ACTA TECHNICA

CIVIL ENGINEERING — C/6

1828

ACTA TECHNICA

A JOURNAL OF THE HUNGARIAN ACADEMY OF SCIENCES

CONTENTS

BOOK REVIEW

APPLICATION OF THE DIFFERENCE METHOD TO THE
GEOMETRICALLY NONLINEAR DIRECTOR THEORY OF BEAMS

CZIBERE, B.[*]

A geometrically nonlinear theory is presented for the plane bending of straight beams with the finite difference energy method. According to the straight line hypothesis the beam is described with two position vector components and two director components; the strains are formed by the dot products of these vectors. The determination of the difference operators is based on the least square method. Using the principle of minimum potential energy, a system of nonlinear algebraic equations is obtained which is solved by the Newton—Raphson iterative method.

1. Introduction

A large deflection analysis of elastic, flexible frame structures is introduced by /1/, /2/. The purpose of the present paper is to demonstrate an energy method to analyze a beam undergoing finite displacements and rotations. The finite difference method is suitable to solve linear problems of continuum mechanics (see /3/), but in the nonlinear case, the procedure does not prove to be convergent. On using the finite difference energy method, unlike the finite difference method, the difference operators are inserted into the integral equations; consequently the convergence becomes much quicker and convergence may be attained in nonlinear problems too. During the analysis we restrict ourselves to plane bending of elastic, straight beams with constant thickness in the undeformed configuration.

In accordance with the straight line hypothesis (see /4/, /5/, /6/) the geometry of the beam is described with the aid of the position vector of the middle line and the so-called director assigned to every point of the middle line. The position vector is kinematically independent of the direc-

---

[*]Czibere, Beáta, H-3529 Miskolc, Kós Károly u. 9, Hungary

CZIBERE, B.
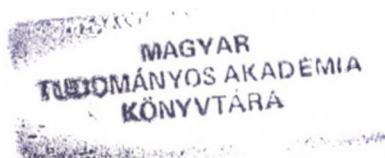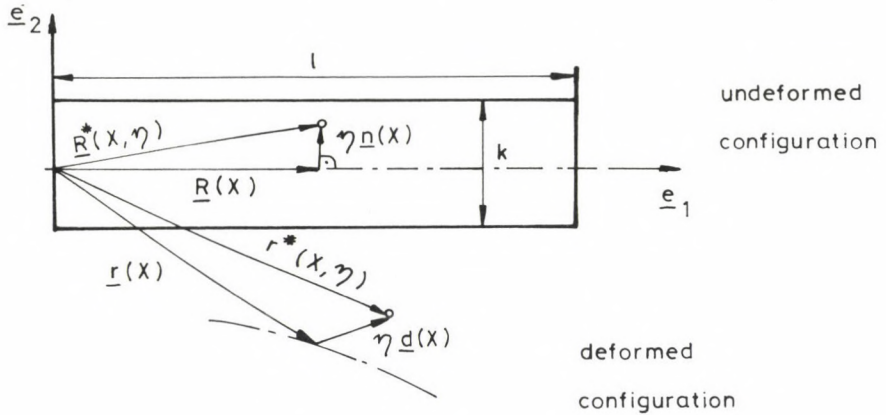
Fig. 1. The geometry of the beam

tor, so we have four degrees of freedom. The director in the undeformed con-
figuration is identical to the unit normal vector of the middle line, and
the change of its length represents the change in the thickness of the beam
under loading.

     Let $\underline{r}$ denote the position vector and $\underline{d}$ the director. The reference
and the actual position vectors of a point outside the middle line of the
beam lying in the $(\underline{e}_1, \underline{e}_2)$ plane (Fig. 1) are as follows:

$$\underline{R}^*(X, \eta) = \underline{R}(X) + \eta\underline{n},$$

$$\underline{r}^*(X, \eta) = \underline{r}(X) + \eta\underline{d}, \quad -\frac{k}{2} \leq \eta \leq \frac{k}{2}, \tag{1}$$

where X, η = Lagrangian coordinates,

      $\underline{n}$ = unit normal vector,

      k = original thickness of the beam.

     The above-mentioned director theory extends the Bernoulli theory to
the following features:

     — the shear strain is under consideration,

     — the thickness of the beam can change under loading.

2. Strains and stress resultants

The components of the Green strain tensor $(\underline{\underline{\varepsilon}})$ in accordance with the director theory (cf. /7/) are formed by dot products as follows:

$$\varepsilon_{11} = \varepsilon_D + \eta \cdot \kappa,$$

$$\varepsilon_D = \frac{1}{2}(\underline{r}' \cdot \underline{r}' - 1), \tag{2.1}$$

$$\kappa = \underline{r}' \cdot \underline{d}', \tag{2.2}$$

$$\varepsilon_{12} = \frac{1}{2}\underline{r}' \cdot \underline{d}, \tag{2.3}$$

$$\varepsilon_{22} = \frac{1}{2}(\underline{d} \cdot \underline{d} - 1), \tag{2.4}$$

where ε_D, κ, ε_{12} and ε_{22} represent the extension, the bending strain, the shear strain, and the thickness strain, $\underline{r}'$ and $\underline{d}'$ denote the derivatives of the vectors $\underline{r}$ and $\underline{d}$ with respect to X. We assume the contribution of the 2nd Piola–Kirchhoff stresses, analogously to the strains in accordance with equations (2.1—2.4):

$$\sigma_{11}(X, \eta) = \sigma_D(X) + \eta\sigma_\kappa(X),$$

$$\sigma_{12}(X, \eta) = \sigma_{12}(X),$$

$$\sigma_{22}(X, \eta) = \sigma_{22}(X). \tag{3}$$

The virtual internal work is

$$\delta A^i = \int_{X=0}^{\ell} \int_{(A)} \sigma_{ij} \cdot \delta\varepsilon_{ij} dAdX. \tag{4}$$

On substituting equations (2.1—2.4), (3) into (4), we obtain

$$\delta A^i = \int_{X=0}^{\ell} \int_{(A)} \left[(\sigma_D + \eta \cdot \sigma_\kappa)(\delta\varepsilon_D + \eta \cdot \delta\kappa) + 2\sigma_{12} \cdot \delta\varepsilon_{12} + \sigma_{22} \cdot \delta\varepsilon_{22} \right] dAdX =$$

$$= \int_{X=0}^{\ell} \left[N \cdot \delta\varepsilon_D + M \cdot \delta\kappa + 2Q \cdot \delta\varepsilon_{12} + T \cdot \delta\varepsilon_{22} \right] dX, \tag{5}$$

where N, M, Q and T represent the stress resultants as normal force, bending moment, shear force, and transversal normal force, respectively. In the case of elastic material, on employing Hooke's law in the plane stress state version (cf. /8/),

$$\underline{\underline{\sigma}} = 2G \left[\underline{\underline{\varepsilon}} + \frac{\nu}{1 - \nu} \varepsilon^* \cdot \underline{\underline{E}}_2 \right],$$
(6)

we get the following formulas for the stress resultants:

$$N = A \frac{2G}{1 - \nu} (\varepsilon_D + \nu \cdot \varepsilon_{22}),$$

$$M = IE\kappa,$$

$$Q = 2AG\varepsilon_{12},$$

$$T = A \frac{2G}{1 - \nu} (\nu \cdot \varepsilon_D + \varepsilon_{22}),$$
(7)

where E = modulus of elasticity in tension,
      G = modulus of elasticity in shear,
      ν = Poisson's ratio,
      $\underline{\underline{E}}_2$ = unit tensor of 2 dimension,
      $\varepsilon^* = \underline{\underline{E}}_2 \cdot\cdot \underline{\underline{\varepsilon}} = \varepsilon_{11} + \varepsilon_{22}$,
      A = area,
      I = moment of inertia.

3. The finite difference representation

In addition to its quick convergence, a further advantage of the energy method is that we need to substitute only first-order derivatives into our formulas. Thus the main problem now is how to calculate the first derivative. Since we require its square, the well-known central difference operators introduced in /9/ cannot be employed. In order to determine the dot products of the derivatives of the director and the position vector in equations (2.1—2.4), we employ the least square minimum method, as presented in the following sections.

For our finite difference discretisation, let us consider an equidistant mesh with step width h. All derivative quantities are approximated
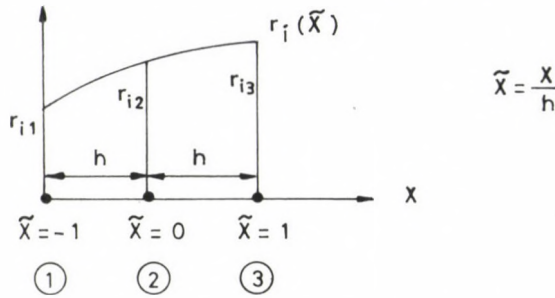
Fig. 2. Finite difference discretisation

by the application of three nodal points. Let us introduce a local co-or-dinate system with the co-ordinate $\tilde{x}$ (Fig. 2). Assume that both components of the position vector and the director are quadratic in $\tilde{x}$:

$$r_i(\tilde{x}) = r_{i2} + \frac{r_{i3} - r_{i1}}{2}\,\tilde{x} + \frac{r_{i3} - 2r_{i2} + r_{i1}}{2}\,\tilde{x}^2,$$

$$d_i(\tilde{x}) = d_{i2} + \frac{d_{i3} - d_{i1}}{2}\,\tilde{x} + \frac{d_{i3} - 2d_{i2} + d_{i1}}{2}\,\tilde{x}^2, \tag{8}$$

where r_{ik}, d_{ik} ($i = 1,2$; $k = 1,2,3$) are the values of the position vector and the director in the k-th nodal point.

The derivatives of formulas (8) with respect to X are

$$\frac{\partial r_i(\tilde{x})}{\partial X} = r_i'(\tilde{x}) = \frac{1}{h}\left[\frac{r_{i3} - r_{i1}}{2} + \left(r_{i3} - 2r_{i2} + r_{i1}\right)\tilde{x}\right],$$

$$\frac{\partial d_i(\tilde{x})}{\partial X} = d_i'(\tilde{x}) = \frac{1}{h}\left[\frac{d_{i3} - d_{i1}}{2} + \left(d_{i3} - 2d_{i2} + d_{i1}\right)\tilde{x}\right]. \tag{9}$$

3.1. Approximation of the extensional, bending, and shear strains

We need to approximate the strains defined by (2.1—2.4) so that they satisfy certain conditions following from the beam theory (e.g. by pure bending the director remains perpendicular to the tangent of the deformed middle line, that is $\varepsilon_{12} = 0$, etc.).

3.1.1. Approximation at internal mesh points

In order to satisfy the conditions mentioned above, we assume that in the neighborhood of an internal point, $\varepsilon_D(\tilde{x})$ and $\kappa(\tilde{x})$ are linear functions and $\varepsilon_{12}(\tilde{x})$ is constant. According to the least square method we have to minimize the three formulas as follows:

$$\rho_{\varepsilon D} = \int_{-1}^{1} \left[c_{01} + c_{11}\tilde{x} - \underline{r}'(\tilde{x}) \cdot \underline{r}'(\tilde{x}) \right]^2 d\tilde{x},$$

$$\rho_{\kappa} = \int_{-1}^{1} \left[c_{02} + c_{12}\tilde{x} - \underline{r}'(\tilde{x}) \cdot \underline{d}'(\tilde{x}) \right]^2 d\tilde{x},$$

$$\rho_{\varepsilon 12} = \int_{-1}^{1} \left[c_{03} - \underline{r}'(\tilde{x}) \cdot \underline{d}(\tilde{x}) \right]^2 d\tilde{x}. \tag{10}$$

Computing the integral expressions for the parameters c_{01}—c_{03} listed below:

$$c_{01} = \frac{1}{2} \int_{-1}^{1} \underline{r}'(\tilde{x}) \cdot \underline{r}'(\tilde{x}) d\tilde{x}, \qquad c_{11} = \frac{3}{2} \int_{-1}^{1} \tilde{x} \cdot \underline{r}'(\tilde{x}) \cdot \underline{r}'(\tilde{x}) d\tilde{x},$$

$$c_{02} = \frac{1}{2} \int_{-1}^{1} \underline{r}'(\tilde{x}) \cdot \underline{d}'(\tilde{x}) d\tilde{x}, \qquad c_{12} = \frac{3}{2} \int_{-1}^{1} \tilde{x} \cdot \underline{r}'(\tilde{x}) \cdot \underline{d}'(\tilde{x}) d\tilde{x},$$

$$c_{03} = \frac{1}{2} \int_{-1}^{1} \underline{r}'(\tilde{x}) \cdot \underline{d}'(\tilde{x}) d\tilde{x},$$

the following difference operators are obtained:

$$/ST1/ = \frac{1}{12h^2} \begin{array}{|c|c|c|} \hline 7 & -8 & 1 \\ \hline -8 & 16 & -8 \\ \hline 1 & -8 & 7 \\ \hline \end{array}, \qquad /ST2/ = \frac{1}{h^2} \begin{array}{|c|c|c|} \hline -1 & 1 & 1 \\ \hline 1 & 0 & -1 \\ \hline 0 & -1 & 1 \\ \hline \end{array}$$

$$/ST3/ = \frac{1}{12h} \begin{array}{|c|c|c|} \hline -3 & 4 & 1 \\ \hline -4 & 0 & 4 \\ \hline 1 & -4 & 3 \\ \hline \end{array}. \tag{11}$$

Further, with the aid of these difference operators, handling them as matrices, the strains can be calculated as follows:

$$\varepsilon_D = \frac{1}{2}\left[r_{ik} \cdot /ST1/_{jk} \cdot r_{ij} + r_{ik} \cdot /ST2/_{jk} \cdot r_{ij} \cdot \tilde{x} - 1 \right] = \varepsilon_D^0 + \varepsilon_D^1 \cdot \tilde{x},$$

$$\kappa = r_{ik} \cdot /ST1/_{jk} \cdot d_{ij} + r_{ik} \cdot /ST2/_{jk} \cdot d_{ij} \cdot \tilde{x} = \kappa^0 + \kappa^1 \cdot \tilde{x},$$

$$\varepsilon_{12} = \frac{1}{2} r_{ik} \cdot /ST3/_{jk} \cdot d_{ij}, \qquad (i = 1,2; \quad j,k = 1,2,3). \tag{12}$$

3.1.2. Approximation at boundary points

In order to satisfy the conditions mentioned in section 3.1, we assume that in the neighborhood of a boundary point the extensional, bending, and shear strains are constant; consequently in this case the three functions to minimize are

$$\rho_{\varepsilon D} = \int_a^b \left[c_{01} - \underline{r}'(\tilde{x}) \cdot \underline{r}'(\tilde{x}) \right]^2 d\tilde{x},$$

$$\rho_{\kappa} = \int_a^b \left[c_{02} - \underline{r}'(\tilde{x}) \cdot \underline{d}'(\tilde{x}) \right]^2 d\tilde{x},$$

$$\rho_{\varepsilon 12} = \int_a^b \left[c_{03} - \underline{r}'(\tilde{x}) \cdot \underline{d}(\tilde{x}) \right]^2 d\tilde{x}, \tag{13}$$

where we integrate from a = -1 to b = 0 at the left-hand side boundary point and from a = 0 to b = 1 at the right-hand side boundary point (see Fig. 2). We obtain the difference operators as in section 3.1.1.:

— left-hand side boundary point:

$$/ST1/ = \frac{1}{12h^2} \begin{array}{|c|c|c|} \hline 13 & -14 & 1 \\ \hline -14 & 16 & -2 \\ \hline 1 & -2 & 1 \\ \hline \end{array}, \qquad /ST3/ = \frac{1}{12h} \begin{array}{|c|c|c|} \hline -6 & 7 & -1 \\ \hline -7 & 6 & 1 \\ \hline 1 & -1 & 0 \\ \hline \end{array},$$

$$\tag{14.1}$$

— right-hand side boundary point:

$$
/ST1/ = \frac{1}{12h^2}
\begin{array}{|c|c|c|}
\hline
1 & -2 & 1 \\
\hline
-2 & 16 & -14 \\
\hline
1 & -14 & 13 \\
\hline
\end{array}
,\qquad
/ST3/ = \frac{1}{12h}
\begin{array}{|c|c|c|}
\hline
0 & 1 & -1 \\
\hline
-1 & -6 & 7 \\
\hline
1 & -7 & 6 \\
\hline
\end{array}
.
$$

$$(14.2)$$

The strains are expressed by

$$
\varepsilon_D = \frac{1}{2}\left[r_{ik} \cdot /ST1/_{jk} \cdot r_{ij} - 1 \right] = \varepsilon_D^0,
$$

$$
\kappa = r_{ik} \cdot /ST1/_{jk} \cdot d_{ij} = \kappa^0,
$$

$$
\varepsilon_{12} = \frac{1}{2} r_{ik} \cdot /ST3/_{jk} \cdot d_{ij}, \qquad (i = 1,2; \quad j,k = 1,2,3). \tag{15}
$$

3.2. Approximation of the thickness strain

Assuming, that the $\underline{d} \cdot \underline{d}$ dot product is quadratic in $\tilde{x}$, the following formulas are obtained:

a) internal points:

$$
\underline{d} \cdot \underline{d} = d_{i2}^2 + \frac{d_{i3}^2 - d_{i1}^2}{2}\tilde{x} + \left(d_{i3}^2 - 2d_{i2}^2 + d_{i1}^2 \right)\frac{\tilde{x}^2}{2}, \tag{16.1}
$$

b) left-hand side boundary point:

$$
\underline{d} \cdot \underline{d} = d_{i1}^2 + \frac{-d_{i3}^2 + 4d_{i2}^2 - 3d_{i1}^2}{2}\tilde{x} + \left(d_{i3}^2 - 2d_{i2}^2 + d_{i1}^2 \right)\frac{\tilde{x}^2}{2}, \tag{16.2}
$$

c) right-hand side boundary point:

$$
\underline{d} \cdot \underline{d} = d_{i3}^2 + \frac{d_{i1}^2 - 4d_{i2}^2 + 3d_{i3}^2}{2}\tilde{x} + \left(d_{i3}^2 - 2d_{i2}^2 + d_{i1}^2 \right)\frac{\tilde{x}^2}{2}, \tag{16.3}
$$

(the origin of the local co-ordinate system is taken at the respective nodal point; $i = 1,2$).

We approximate $\varepsilon_{22}(\tilde{x})$ in the neighborhood of each point with a linear function. The six new difference operators obtained analogously to the method employed in 3.1.1. and 3.1.2. are listed below:

a) internal points:

$$/ST4/ = \frac{1}{6} \begin{bmatrix} 1 & 0 & 0 \\ 0 & 4 & 0 \\ 0 & 0 & 1 \end{bmatrix}, \qquad /ST5/ = \frac{1}{2} \begin{bmatrix} -1 & 0 & 0 \\ 0 & 0 & 0 \\ 0 & 0 & 1 \end{bmatrix}, \qquad (17.1)$$

b) left-hand side boundary point:

$$/ST4/ = \frac{1}{12} \begin{bmatrix} 11 & 0 & 0 \\ 0 & 2 & 0 \\ 0 & 0 & -1 \end{bmatrix}, \qquad /ST5/ = \begin{bmatrix} -1 & 0 & 0 \\ 0 & 1 & 0 \\ 0 & 0 & 0 \end{bmatrix}, \qquad (17.2)$$

c) right-hand side boundary point

$$/ST4/ = \frac{1}{12} \begin{bmatrix} -1 & 0 & 0 \\ 0 & 2 & 0 \\ 0 & 0 & 11 \end{bmatrix} \qquad /ST5/ = \begin{bmatrix} 0 & 0 & 0 \\ 0 & -1 & 0 \\ 0 & 0 & 1 \end{bmatrix}, \qquad (17.3)$$

Using these matrices, we get that the thickness strain is

$$\varepsilon_{22} = \frac{1}{2}\left[d_{ik} \cdot /ST4/_{jk} \cdot d_{ij} + d_{ik} \cdot /ST5/_{jk} \cdot d_{ij} \cdot \tilde{x} - 1 \right] = \varepsilon_{22}^0 + \varepsilon_{22}^1 \cdot \tilde{x},$$

$$(i = 1,2; \quad j,k = 1,2,3). \qquad (18)$$

4. Application of the principle of minimum potential energy

The strain energy in the neighborhood of a nodal point can be expressed as:

$$W^E = \frac{1}{2} \int_a^b \left\{ A\frac{2G}{1-\nu} \left[(\varepsilon_D^0 + \tilde{x}\varepsilon_D^1)^2 + 2\nu(\varepsilon_D^0 + \tilde{x}\varepsilon_D^1)(\varepsilon_{22}^0 + \tilde{x}\varepsilon_{22}^1) + (\varepsilon_{22}^0 + \tilde{x}\varepsilon_{22}^1)^2 \right] + \right.$$

$$\left. + EI(\kappa^0 + \tilde{x}\kappa^1)^2 + 4AG(\varepsilon_{12})^2 \right\} h d\tilde{x}; \qquad (19)$$

here the interval of the integral is

a) for internal mesh points: from $a = -\frac{1}{2}$ to $b = \frac{1}{2}$;

CZIBERE, B.
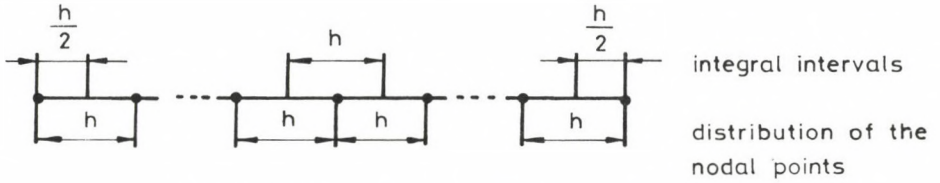

integral intervals

distribution of the
nodal points

Fig. 3. Integral intervals by computing the strain energy

b) for left-hand side boundary points: from $a = 0$ to $b = \frac{1}{2}$;

c) for right-hand side boundary points: from $a = -\frac{1}{2}$ to $b = 0$ (see Fig. 3).

On substituting the formulas (12), (15) and (18) into the integral expression (19), and carrying out the integration, we obtain the strain energy in the following form:

$$W^E = \frac{1}{2} \, \underline{\varepsilon} \cdot \underline{\underline{A}} \cdot \underline{\varepsilon}, \tag{20}$$

where the vector $\underline{\varepsilon}$ has 7 discrete strain components:

$$\underline{\varepsilon} = \left[\, \varepsilon_D^0 \ \ \varepsilon_D^1 \ \ \kappa^0 \ \ \kappa^1 \ \ \varepsilon_{12} \ \ \varepsilon_{22}^0 \ \ \varepsilon_{22}^1 \, \right],$$

and $\underline{\underline{A}}$ denotes the work matrix independent of the strains.

The tangential stiffness matrix with reference to three nodal points is

$$/S^E/_{ij} = \frac{\partial^2 W^E}{\partial x_i^E \, \partial x_j^E} = \frac{\partial \varepsilon_k}{\partial x_i^E \, \partial x_j^E} \cdot A_{kn} \cdot \varepsilon_n + \frac{\partial \varepsilon_k}{\partial x_i^E} \cdot A_{kn} \cdot \frac{\partial \varepsilon_n}{\partial x_j^E},$$

$$(i,j = 1,2,3; \qquad k,n = 1,2,\ldots,7), \tag{21}$$

where $\underline{x}^E = \left[r_{11} \ r_{21} \ d_{11} \ d_{21} \ r_{12} \ r_{22} \ d_{12} \ d_{22} \ r_{13} \ r_{23} \ d_{13} \ d_{23} \right]$.

The total potential energy is defined by

$$\Pi = W - A^a, \tag{22}$$

where $W = \Sigma(W^E)$ denotes the strain energy of the beam and A^a represents the external work.

In accordance with the principle of minimum potential energy one can write

$$\delta \Pi = \left(\frac{\partial W}{\partial \underline{x}} - \frac{\partial A^a}{\partial \underline{x}} \right) \delta \underline{x} = 0, \tag{23}$$

where $\underline{x} = \left[r_{in}, d_{in} \right]$, $(i = 1,2; n = 1,2,\ldots,np)$, and np is the number of the nodal points.

On applying the energy principle, a following system of nonlinear equations is obtained:

$$\underline{G}(\underline{x}) = \frac{\partial W}{\partial \underline{x}} - \frac{A^a}{\partial \underline{x}} = \underline{F} - \underline{P}^a = 0, \tag{24}$$

which we can easily solve by the Newton–Raphson iterative method:

$$\underline{\underline{S}}(\underline{x}^k) \cdot (\underline{x}^k - \underline{x}^{k+1}) = \underline{F}(\underline{x}^k) - \underline{P}^a, \tag{25}$$

where $\underline{\underline{S}}$ is the global tangential stiffness matrix

$$\underline{\underline{S}} = \left[\frac{\partial^2 W}{\partial x_i \, \partial x_j} \right], \qquad (i,j = 1,2).$$

5. Numerical results

The show the effectiveness of the procedure introduced above, some numerical examples are presented in this section. We will study a clamped beam, loaded at its free end by a concentrated and step-by-step increasable load.

5.1. Determination of the Eulerian critical buckling load

In this problem our calculation is based on the fact that on gradually increasing the pressing load, the determinant of the system of equations changes signs at the critical load. By increasing the number of the nodal points, the procedure converges to the exact solution, as it is shown in Table 1.

Table 1. Critical buckling load: The error of the calculation
(The length-to-thickness ratio is 1/100)

Nodal points	5	7	9	11	15
Error /%/	3.8	1.72	0.96	0.61	0.31

5.2. Determination of the curved shapes of a beam with a pressing load

Figure 4 shows a cantilever beam loaded by step-by-step increased pressing load. The procedure is started by the Eulerian critical load and, in addition, a small transversal load (of magnitude 1/1000 of the critical
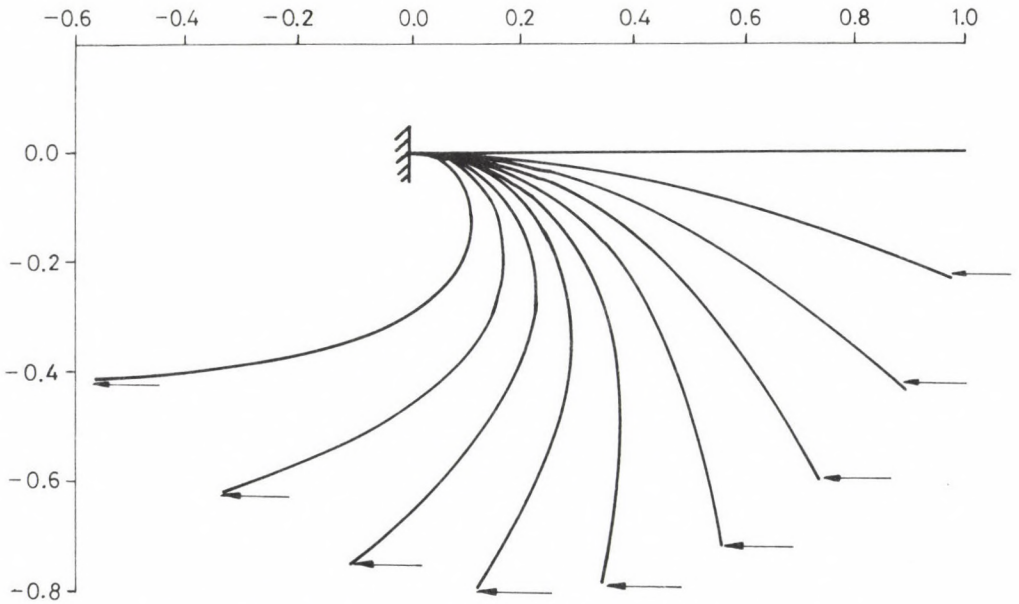
Fig. 4. Cantilever beam with step-by-step increased pressing load

Table 2. Cantilever beam with a step-by-step increased pressing load (P).
Summary of the solutions. The results correspond to the deflection at the
end of the beam (w)

Load step	P/P_{crit}	w/ℓ Numeric. res.	w/ℓ Analytic. res.	Error /%/
1	1.015	-0.2223	-0.220	1.04
2	1.063	-0.4227	-0.420	0.64
3	1.152	-0.5948	-0.593	0.30
4	1.293	-0.7196	-0.719	0.08
5	1.518	-0.7917	-0.792	-0.04
6	1.884	-0.8032	-0.803	0.02
7	2.541	-0.7504	-0.750	0.05
8	4.029	-0.6245	-0.625	0.08
9	9.116	-0.4212	-0.421	0.05

load) is applied only at the first step of iteration. The length-to-thick-
ness ratio is 1/100 and 31 nodal points are employed. The numerical results
and the analytical results presented in /10/ are compared in Table 2.

5.3. Large deflection analysis of a cantilever beam

A cantilever beam loaded by step-by-step increased transversal load is
analyzed. Figure 5 shows the deformed shapes of the beam by five load steps.
The numerical results presented in /11/ are compared in Table 3.
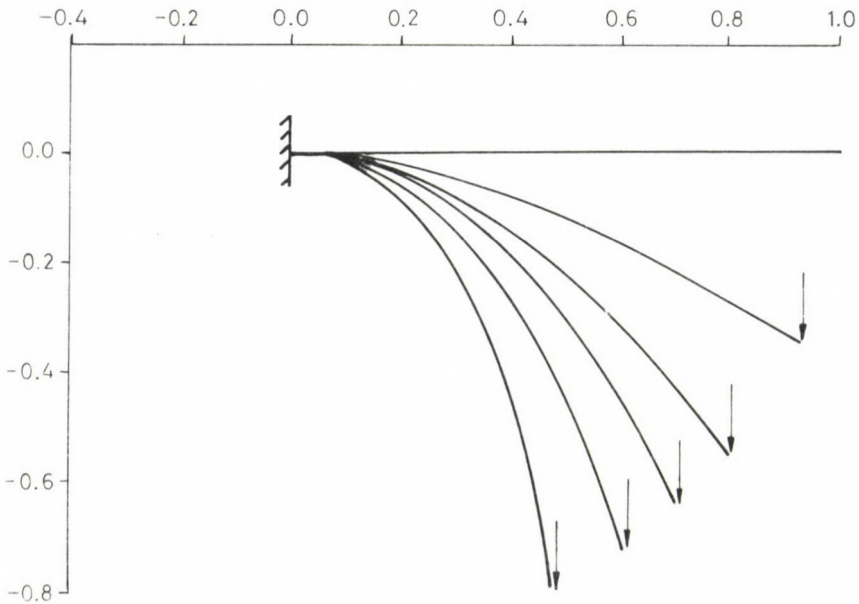
Fig. 5. Cantilever beam with a transversal load

Table 3. Cantilever beam with a transversal load. Summary of
the solution. The coordinates (r_1, r_2) correspond to the end
of the beam

Load step	Numerical results		Analytical results	
	r_1/ℓ	r_2/ℓ	r_1/ℓ	r_2/ℓ
1	0.87014	-0.44873	0.87155	-0.44561
2	0.79840	-0.54715	0.80028	-0.54367
3	0.71097	-0.63774	0.71318	-0.63401
4	0.60578	-0.72071	0.60818	-0.71669
5	0.47384	-0.79966	0.47639	-0.79483

5.4. Bending to a full circle

The deformed shape of a cantilever beam loaded by a moment at its end is a circular arc. On increasing the load in 10 increment steps to reach the bending moment required to form a full circle and using 21 nodal points, the solution is obtained with 10 iterations in each load step. Figure 6 shows the deformed shapes of the beam at every second load increment.
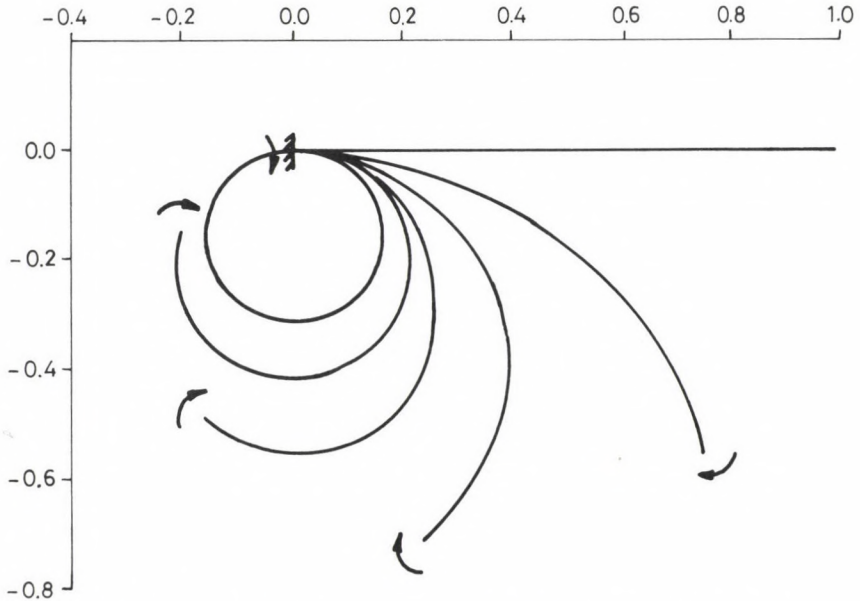
Fig. 6. Bending to a full circle: the deformed shapes of the beam

5.5. Investigation of the effect of the shear strain

As the last example we restrict ourselves to the linear analysis of a cantilever beam, loaded at its free end by a transversal load (P). In this linear case, in consideration of the shear strain, the deflection at the end of the beam is (see /12/)

$$w^{whole} = w^{Kirchh} + w^{shear},$$

where $w^{Kirchh} = \dfrac{P\ell^3}{3IE}$, $w^{shear} = \dfrac{6}{5} \cdot \dfrac{P\ell}{AG}$.

Table 4 shows the analytical and the numerical results in case of different length-to-thickness ratio.

Table 4. The effect of the shear strain by a cantilever beam. The results correspond to the deflection at the end of the beam (w).

$$(w^{whole} = w^{Kirchh} + w^{shear})$$

Length-to-thickness ratio	Analytical results			Numerical results
	w^{Kirchh}/ℓ	w^{shear}/ℓ	w^{whole}/ℓ	w^{whole}/ℓ
1/100	0.16	0.0000128	0.1600128	0.1602106
5/100	0.16	0.00032	0.16032	0.1607520
10/100	0.16	0.00128	0.16128	0.1614289
15/100	0.16	0.00288	0.16288	0.1625419
20/100	0.16	0.00512	0.16512	0.1660984

These five examples show that our results obtained by the above numerical method are in good agreement with those obtained analytically.

REFERENCES

1. Gáspár, Zs.: Ideálisan rugalmas rúdszerkezetek stabilitásvizsgálata az egyensúlyi módszerrel. Budapest, 1972

2. Gáspár, Zs.: Rugalmas rúdszerkezetek nagy elmozdulásának vizsgálata. Budapest, 1976

3. Szilard, R.: Finite Berechnungsmethodes der Strukturmechanik. Band 1, Stabwerke. Verlag Wilh. E. & S., 1982

4. Naghdi, P.: The theory of shells and plates. Handbuch der Physik, Band VIa/2. Springer, 1972, 425—640

5. Antman, S. S.: Director theories of rods. Handbuch der Physik, Band VIa/2. Springer, 1972, 665—669

6. Schoop, H.: Skript zur Vorlesung "Schalentheorie". Techn. Univ. Berlin

7. Schoop, H. - Lübcke, E.: Einfache finite Balken- und Bogenelemente mit objektiven nichtlinearen Verzerrungen bei ebener Biegung. Techn. Univ. Berlin, Forschungsbericht Nr. 6, 1988

8. Schoop, H.: Skript zur Vorlesung "Finite Elemente in der nichtlinearen Membran- und Balkentheorie". Techn. Univ. Berlin

9. Collatz, L.: The numerical treatment of differential equations. Springer, 1966

10. Kozák, I. - Szabó, I.: Szilárdságtan VI. (lecture notes). Tankönyvkiadó, Budapest, 1977

11. Popov, E. P.: Theory and calculation of flexible, elastic beams (in Russian). Moscow, Nauka, 1986

12. Gummert, P. - Reckling, K. A.: Mechanik. Vieweg & Sohn, 1987

COMPILATION OF THE FIRST HUNGARIAN NETWORK-LEVEL
PAVEMENT MANAGEMENT SYSTEM (PMS)

GÁSPÁR, L. Jr.*

The first Hungarian network-level PMS relies on Markov matrices. The system can be used for the calculation of the funds needed at various condition levels, for the regional distribution of given amounts of financial means at the minimization of national economy costs and for the determination of the economic and the technical consequences of subsequent modifications in the funds distribution.

1. Introduction

It can be observed all over the world that the financial means available for highway purposes are more and more behind the actual needs. Although a growing share of these funds is used for maintenance and preservation tasks, even these financial means decrease continually in several countries — among others, in Hungary — lately. This fact, naturally, influences the actual national roads policy, our aim can only be the deceleration of the general condition deterioration.

That is why the optimal distribution and allocation of rather limited financial means have become even more important than before. In the latest years, a significant development could be seen in the actual method of the allocation of highway funds between counties (highway directorates). The former simple procedure relying upon normative values that were functions of road length, pavement type and, slightly, of traffic size were gradually substituted by methods utilizing information about the actual pavement condition. Recently the need has emerged that this funds allocation should be made as objective and reliable as possible. This intention was declared also

---

*Gáspár, László ifj., H-1158 Budapest, Szücs I. u. 2, Hungary

by the professional managing authorities. As objective preconditions of this development it can be mentioned the availability of the necessary data (insufficient quantity and accuracy) as well as of the appropriate computer technical background necessary for data retrieval, processing and the elaboration of allocation model.

Thus, the development of the first Hungarian network-level PMS has been performed among the above circumstances.

2. Scope of the task, network-level and project-level PMS

The research work presented here aimed at the compilation of the first version of the mathematical model of the Hungarian network-level PMS /1/, more precisely its first version was to be established.

The model relies upon the available information on the highway network, traffic, pavement structure, cost etc. The main influencing technical-economic factors were realistically considered and, at the same time, the limitations of available information were also taken into account. Compared with the preceding methods, the establishment of optimization system can be seemed as a significant step forward although several necessary future development directions can already be pointed out /2—4/.

The model had to have the following main functions: determination of the necessary amount of funds ensuring a given future pavement condition, as well a reliable regional allocation at given limitation of available financial means. When establishing the model, the sometimes controversary requirements of high scientific level and of the easy practical applicability were also considered having a direct effect on the complexity and the size of the mathematical model, as well as on the approximations and negligences applied.

In 1988 an expert team under the supervision of the Highway Department of Ministry of Transport investigated the preconditions for the development of the first Hungarian PMS, its possible time-table and the expected research expenditures. Relying on the actual situation, it was concluded that the creation of the first working version of the project-level PMS in Hungary needed still several-year intensive research activities, while the elaboration of the first Hungarian variant of network-level PMS appeared to be realistic during 1989—1990 /11/.

According to the investigations performed so far, for the project-level variant the adaptation of the HDM-III model of World Bank seems to be the most suitable, however, it also needs still great efforts. Anyway, it would be absolutely advantageous to apply the procedure of World Bank because of the existing and the future financial relationships with this institution.

The network-level system should be established prior to the other one not only because of the fact that the distribution of the financial means between various regions (counties) preceeds even logically the optimal ranking of actual condition improving interventions from technical-economic point of view -- that is, the elaboration of a project-level PMS -- but it should be preferred as a consequence of following reasons:

 -- the deficiencies and the eventual limited reliability of the existing relevant do not hinder in such extent the elaboration of the network-level PMS as that of the project-level PMS since in the former case mean values and even only partly homogeneous data sets can be used,

 -- for the creation of the network-level PMS there is already an existing method that can serve as a starting point of the new system,

 -- even the first version of the project-level PMS can only be properly be operated if major organisation changes of several institutions (e.g. highway directorates, design and construction firms) are carried out; however, this rather time-consuming and complex series of measures is not needed for the network-level variant.

Thus, the Institute for Transport Sciences (KTI) elaborated -- on behalf of National Highway Directorate the mathematical model of first Hungarian network-level PMS in 1989—1990.

The system developed deals only with the maintenance-operation funds excluding e.g. the institutional costs, the winter maintenance and traffic engineering expenditures.

Several preliminary research reports have been made in the theme /2--6/. The final report /7/ summarizes the whole system and the results obtained.

The model features and the application areas will be dealt with subsequently. The computer and mathematical aspects -- carried out by the mathematicians dr. András BAKÓ and dr. Tamás SZÁNTAI -- are presented in another article /1/.

3. Selection of the model

3.1. Preliminary investigations

The development of the network-level model needed various preliminary investigations.

The decision about the pavement types to be included in the system was considered as one of the first tasks. For this purpose the distribution of the whole national highway network area according to pavement types was analyzed. (Instead of the length, the area was preferred here because the intervention costs in the model can be related only m^2; thus, area ratios were applied in the system.)

The funds distribution in 1990 considered several parameters that were usually conform with the engineering judgement. However, in the lack of an appropriate model, their coincidence could not have been investigated and the possibility of the optimization did not exist.

For the model only three main intervention alternatives (routine maintenance, surface dressing and asphalt overlay) were chosen. It can be mentioned here that the maximum number of parameters applied is strongly limited by the need of manageability of the matrix which the model relies on.

Among the traffic parameters, AADT and N (number of 100 kN axle loads passing daily) were taken into consideration. Although the actual heavy axle load has a direct connection with the bearing capacity loss of pavement structure the parameter AADT was preferred partly because of its being more widely known than the other one and partly because some other pavement deterioration forms — not only the loss of bearing capacity — should be considered in this complex investigation.

3.2. Selected methodology

For the solution of the task outlined a methodology realistically taking into account realistically both the possibilities and the constraints had to be chosen.

The following "existing possibilities" are highlighted here:
— the available road data sets,
— former Hungarian funds distribution experience,
— presentation of similar foreign systems,
— set of mathematical means for the treatment of this problem,

— the goal-oriented expert team including experienced highway engineers and mathematicians.

The following objective difficulties and constraints of the establishment of the model can be mentioned:

— the rather limited time available for the elaboration of model,
— only a part of the huge information mass of the country-wide suitability rating initiated in 1979 is available for the data processing prior to the compilation of model,
— a certain share of the data available has not sufficient accuracy because e.g. the existing data base does not contain the consequences of the recent changes in the kilometrage of highways,
— the use of the time series is more or less disadvantageously influenced by the fact that the condition parameters were often evaluated in various time-points using different methods and, in some cases, the results of these procedures have no correlation between each other,
— no domestic relationships are available between pavement condition and vehicle operating costs, although they would definitely help the determination of a well-founded optimum criteria,
— there are still no reliable methods for the determination of the optimum ratio between development and maintenance funds, for the forecast of operation costs and for the well-established estimation of institutional costs, thus, the exact assumption of the funds limit for the model encounters difficulties even if the total amount of Road Funds is known.

Taking into account all of these aspects, the Markov-type transition probability matrix was chosen from among several methods published in the literature. One of the reasons was that it is rather clear, besides it does not need long time series as a precondition. For the sake of the practical applicability only limited numbers of condition variations, pavement types, traffic volumes and intervention variants were taken for the compilation of the model.

4. Markov-type transition probability matrix

The Markov-type transition probability matrix — in case of a certain pavement type, traffic size and intervention strategy — supplies in the

model the distribution of the probabilities of the transition of a given
condition variant to another one or of its remaining in the same variant·
during a certain period (e.g. 1 year).

Hereafter the choice of the variables of the matrix, the determination
of various condition variants, the establishment of matrix elements and,
finally, the interpretation of matrix will be dealt with.

4.1. Matrix variables

The variables of matrix are: pavement type, traffic volume, interven-
tion variants. Subsequently the background of the selection of actual va-
riants applied in the system will be presented.

As pavement types, asphalt concrete and asphalt macadam pavements were
chosen. (In the first group all of the rolled asphalt types, while in the
other one the coated chippings, mixed and impregnated asphalt macadams are
included.) It was also considered that the rest of the highway network
— rigid and unpaved sections — have deterioration characteristics basical-
ly different from those of the two selected flexible pavement groups.

The following procedure is recommended for the funds distribution in
the case of roads with non-asphalt pavements:

(a) The categories "surface dressing and oiled macadam pavement"
    — with a total length of some 6000 km /8/ — are considered as
    asphalt macadam pavements. This decision can be explained by the
    fact that "surface dressing" means here a surface treatment on
    water-bound macadam pavements and the deterioration features of
    these pavements are not very unlike to the asphalt macadam pave-
    ments because of technological reasons.

(b) The situation is similar in the case of water-bound macadam pave-
    ments (total length: only 116 km), so, for the sake of simplicity,
    they can be classed among the asphalt macadams in the distribution
    procedure of funds.

(c) The cement concrete, stone and paving brick pavements as well as
    the unpaved (earth) roads have technological features and, con-
    sequently, a deterioration process basically different from those
    of the asphalt pavements and so, they cannot be ranked to the same
    class. That is why a separate share of funds should be ensured
    for them.

(d) As the first step of funds distribution, a given amount of money should be separated for the rigid (cement concrete, stone and paving brick pavements). It should be achieved that the funds ratio of these pavements should be similar to that of the asphalt pavements.

As a consequence, the actual values of last year or of the 2 last years but one should be used, that is the amount of funds and the percentage used for the maintenance and operation of both road types. This percentage will be considered when the separation of certain part of the total national funds for these pavement types is decided.

For the characterization of low, medium and high traffic, following classes were chosen here: 0—3000 pcu/day, 3001—8000 pcu/day and min. 8001 pcu/day.

The following three intervention variants were preferred: routine maintenance — surface dressing — asphalt overlay. (It should be noted that several foreign PMS apply also the variant "do nothing", as well. It was decided, however, to apply in our system only the variant "routine maintenance" even in the case of slightest intervention variant when the necessary routine maintenance activities have to be performed after the initiation of first cracks and pot-holes. It cannot be accepted that the pavement would be "left alone" without any maintenance.)

Taking into account the afore-mentioned facts, theoretically 2x3x3 = 18 matrices should be made; two of them (surface dressing above 8000 pcu/day both pavement types), however, were excluded because of technological reasons. So, the elaboration of 16 matrices was aimed at. (It should be emphasized that the asphalt macadam pavements above 8000 pcu/day traffic are rather rare; so, in a later development phase also these two matrices can be excluded. In the first version, however, they were still included.)

4.2. Determination of the condition variants in the matrix

The rows and the columns of Markov transition probability matrices are formed by pavement condition variants. Of the condition notes supplied by the country-wide highway suitability surveys, those are utilized for this calculation on one hand, of which sufficient data were available with even-

tual time series, on the other hand, which were considered of basic im-
portance from the view-point of the deterioration process. So, the following
pavement condition parameters were selected:

— pavement structure bearing capacity note,
— longitudinal unevenness note,
— pavement surface quality note.

We are convinced that the ranking of these condition parameters into
5 quality classes is of sufficient accuracy for the intervention decisions.
(It can be noted that in the United Kingdom only 3-grade and in the former
GDR 4-grade evaluation has been used recently.)

The quality levels of various parameters are:

— Bearing capacity
    1   good
    2   sufficient
    3   fair
    4   at the end of planned life
    5   after the end of planned life
— Longitudinal unevenness
    using Bump Integrator   by visual evaluation
    1   good   1 good
    2   sufficient
    3   fair   3 fair
    4   insufficient
    5   unbearable   5 poor
    — surface quality
      1   good
      2   sufficient
      3   fair
      4   insufficient
      5   unbearable

For the sake of the uniformity, a 3-grade evaluation was selected for
the pavement longitudinal unevenness. So, theoretically 5x5x3 = 75 condition
variants would be available. For the mathematical solvability of the problem
and for the approximation to the practical conditions, however, the number of
condition variants had to be by all means reduced.

That is why the condition data of the national highway network in
5 counties were evaluated. As a result, the actual condition variants not

Table 1. Condition variant groups of Markov-type
transition matrices

Number	Condition variants
1.	111
2.	112
3.	113 + 114 + 115
4.	131 + 132 + 151
5.	133 + 152
6.	134 + 135
7.	153 + 154 + 155
8.	211
9.	212
10.	213
11.	231 + 251
12.	232 + 252
13.	233 + 214
14.	234 + 215 + 235 + 253 + 254 + 255
15.	311
16.	312 + 331
17.	313 + 314
18.	332 + 351
19.	333 + 352 + 353
20.	334 + 315 + 335
21.	355 + 354
22.	411
23.	412
24.	413 + 414
25.	432 + 431
26.	433
27.	434 + 415 + 435
28.	452 + 451
29.	453
30.	454
31.	455
32.	511
33.	512
34.	513
35.	514 + 515
36.	532 + 531 + 551
37.	533 + 552
38.	534 + 535
39.	553
40.	554
41.	555

Legend: 135 condition variant of a pavement with
bearing capacity note 1 + pavement un-
evenness note 3 + surface quality note 5

exceeding 2.5 km in the sample selected, that is not exceeding approximately
10.0 km in the whole national highway network were determined. (An example
for the condition variants: 135 means the simultaneous occurrence of bearing
capacity note 1, longitudinal unevenness note 3 and surface quality note 5.)
This relatively rare condition variant was not considered as a separate one
but it was united with a similar (sufficiently frequent) condition variant.
After this calculation, the 41 condition variants presented in Table 1 were
considered in the model.

4.3. Calculation of matrix elements

Each element of the matrix — that is the decimal probability of the
transition of a certain condition variant to another one in one year, in
case of a given pavement type, traffic volume size and intervention strate-
gy — is calculated on the basis of the results gained by the processing of
actual domestic data or, in lack of them, by interpolation.

The available highway network and pavement structural data set was
processed using the following method. First the changings of the condition
variants in 1984 and in 1989 were determined for some 2500 road sections
with various length where no overlay or surface dressing was made during the
investigation period. This processing that was performed taking into consi-
deration the pavement and traffic categories already mentioned, supplied the
distribution of condition variants after 5 years in percentage. (E.g. in the
case of asphalt concrete pavements with an AADT of 3000—8000 pcu/day and
with condition variant 111: 89% remains in the same category, 6% deterio-
rates to the category 112 and 5% to 211 after 5 years.) These percentage
changings were divided by 5 in order to relate them to 1 year. The calcula-
tion was made in each variant if min. 5 km total length was available. These
percentage distributions — after dividing by 100 and rounding off — became
the matrix elements. Where no actual data were available interpolation (or
sometimes extrapolation) was done. In case of surface dressing and asphalt
overlay the condition notes before and after the intervention were compared
in order to obtain information about the typical condition changing.

A row-vector situated under the matrix is connected with it. Every
element of this vector means the unit cost for 1 m^2 at the given interven-
tion type performed on the section that has a condition variant specified
above the appropriate column of the matrix. This unit cost is identic in the
whole country.

4.4. The interpretation of the matrix

Any of the 16 matrices has a size of 41x41. According to the condition variants presented in Table 2, using their numbering, the matrix has the following structure. (Horizontally the condition variants of first year — the basic situation —, while vertically the expected condition distribution of second year can be found.)

E.g. the symbol a_{23} in the matrix means the probability of the transition of a pavement with condition variant 2 to condition variant 3 in the next year (at the pavement type, the traffic volume and the intervention strategy of the matrix in question). If the probability is 20%, the value of a_{23} is 0.20.

The sum of each column is 1.0 because all (100%) of the sections characterized by any condition variant will get into one of the condition variants next year.

Obviously, after only routine maintenance the matrix elements can be found on the diagonal or under it, according to the general deterioration. At the same time, surface dressing especially asphalt overlay pushes the

Table 2. The structure of a Markov transition probability matrix

	1	2	3	4	5	.	.	.	.	.	41
1	a_{11}	a_{21}									
2	a_{12}	a_{22}									
3		a_{23}									
4	a_{14}										
5		a_{25}									
.											
.											
.											
.											
41											$a_{41,41}$
	1	1	1	1	1	.	.	.	.	.	

GÁSPÁR, L. Jr.

	1	2	3	4	5	6	7	8	9	10	11	12	13	14	15	16	17	18	19	20	21	22	23	24	25	26	27	28	29	30	31	32	33	34	35	36	37	38	39	40	41
1	0.60																																								
2		0.55																																							
3		0.10	0.45																																						
4				0.70																																					
5					0.65																																				
6						0.70																																			
7							0.60																																		
8	0.40							0.75																																	
9		0.35							0.60																																
10			0.20							0.55																															
11				0.20								0.80																													
12				0.10									0.10	0.75																											
13			0.35		0.35										0.55																										
14						0.30	0.40							0.80																											
15								0.25								0.50																									
16									0.40		0.10						0.75																								
17									0.45								0.55																								
18																		0.70																							
19												0.25	0.45						0.55																						
20														0.20						0.90																					
21																					0.85																				
22																0.50						0.50																			
23																						0.15	0.35																		
24																	0.45						0.15	0.80																	
25																0.25		0.30							0.80																
26																										0.95															
27																					0.10					0.05	0.90														
28																												0.90													
29																		0.45							0.05			0.10	0.85												
30																					0.15									0.70											
31																															0.75										
32																				0.20												0.80									
33																						0.15	0.50									0.20	0.90								
34																									0.20									0.10	0.90						
35																																			0.10	0.90					
36																								0.15												0.10	0.90				
37																																					0.10	0.65			
38																								0.10															0.90		
39																										0.15														0.90	
40																									0.30													0.35	0.10	0.10	0.85	
41																											0.25													0.15	1.00
Unit cost, HUF/m²	0.0	3.0	6.0	2.0	3.0	8.0	8.0	1.0	3.5	5.0	1.5	3.0	6.0	7.5	2.0	2.5	4.5	2.5	3.5	12.0	9.5	1.5	3.0	6.0	2.5	5.0	12.0	2.5	4.5	8.0	15.0	2.0	3.0	5.5	13.5	2.5	4.0	13.0	6.0	11.5	15.0

Fig. 1. Markov-type transition probability matrix of asphalt concrete pavements with min 8001 pcu/day traffic volume, in the case of routine maintenance only

elements that are different from 0 into the upper part of the matrix as a consequence of the general condition improvement. (Naturally, some elements can be found on the diagonal in this case, too.)

Figure 1 presents, as an example, a matrix used for asphalt concrete pavements.

4.5. Intervention unit costs

The unit costs of various intervention types (only routine maintenance, surface dressing, asphalt overlay) that can be found as row-vectors under the matrices, constitute an important part of the model.

Related to this problem, two questions arise: the actual series value of intervention costs belonging to a given matrix and its 41 starting condition variants, as well as the decision about the use of country-wide unified or regional costs.

For the first question, it is evident that the interventions needed to repair the various condition variants have different prices:

— in the case of routine maintenance activities (it includes potholing, crack filling, fine patching and repair on a large area) it can gradually increase from 0 t/km to 10 t/km,

— in the case of surface dressing a double dressing is considered if the original condition is relatively poor (between about the condition variants 25 and 41).

— the thickness of new overlay increases from the minimum 3 cm up to 10 cm together with the condition deterioration.

The decision about the country-wide unified unit costs was preceded by a detailed preliminary investigation. First the important unit costs (single and double surface dressing, 3 cm asphalt overlay) were collected — by the help of a phone inquiry — in various Highway Directorates with the following results.

(a) Single surface dressing
unit costs: min. 20 HUF/m^2
                    max. 35 HUF/m^2
            mean value: 27 HUF/m^2
            standard
            deviation: 5 HUF/m^2

(b) Double surface dressing
unit costs: min. 34 HUF/m^2
                       max. 60 HUF/m^2
        mean value: 43 HUF/m^2
        standard
        deviation: 8 HUF/m^2

(c) 3 cm new asphalt overlay
unit costs: min. 160 HUF/m^2
                       max. 275 HUF/m^2
        mean value: 202 HUF/m^2
        standard
        deviation: 27 HUF/m^2.

Although the variation coefficient of the unit costs is between 0.13 and 0.18 (that is rather high), the order of the unit costs in various Highway Directorates is not comform at all with the regional geological conditions. No regularity can be observed according to which the regions with some quarries and/or sufficient local aggregates would have the lowest intervention unit costs.

Three main reasons explained our decision about the application of country-wide unified average unit costs:

— the regional unit costs are influenced by several parameters that should not be included in the system,

— the realistic regional unit costs would be disadvantageous in the funds distribution for the Highway Directorates that maintain their network economically,

— the use of several unit costs would complicate considerably the "funds need determination" part of the model.

4.6. Intervention shares on asphalt concrete and asphalt macadam pavements

The shares of interventions (here only surface dressing and asphalt overlay) on both pavement types should also be included into the model as a constraint.

Before deciding about this constraint, the shares of these pavement types in various traffic classes were investigated, with the following results:

	A—C	D—E
	traffic classes	
asphalt concrete pavement	11%	38%
asphalt macadam pavement	33%	—

The percentage values relate to the total area of national highway network.

If a relatively high weighing factor were contributed to asphalt concrete pavements, some important asphalt macadam pavement would get into a disadvantageous situation. A similar result would be obtained if a strong weighing were done as a function of traffic size. Instead, it was decided that the traffic, the pavement type and condition were simultaneously considered at the weighing procedure.

Thus, in the initial phase the total areas of "poor quality" asphalt concrete and asphalt macadam pavements were calculated separately and the shares of them were considered as prescribed shares of interventions. However, it is important to emphasize that the "poor quality" was interpreted differently for asphalt concretes as for asphalt macadams.

In the case of asphalt concrete pavements:

— 0—3000 pcu/day: sections with a condition variant containing at least a note 5,

— 3001—8000 pcu/day: sections with a condition variant containing also a note 5 or 4,

— min. 8001 pcu/day: sections with a condition variant containing also a note 5 or 4

were taken into account in the calculation.

In the case of asphalt macadam pavements:

— 0—3000 pcu/day: sections with a condition variant containing at least a note 5,

— 3001—8000 pcu/day: sections with a condition variant containing at least a note 5,

— min. 8001 pcu/day: sections with a condition variant containing also a note 5 or 4

were taken into account in the calculation.

The shares of these two areas became the prescribed area shares of major condition improving interventions.

5. Application areas

The network-level PMS-model can be used primarily for the solution of three tasks:

— determination of the necessary funds need for ensuring a given condition level, at a certain optimum criteria,

— regional and functional distribution of a certain amount of money, under constraints and a given optimum criteria,

— evaluation of the technical and the economic effect of subsequent funds distribution modification.

6. Determination of necessary funds

6.1. Basic principles

Also the maintenance funds need can be determined by the help of 16 Markov-type transition probability matrices and of the connected intervention unit costs.

Evidently, the actual funds need relates to a desired condition level. In the practice, it means usually one of the following:

— minimisation of the shares of some "good" condition variants and/or

— maximisation of the shares of some "poor" condition variants or

— the former condition distribution is required also in the future,

— various constraints are selected for certain pavement types and traffic alternatives.

In a general case, the shares of various condition variants can be maximised, minimised, fixed or not regulated at all.

6.2. Some trial run experiences

The practical applicability of the mentioned principles was investigated by several trial runs and the evaluation of their results.

In a trial run, the following constraints were assumed as future conditions: the area shares of the sections of condition variants 6, 14, 20, 21, 27—41 (see Table 1) should not decrease after the intervention. The shares of the other condition variants were not limited at all. Because of the relatively few condition constraints the total funds need is only

$2.08 \cdot 10^9$ HUF (610 million HUF for routine maintenance, 646 million HUF for surface dressing and 826 million HUF for asphalt overlay). If the shares of areas undergoing an intervention are considered, the following results can be obtained: new asphalt overlay on 1.2%, surface dressing on 11.0%, routine maintenance (mainly patching) on 87.8%.

Then another trial run was performed when the influence of the increase of constraints on the funds need and the actual shares within the need was investigated. In this case, besides the constraints mentioned before (upper limitation of "poor" condition variants), it was also specified that the area shares of the "good" condition variants — variants 1, 2, 4 and 8 according to Table 1 — should not decrease.

The following areea shares resulted:

111.7 million m^2 (73.0%) routine maintenance

8.2 million m^2 (5.4%) surface dressing

32.8 million m^2 (21.6%) asphalt overlay

Total: 152.7 million m^2

The cost shares resulted:

422 million HUF (2.8%) routine maintenance

264 million HUF (1.7%) surface dressing

14 410 million HUF (95.5%) asphalt overlay

Total: 15 096 million HUF

When evaluating the above results, it is striking that the attempt to preserve the shares of the sections of almost perfect condition needs a rather high extra cost. The former 2000 million HUF increased here by 650%. It is interesting to observe that the share of asphalt overlay considerably grows. In the first version, only 1.2% of the total area needed an overlay, while it grew to 21.6% after the increase of constraints. (This change can be taken as the transformation of the former 90-year strengthening life cycle into one under 5 years according to the new alternative. It should be emphasized, however, here that nowadays an extremely deteriorated general condition prevails and so, if following this strategy, after few years it will not be necessary to intervene on one-fifth of the network.)

7. Funds distribution

7.1. Basic principles

In practice it occurs frequently that certain financial means should be divided for various purposes and regions.

In this case, the minimisation of a value proportional to the vehicle operating costs is considered as object function while the traffic and the pavement type constraints are also taken into account. It is a good question why not the sum of the vehicle operating costs and the intervention costs — that is approximately the national economy expenditures — shall be maximised. At present this aim cannot be attained because we have no information on the actual vehicle operating costs and these absolute data would be needed for accomplishing the summation with the absolute values of intervention costs. As long as only relative values connected with the vehicle operating costs /10/ are used in the lack of more accurate data, only the minimization of one of these parameters can be selected as an object function. For this purpose, the vehicle operating costs, as the more significant one on national economy level, are chosen.

Before the optimisation the calculation already mentioned should be done according to which the shares of necessary interventions on asphalt concrete and asphalt macadam pavements — separately for surface dressings and asphalt overlays are given as a preliminary constraint.

The first step of the distribution of funds is the country-wide distribution of available financial means according to intervention categories, pavement types, condition variants and traffic sizes.

After having done this optimisation from the point of view of traffic operating costs, the regional distribution follows. This time no more weighing is needed, the distribution is made simply according to the area shares of sections with given characteristics (AADT, pavement type, condition variant) in various counties.

The selected object function is the minimisation of following sum:

$$\sum_{i=1}^{41} , A_i \cdot AADT_i^a \cdot H_i, \quad \text{where}$$

A_i — specific vehicle operating cost parameter as a function of i-th condition variant and the relative share of heavy traffic (Fig. 2),

Pavement condition and type					In case of "n"			
					0.10	0.15	0.20	0.25
very good	good	fair	poor	very poor	fuel cost factor			
AB					1.00	1.00	1.00	1.00
AM	AB				1.05	1.04	1.04	1.04
	AM	AB			1.08	1.06	1.06	1.04
		AM	AB		1.21	1.19	1.16	1.14
			AM	AB	1.26	1.24	1.21	1.19
				AM	1.40	1.37	1.35	1.32

Legend: n — the ratio of the heavy (min. 30 kN) axle load vehicles and all vehicles on
        the section
     AB — asphalt concrete
     AM — asphalt macadam

Fig. 2. Extra fuel cost factors of roads with various pavement types and heavy traffic
ratios

$AADT_i^a$ — annual average daily traffic weighed by the road area of i-th
        condition variant (pcu/day),

H_i — total length of sections in i-th condition variant.

This sum of products can be calculated, naturally, also before the
intervention and so, the effect of various condition improving intervention
strategies on the vehicle operating costs can be evaluated. (Increase? De-
crease? To what extent?)

For the use of Fig. 2, the classification of 41 condition variants
into five groups shown in the figure is needed. The three condition note
variations were put into classes as follows:

   — "very good condition": if the sum of three condition notes is
     maximum 6,
   — "good condition": if the sum of three condition notes is between 7
     and 9, and none of them is note 5,
   — "medium condition": if the sum of three condition notes is between
     10 and 12 as well as none of them is note 5,
   — "poor condition": only one of the condition notes is 5,
   — "very poor condition": two or three of the condition notes are 5.

The value "a", the ratio of vehicles with heavy axle loads and all
motor vehicles, is to be calculated by putting into the numerator the sum of
camions, trailers, busses and heavy trucks.

Taking into account the afore-mentioned facts, the product $A_i \cdot AADT_i^a \cdot L_i$ is calculated for each condition-pavement type-traffic variant. These products are summarized for every variant in order to obtain the parameter K_k of the initial condition of the network that is proportional to the vehicle operating costs.

The areas of the various condition-pavement type-traffic variants change after the distribution of the available funds because a slight per-centage of the network receives an overlay, a higher share a surface dressing while only routine maintenance is carried out on the majority of the total area.

For a new condition distribution, naturally, the parameter K_1 pro-portional to the actual vehicle operating costs can be calculated following the same principles. (The first element of the product is unchanged, the second one can be considered constant while the third one, usually, changes. As a consequence, the total sum of products will also be different.)

As a part of this computerised model, the optimal variant with lowest K_1 value /1/ can be determined using linear programming.

The K_1 value of optimal variant can exceed the former K_k value, proving that the available financial means are not sufficient for the pre-servation of the original condition level. While if K_k is below K_k, then, fortunately, a more favourable situation than the former one can be at-tained.

Afterwards the regional (county) funds allocation means only a simple proportioning where the funds shares of various condition-pavement type-traffic variants are divided among the counties according to the shares of the total area of their highway sections with given parameters in the entire national area.

7.2. Experience of some trial runs

Owing to the fact that the value of the funds ($7.0 \cdot 10^9$ HUF) assumed in the first trial run is above the presently realistic level, for the further variants the funds assumed were gradually reduced, that is $6 \cdot 10^9$ HUF, then $5 \cdot 10^9$ HUF, then $4 \cdot 10^9$ HUF and, finally, $3 \cdot 10^9$ HUF were distributed.

Our main direction of investigation was how the actual funds level influences the shares of three intervention types. Figure 3 informs about the changing of the shares used for routine maintenance, surface dressing
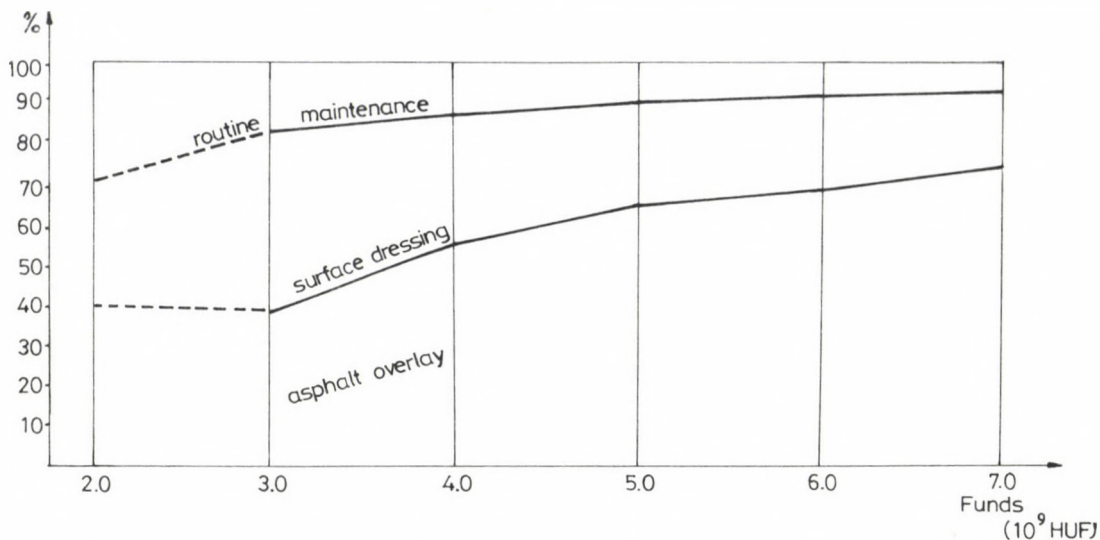
Fig. 3. Relationship between the quantity of funds and the shares of intervention types

and new asphalt overlay in the allocation according to this model as a function of available funds.

The following main results were obtained:

— in case of the allocation of $3.0 \cdot 10^9$ HUF funds only one-third of the financial means was used for asphalt overlays, the highest share is spent for surface dressings,

— increasing of funds, the financial means allocated to asphalt overlay considerably grow while the shares of other two intervention types, evidently, decrease;

— among the areas of various intervention types not so high percentage changes can be observed since the unit costs of routine maintenance and surface dressing gradually decrease accordingly, as — together with the increase of total funds — asphalt overlay is applied on the worst sections that obtained earlier only patching or surface dressing.

Figure 4 analyses how the funds increased by $1.0 \cdot 10^9$ HUF steps influence the vehicle operating costs (or the parameter proportionate to them). There is a definite tendency that the "savings" (reduced fuel costs) are smaller and smaller as the total funds grow. This statement is, naturally, not surprising at all, because the extra funds permit to repair not only the very poor but also the less bad sections. In the latter case, evidently, a lower fuel costs reduction can be attained by the interventions.

Savings in the parameter proportional
to fuel costs as a consequence of addi-
tional 10^9 HUF funds (10^9 HUF)
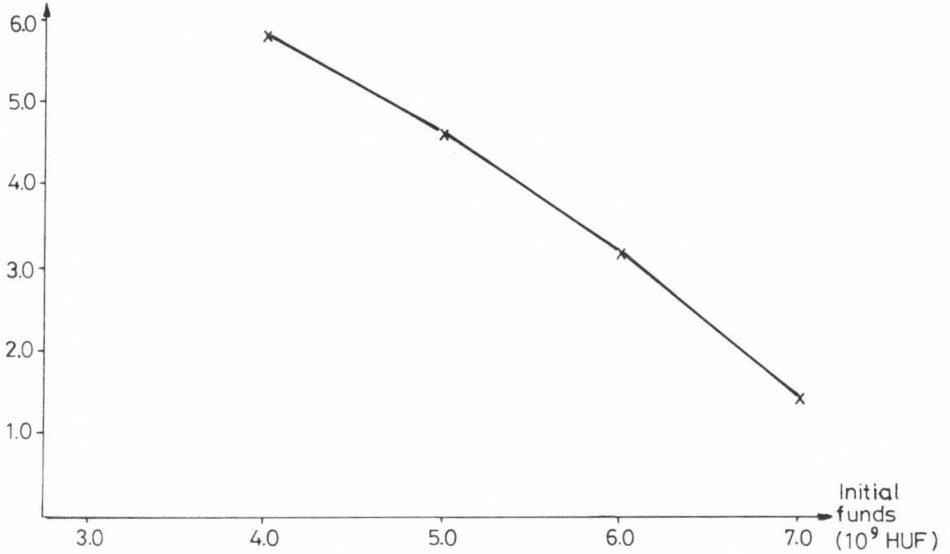
Fig. 4. The savings in the parameter proportional to fuel costs resulting from
additional 10^9 HUF funds, at various initial funds levels

8. Evaluation of the consequences of subsequent modification
in the funds distribution

It was a frequent case (and presumably it will be also in the future)
that not the optimum funds distribution is implemented. (The reasons can be,
among others, the consideration of local aspects, the need of the concentra-
tion of financial means, the necessity of an internal regrouping of money.)
It is a just claim to evaluate the technical and the economic consequences
of such modification.

The technical consequence is the resulting condition distribution of
the network concerned. It can be easily obtained using the appropriate Mar-
kov transition probability matrices and forecasting the conditions in the
following year according to the changed intervention spectrum.

The economic consequence can be evaluated by the calculation of total
vehicle operating costs (or the parameter proportional to them). The deter-
mination of this sum of products, after the changed intervention alter-
native, makes it possible to estimate the losses in national economy costs

caused by the new decisions. (An improvement cannot be attained because the optimum variant was originally developed.)

9. The significance of the model

The significance of the first Hungarian network-level PMS-model can be summarized as follows:

- the determination and the distribution of maintenance-operation funds are carried out here considering several influencing factors,
- at the optimization not only the poor but all condition data of network are taken into account,
- the distribution of funds is done excluding the local subjective parameters,
- as the last step, some other aspects can be applied in the system,
- the system can readily be developed further.

Table 3. Organizational indices in various counties

County	Patching	Surface dressing (cut-back)	Surface dressing (emulsion)	Asphalt concrete type AB-12 (3 cm)
	regional parameters			
Pest	1.00	1.00	1.00	1.00
Nógrád	0.95	0.91	0.97	0.94
Győr-Sopron	0.90	1.03	1.03	0.99
Komárom	0.99	1.03	1.03	0.97
Borsod-Abaúj-Zemplén	0.99	0.91	0.97	1.00
Heves	0.97	0.91	0.92	0.95
Szabolcs-Szatmár-Bereg	0.98	0.97	1.00	0.97
Hajdú-Bihar	0.99	1.00	1.00	0.99
Baranya	0.97	0.91	0.97	0.95
Somogy	1.00	1.06	1.00	1.00
Tolna	0.99	0.97	1.00	0.97
Csongrád	1.00	1.06	1.05	0.99
Bács-Kiskun	0.99	1.03	1.00	0.98
Jász-Nagykun-Szolnok	0.99	1.03	1.00	0.98
Békés	0.99	1.03	1.03	0.99
Vas	0.97	0.91	0.97	0.95
Zala	0.97	0.89	0.95	0.95
Veszprém	0.97	0.91	0.97	0.95
Fejér	0.98	1.00	1.00	0.95

The regional unit costs cannot be directly used partly because of the lack of accurate post-calculating data, partly as a consequence of the necessity for the limitation of the computer model size to ensure its manageability. Since the experts of Highway Directorates have already emphasized repeatedly the advantages of the use of regional unit costs, the following intermediate solution can be suggested. The primary regional distribution of funds should be performed using country-wide unified cost values, then the actual county intervention area shares are determined, by the help of the pricing (organisational) parameters /9/ shown in Table 3. This modification can be carried out by norming preserving, evidently, the sum of the country-wide funds to be distributed.

REFERENCES

1. Bakó, A.: The computer model of the first Hungarian network-level PMS. Közlekedésépítés- és Mélyépítéstudományi Szemle 1992/2 (in Hungarian)

2. Elaboration of Hungarian network-level PMS model. Final report of the KTI-theme no. 0000 86020 9. 1989. (Gáspár, L. Jr., in Hungarian)

3. The Hungarian network-level PMS. Report of the KTI-theme no. 243-008-1-0 March 1990. (Gáspár, L. Jr., in Hungarian)

4. The Hungarian network-level PMS. Report of the KTI-theme no. 243-008-1-0 May 1990. (Gáspár, L. Jr., in Hungarian)

5. The Hungarian network-level PMS. Report of the KTI-theme no. 243-008-1-0 June 1990. (Gáspár, L. Jr., in Hungarian)

6. The Hungarian network-level PMS. Report of the KTI-theme no. 243-008-1-0 July 1990. (Gáspár, L. Jr., in Hungarian)

7. The Hungarian network-level PMS. Report of the KTI-theme no. 243-008-1-0 August 1990. (Gáspár, L. Jr., in Hungarian)

8. Main highway data 1991. Highway Management and Coordination Directorate 1992 (in Hungarian)

9. Investigation of the changing in highway construction and maintenance prices taking into consideration the regional characteristics. Faculty of Construction and Organization Institute, Ybl Miklós Construction Industry Technical College. Theme number SzM-MÉSZI-10/89. (Varga, L., in Hungarian)

10. Takács, F.: A practical method for the analysis of the economical effectiveness of highway investments. KÖZDOK, Budapest 1986. KTI-publication no. 20 (in Hungarian)

11. Investigation of the conditions for the establishment of PMS in Hungary. Report of Transport Sciences Association expert team 1988 (Leader: Gáspár, L. Jr., in Hungarian)

NUMERICAL METHOD FOR THE SOLUTION OF THE DIFFERENTIAL EQUATIONS DESCRIBING THE STABILITY BEHAVIOUR OF VISCOELASTIC STRUCTURES OF ONE DEGREE OF FREEDOM

IJJAS, GY.[*]

As follows from the nature of the phenomenon, the determination of the behaviour of viscoelastic structures in the environment of the loss of stability involves numerical problems such as the multivaluedness of the solution, the infinity of the derivative and case of the internal parameter, the singularity of the solution. Numerical methods to eliminate these problems are presented in this paper.

Introduction

The stability problems of viscoelastic structures can be divided into two major groups.

One of them includes the cases where the inertia of the structure is taken into consideration. The other includes the cases where the inertia of the mass of the structure is neglected.

The cases falling within the first group are hardly discussed in the literature and the present work is not intended either to discuss the cases where the inertia of the structure is taken into consideration. However, presentation of a simple structure of inertial mass seems to be still reasonable to make the investigation neglecting the inertia of the mass more understandable.

A three-hinged structure consisting of two rods made of Maxwellian fluid with the mass of the structure concentrated at the upper hinge is illustrated in Fig. 1. In Fig. 2 a continuous line shows the vertical dis-

---

[*]Ijjas, György, H-1147 Budapest, Öv u. 165, Hungary

Fig. 1

Fig. 2
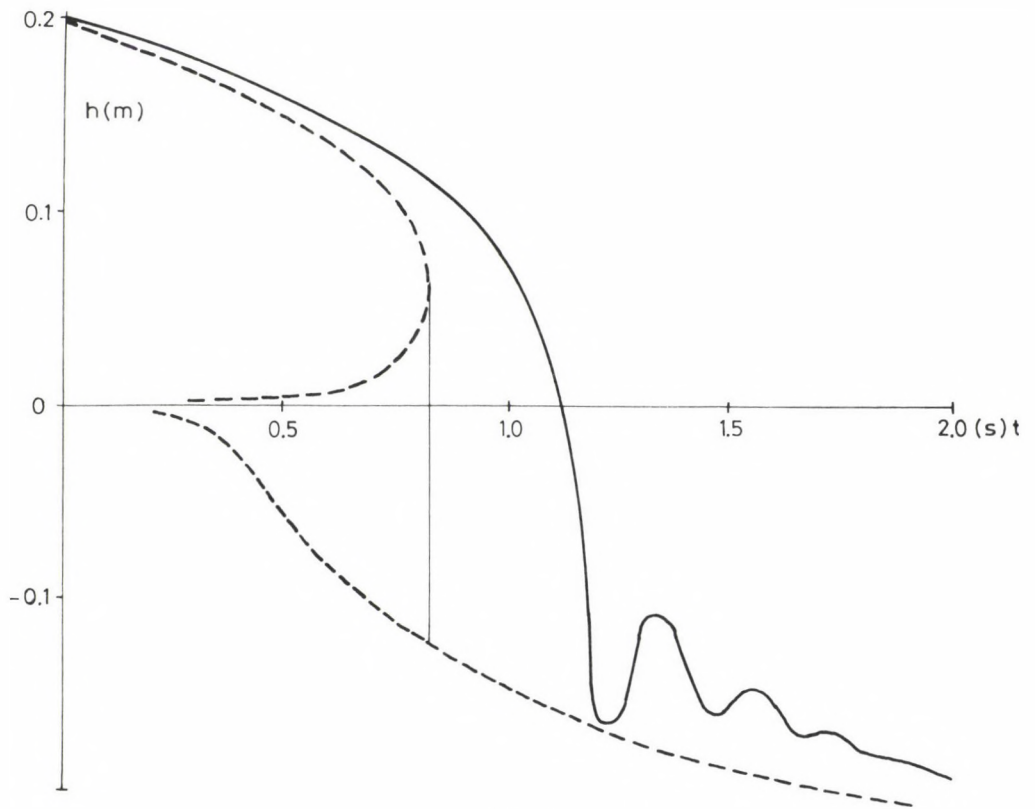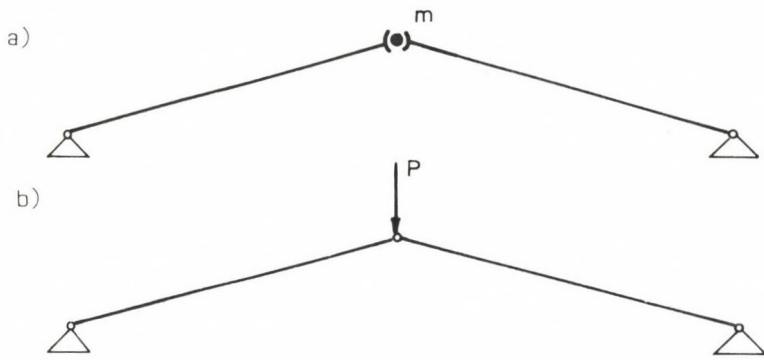
placement of the upper point of the structure as a function of time. As far as is known today, no distinctions can be made between the stable and unstable states of motion of the structure, unless the inertia of the mass of the structure is neglected.

However, if the inertia of the mass of the structure is neglected, then a viscoelastic structure will loose its stability, by the definition, when the first time derivative of the co-ordinates of motion of the structure tends towards infinite. It was discovered by Hult (1962). The connection of this definition and the potential energy has been discovered /Ijjas (1982)/. In this case the structure shown in Fig. 1a can be replaced by the structure shown in Fig. 1b. However, the curve describing the behaviour of the structure splits into two parts (shown by the broken lines in Fig. 2). The curve in the upper part of the figure "bends back" as a function of time, the point associated with the vertical tangent being the displacement point corresponding to the critical time (where the structure looses its stability). The broken line in the lower part of the figure describes the behaviour of the structure after snapdown. The section of the upper curve before critical time and the section of the lower curve after critical time can only be interpreted physically. The vertical straight line between the two curve sections, which is the tangent of the upper curve was constructed.

It follows from the previous part that problems would obviously developed in the process of solution of the differential equations describing the behaviour of the viscoelastic structures in the environment of the loss of stability if the inertia of the mass of the structures was neglected. Namely, a method using derivatives in the course of solution cannot be used to solve differential equation if the derivatives getting to be infinite. This paper is intended to present an algorithm by means of which this numerical problem can be avoided.

To simplify the problem, the differential equation describing the behaviour of the investigated structure can be solved in a closed form. The behaviour of the structure shown in Fig. 1b has also been investigated by Huang (1967) and Szalai (1989).

Description of the behaviour of Mises' viscoelastic structure

The equation describing the behaviour of the structure shown in Fig. 1b will be derived in detail for clear understanding. The strain of one of the rods as a function of the rise of the structure is:

$$\Delta = s - s_0 = \frac{L}{2}\left[\left(\frac{h^2}{L}\right)^2 - \left(\frac{h_0}{L}\right)^2\right], \tag{1}$$

provided that $h_0 < L$. Namely, in this case the following approximations can be assumed:

$$s = \sqrt{L^2 + h^2} \approx L\left[1 + \frac{1}{2}\left(\frac{h}{L}\right)^2\right]; \tag{2}$$

$$s_0 = \sqrt{L^2 + h_0^2} \approx L\left[1 + \frac{1}{2}\left(\frac{h_0}{L}\right)^2\right]. \tag{3}$$

Based on the above approximations, the force acting in a rod is

$$F = -\frac{PL}{2h}. \tag{4}$$

In equations (1)—(4), h is the rise of the structure that is the function of time. If the rods are made of Maxwellian fluid, their constitutive equation will be:

$$kb\,\dot{\Delta} = kF + b\dot{F}, \tag{5}$$

where k is the coefficient of the spring and b is the viscosity coefficient of the dashpot. (The dot is the symbol of derivation with respect to time.)

Taking into account equations (1) and (4), the derivatives with respect to time of the compressive strain and compressive force working in the rod (P = constant!) are

$$\Delta = \frac{h}{L}\,\dot{h}; \tag{6}$$

and

$$\dot{F} = \frac{PL}{2h^2}\,\dot{h}, \tag{7}$$

respectively.

If equations (4), (6) and (7) are substituted into equation (5), the following relationship will be obtained after suitable arrangement:

$$\dot{h} = \frac{1}{\dfrac{b}{k}\left[\dfrac{1}{h} - \dfrac{2kh^2}{PL^2}\right]}. \tag{8}$$

This is a differential equation with separable variables, and can be integrated in closed form.

Taking into account that after elastic deformation the height of the middle of the structure is $h = h_0$ at time $t_0 = 0$, the result of the integration will be:

$$\frac{b}{k} \left[\ln \left| \frac{h}{h_0} \right| - \frac{2}{3} \left[h^3 - h_0^3 \right] \right] = t. \tag{9}$$

The value of h_0, that is the height of the middle of the structure after the elastic ("creepless") deformation just after the application of the load, is obtained from the following equation:

$$h_0^3 - h_{og}^2 h_0 + \frac{PL^2}{k} = 0 \tag{10}$$

where h_{og} is the height of the middle of the structure before the application of the load.

The h—t relation that can be obtained from equation (9) has been plotted in Fig. 3, but its parameters are different from those in Fig. 2.

The parameters of the function can be seen in the figure. If a numerical method including derivatives was used to solve the differential equation describing the behaviour of the structure, this process would certainly fail near the point where the structure looses its stability. Therefore, use of the process describing below is recommended.

An algorithm, preferably a fourth-order Runge—Kutta method shall be used to start with the solution of the differential equation. (For description of the Runge—Kutta method see any textbook dealing with numerical methods, e.g. the book of Stiefel (1970).) Practically, we have to begin by trial and error to presume the length of the intervals of the independent variable. Those are the first steps of the Runge—Kutta method, unless some preliminary estimate of the loss of stability is available. Checking procedures have been built into the process of solution. Thus we investigated the ratio of the values of the solution belonging to the subsequent intervals, and the length of the steps of the solution was corrected accordingly. The variation of the derivative was investigated too. This protection served on the one hand to control the running of the program and, on the other hand, to get the best approximation of the critical time. Then the solution was developed into Taylor series, using the arc length as the independent

$$h_{og} = 0.2 \, m$$

$$h_0 = 0.191078608 \, m$$

$$\frac{2k}{3PL^2} = 1000 \frac{1}{m^3}$$

$$\frac{b}{k} = 0.1 \, s$$

$$L = 5.0 \, m$$
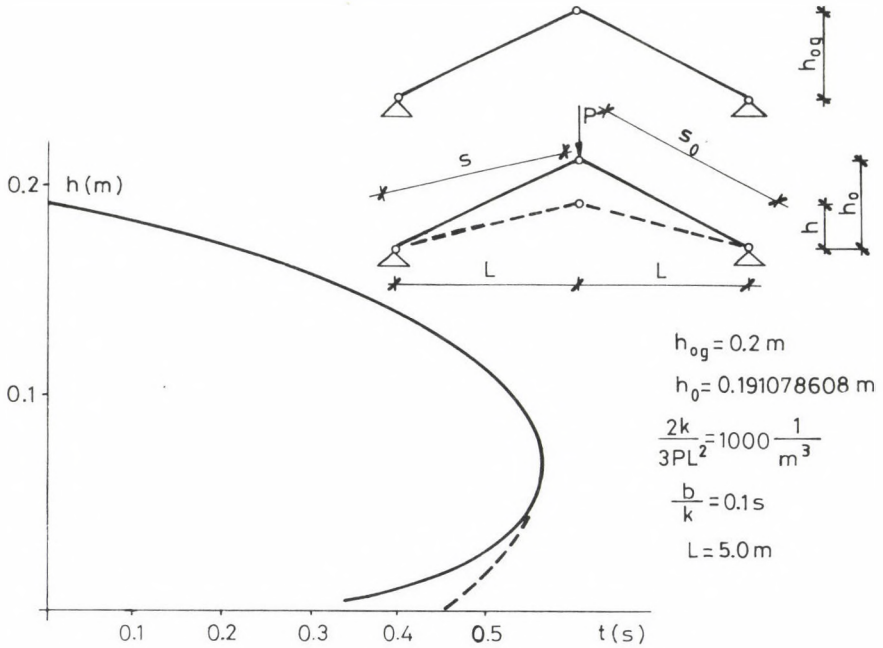
Fig. 3

variable. This was a very useful method, because in this case, no calcula-
tion of the mixed derivatives is necessary even in case of more variables
/Bronstein and Semendiaev (1987)/.

The arc length, on which the Taylor series was developed, was chosen
so that the ratio of the independent co-ordinates (the time) of the first
and last basic point was within 2%.

A numerical derivation formula was used to generate the coefficient of
the Taylor series.

The numerical derivatives can be determined only on the basis of non-
equidistant points in this case. Although the derivation of the appropriate
formulae is theoretically not difficult, it is a time-consuming job. For-
mulae of derivatives based on equidistant points are available in the li-
terature and these were employed to check the derivation. Although formulae
for numerical derivatives based on six equidistant points is found in the
literature /Bickley (1941)/, its accuracy is better only in the case of the
first and third derivative as compared with the numerical derivation for-
mulae based on five equidistant points. These formulae would deprive us of a
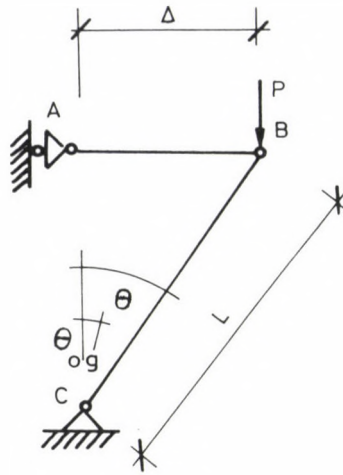
Fig. 4

solution of closed form serving for the determination of the critical time too.

Namely, a closed form solution can be obtained for the determination of the extreme value of the arch length-time (that is the critical time). In this case the critical time is the root of the cubic equation that has to be found.

This process has been applied to investigate not only the structure presented above but in case of some similar structures discussed elsewhere /Ijjas (1991)/. The analytical solution describing the behaviour of these structures is known too.

The structure investigated is illustrated schematically in Fig. 4. The structure consists of two parts. The rod denoted by AB, was made of Max-wellian-fluid in one case while being a Dischinger model in the other case. Both models consist of a linear spring and a dashpot connected in series. In case of the Maxwellian fluid, the dashpot is a Newtonian fluid, while in case of the Dischinger model it was an ageing material. The rod denoted by BC was infinitely rigid in both cases.

In case of Maxwellian-fluid, the analytical solution describing the behaviour of the structure /Ijjas (1991)/ is:

$$\frac{b}{k} \left[\frac{kL}{P} \left(\cos \theta - \ln \tan \frac{\theta}{2} \right) - \ln \tan \theta \right]_{\theta_o}^{\theta} = t, \tag{11}$$

where b and k are material constants, t is the time while the meaning of P and L can be understood from the figure.

In case of Dischinger model, the equation describing the behaviour of the structure is

$$-\frac{1}{\lambda} \ln \left\{1 - \frac{1}{\phi_{max}} \left[\left(\frac{kL}{P} \cos \theta + \ln \tan \frac{\theta}{2} \right) - \ln \tan \theta \right] \right\}\Big|_{\theta_0}^{\theta} = t, \qquad (12)$$

where λ and ϕ_{max} are additional material constants.

Our experience gained in the course of the investigations is summed up below.

The accuracy of the critical time obtained by means of the numerical method described above lay within 2% in every case, certainly because the Taylor series was started "near" the critical time. However, a practical criterion cannot be specified for this "nearness". In can only be recommended to work by trial and error.

The investigations showed too that the deformation that belonged to the critical time and was given as a function of the arc length deviated from the correct value by a large amount using this method. In some cases the accuracy lay within 1% but e.g. in case of Mieses' structure discussed earlier, the expansion resulted in a difference of almost 50% in the value of the height of the middle of the structure that belonged to the critical time as compared with the analytical value.

E.g. the analytical solution for the structure presented at the beginning of this work resulted in a value of 0.562942548 s for the critical time and in a value of 0.069336127 m for the height of the structure while in case of Taylor series, the value of the critical time lay at 0.570701265 s (within 2%) and the value of the height of the structure associated with the critical time 0.047418857 m (a difference of approximately 50%). The considerable deviation can be attributed to the fact that at the time of the loss of stability, the first derivative with respect to time is infinite.

So we start the Runge—Kutta process in the knowledge of critical time again. That process was stopped near the critical time where the accuracy of nearness was determined in advance. The values of deformation so obtained was accepted as the values of deformation that belongs to the critical time. In every case, the solutions so obtained lay always near the values obtained for the deformation that belongs to the critical time in the analytical solution, the deviation lying within 5%.

In case of the structure presented at the beginning of this paper, a value of 0.072579485 m was obtained in this way for the height of the middle of the structure that belongs to the critical time. The difference as compared with the analytical value lying within 5%.

Generalization of the process for the multivariable case

If the behaviour of the structure is described by a differential equation system, each of the different independent variables will describe the motion of a point of the system of finite degree of freedom. Obviously, the displacement-time relationships giving the behaviour of every single point can be handled independently and the Taylor expansion as a function of the arc length can be developed for each relationship of this type independently whereas the critical time can be estimated in a way similar to that described above. Namely, in case of expansion according to the arc length, the Taylor series contains no mixed derivatives.

Otherwise, in case of one independent variable, the solution can be carried out directly by means of the Runge--Kutta method or some other method after changing the variables that is, no use of the Taylor series is necessary. In the example presented, we used the Taylor series only because of generalization at a later date.

Determination of the change in the internal parameter

The deformation characteristics of viscoelastic structures consist of two components such as elastic (instantaneous) deformation and viscous (slow) deformation. Structures consisting of springs and dashpots have been used to model the viscoelastic materials, where the springs simulated the elastic component while the dashpots the viscous component.

In the course of the investigation of viscoelastic structures, e.g. if we want to determine the potential energy of the structure, determination of the change in the internal parameter(s) as a function of time may be necessary. In our example, the movement of the dashpot can be determined in the following way:

On the basis of Biot's work /Biot (1955)/, the "quasi" equilibrium equation of the structure shown in Fig. 1 is

$$- \frac{PL}{2h} - k \left(\Delta - \Delta_d \right) = 0, \tag{13}$$

where Δ_d is the parameter describing the movement of the dashpot of the Maxwellian model. The differential equation giving the relationship between the total deformation belonging to equation (13) and the movement of the dashpot is

$$b \frac{d\Delta_d}{dt} = k \left(\Delta - \Delta_d \right). \tag{14}$$

The Δ_d can be expressed from equation (14) while Δ can be given as a function of h (see equation (1)). Thus, the following equation is obtained for Δ_d as a function of h:

$$\Delta_d = \frac{1}{2} \left[\frac{PL}{kh} + \frac{h^2 - h_{og}^2}{L} \right]. \tag{15}$$

Since the relationship between h and t is known (see formula (9)), the relationship between Δ_d and t becomes known too as was illustrated in Fig. 5. There is an interval of t where two values of dependent variables belong to one independent variable as seen in the Figure. The function is singular at the time of the loss of stability (denoted by C in the figure).

However, the method outlined above, suited to provide useful information about the change in internal parameter Δ_d as a function of time, can be used only if the number of the external and internal parameters is identical. Namely, in this case, there exists a unique solution of the system of equations similar to equation (13), as a function of Δ or of the appropriate external parameters. If it is needed to produce this function as a solution of equation (14), it is quite obvious what kind of numerical problems should be solved.

Since we have proved /Ijjas (1991)/ that $d \Delta_d/dh = 0$ holds at the instant of the loss of stability, the following process can be recommended. Let both sides of equation (14) be multiplied by dt/dh. Thus h will be the independent variable of this equation. Differential quotient dt/dh can be determined from equation (8), while Δ_d can be obtained as a function of h by means of the usual numerical methods.

Accordingly, taking equation (1) or (8) into consideration, equation (14) can be written as
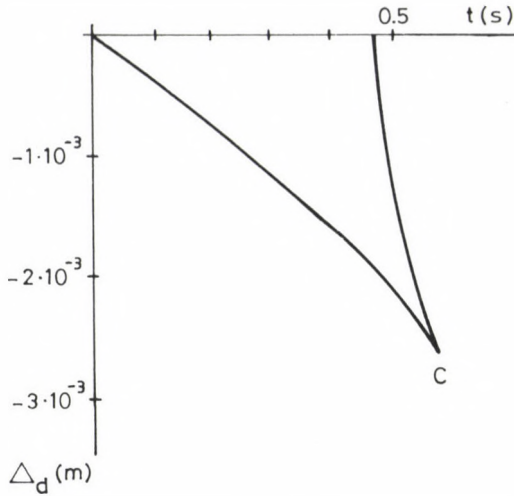
Fig. 5

$$\frac{d\Delta_d}{dh} = \left[\frac{1}{h} - \frac{2kh^2}{PL^2}\right]\left[\frac{h^2 - h_{og}^2}{2L} - \Delta_d\right]. \tag{16}$$

The differential equation so obtained can be solved without any difficulty
and the relationship between Δ_d and t can be determined by means of the cal-
culated values if necessary. In Fig. 6, the solution of equation (14), that
belongs to the initial values h = 0.191078609 and Δ_d = 0, is illustrated. If
it is needed to determine the relationship between Δ_d and t, the change of
the height of the middle of the structure (h) as a function of time (t) can
be obtained from the solution of equation (8) while the relationship between
Δ_d and h can be obtained from the solution of equation (16). If these re-
lationships are known, the relationship between t and Δ_d, can be given
which is of course identical with that presented in Fig. 3, obtained by
means of equations (16) and (9).

Generalization of the process

For the purpose of generalization, let the equation describing the be-
haviour of the viscoelastic structure /Biot (1955)/ be written as:
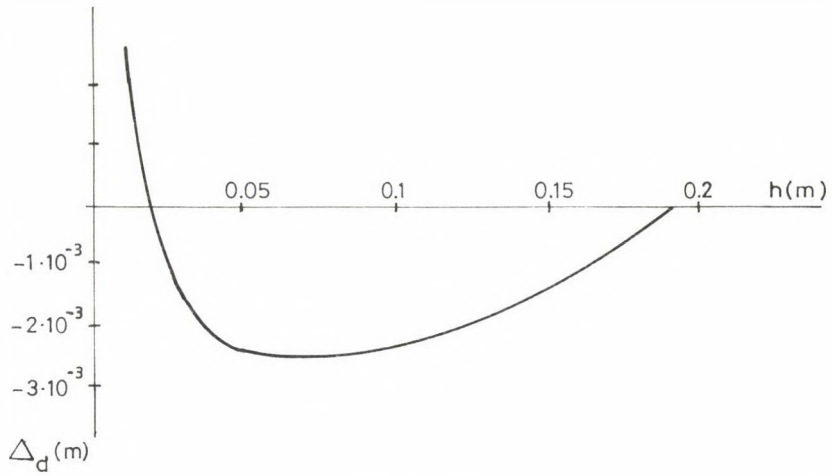
Fig. 6

$$\frac{\partial V}{\partial qi} + \frac{\partial D}{\partial \dot{q}_i} = 0. \tag{17}$$

where V — is the potential energy of the loaded structure,

D — is the dissipation function,

q_i — is the parameter describing the behaviour of the system.

The quadratic form D is a function of the time derivatives of the internal parameters. Since a quadratic form can be transformed into a sum of squares by suitable co-ordinate transformation, the system of equations (17) can be written so that the time derivative of only one internal parameter appears in one equation. In this case, any equation containing the time derivative of the internal parameter can be multiplied by the reciprocal of the time derivative of the appropriate external parameter. Now the internal parameters appears in the differential equation(s) as the derivative with respect to the appropriate external parameter. Differential expressions like e.g. the right side of equation (8) can be written in place of the reciprocals of the derivatives of the external parameters appearing in the equation(s) elsewhere because of the multiplication. That means that the different derivatives with respect to time are expressed from the linear differential equations describing the change in the external parameters and substituted into the equation(s) in the way described above. In this way, a

differential equation system corresponding to equation (16), depending on the internal parameters exclusively, is obtained.

Summary

As follows from the nature of the phenomenon, numerical problems arise in the way of solving the differential equation describing the behaviour of viscoelastic structures in the environment of the loss of stability. Such problems are the multivaluedness of the solution, the infinity of the derivative and, in case of internal parameters, the singularity of the solution. In this paper, methods to eliminate these problems are recommended. Expansion according to the arc length has been used to eliminate the multivaluedness of the solution in the environment of the loss of stability in the course of determination of the relation determining the displacement of the structure. Also, a process to improve the accuracy has been recommended because, dissimilarly to the acceptable accuracy of the critical time obtained by means of the process, the deviation of the value of the deformation that belongs to the critical time is considerable compared with the exact value.

The singularity of the relation describing the internal parameter as a function of time can be eliminated by determining first the internal parameter as a function of the appropriate displacement (external parameter) of the structure. If the relationship between the internal and external parameter is known then the relationship between the internal parameter and the time can be easily determined according to the method presented earlier. The problem of singularity is avoided using that indirect way of solution.

APPENDIX

The following formulae can be used to determine the derivatives of a function, based on five non-equidistant points:

$$\frac{dt}{ds} = \frac{A_1}{N_1} t_1 + \frac{B_1}{N_2} t_2 + \frac{C_1}{N_3} t_3 + \frac{D_1}{N_4} t_4 + \frac{E_1}{N_5} t_5; \tag{A.1}$$

$$\frac{d^2t}{ds^2} = \frac{A_2}{N_1} t_1 + \frac{B_2}{N_2} t_2 + \frac{C_2}{N_3} t_3 + \frac{D_2}{N_4} t_4 + \frac{E_2}{N_5} t_5; \tag{A.2}$$

$$\frac{d^3t}{ds^3} = \frac{A_3}{N_1} t_1 + \frac{B_3}{N_2} t_2 + \frac{C_3}{N_3} t_3 + \frac{D_3}{N_4} t_4 + \frac{E_3}{N_5} t_5; \tag{A.3}$$

$$\frac{d^4t}{ds^4} = \frac{A_4}{N_1} t_1 + \frac{B_4}{N_2} t_2 + \frac{C_4}{N_3} t_3 + \frac{D_4}{N_4} t_4 + \frac{E_4}{N_5} t_5; \tag{A.4}$$

$$N_1 = (s_0 - s_1)(s_0 - s_2)(s_0 - s_3)(s_0 - s_4); \tag{A.5}$$

$$N_2 = (s_1 - s_0)(s_1 - s_2)(s_1 - s_3)(s_1 - s_4); \tag{A.6}$$

$$N_3 = (s_2 - s_0)(s_2 - s_1)(s_2 - s_3)(s_2 - s_4); \tag{A.7}$$

$$N_4 = (s_3 - s_0)(s_3 - s_1)(s_3 - s_2)(s_3 - s_4); \tag{A.8}$$

$$N_5 = (s_4 - s_0)(s_4 - s_1)(s_4 - s_2)(s_4 - s_3); \tag{A.9}$$

$$A_1 = (s_2 - s_1)(s_2 - s_3)(s_2 - s_4); \tag{A.10}$$

$$B_1 = (s_2 - s_0)(s_2 - s_3)(s_2 - s_4); \tag{A.11}$$

$$\begin{aligned}
C_1 = &(s_2 - s_1)(s_2 - s_3)(s_2 - s_4) + \\
&(s_2 - s_0)(s_2 - s_3)(s_2 - s_4) + \\
&(s_2 - s_0)(s_2 - s_1)(s_2 - s_4) + \\
&(s_2 - s_0)(s_2 - s_1)(s_2 - s_3);
\end{aligned} \tag{A.12}$$

$$D_1 = (s_2 - s_0)(s_2 - s_1)(s_2 - s_4); \tag{A.13}$$

$$E_1 = (s_2 - s_0)(s_2 - s_1)(s_2 - s_3); \tag{A.14}$$

$$\begin{aligned}
A_2 = 2/&(s_2 - s_1)(s_2 - s_3) + (s_2 - s_1)(s_2 - s_4) + \\
&(s_2 - s_3)(s_2 - s_4)/;
\end{aligned} \tag{A.15}$$

$$B_2 = 2/(s_2 - s_3)(s_2 - s_4) + (s_2 - s_0)(s_2 - s_4) +$$
$$(s_2 - s_0)(s_2 - s_3)/; \tag{A.16}$$

$$C_2 = 2/(s_2 - s_0)(s_2 - s_1) + (s_2 - s_0)(s_2 - s_3) +$$
$$(s_2 - s_0)(s_2 - s_4) + (s_2 - s_1)(s_2 - s_3) +$$
$$(s_2 - s_1)(s_2 - s_4) + (s_2 - s_3)(s_2 - s_4)/; \tag{A.17}$$

$$D_2 = 2/(s_2 - s_0)(s_2 - s_1) + (s_2 - s_0)(s_2 - s_4) +$$
$$(s_2 - s_1)(s_2 - s_4)/; \tag{A.18}$$

$$E_2 = 2/(s_2 - s_0)(s_2 - s_1) + (s_2 - s_0)(s_2 - s_3) +$$
$$(s_2 - s_1)(s_2 - s_3)/; \tag{A.19}$$

$$A_3 = 6/(s_2 - s_1) + (s_2 - s_3) + (s_2 - s_4)/; \tag{A.20}$$

$$B_3 = 6/(s_2 - s_0) + (s_2 - s_3) + (s_2 - s_4)/; \tag{A.21}$$

$$C_3 = 6/(s_2 - s_0) + (s_2 - s_1) + (s_2 - s_4) + (s_2 - s_3)/; \tag{A.22}$$

$$D_3 = 6/(s_2 - s_0) + (s_2 - s_1) + (s_2 - s_4)/; \tag{A.23}$$

$$E_3 = 6/(s_2 - s_0) + (s_2 - s_1) + (s_2 - s_3)/; \tag{A.24}$$

$$A_4 = B_4 = C_4 = D_4 = E_4 = 24. \tag{A.25}$$

The above formulae can be produced by derivation of the Lagrangian interpolation polynomial /Stiefel (1970)/. To determine the derivatives based on non-equidistant points, an algorithm can be worked out on the basis of Holnapy's method /Holnapy (1974)/ as well. The formulae for the time derivatives according to arc length can be applied accordingly to the derivatives of other variables according to arc length.

REFERENCES

Bickley, W. G. (1941): Formulae for numerical differentiation. Mat. Gaz. 25, 19—27

Biot, M. A. (1955): Variational principles in irreversible thermodynamics with application to viscoelasticity. Physical Review, Vol. 97. No. 6 (March 15), 1463—1469

Bronstein, J. N. - Semendiaiev, K. A. (1987): Handbook of mathematics (in Hungarian). Műszaki Könyvkiadó, 520—521

Hoff, N. J. (1956): Creep buckling. The Aeronautical Quarterly, Vol. 7. 1—20

Holnapy, D. (1974): Numerical algorithm for determination of the differential operators of boundary value problems (in Hungarian). Műszaki Tudomány No. 48, 357—367

Huang, N. C. (1966): Numerical creep buckling of some simple structures. IRPA Report, 66—80

Huang, N. C. (1967): Nonlinear creep buckling of some simple structures. J. of Applied Mechanics, Trans. ASME, 651—

Hult, J. (1962): Oil canning problems in creep (published in "Creep in structures", ed. by Hoff). Springer Verlag, 161—173

Ijjas, Gy. (1991): Loss of stability of structures of viscoelastic material (published in "Special Problems of the Theory of Stability in Engineering", ed. by Kollár, in Hungarian). Akadémiai Kiadó, Budapest

Stiefel, E. (1970): Einführung in die numerische Mathematik. Verlag B.G. Teubner, Stuttgart

Szalai, L. (1989): Creep resistance of a bouncing three-hinged rod structure (in Hungarian). Architectural Research & Development, Vol. 22. No. 3, 160—167

ON THE USE OF A RANKINE HALF BODY SHAPE AS A SHARP CRESTED LINEAR WEIR OR RANKINE WEIR

KESHAVA MURTHY, K.[*] – RAMAKRISHNA RAO, A.[*]

In this paper, it is shown that if the two-dimensional Rankine half body of focal length μ (distance between the line source and the stagnation point) obtained by superposing a uniform flow over a line source, is kept in a rectangular channel of width equal to the maximum width of the half body ($2\Pi\mu$ at infinity), the rate of flow in the intervening space acting as a sharp crested notch is very nearly a linear function of the head above the channel bed, for flows above a minimum base height and is valid for a short distance of 5μ above the bed. The range of linear relationship between discharge and the head can be considerably improved by increasing the width of the channel (equal to increasing the width of the weir uniformly throughout) by 0.4μ (for symmetrical weirs), so that for all flows above a depth of 2μ above the crest, the discharge is proportional to the head measured above a reference plane or datum, situated at 0.47μ above the crest, in the range $2 \leq h/\mu \leq 40$ within a maximum error of $\pm 0.5\%$. The significant feature of the weir is that it is not a compound weir, and the entire weir is defined by one equation (unlike Sutro and other linear weirs) a portion of it above the crest acting as its own base. Experiments with 3 weirs having $2\Pi\mu = 10, 30, 40$ cm /base width of the weir = $(2\Pi\mu + 0.4\mu)$/confirms the theory by giving a constant average coefficient of discharge of 0.61, 0.64 and 0.66 respectively for the 3 weirs.

1. Introduction

The study of proportional weirs or notches (used synonymously) is not only of interest in the study of fundamental hydraulics, but also because of its relevance to several engineering problems. The recent interest in proportional weirs is stimulated by the concept of reference plane or datum in the design of weirs /6/. It has been well established that weirs which pass a discharge $Q \propto H^n$, where H = head causing flow, for $n < 3/2$, can be designed only with bases /8/. They are classified under 'Compensating weirs'.

---

[*]Keshava Murthy, K. and Ramakrishna Rao, A., Dep. of Civil Engineering Indian Institute of Science, Bangalore 560 012, INDIA

The linear proportional weirs for which n = 1 is one such case. The earliest attempt to this problem was made by Stout /15/ and later modified by Sutro /3, 2/. Recent works on linear proportional weirs include those of Keshava Murthy and Pillai /8/, Rao and Bhukari /11/, Sreenivasulu and Raghavendran /14/, Fonck /5/. The linear proportional weirs are of considerable applications in several fields. As simple discharge measuring devices in Hydraulic Engineering and irrigation; as dosing devices in Chemical Engineering; as outlet weirs in grit chambers (sedimentation tanks) to maintain constant average velocity irrespective of flow fluctuations in discharge /1, 9, 4/. The several designs and their applications have been highlighted and discussed in earlier publications. However, in all the previous solutions, the weir consisted of a base over which a designed complimentary weir is fitted, the two being defined by different equations. In this paper, we discuss a novel weir using the Rankine half body, the significant feature of which is that the entire weir is defined by one single equation, a portion of the weir above the crest acting as the base. This accidentally serves as an example of a self basing weir /10/. The rate of flow in this weir for flows above a depth, is proportional to the head measured above a reference plane, within an allowable error of ± 0.5%. We treat this problem as a theoretical problem in hydraulics, leaving aside the detailed experimental work required for standardization and subsequent field use to another study. The experiments conducted have the limited objective of just checking the theory.

2. Rankine half body — quadratix of Hippias

A uniform flow defined by w = UZ superposed on a line source defined by w = mlnZ results in the flow, whose velocity potential is given by /13/.

$$\phi = UR\cos\theta + m\ln R. \tag{1}$$

The streamline ψ = 0 is given by

$$R = \frac{m}{u} \frac{\theta}{\sin\theta} = \frac{\mu\theta}{\sin\theta} \text{ (say)}$$

or

$$y = \mu\theta. \tag{2}$$
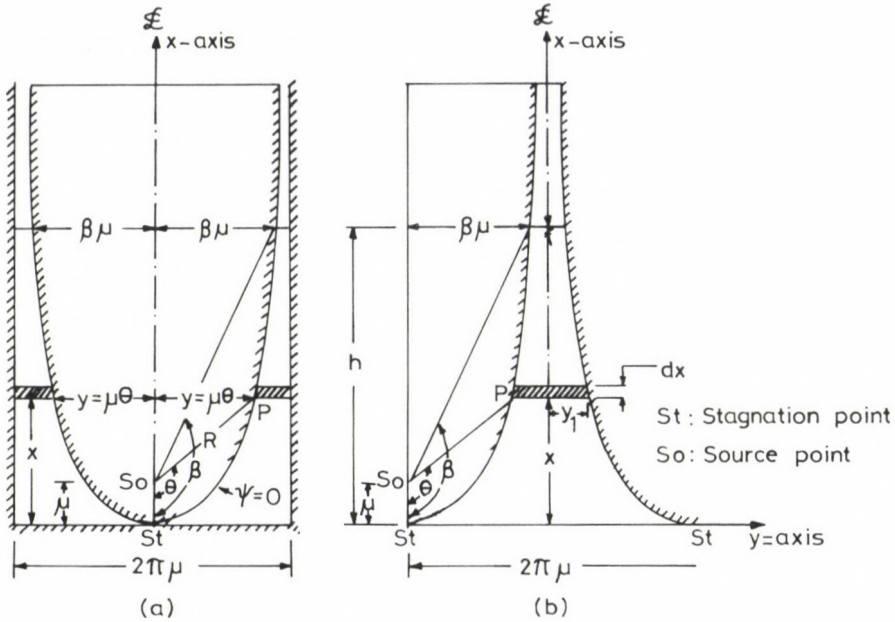
Fig. 1. Rankine half body weir

The vertical distance, y, of any point, P, on this curve, from the x-axis is proportional to the angle, θ, made by the radial line through the source and the point P with the x-axis. This curve is well known in analytical geometry as the 'Quadratrix of the Hippias' /12/, known commonly to Engineers as the Rankine half body. The curve is shown in Fig. 1 and the co-ordinates (x, y) of the points on the curve are given in Table 1 (columns 2 and 3). The distance between the stagnation point and the source, called the focal length is μ. The thickness of the body at the point of source is $\pi\mu$ and the maximum thickness (at ∞) is twice this thickness. The curve is easily drawn by the Rankine's graphical method /13/.

3. Modified Rankine half body weir — discharge equation

If the Rankine half body of focal length μ is placed in a channel of width equal to the maximum width of the half body = $2\pi\mu$ (Fig. 1a), we get a weir shape as shown in Fig. 1b. The co-ordinates of the point on the weir are given in Table 1 (columns 2 and 4). The discharge through this weir is equal to

$$q = 2C_d \sqrt{2g} \int_0^h \sqrt{h-x} \; (\Pi\mu-y) \; dx \qquad (3)$$

where y is defined by Eq. (2), C_d is the coefficient of discharge (approximately equal to 0.6) assumed to be constant which is valid for sharp crested weirs and streamlined flows. Equation (3) can be written as

$$q = 2C_d \sqrt{2g} \int_0^h \sqrt{h-x} \; (\Pi\mu)dx - 2C_d \sqrt{2g} \int_0^h \sqrt{h-x} \; y \; dx = I_1 - I_2, \qquad (4)$$

where

$$I_1 = K \int_0^h \sqrt{h-x}(\Pi\mu) \; dx \qquad (4a)$$

$$I_2 = K \int_0^h \sqrt{h-x} \; ydx \qquad (4b)$$

and

$$K_8 = 2C_d \sqrt{2g}.$$

It can be easily evaluated (as for a rectangular weir) and is found to be

$$I_1 = \frac{4}{3} C_d \sqrt{2g} \left(\frac{h}{\mu}\right)^{3/2} \Pi\mu^{5/2} = \frac{2}{3} K \; (h/\mu)^{3/2} \; \Pi\mu^{5/2}. \qquad (5)$$

As $y = \mu\theta$, $x = \mu(1 - \frac{\theta}{\tan\theta})$ and $dy = \mu d\theta$, substituting in Eq. (4b),

$$I_2 = \frac{2}{3} K \int_0^\beta \left(\frac{\theta}{\tan\theta} - \frac{\beta}{\tan}\right)^{3/2} \mu^{5/2} \; d\theta. \qquad (6)$$

Hence

$$q = I_1 - I_2 = K_1 \mu^{5/2} \left[\left(1 - \frac{\beta}{\tan}\right)^{3/2} \Pi - \int_0^\beta \left(\frac{\theta}{\tan\theta} - \frac{\beta}{\tan\beta}\right)^{3/2} d\theta\right] \qquad (7)$$

where

$$K_1 = \frac{2}{3} K = \frac{4}{3} C_d \sqrt{2g}.$$

4. Numerical integration

As the direct integration of Eq. (7) is not possible, numerical integration is resorted to, to get discharge values for the head h. Numerical integration has been performed using 'Simpson's rule'. The Horizon 3 computer is employed. The step size taken in numerical integration is 1/1000 of a radian which is found to yield results with sufficient accuracy.

5. Addition of vertical slot

A graph of non-dimensional discharge Q (= $q/k\mu^{5/2}$) versus the non-dimensional head H (= h/μ) for the modified weir (Fig. 1b) is shown in Fig. 2. It is seen that for flows $H \geq 2$, the rate of flow is nearly a linear
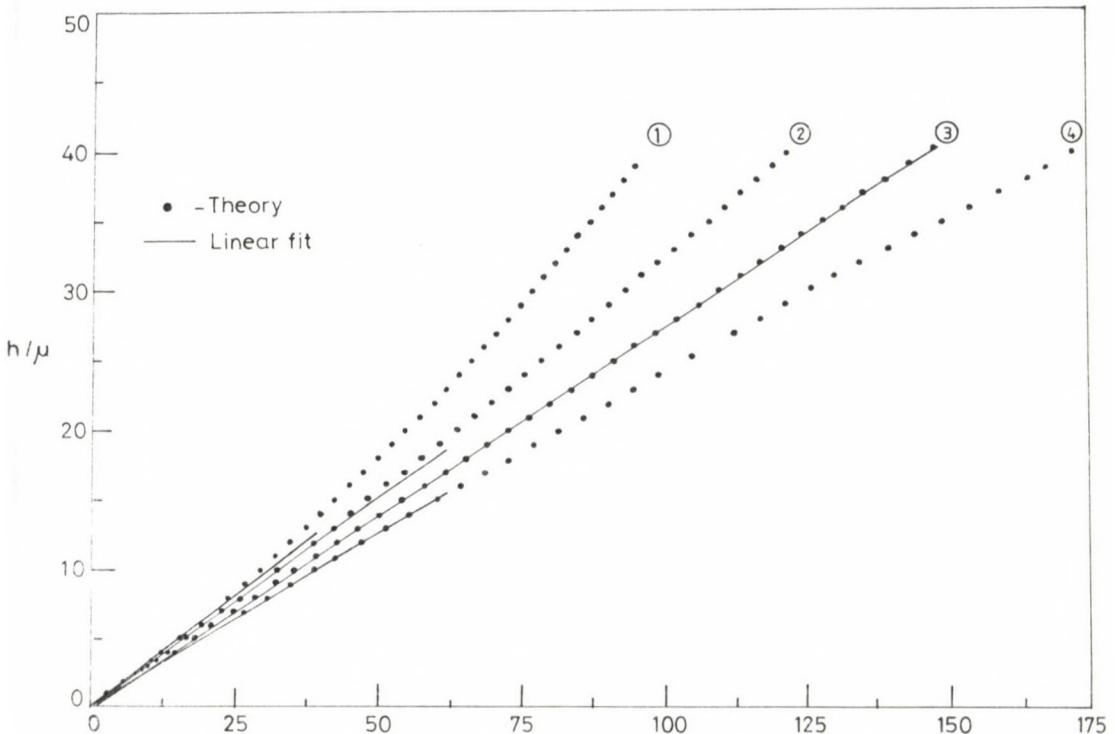
Fig. 2. Theoretical discharge vs. head curve
(1 — whithout additional slot /Eq. 7/, 2 — with addition of 0.2 μ vertical slot /Eq. 8/, 3 — with addition of 0.4 μ vertical slot /Eq. 8/, 4 — with addition of 0.6 μ vertical slot /Eq. 8/)
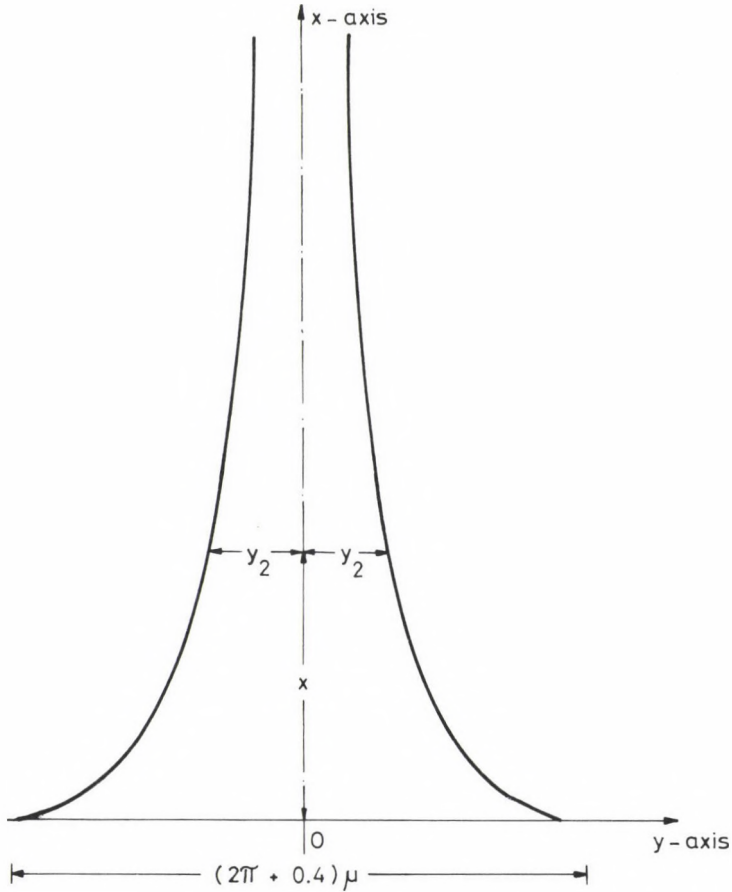
Fig. 3. Modified Rankine half body weir

function of the head for a depth of flow up to 5, i.e. for the limited range $2 \leq h/u \leq 5$. However, an addition of a small vertical slot to the weir, amounting to increasing the width of the weir throughout (or increasing the width of the channel in Fig. 1a) by 0.2 μ, 0.4 μ, 0.6 μ (for symmetrical weirs) improves the linear relationship between Q and H considerably. The theoretical discharge in the modified Rankine weir with the addition of a vertical slot of width nμ (symmetrical) is given by

$$q = \frac{2}{3} (n\mu)C_d \sqrt{2g} \ h^{3/2} + 2C_d \sqrt{2g} \int_0^h \sqrt{h-x} \ (\Pi\mu-y)dx$$

$$Q_t = \frac{2}{3} K \ (n\mu) \ h^{3/2} + \frac{2}{3} (\Pi\mu)K \ h^{3/2} - I_2 \qquad\qquad (8)$$
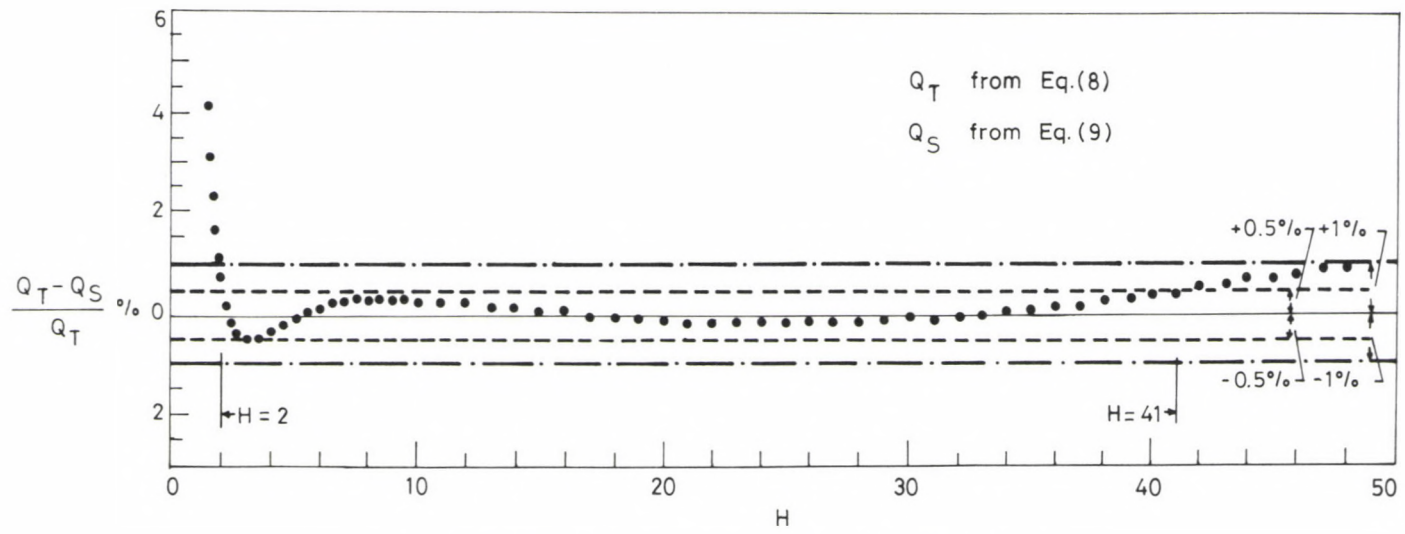
Fig. 4. Percentage variation of theoretical discharges with H

Table 1. Co-ordinates of the points on the Rankine half body
(Fig. 1), modified Rankine half body (Fig. 3) and K-R weir
(Fig. 4)

Sl No	$\frac{x}{\mu}$	$\frac{Y_1}{\mu}$	$\frac{Y_2}{\mu}$	$\frac{Y_3}{\mu}$
1	2	3	4	5
1	0	0.000	3.142	3.342
2	0.1	0.542	2.599	2.799
3	0.2	0.759	2.382	2.582
4	0.3	0.921	2.221	2.421
5	0.4	1.053	2.089	2.289
6	0.5	1.166	1.976	2.176
7	0.6	1.264	1.877	2.077
8	0.7	1.353	1.789	1.989
9	0.8	1.432	1.710	1.910
10	0.9	1.504	1.637	1.837
11	1.0	1.571	1.571	1.771
12	1.5	1.837	1.305	1.505
13	2.0	2.029	1.113	1.313
14	2.5	2.175	0.967	1.167
15	3.0	2.289	1.053	0.253
16	3.5	2.381	0.761	0.961
17	4.0	2.456	0.686	0.886
18	4.5	2.518	0.624	0.824
19	5.0	2.570	0.571	0.771
20	6.0	2.654	0.488	0.688
21	7.0	2.716	0.425	0.625
22	8.0	2.765	0.376	0.576
23	9.0	2.804	0.337	0.537
24	10.0	2.836	0.305	0.505
25	11.0	2.863	0.279	0.479
26	12.0	2.885	0.257	0.457
27	13.0	2.904	0.237	0.437
28	14.0	2.921	0.221	0.421
29	15.0	2.935	0.207	0.407
30	16.0	2.948	0.194	0.394
31	17.0	2.959	0.183	0.383
32	18.0	2.969	0.173	0.373
33	19.0	2.978	0.164	0.364
34	20.0	2.986	0.156	0.356
35	21.0	2.993	0.149	0.349
36	22.0	3.000	0.142	0.342
37	23.0	3.006	0.136	0.336
38	24.0	3.011	0.130	0.330
39	25.0	3.017	0.125	0.325
40	26.0	3.021	0.120	0.320
41	27.0	3.026	0.116	0.316
42	28.0	3.032	0.112	0.312
43	29.0	3.034	0.108	0.308
44	30.0	3.037	0.104	0.304
45	31.0	3.041	0.101	0.301
46	32.0	3.044	0.098	0.298
47	33.0	3.047	0.095	0.295

Table 1 (cont.)

1	2	3	4	5
48	34.0	3.049	0.092	0.292
49	35.0	3.052	0.090	0.290
50	36.0	3.055	0.087	0.287
51	37.0	3.057	0.085	0.285
52	38.0	3.059	0.082	0.282
53	39.0	3.061	0.080	3.261
54	40.0	3.063	0.078	3.263

Y_1 = half breadth of the Rankine half body (Fig. 1)
Y_2 = half breadth of the modified Rankine half body (Fig. 3)
Y_3 = half breadth of the K-R weir (Fig. 4)

$$Y_1 + Y_2 = \frac{\pi\mu}{2}, \; Y_3 = Y_2 + 0.2\,\mu$$

which is seen as Eq. (4) with an additional term, due to the discharge in the vertical slot. Figure 2 shows the plot of the theoretical discharge vs. head for 3 values of n, viz., n = 0.2, 0.4 and 0.6.

It is seen that the addition of the vertical slot helps in extending the linear relationship of Q and H beyond H = 2. The addition of 0.4 μ slot (for symmetrical weirs) results in an optimum design giving the linear relationship valid to a depth of H = 40. The correlation coefficient for the straight line fit (for the range $2 \leq H \leq 40$) is found to be maximum for an addition of 0.4 μ strip (symmetrical weir). In this range, the discharge is proportional to the head measured above a reference plane situated at 0.47 μ above the crest. The weir is shown in Fig. 4 and the co-ordinates of the points on the curve are given in Table 1 (columns 2 and 5). The linear relationship between Q and H for n = 0.4 is given by.

$$Q_S = 4.97\, C_d\, \sqrt{2g}\; \mu^{5/2} \left(\frac{h}{\mu} - 0.47 \right),\; 2 \leq \frac{h}{\mu} \leq 40. \tag{9}$$

The values of Q_T with n = 0.4 obtained form Eq. (8) and Q_S form Eq. (9) are compared as percentage difference, i.e. $(Q_T - Q_S)/Q_T\%$ with H is shown in Fig. 4. It can be seen that for the range $2 \leq H \leq 40$, the maximum percentage deviation is only $\pm$ 0.5%.

Thus it is confirmed form the above theoretical considerations that Modified Rankine half body weir can be used effectively as a linear proportional weir for a sufficiently high range of heads, ie. $2 \leq H \leq 40$ with an accuracy of theoretical discharge of 100 $\pm$ 0.5%.
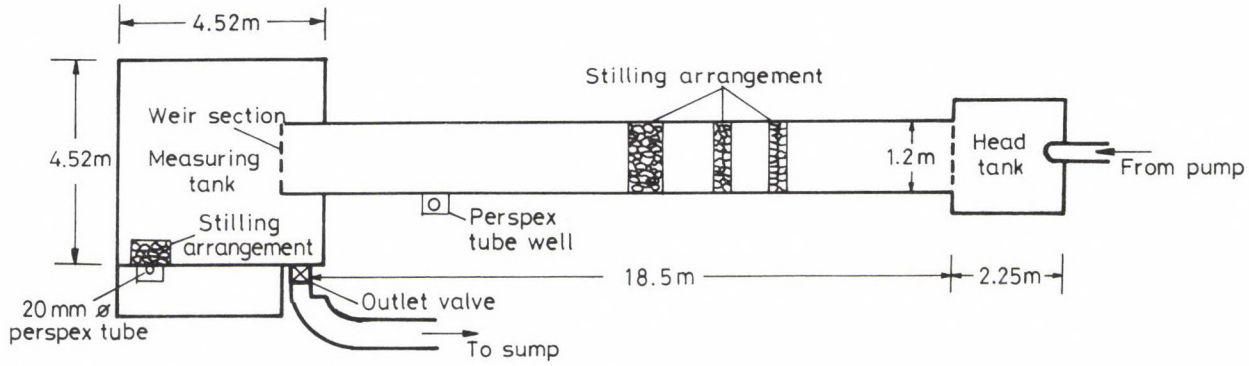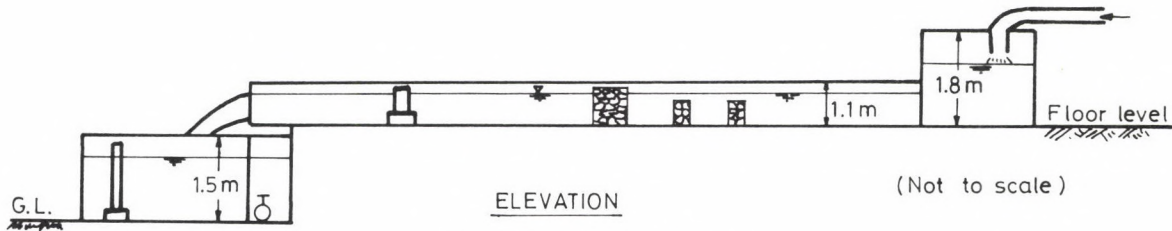
Fig. 5. Experimental set-up

Fig. 6. Side view of flow through modified Rankine half body weir, showing nappe

6. Experiments

Experiments were conducted on 3 weirs shown in Fig. 4 having $2\pi\mu$ = 10, 30, and 40 cm (width of the weir = $/(2\pi + 0.4)\mu/$. The experimental details are shown in Figs 5 and 6. The weirs were cut in 1/4" (6 mm) mild steel plates. The boundary of the weir was carefully marked on the plate by a scratch awl. The opening was then cut roughly by a band saw machine and then accurately filed to the required shape. The weir had a sharp edge of 1/6" (1.5 mm) with a 45° chamfer. The weir was fixed at the end of a rectangular channel 63 ft. long (19.2 mm), 3'11 1/4" wide (1.2 m) and 3'7 1/4" (1.1 mm) deep with its crest 1' (0.3 m) above the channel bed. The water was fed through a head tank measuring 7.4 1/2" x 7'4 1/2" x 5'10 7/8" (2.25 m x 2.25 m x 1.8 m) to which water was supplied by two pumps, having combined maximum capacity of 200 l.p.s (7 cusecs). The head over the weir was measured in a
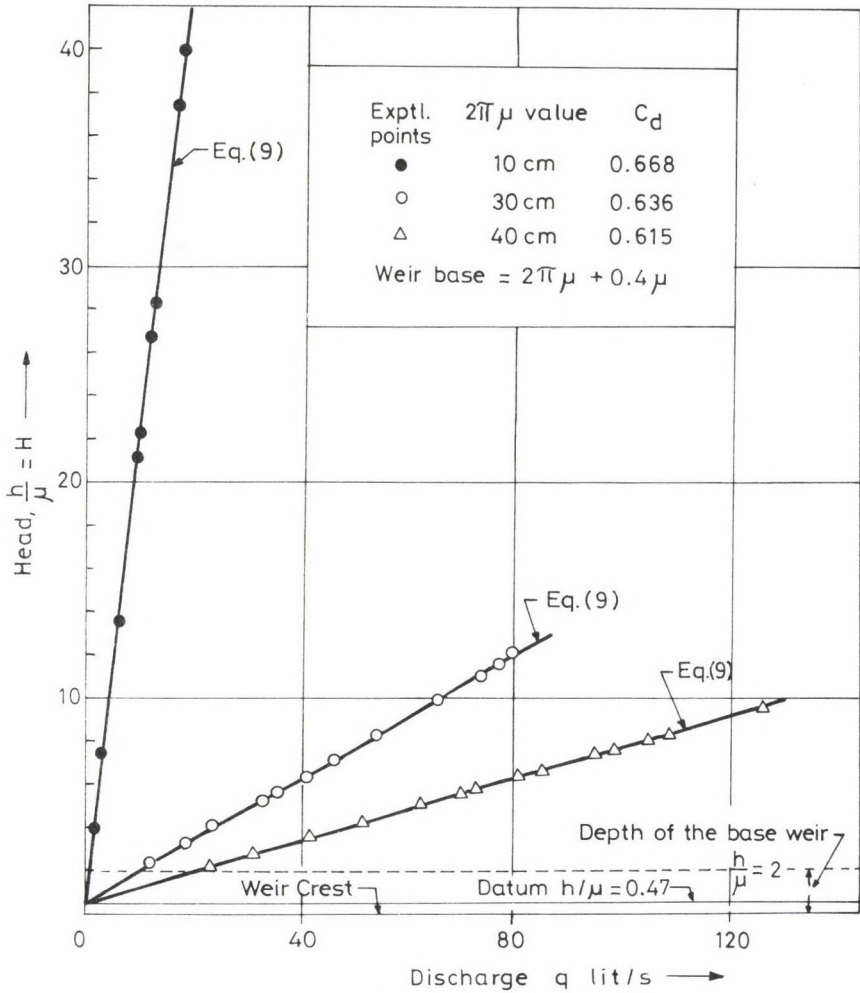
Fig. 7. Experimental verification of modified rankine half body as a linear proportional weir

stilling well situated 6 m from the weir with an electronic point gauge hav-
ing a least count of 1/1000' (0.3 mm). The volume of water collected was
measured in a tank measuring 14'10" x 14'10" x 4'11" (4.52 m x 4.52 m x 1.5
m) through readings in a perspex tube of 3/4" (20 mm) ID connected to the
tank at the bottom at one end. The rate of flow was determined by finding
the time taken for the water level to rise from one indicator fixed in the
perspex tube to another fixed exactly at a distance of 50 cm. The indicators
were connected to the leads of an electronic timer through a start and stop
mechanism. The time to collect the fixed volume of water was recorded to an
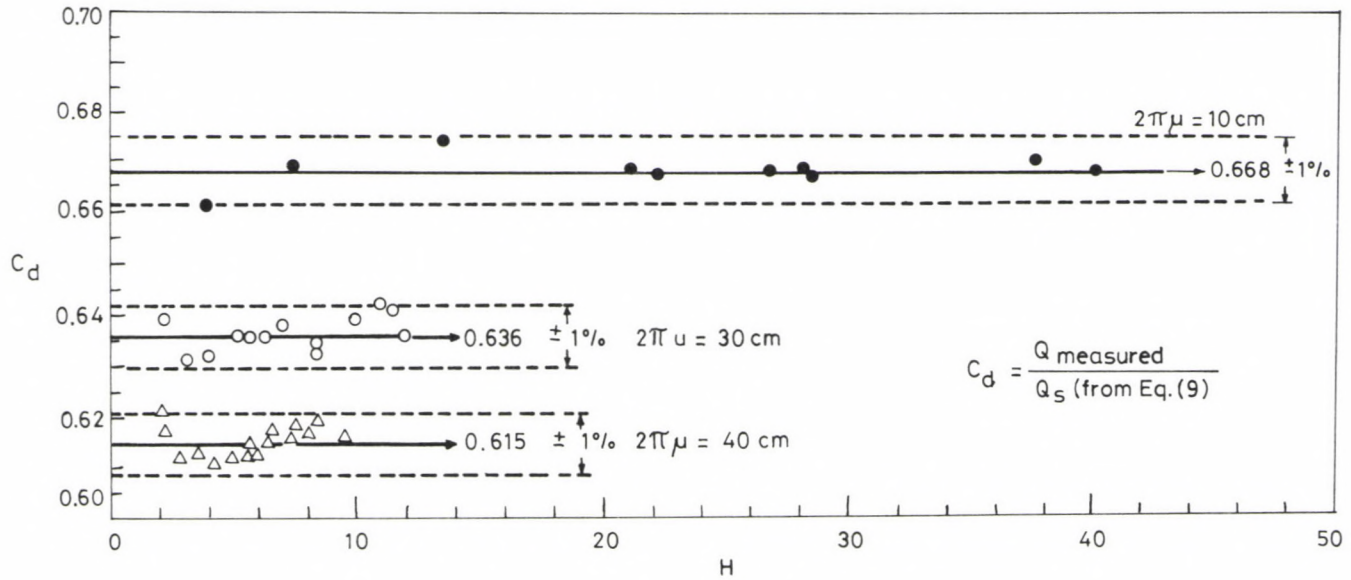
Fig. 8. Experimental variation of C_d with H

accuracy of 0.001 sec for each discharge. Each experiment was repeated twice
to ensure accuracy. At least 30 min were allowed between two experiments to
allow water level to stabilize. The experimental results of the non-dimen-
sional discharge $q/K\mu^{5/2}$ against the non-dimensional head h/μ are shown in
Fig. 7 for the 3 weirs.

7. Experimental results and discussion

It is evident from Fig. 7, for the 3 weirs that for flows $h/\mu \geq 2$, the
discharge has a linear relationship with the head measured above the datum
or reference plane situated at $0.47\ \mu$ above the crest, which relationship
exists to a depth of up to $40\ \mu$, within an error of $\pm$ 0.5% beyond which the
discharge-head relationship deviates from the linear relationship. From
Fig. 8, it is seen that C_d is constant for each weir within the limits of
experimental errors. However, the average value of C_d varies from 0.61 to
0.66 for the 3 weirs tested. It is not possible to generalize the nature of
variation of C_d with the dimensions of the weir with the limited experiments
conducted.

8. Conclusions

It is shown that the Rankine half body shape (Quadratrix of Hippias)
obtained by superposing a uniform flow over a line source can be effectively
used as a measuring notch. The flow in the intervening shape obtained by
placing a Rankine half body of focal length μ in a channel having its width
equal to the maximum width of the half body, i.e. $2\pi\mu$ (at ∞) produces a flow
having a linear relationship with the head, for flows above a minimum head,
to a small of depth of up to $5\ \mu$. The addition of a small vertical slot of
width varying from $0.2\ \mu$ to $0.6\ \mu$ (equivalent to increasing the width of the
weir uniformly throughout) is found to have a beneficial effect on the li-
nearity of the discharge — head relationship. Further it is found that the
addition of $0.4\ \mu$ slot (for symmetrical weirs) has the optimum effect, in
that the discharge is proportional to the head measured above a reference
plane situated at $0.47\ \mu$ above the crest, for all flows above a depth of
flow $2\ \mu$ and is valid up to $40\ \mu$, i.e. in the range $2 \leq h/\mu \leq 40$, within an
error of $\pm$ 0.5%. The experiments conducted on weirs testify the theory by

giving a constant average coefficient of discharge C_d for each weir. The weir should prove useful as a simple discharge measuring device, which can be designed as a high discharge coefficient weir, and also as an outlet weir for grit chambers (sedimentation tanks) of rectangular sections to maintain constant average velocity for different flows.

ACKNOWLEDGEMENTS

REFERENCES

1. Babbit, H. E. - Baumann, E. R.: Sewerage and sewage treatment. New York, John Wiley and Sons, 1955, 125—126

2. Banks, R. B.: A note on the generalized weir equation. Dept. of Civil Engineering, North Western University, Paper HP 0654, Illinois, No. 20, 1954

3. Cowgill, P.: The mathematics of weir forms. Quart. Appl. Maths. Vol. 11, No. 2 (1949), p. 142.

4. Davis, C. V.: Handbook of applied hydraulics. 2nd edn. McGraw—Hill Book Company, New York, N.Y. 1952, 1106—1107

5. Fonck, R. M.: Datum line for linear proportional weirs. Journal of App. Mech. ASME, Jan. 1978, Vol. 45, mÜ 22%

6. Keshava Murthy, K.: On the design of quadratic weirs. Journal of the Franklin Institute (Academic Press), Vol. 287, No. 2, Feb. 1969, 159—174

7. Keshava Murthy, K. - Gopalakrishna Pillai, K.: Modified proportional V-notch weirs. Journal of Hydraulic Division, ASCE, May 1978, 775—791

8. Keshava Murthy, K. - Gopalakrishna Pillai, K.: Design of a constant accuracy linear proportional weir. Journal of Hyd. Division, ASCE, April 1978, 527—541

9. Keshava Murthy, K. - Seshagiri, N.: A generalized mathematical theory and experimental verification of proportional notches. Journal of the Franklin Institute (Academic Press), Vol. 285, No. 5, May 1968, 347—363

10. Keshava Murhty, K. - Giridhar, D. P.: On the theory and design of self basing weirs. Under publication.

11. Lakshmana Rao, N. S. - Abdul Bhukari, C. H.: Linear proportional weirs with trapezoidal bottom. Journal of Hydraulic Research, IAHR, Vol. 9, No. 3, 1971, 413—427

12. Robert C. Weast - Samuel M. Selby: Handbook of tables for mathematics. 4th edn. 1970, p. 380

13. Saloman Eskinazi: Principles of fluid mechanics. Allyn and Bacon, Inc. Boston, 1962, p. 113

14. Sreenivasulu, P. - Raghavendran, R.: Linear proportional weirs. Journal of Hydraulic Division, ASCE, Vol. 96, No. 2, Feb. 1970, 379—390

15. Stout, O. V. P.: A new form of weir notch. Trans. of the Nebraska Engineering Society, Vol. 1, No. 1, 1987, p. 13

DETERMINATION OF THE SHEAR CENTER AND SHEAR FACTORS OF BEAM CROSS SECTIONS USING THE FINITE ELEMENT METHOD

PÁCZELT, I.[*]

(Received: 4 September 1992)

This work deals with the determination of the shear center and shear factors of a cross section consisting of a homogeneous isotropic material in each subdomain. Bernoulli's hypothesis has been adopted to calculate the bending stress while a stress function determined by means of the finite element method, using variation principles, has been introduced to calculate the stress resulting from shear. Numerical examples are presented to illustrate the efficiency of the method recommended.

1. Fundamental relationships, stress states

1.1. Bending stress

Let a prismatic beam be investigated. Let the longitudinal axis of the beam passing through the center of gravity of the cross section be denoted by z while the axes of the cross section, perpendicular to each other, by x and y. Assume axes x and y are of arbitrary orientation and axes x, y, z constitute a right-twisted system. Let the unit vectors pointing towards the mentioned axes be denoted by $\underline{e}_x$, $\underline{e}_y$, $\underline{e}_z$.

Let the tensor of second order moments in the center of gravity be denoted by $\underline{\underline{I}}_S$. Now, with the neutral line of the cross section denoted by $\underline{a}$ (see Fig. 1), the bending moment vector is

$$\underline{M} = \int_A \underline{R} \times (\underline{a} \times \underline{R}) \, dA = \underline{\underline{I}}_S \cdot \underline{a}, \tag{1}$$

that is

$$\underline{a} = \underline{\underline{I}}_S^{-1} \cdot \underline{M}, \tag{2}$$

[*]Páczelt, István, H-3529 Miskolc, Perczel M. u. 30, Hungary
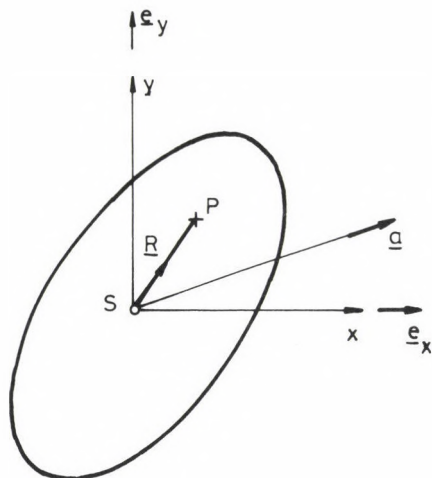
Fig. 1. Axes x, y in the center of gravity of the cross section, position vector
$\underline{R} = x\ \underline{e}_x + y\ \underline{e}_y$, vector $\underline{a}$ identifying the neutral line
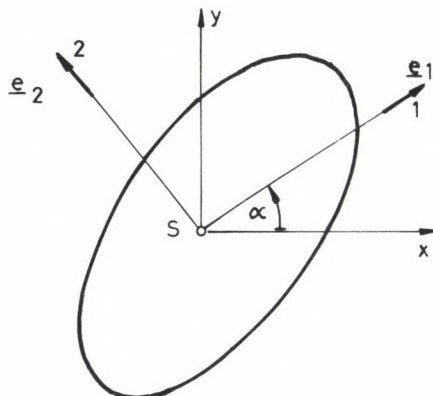
Fig. 2. Principal axes 1 and 2 of the cross section, α-angle to principal axes

where

$$\underline{\underline{I}}_S = \begin{bmatrix} I_x & -I_{xy} \\ -I_{yx} & I_y \end{bmatrix},$$

$$\underline{\underline{I}}_S^{-1} = \frac{1}{I_x\ I_y - I_{xy}^2} \begin{bmatrix} I_y & I_{xy} \\ I_{xy} & I_x \end{bmatrix} \tag{3a,b}$$
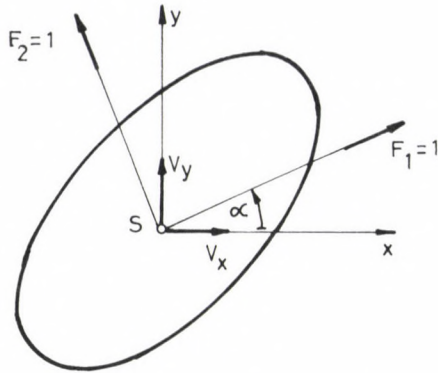
Fig. 3. Shear forces V_x, V_y and/or F_1, F_2
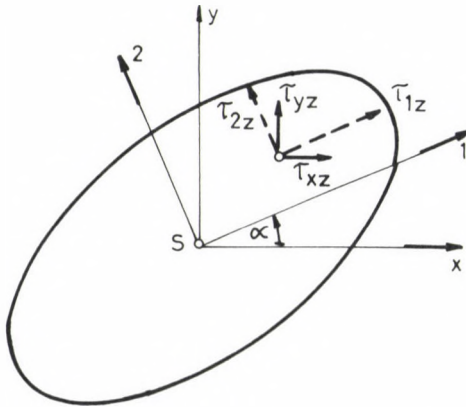
Fig. 4. Shear stresses in the x, y system: τ_{xz}, τ_{yz};
shear stresses in the 1, 2 system: τ_{1z}, τ_{2z}

I_x, I_y the second order moment calculated for axes x and y, respec-
tively,

I_{xy} the second order moment calculated for the pair of axes,

$$\left(I_x = \int_A y^2 \, dA, \ I_y = \int_A x^2 \, dA, \ I_{xy} = \int_A xy \, dA \right).$$

The principal axes of the cross section being set by vectors $\underline{e}_1$ and $\underline{e}_2$
(Fig. 2).

Normal bending stress:

$$\sigma_2 = (\underline{a} \times \underline{R}) \cdot \underline{e}_z = -\underline{e}_z \cdot (\underline{R} \times \underline{\underline{I}}_s^{-1} \cdot \underline{M}). \tag{4}$$

Let forces V_x, V_y pointing towards axes x and y act upon the beam at point $z = \ell$ (Fig. 3). Now bending moment

$$\underline{M} = M_x \, \underline{e}_x + M_y \, \underline{e}_y \tag{5}$$

arises in section z, where

$$M_x = -(\ell - z) \, V_y, \quad M_y = (\ell - z) \, V_x. \tag{6a,b}$$

From (4), by use of (5)—(6):

$$\sigma_z = -(\ell - z)(c_x \cdot x + c_y \cdot y), \tag{7}$$

where

$$c_x = \frac{I_x \, V_x - I_{xy} \, V_y}{I_x \, I_y - I_{xy}^2} \tag{8a}$$

$$c_y = \frac{I_y \, V_y - I_{xy} \, V_x}{I_x \, I_y - I_{xy}^2} \tag{8b}$$

1.2. Shear stress

As a result of shear forces V_x and V_y, also a shear stress vector $\underline{\tau} = \tau_{xz} \, \underline{e}_x + \tau_{yz} \, \underline{e}_y$ arises in addition to bending stress σ_z (Fig. 4). Since the beam is prismatic, $\underline{\tau}$ is independent of z that is

$$\underline{\tau} = \underline{\tau}(x,y) \tag{9}$$

Scalar equation

$$\frac{\partial \tau_{xz}}{\partial x} + \frac{\partial \tau_{yz}}{\partial y} + \frac{\partial \delta_z}{\partial z} = 0 \tag{10}$$

obtainable from equilibrium equation $\underline{\underline{T}} \cdot \nabla = \underline{0}$ can be satisfied in case of a homogeneous isotropic material by introducing stress function $\psi = \psi(x,y)$ provided we try to find the stress function co-ordinates in the form

$$\tau_{xz} = G \frac{\partial \psi}{\partial x} - \frac{1}{2(1 + \nu)} (c_x x^2 + c_y 2\nu xy) \equiv G \frac{\partial \psi}{\partial x} - A(x,y) \tag{11a}$$

and

$$\tau_{yz} = G \frac{\partial \psi}{\partial y} - \frac{1}{2(1 + \nu)} (c_x 2\nu xy + c_y y^2) \equiv G \frac{\partial \psi}{\partial y} - B(x,y) \tag{11b}$$

where G -- shear elasticity modulus,

ν — Poisson's number.

Introducing the tensor of material constants

$$\underline{\underline{D}} = \begin{bmatrix} G & 0 \\ 0 & G \end{bmatrix}, \tag{12}$$

the shear stress will be

$$\underline{\tau} = \underline{\underline{D}} \cdot \nabla \psi - \left[A(x,y) \underline{e}_x + B(x,y) \underline{e}_y \right] \equiv \underline{\underline{D}} \cdot \nabla \psi - \underline{c}(x,y). \tag{13}$$

Note that K. S. Surana uses the potential energy minimum principle by introducing warping function $\underline{\psi}(x,y)$ in his work /4/, making use of the work of Mason and Hermann /5/. The functional used is incomparably more complicated than that used by us.

1.3. Basic equation, boundary conditions, fitting conditions

Basic equation

$$(\nabla \cdot \underline{\underline{D}} \cdot \nabla \psi) = 0 \tag{14}$$

applying to ψ follows from equation (13) for $\underline{\tau}$ according to equilibrium equation (10). Stress

$$\tau_n = \underline{e}_z \cdot \underline{\underline{T}} \cdot \underline{n} = \underline{\tau} \cdot \underline{n} = \underline{n} \cdot \underline{\underline{D}} \cdot \nabla \psi - \underline{n} \cdot \underline{c} \tag{15}$$

arises on the boundary of normal $\underline{n}$.

Dynamic fitting conditions

$$\tau_n = 0 \tag{16}$$

and

$$\tau_n^e + \tau_n^j = 0 \tag{17}$$
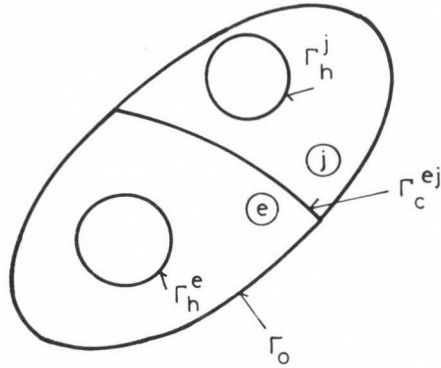
Fig. 5. The case of multiply connected domain

can be written for boundaries Γ_o and Γ_h of the cross section and for the internal boundary between the domains, e.g. for boundary Γ_c^{ej} of domains e and j, respectively (Fig. 5).

It is quite easy to make sure that the stresses according to (7) and (11a,b) satisfy the compatibility equations /2, 3/. (From among the six equations, it is only the two non-trivially satisfied equations given below that need to be investigated):

$$2\,\frac{\partial^2 \varepsilon_x}{\partial y\,\partial z} = \frac{\partial}{\partial x}\left(-\frac{\partial \gamma_{yz}}{\partial x} + \frac{\partial \gamma_{xz}}{\partial y}\right)$$

$$2\,\frac{\partial^2 \varepsilon_y}{\partial z\,\partial x} = \frac{\partial}{\partial y}\left(-\frac{\partial \gamma_{zx}}{\partial y} + \frac{\partial \gamma_{yz}}{\partial x}\right).$$

Since

$$\varepsilon_x = -\frac{\delta_z}{E}\,\nu = \varepsilon_y \qquad \text{and} \qquad \gamma_{yz} = \frac{\tau_{yz}}{G}\,, \quad \gamma_{zx} = \frac{\tau_{zx}}{G}\,,$$

the above statement is true also in this case. That means that the displacement field associated with the stress tensor field is compatible, it satisfies the continuity conditions. Therefore, the kinematic fitting condition will be automatically satisfied provided fields ψ along the boundary of the subdomains are continuous. Thus this condition need not be prescribed.

1.4. Formulation of variation principles

1.4.1. Principle 1

The solution to the above boundary condition problem comes from the stationarity condition of functional

$$L_1 = \frac{1}{2} \sum_e \int_{A^e} \nabla \psi \cdot \underline{\underline{D}} \cdot \nabla \psi \, dA - \sum_e \int_{\Gamma^e_{\cdot o}} \psi \underline{c} \cdot \underline{n} \, d\Gamma. \tag{18}$$

That is, all the fields satisfying variation equation

$$\delta L_1 = 0 \tag{19a}$$

correspond to actual fields. And indeed, considering the variation of L_1 according to fields ψ^e independent for each element (making use of the Gauss—Ostrogradski theorem and requiring that the fields be continuous according to class C^0 along internal boundaries Γ_c), we obtain that

$$\delta L_1 = \sum_e \left[-\int_{A^e} \delta\psi \, (\nabla \cdot \underline{\underline{D}} \cdot \nabla\psi) dA + \int_{\Gamma^e_o} \delta\psi \, (\underline{n} \cdot \underline{\underline{D}} \cdot \nabla\psi - \underline{n} \cdot \underline{c}) d\Gamma' \right]$$

$$\tag{19b}$$

$$\dots + \int_{\Gamma^{ej}_c} \delta\psi \left[(\underline{n}^e \cdot \underline{\underline{D}}^e \cdot \nabla\psi^e - \underline{n}^e \cdot \underline{c}^e) + (\underline{n}^j \cdot \underline{\underline{D}}^j \cdot \nabla\psi^j - \underline{n}^j \cdot \underline{c}^j) \right] d\Gamma + \dots = 0$$

where the vanishing of the different integrals results in basic equation (14), boundary condition (16) and dynamic fitting condition (17).

1.4.2. Principle 2

Suppose function ψ used for approximation satisfies basic equation (14). Now the first surface integral of functional (18) can be transformed into line integral:

$$\int \nabla\psi \cdot \underline{\underline{D}} \cdot \nabla\psi \, dA = \int (\nabla\psi \cdot \underline{\underline{D}} \cdot \nabla\psi) dA - \int \psi (\nabla \cdot \underline{\underline{D}} \cdot \nabla\psi) dA =$$

$$= \int (\underline{n} \cdot \underline{\underline{D}} \cdot \nabla\psi) \psi \, d\Gamma.$$

The continuity of ψ at the boundary of the elements can be controlled by means of multiplicator μ defined for the boundary of the element.

The functional resulting in the solution is

$$L_2 = \frac{1}{2} \sum_e \int_{\Gamma^e} \psi(\underline{n} \cdot \underline{\underline{D}} \cdot \nabla\psi)d\Gamma -$$

$$- \sum_e \int_{\Gamma^e} \mu(\underline{n} \cdot \underline{\underline{D}} \cdot \nabla\psi)d\Gamma + \sum_e \int_{\Gamma^e} \mu \, \underline{c} \cdot \underline{n} \, d\Gamma. \tag{20a}$$

By means of the stationarity condition,

$$\delta L_2 = 0 = \sum_e \int_{\Gamma^e} (\psi - \mu) \, \underline{n} \cdot \underline{\underline{D}} \cdot \nabla\delta\psi \, d\Gamma$$

$$\text{(the continuity of } \psi\text{)}$$

$$- \sum_e \int_{(\Gamma_o^e, \Gamma_h^e)} \delta\mu(\underline{n} \cdot \underline{\underline{D}} \cdot \nabla\psi - \underline{c} \cdot \underline{n})d\Gamma \tag{20b}$$

$$\ldots - \int_{\Gamma_c^{ej}} \delta\mu\left[(\underline{n}^e \cdot \underline{\underline{D}}^e \cdot \nabla\psi^e - \underline{c}^e \cdot n^e) + (\underline{n}^j \cdot \underline{\underline{D}}^j \cdot \nabla\psi^j - \underline{c}^j \cdot \underline{n}^j)\right]d\Gamma - \ldots$$

that is, also the dynamic boundary conditions and fitting conditions have been obtained. In case of a homogeneous isotropic material, $\underline{\underline{D}} = G\underline{\underline{I}}$, $\underline{\underline{I}}$ being idemtensor.

1.5. Shear center

The resultant of stresses $\underline{\tau}$ resulting from shear goes through the shear center /3/. The moment for the center of gravity can be calculated in two different ways that is, on the basis of stresses $\underline{\tau}$ or on the basis of the shear forces acting upon the cross section:

$$\underline{M}_s = \int_A \underline{R} \times \underline{\tau} \, dA = \underline{R}_c \times (V_x \, \underline{e}_x + V_y \, \underline{e}_y) = \underline{R}_c \times (F_1 \, \underline{e}_1 + F_2 \, \underline{e}_2) \tag{21}$$

where the position vector of the shear center is $\underline{R}_c = x_c \, \underline{e}_x + y_c \, \underline{e}_y = \xi_x \, \underline{e}_1 + \eta_c \, \underline{e}_2$ (Fig. 6).
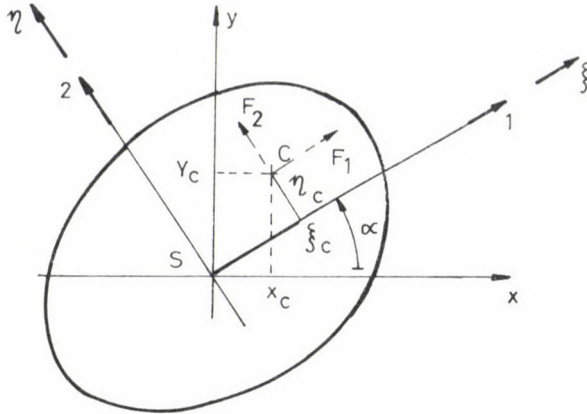
<u>Fig. 6.</u> Co-ordinates of shear center C: x_c, y_c and/or ξ_c, η_c

From the above equation, scalar equation

$$\int_A (x\,\tau_{yz} - y\,\tau_{xz})dA = x_c\,V_y - y_c\,V_x = \xi_c\,F_2 - \eta_c\,F_1$$

is obtained.

Let the shear force defined as load $V = 1$, $V_y = 0$) (or $F_1 = 1$, $F_2 = 0$) be denoted by $\tau^{(1)} = \tau_{xz}^{(1)}\,\underline{e}_x + \tau_{yz}^{(1)}\,\underline{e}_y$ while that defined as load $V_x = 0$, $V_y = 1$ (or $F_1 = 0$, $F_2 = 1$) by $\tau^{(2)}$.

Thus

$$\left.\begin{matrix} x_c \\ \xi_c \end{matrix}\right\} = \int_A (x\,\tau_{yz}^{(2)} - y\,\tau_{xz}^{(2)})dA \qquad \left\{\begin{matrix} V_x = 0,\ V_y = 1 \\ F_1 = 0,\ F_2 = 1 \end{matrix}\right. \tag{22a}$$

$$\left.\begin{matrix} y_c \\ \eta_c \end{matrix}\right\} = -\int_A (x\,\tau_{yz}^{(1)} - y\,\tau_{xz}^{(1)})dA \qquad \left\{\begin{matrix} V_x = 1,\ V_y = 0 \\ F_1 = 1,\ F_2 = 0 \end{matrix}\right. \tag{22b}$$

where

$$x_c = \xi_c \cos\alpha - \eta_c \sin\alpha$$

$$y_c = \xi_c \sin\alpha + \eta_c \cos\alpha. \tag{22c}$$

1.6. Shear factors

In the Timoshenko beam model, the cross section remains flat, its angular displacement being affected also by the shear strain /6/. To be flat means in this case that the value of the shear stress is constant which is, of course, not true in practice because the mantle of the beam is unloaded. A shear factor may be introduced so that the shear energies associated with the constant shear stress and the actual stress will be identical.

Let the case of the rectangle under shear, known from the theory of strength, be investigated as an example. We can write that, from force F acting in the direction of x (Fig. 7), the average value of the shear stress varies according to relationship

$$\tau = \tau_{xz} = \frac{3}{2}\frac{F}{A}\left(1 - \frac{x^2}{a^2}\right)$$

where A = 2ab is the surface of the rectangle, the shear stress of an approximately constant value being

$$\tau_o = \frac{F}{A}.$$

Writing the identity of the strain energies, we obtain that

$$\frac{1}{2}\int \tau\gamma\,dV = \frac{1}{2}\int \frac{\tau^2}{G}\,dV = \frac{1}{2}\tilde{\kappa}\int \frac{\tau_o^2}{G}\,dV.$$

Assuming a beam element of unit length in the direction of the axis, the integrals in question will be

$$\int_{-a}^{a} \frac{b}{G}\left(\frac{3}{2}\frac{F}{A}\left(1 - \frac{x^2}{a^2}\right)\right)^2 dx = \tilde{\kappa}\left(\frac{F}{A}\right)^2 \frac{1}{G}A$$

resulting in a shear factor of $\tilde{\kappa} = 6/5$.

Using a method of the theory of elasticity /6/, relationship $\tilde{\kappa} = (12 + 11\,\nu)/(10\,(1 + \nu))$ can be used for calculation.

In the general case, the shear factors are defined in the direction of the principal axes of the cross section. Stress field $\underline{\tau}^{(1)}$ or $\underline{\tau}^{(2)}$ will
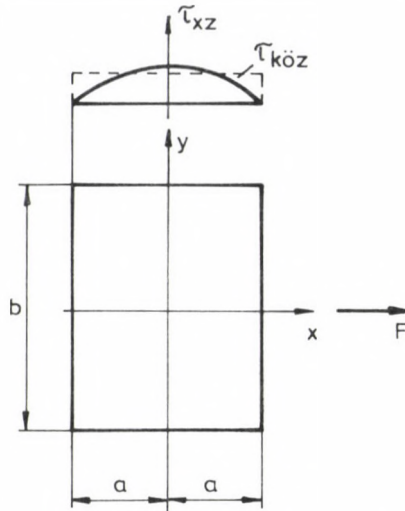
Fig. 7. Shear of the cross section of a rectangle

result from the shear force pointing in the direction of unit principal axis $F_1 = 1$ or $F_2 = 1$, respectively.

The identity of the strain energies is expressed by the following relationships where the strain energy associated with the shear boundary value problem is given on the right side while the value of energy associated with the approximate average stress, multiplied with shear factor κ_p, on the left side:

$$\text{by } F_1 = 1,\ F_2 = 0 \qquad \frac{1}{2}\int_A \frac{\left(\tau_{xz}^{(1)}\right)^2 + \left(\tau_{yz}^{(1)}\right)^2}{G}\, dA = \frac{1}{2}\tilde{\kappa}_1 \int_A \frac{dA}{A^2 G}$$

$$\text{by } F_1 = 0,\ F_2 = 1 \qquad \frac{1}{2}\int_A \frac{\left(\tau_{xz}^{(2)}\right)^2 + \left(\tau_{yz}^{(2)}\right)^2}{G}\, dA = \frac{1}{2}\tilde{\kappa}_2 \int_A \frac{dA}{A^2 G}$$

(23a,b)

When writing the boundary value problem, values

$$V_x = \cos \alpha, \qquad V_y = \sin \alpha \qquad\qquad (23c)$$

shall be substituted for constants c_x and c_y (8a,b), respectively from force $F_1 = 1$ acting in the direction of principal axis 1 while in case of force $F_2 = 1$ acting in the direction of principal axis 2,

$$V_x = -\sin \ \alpha, \qquad V_y = \cos \ \alpha. \tag{23d}$$

In case of a composite cross section where G is assumed to vary for each subdomain, the values can be simply determined by numerical integration of the integrals on the left side while summation of the integrals on the right side according to $1/A^2 \sum_i A^i/G_i$ (where A_i, G_i — area and shear modulus of elasticity of the surface of the subdomain). The shear factors defined in the x,y system can be calculated on the basis of formula (A.12) given in the Appendix, taking relationship $\kappa_p = 1/\tilde{\kappa}_p$ into consideration.

2. Use of the finite element method

2.1. Field approximation

The finite element method is used to approximate the fields that is,

$\psi^e = \underline{\underline{N}}^e \ \underline{\psi}^e$ in case of principle 1 while

$\psi^e = \underline{\underline{\Psi}}^e \ \underline{a}^e$

$\mu^e = \underline{\underline{N}}^e \ \underline{q}^e$ in case of principle 2, $\tag{25}$

where $\underline{\underline{N}}^e$, $\underline{\underline{\Psi}}^e$ — approximation matrices,

$\qquad \underline{\psi}^e$ — vector of the nodal values of function ψ,

$\qquad \underline{a}^e$ — vector of constants,

$\qquad \underline{q}^e$ — vector of the nodal values of μ.

Approximating the gradient in functional (18) in the form

$$\nabla\psi^e = \left[\begin{array}{c} B_x \\ B_y \end{array}\right]^e \underline{\psi}^e = \underline{\underline{B}}^e \ \underline{\psi}^e, \qquad \nabla\psi^e = \left[\begin{array}{c} W_x \\ W_y \end{array}\right]^e \underline{a}^e = \underline{\underline{W}}^e \ \underline{a}^e \tag{25}$$

where

$$\underline{\underline{B}}^e_x = \frac{\partial \underline{\underline{N}}^e}{\partial x}, \qquad \underline{\underline{B}}^e_y = \frac{\partial \underline{\underline{N}}^e}{\partial y}, \qquad \underline{\underline{W}}^e_x = \frac{\partial \underline{\underline{\Psi}}^e}{\partial x}, \qquad \underline{\underline{W}}^e_y = \frac{\partial \underline{\underline{\Psi}}^e}{\partial y},$$

the functional to be minimized will be

$$L_1 = \frac{1}{2} \sum_e \underline{\psi}^{eT} \int_{A^e} \underline{\underline{B}}^{eT} \underline{\underline{D}}^e \underline{\underline{B}}^e \, dA \, \underline{\psi}^e - \sum_e \underline{\psi}^{eT} \int_{\Gamma^e} \underline{N}^{eT}(\underline{c} \cdot \underline{n}) d\Gamma =$$

$$= \frac{1}{2} \sum_e \underline{\psi}^{eT} (\underline{\underline{K}}^e \underline{\psi}^e - 2 \underline{f}^e) = \frac{1}{2} \underline{\psi}^T \underline{\underline{K}} \underline{\psi} - \underline{\psi}^T \underline{f} \qquad (26a)$$

on the one hand, while

$$L_2 = \frac{1}{2} \sum_e \underline{a}^{eT} \int_{\Gamma^e} \underline{\underline{\psi}}^{eT} \underline{n}^{eT} \underline{\underline{D}}^e \underline{\underline{w}}^e \, d\Gamma \, \underline{a}^e - \sum_e \underline{g}^{eT} \int_{\Gamma^e} \underline{N}^{eT}(\underline{n}^{eT} \underline{\underline{D}}^e \underline{\underline{w}}^e) \, d\Gamma \, \underline{a}^e +$$

$$\qquad (26b)$$

$$+ \sum_e \underline{g}^{eT} \int_{\Gamma^e} \underline{N}^{eT}(\underline{c} \cdot \underline{n}) \, d\Gamma = \frac{1}{2} \sum_e \underline{a}^{eT} \underline{\underline{S}}^e \underline{a}^e - \sum_e \underline{g}^{eT} \underline{\underline{V}}^{eT} \underline{a}^e + \sum_e \underline{g}^{eT} \underline{f}^e$$

on the other hand.

Here $\underline{\underline{K}}^e$ — stiffness matrix of element e ($\underline{\underline{K}}$ being the stiffness matrix of the system),

$\underline{f}^e$ — load vector of element e ($\underline{f}$ being the load vector of the system),

that is

$$\underline{\underline{K}}^e = \int_{A^e} \underline{\underline{B}}^{eT} \underline{\underline{D}}^e \underline{\underline{B}}^e \, dA, \qquad \underline{\underline{D}}^e = \begin{bmatrix} G & 0 \\ 0 & G \end{bmatrix}^e \qquad (27)$$

$$\underline{\underline{S}}^e = \frac{1}{2} \int_{\Gamma^e} (\underline{\underline{\psi}}^{eT} \underline{n}^{eT} \underline{\underline{D}}^e \underline{\underline{w}}^e + \underline{\underline{w}}^{eT} \underline{\underline{D}}^e \underline{n}^e \underline{\underline{\psi}}^e) \, d\Gamma, \qquad \underline{\underline{V}}^{eT} = \int_{\Gamma^e} \underline{N}^{eT} \underline{n}^{eT} \underline{\underline{D}}^e \underline{\underline{w}}^e \, d\Gamma$$

$$\underline{n}^{eT} = [n_x, n_y]^e$$

$$\underline{\underline{f}}^e = \int_{\Gamma^e} \frac{1}{2(1 + \nu)} \underline{N}^T (c_x x^2 + c_y 2\nu xy) \underline{e}_x \cdot \underline{n} \, d\Gamma$$

$$+ \int_{\Gamma^e} \frac{1}{2(1 + \nu)} \underline{N}^T (c_x 2\nu xy + c_y y^2) \underline{e}_y \cdot \underline{n} \, d\Gamma. \qquad (28)$$

In case of isoparametric elements, normal $\underline{n}$ in (28) can be determined in the usual way.
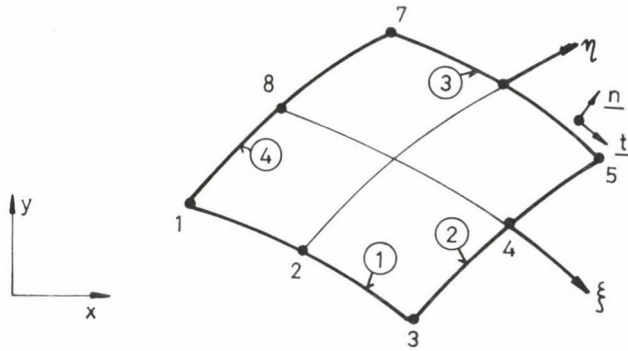
Fig. 8. Isoparametric element

Consider the isoparametric element with 8 nodes, illustrated sche-
matically in Fig. 8. Let the local co-ordinate system be denoted by ξ, η.
Now the tangent vector of boundary $\eta' = 1$ is

$$\underline{t} = \frac{\partial \underline{r}}{\partial \xi} = \frac{\partial \underline{r}}{\partial x} \frac{\partial x}{\partial \xi} + \frac{\partial \underline{r}}{\partial y} \frac{\partial y}{\partial \xi} = \underline{e}_x \frac{\partial x}{\partial \xi} + \underline{e}_y \frac{\partial y}{\partial \xi} \; .$$

Since relationship

$$x = \sum_i N_i(\xi, \eta) \; x_i \qquad\qquad (x \longleftrightarrow y)$$

(x_i, y_i being nodal co-ordinates, N_i shape function) applies to mapping be-
tween systems (x, y) and (ξ, η).

Along boundary 3 in question,

$$\underline{n} = \underline{e}_z \times \frac{\underline{t}}{|\underline{t}|} = \left(- \underline{e}_x \sum_i \frac{\partial N_i}{\partial \xi} y_i + \underline{e}_y \sum_i \frac{\partial N_i}{\partial \xi} x_i \right) \frac{\underline{t}}{|\underline{t}|} \; . \qquad (29a)$$

Then, in a similar way, the normals along the other boundaries can be
simply produced:
Side 1:

$$\underline{n} = \frac{1}{|\underline{b}|} \left(\underline{e}_x \sum_i \frac{\partial N_i}{\partial \xi} \Big|_{\eta=-1} y_i - \underline{e}_y \sum_i \frac{\partial N_i}{\partial \xi} \Big|_{\eta=-1} x_i \right) \qquad (29b)$$

Side 2:

$$\underline{n} = \frac{1}{|\underline{b}|} \left(\underline{e}_x \sum_i \frac{\partial N_i}{\partial \eta}\Big|_{\xi=1} y_i - \underline{e}_y \sum_i \frac{\partial N_i}{\partial \eta}\Big|_{\xi=1} x_i \right) \tag{29c}$$

Side 3:

$$\underline{n} = \frac{1}{|\underline{b}|} \left(- \underline{e}_x \sum_i \frac{\partial N_i}{\partial \eta}\Big|_{\xi=-1} y_i + \underline{e}_y \sum_i \frac{\partial N_i}{\partial \eta}\Big|_{\xi=-1} x_i \right) \tag{29d}$$

where $\underline{b}$ stands for the absolute value of the vector in parantheses in expression $\underline{n}$, e.g.

$$|\underline{b}| = \sqrt{ \left(\sum_i \frac{\partial N_i}{\partial \eta} y_i \right)^2 + \left(\sum_i \frac{\partial N_i}{\partial \eta} x_i \right)^2 }$$

on side 2.

2.2. The equation system to be solved

2.2.1. In case of L_1, equation system

$$\frac{\partial L_1}{\partial \psi} = \underline{0} = \underline{\underline{K}} \, \underline{\psi} - \underline{f} \tag{30}$$

is obtained, whence nodal vector $\underline{\psi}$ can be determined.

2.2.2. In case of L_2

$$\delta L_2 = \sum_e \delta \underline{a}^{eT} \frac{\partial L_2}{\partial \underline{a}^e} + \sum_e \delta \underline{g}^{eT} \frac{\partial L_2}{\partial \underline{g}^e} = 0, \tag{31}$$

$$\frac{\partial L_2}{\partial \underline{g}^e} = \underline{0} = \underline{\underline{S}}^e \, \underline{a}^e - \underline{\underline{V}}^e \, \underline{g}^e, \tag{32}$$

$$\underline{a}^e = (\underline{\underline{S}}^e)^{-1} \, \underline{\underline{V}}^e \, \underline{g}^e \equiv \underline{\underline{Z}}^e \, \underline{g}^e \tag{33}$$

follows from $\underline{a}^e$ which is independent for each element, because L_2 is a function of L_2 $(\underline{a}^e, \underline{g}^e)$.

Substituting (33) into (26b),

$$L_2 = \frac{1}{2} \sum_e \underline{q}^{eT} \, \underline{\underline{v}}^{eT} (\underline{\underline{S}}^e)^{-1} \, \underline{\underline{v}}^e \, \underline{q}^e - \sum_e \underline{q}^{eT} \, \underline{\underline{v}}^{eT} (\underline{\underline{S}}^e)^{-1} \, \underline{\underline{v}}^e \, \underline{q}^e + \sum_e \underline{q}^{eT} \, \underline{f}^e$$

that is

$$L_2 = -\frac{1}{2} \sum_e \underline{q}^{eT} \, \underline{\underline{Q}}^e \, \underline{q}^e + \sum_e \underline{q}^{eT} \, \underline{f}^e = -\frac{1}{2} \underline{q}^T \, \underline{\underline{Q}} \, \underline{q} + \underline{q}^T \, \underline{f} \tag{34}$$

where

$$\underline{\underline{Q}}^e = \underline{\underline{v}}^{eT} \, (\underline{\underline{S}}^e)^{-1} \, \underline{\underline{v}}^e ,$$

$\underline{\underline{Q}}$ — stiffness matrix of the system,

$\underline{q}$ — nodal vector of the multiplicator field of the system.

Equation system

$$\underline{\underline{Q}}\underline{q} = \underline{f}$$

is obtained from the maximum of L_2, from which $\underline{q}$, then nodal multiplicator vector $\underline{q}^e$ of element e and, on the basis of (33), the vector of constants $\underline{a}^e$ can be determined. This latter being available, field ψ^e and then, by means of (13), tangential stress τ can be calculated.

3. Use of FEM-3D finite-element program system

On the basis of variation principle 1, eight or six nodal isoparametric finite elements have been built into the FEM-3D finite element program system /7/.

The program shall be run twice to solve the problems. First the torsional rigidity and other characteristics of the cross section are determined on the basis of /8/.

In the knowledge of the directions of the principal axes, the second running can take place. Because of determination of the shear factor, loads $F_1 = 1$ and $F_2 = 1$ shall be adjusted to determine the co-ordinates of the shear center. When the program runs for the second time, nodal vector $\underline{\psi}$ shall be determined first from the equation system (30) assigned to the shear boundary value problem, using the load vector of the element calculated according to (28) where constants c_x and c_y are obtained from (8a,b) by
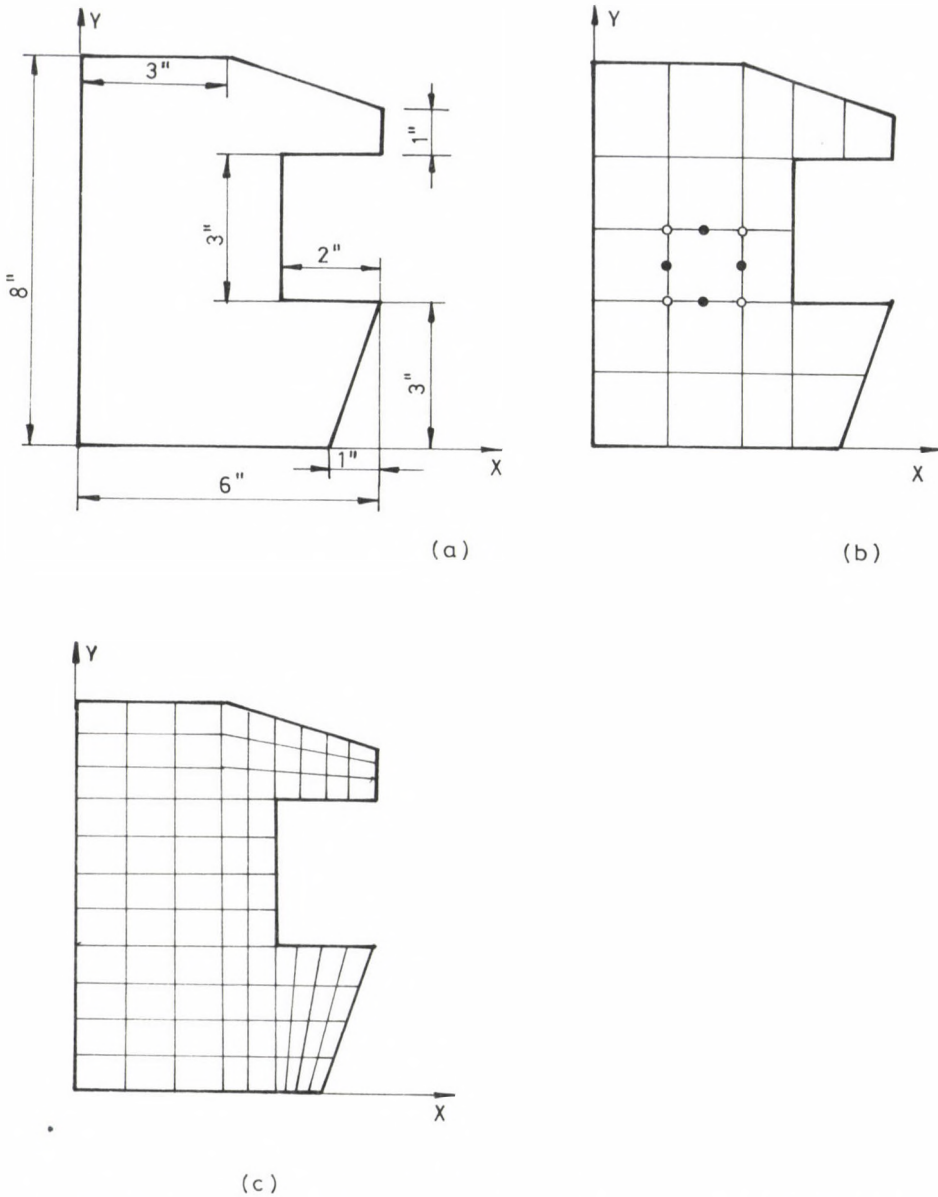
Fig. 9. Beam cross section, coarse and fine division in finite elements /a) Geometrical dimensions; b) Coarse: NUMNP = 80, NUMEL = 19; c) Fine: NUMNP = 330, NUMEL = 94/

PÁCZELT, I.

Table 1

Task 1

Cross section characteristic	SURANA NUMNP = 80 NUMEL = 19	Authors coarse resolution NUMNP = 80 NUMEL = 19	fine NUMNP = 333 NUMEL = 94
Surface		39	
Center of gravity co-ordinates			
x_S		2.51282	
y_S		3.8744	
Second-order moments			
I_x		215.09	
I_y		91.2436	
I_{xy}		-6.94822	
Polar angle of principal axis α (degrees)		3.20134	
I_1		215.478	
I_2		90.8544	
Shear center			
x_C	1.75122	1.178	1.736
y_C	3.8784	3.876	3.876
Shear factors			
$\tilde{\kappa}_1$	—	1.257	1.257
$\tilde{\kappa}_2$	—	1.492	1.500
$\tilde{\kappa}_x$	1.19959	1.258	1.258
$\tilde{\kappa}_y$	1.48019	1.491	1.499
$\tilde{\kappa}_{xy}$	-0.00577	-0.1303	-0.013
I_c (torsional rigidity)	146.45	146.11	145.03
I_ω (sectorial moment of inertia)	—	317.3	306.8

means of (23c,d), then, from (22a,b), co-ordinates ξ_c, η_c of the shear centre, from (23a,b), the value of the shear factors associated with principal axes $\tilde{\kappa}_1$ and $\tilde{\kappa}_2$ and finally, on the basis of formula (A.12) in the Appendix, the values ($\kappa = 1/\tilde{\kappa}$) κ_x, κ_{xy}, κ_y shall be calculated.

Of course, the program is also capable of displaying graphically the values τ_{xz}, τ_{yz}, σ_{red} of the stressed state resulting from shear.

Task 2

Table 2

Cross section characteristics	SURANA	coarse NUMNP = 69 NUMEL = 14	Author's fine resolution NUMNP = 221 NUMEL = 56	fine NUMNP = 603 NUMEL = 168
Surface		7.0		
Center of gravity co-ordinates				
x_S		2.7143		
y_S		0.75		
Second-order moments				
I_x		1.6458		
I_y		21.762		
I_{xy}		0		
Polar angle of principal axis α (degrees)		0		
I_1		1.6458		
I_2		21.762		
Shear center				
x_C	-0.03638	-0.05678	-0.06637	0.03589
y_C	0.75	0.75	0.75	0.75
Shear factors				
$\tilde{\kappa}_1$	1.269	1.297	1.303	1.304
$\tilde{\kappa}_2$	19.385	19.48	19.58	19.52
$\tilde{\kappa}_x$	1.269	1.297	1.303	1.304
$\tilde{\kappa}_y$	19.385	19.48	29.58	19.52
$\tilde{\kappa}_{xy}$	0	0	0	0
I_C (torsional rigidity)	1.6643	1.6166	1.606	1.6031
I_ω (sectorial moment of inertia)	—	5.223	5.258	5.278

4. Numerical examples

Presented below are some numerical examples to illustrate what has been said above.

4.1. Example 1

The cross section taken from /4/ is illustrated, together with the distribution of the finite elements, in Fig. 9. NUMEL is the number of elements while NUMNP the number of nodal points.

Material characteristics: $E = 29 \cdot 10^4$ lb/inch, $\nu = 0.22$.

PÁCZELT, I.

Table 3

Task 3

Cross section characteristics	Thin section /Ponomariov, Vol. 2/	Author's resolution NUMNP = 437 NUMEL = 108
Surface	780	780
Center of gravity co-ordinates x_S y_S		22.65 0
Second-order moments I_x I_y I_{xy}	$0.1234 \cdot 10^7$	$0.1235 \cdot 10^7$ $0.3520 \cdot 10^6$
Polar angle of principal axis α (degrees) I_1 I_2	0	0 $0.1235 \cdot 10^7$ $0.3520 \cdot 10^6$
Shear center x_c y_c	−31.2 0	−29.65 0
Shear factors $\tilde{\kappa}_1$ $\tilde{\kappa}_2$		3.50 3.828
$\tilde{\kappa}_x$ $\tilde{\kappa}_y$ $\tilde{\kappa}_{xy}$		3.50 3.828 0
I_c (torsional rigidity) I_ω (sectorial moment of inertia)	2340 $0.1355 \cdot 10^{10}$	2353 $0.1355 \cdot 10^{10}$

Table 4

		x_c	$\tilde{\kappa}_x$	$\tilde{\kappa}_y$
	0.25	−0.06637	1.303	19.58
	0.30	−0.08292	1.303	19.62
ν	0.35	−0.09824	1.303	19.66
	0.40	−0.1125	1.303	19.70
	0.45	−0.1257	1.303	19.75

Fig. 10. Example 2: Beam cross section, division in finite elements /a) Geometrical dimensions; b) Coarse: NUMNP = 69, NUMEL = 14; c) Author's fine 1: NUMNP = 221, NUMEL = 56; d) Author's fine 2: NUMNP = 603, NUMEL = 168/
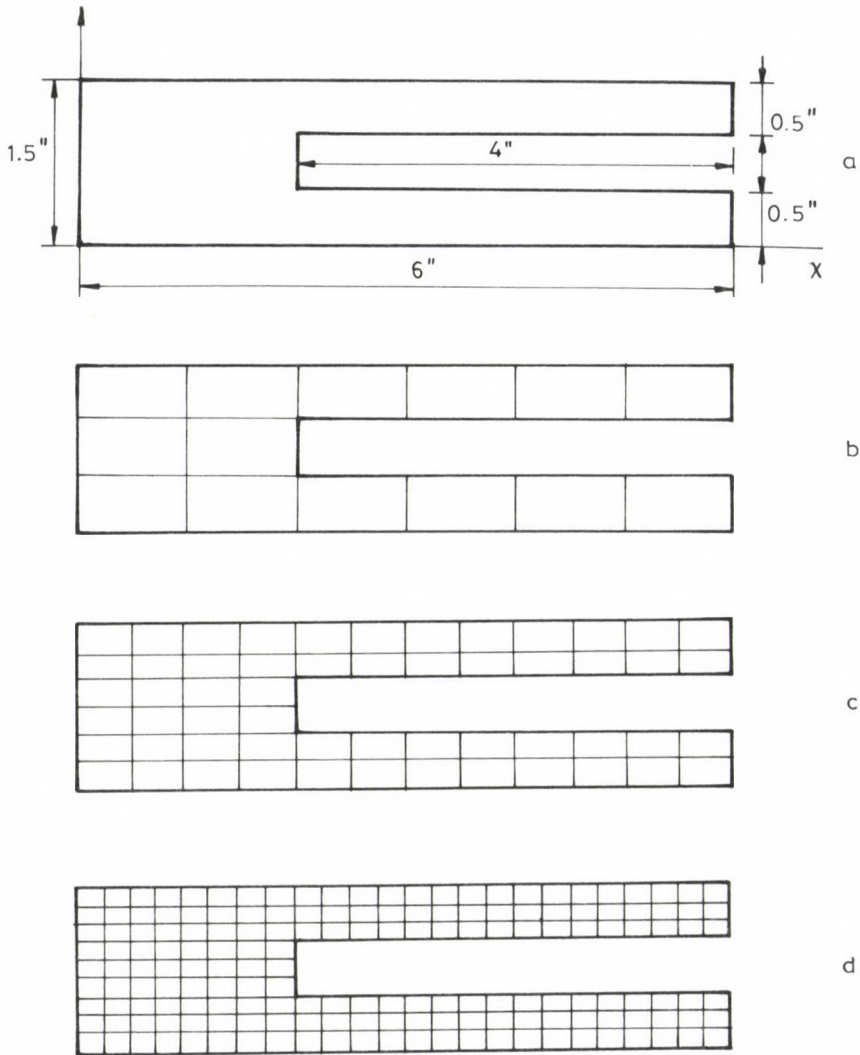
Fig. 10

4.2. Example 2

The values determined by Surana /4/ for the characteristics of the cross section of a beam, illustrated in Fig. 10, are tabulated in Table 2. Material characteristics: $E = 30.50^4$ lb/inch^2, $\nu = 0.25$.

Table 4 permits the effect of Poisson's number ν to be studied.

Fig. 11. Thin-walled open section /a) Geometry in case of the Vlasov theory; b) Distortion function ω, c) Geometry in case of the finite element model, d) Finite element mesh/

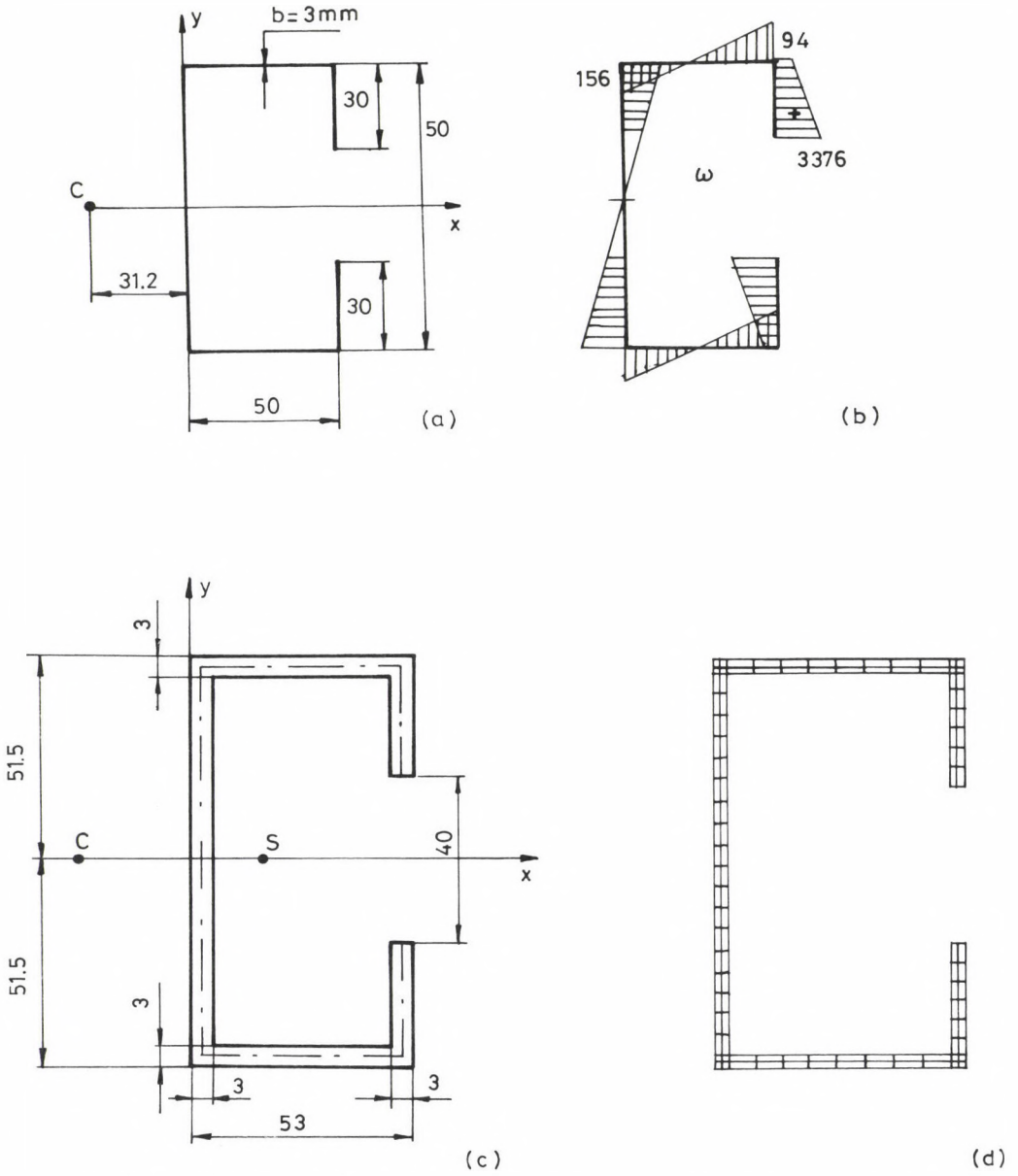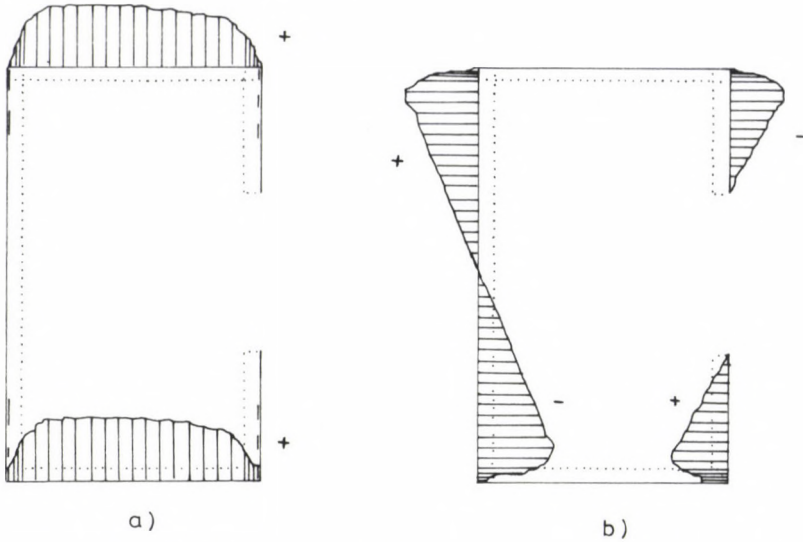Fig. 12. Example 3: Stresses τ_{xz} and τ_{yz} along the boundary, arising as a result of load $V_x = 1$ of direction x /a) min./max. values: $-6.064 \cdot 10^{-5}/3.6921 \cdot 10^{-3}$ N/mm^2, b) min./max. values: $-2.745 \cdot 10^{-3}/2.7453 \cdot 10^{-3}$ N/mm^2/
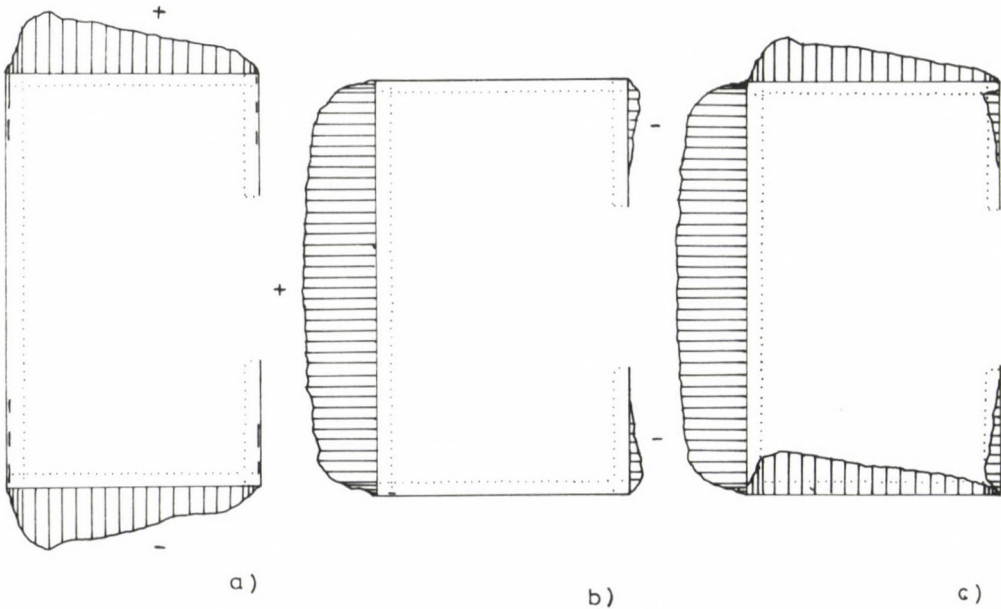

Fig. 13. Example 3: Stresses τ_{xz}, τ_{yz} and/or σ_{red} along the boundary, arising as a result of load $V_y = 1$ of direction y /a) min./max. values: $-2.688 \cdot 10^{-3}/2.6889 \cdot 10^{-3}$ N/mm^2; b) min./max. values: $-6.332 \cdot 10^{-4}/3.8945 \cdot 10^{-3}$ N/mm^2; c) min./max. values: $9.7068 \cdot 10^{-6}/6.7455 \cdot 10^{-3}$ N/mm^2/

4.3. Example 3

A thin-walled beam cross section is illustrated in Fig. 11. Material characteristics: $E = 2 \cdot 10^5$ MPa, $\nu = 0.3$. Table 3 also shows the results of calculation for the cross section shown in Fig. 11, based on the Vlasov theory.

Figure 12 shows tangential stresses τ_{xz} and τ_{yz}, resulting from unit load of direction x, along the boundary of the cross section. As clearly seen, the value of stress τ_{xz} lies by two orders of magnitude below the maximum value, that is, the stress arising in the corners is practically zero.

The same stresses but in association with the shear force of direction y are illustrated in Fig. 13.

Figure 13c shows stress σ_{red}. The value of the reduced stress arising in the corners lies by three orders of magnitude below the maximum value, a good approximation indeed.

4.4. Example 4

Consider the shear factor of a square cross section as a function of Poisson number ν.

Cowper /6/ determined a value of

$$\kappa = \frac{10(1 + \nu)}{12 + 11\nu} = \frac{1}{\tilde{\kappa}}$$

in his work.

The values we have obtained on the basis of energetic considerations for a square with 8 nodal points (8x8 elements) are tabulated in Table 5. As seen, the difference lies below 4%.

4.5. Example 5

8x16 elements have been assumed in the rectangle shown in Table 6. The Table includes shear factors κ_p depending on ν. According to Cowper,

$$\tilde{\kappa}_x = \tilde{\kappa}_y = 1/\tilde{\kappa}_{COWPER}$$

while, according to the definition of $\tilde{\kappa}_p$ we used,

Table 5. Shear factor of the square

ν	κ_{Cowper} /6/ $$COWPER = \frac{10(1 + \nu)}{12 + 11\nu}$$	8x8 elements NUMNP = 225 NUMEL = 64 $\kappa = 1/\tilde{\kappa}$	$\dfrac{\kappa}{\kappa_{COWPER}}$ 100%
0.2	0.845094	0.83056	98.28
0.25	0.847457	0.82919	94.84
0.3	0.84968	0.82850	97.50
0.35	0.85172	0.82713	97.11
0.4	0.85368	0.82576	96.73
0.45	0.85546	0.82410	96.33

Table 6

8·16 elements
NUMNP = 433
NUMEL = 128

$E = 2 \cdot 10^5$ Mpa
$A = 2 \cdot 10^4$ mm^2
$I_x = 0.666 \cdot 10^8$ mm^4
$I_y = 0.166 \cdot 10^8$ mm^4
$I_c = 0.4574 \cdot 10^8$ mm^4
$I_\omega = 0.2033 \cdot 10^{11}$ mm^6

ν	$\tilde{\kappa}_x$	$\tilde{\kappa}_y$
0.20	1.239	1.200
0.25	1.256	1.200
0.30	1.275	1.201
0.35	1.294	1.201
0.40	1.315	1.201
0.45	1.335	1.201

$$\tilde{\kappa}_x \neq \tilde{\kappa}_y.$$

In the range of $0.2 \leq . \leq 0.45$ assumed in the example,

$$\vartheta = \frac{\frac{1}{\tilde{\kappa}_x} - \kappa_{COWPER}}{\kappa_{COWPER}}$$

varies between 0.124 and 0.198.
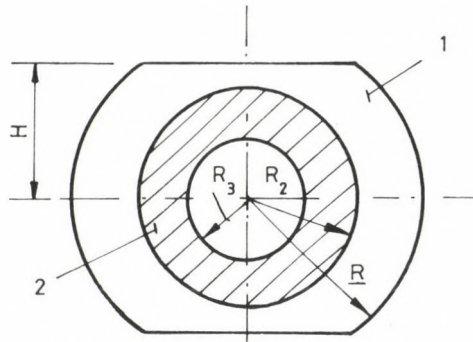
R$_3$ / R = 0.5   H / R = 0.8

R$_2$ / R = 0.7   R = 100 mm

Fig. 14. Geometry of a composite cross section
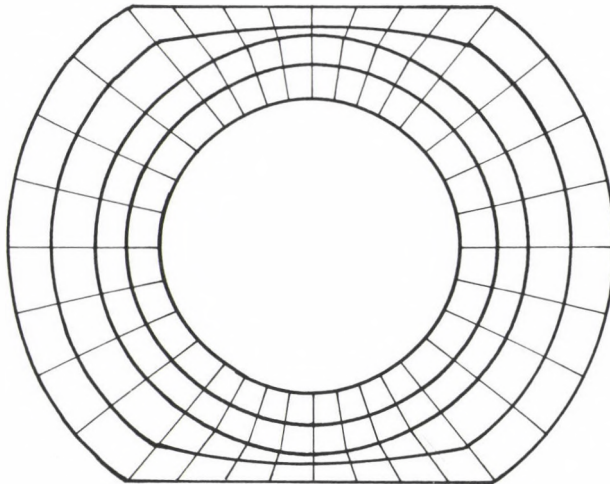
Fig. 15. Geometry of a composite cross section divided in finite elements

4.6. Example 6

Finally, let the values of the shear factors of a composite cross section be determined.

Material characteristics of the cross section illustrated in Fig. 14:

Domain 1: $E = 2.14 \cdot 10^5$ MPa, $\nu = 0.3$.

Domain 2: $E = 5.8 \cdot 10^5$ MPa, $\nu = 0.3$.

With the division of finite elements according to Fig. 15:

$$\tilde{\kappa}_x = 1.243 \qquad \tilde{\kappa}_y = 1.241$$

Other geometrical characteristics of the cross section:

$$
\begin{aligned}
A &= 0.20292 \cdot 10^5 \text{ mm}^2 \\
I_x &= 0.48175 \cdot 10^8 \text{ mm}^4 \\
I_y &= 0.71215 \cdot 10^8 \text{ mm}^4 \\
I_c &= 0.13153 \cdot 10^{14} \text{ N} \cdot \text{mm}^2 \\
I_\omega &= 0.9295 \cdot 10^{15} \text{ N} \cdot \text{mm}^4
\end{aligned}
$$

In case of an identical material ($E = 2.14 \cdot 10^{15}$),

$$\tilde{\kappa}_x = 1.853, \qquad \tilde{\kappa}_y = 1.697,$$

furthermore,

$$
\begin{aligned}
I_c &= 0.90237 \cdot 10^{13} \text{ N} \cdot \text{mm}^2, \\
I_\omega &= 0.1927 \cdot 10^{16} \text{ N} \cdot \text{mm}^4,
\end{aligned}
$$

or

$$
\begin{aligned}
I_c/G &= I_c/0.8231 \cdot 10^5 = 0.10939 \cdot 10^9 \text{ mm}^4, \\
I_\omega/E &= I_\omega/2.14 \cdot 10^5 = 0.9006 \cdot 10^{10} \text{ mm}^6,
\end{aligned}
$$

where

$$G = E/2 \, (1 + \nu).$$

5. Conclusions

The finite element model presented is a rather efficient method to clear the geometrical characteristics of the beam cross section in two steps. In the first step, the conventional geometrical characteristics such as surface, most important moments of inertia, St. Venant's torsional rigidity I_c and/or the second-order moment associated with warping are determined while in the second step -- in the knowledge of the principal axes of the cross section — the co-ordinates of the shear center and/or shear factor $\tilde{\kappa}_p$ are calculated by means of the variation principle described in this work. Presented in Appendix are the variation principle based on the total potential energy associated with the Timoshenko beam model which takes the shear strain into consideration, as well as the calculations to obtain the equilibrium equations and dynamic boundary conditions.

The calculation based on the first variation principle seems to be more expedient than that based on the second variation principle because in the first case, the stiffness matrix and the load vector can be produced in a simpler way.

APPENDIX

Total potential energy of the beam

Let x and y be the axes falling within the cross section going through the center of gravity of the cross section while z the centreline of the beam. Material characteristics of the beam: Young modulus E and/or shear modulus of elasticity G. Displacements of the points of the beam result from angular displacements ϕ_x and ϕ_y of the beam cross section around axes x and y. Assume the cross section remains flat also after deformation that is,

$$w = \phi_x y - \phi_y x = \phi_\xi \eta - \phi_\eta \xi. \tag{A.1}$$

Let the displacement of the point of the beam in directions x and y be denoted by u and v, respectively. The principal axes of the cross section are straights 1 and 2, the displacements in these directions are u and v while the angular displacements of the cross section ϕ_ξ and ϕ_η, respectively (Fig. A.1).
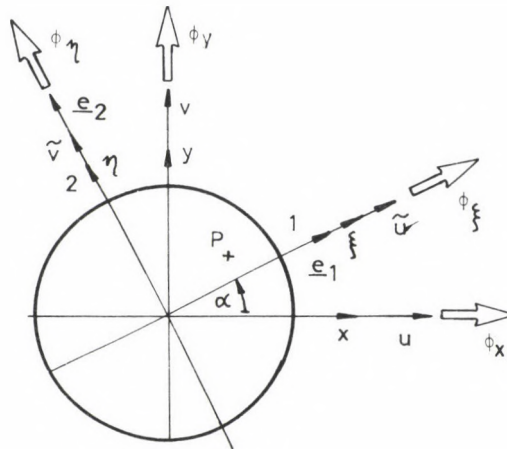
Fig. A.1. Co-ordinate systems, displacement co-ordinates, angular displacement co-ordinates

The specific elongation in the direction of axis z is

$$\varepsilon_z = \frac{dw}{dz} = w' = \phi_x' y - \phi_y' x \tag{A.2}$$

while the angular distortion

$$\gamma_{1z} = \frac{\partial \tilde{u}}{\partial z} + \frac{\partial w}{\partial \xi} = \tilde{u}' - \phi_\eta \tag{A.3}$$

$$\gamma_{2z} = \frac{\partial \tilde{v}}{\partial z} + \frac{\partial w}{\partial \eta} = \tilde{v}' + \phi_\xi . \tag{A.4}$$

Acting along axis z of the beam are loads p_x and p_y and/or moment m_x and m_y distributed among lines x and y, respectively.

The concentrated moments and forces are M_x, M_y and F_x, F_y in the direction of x and y, respectively.

The following transformation relationships apply:

$$\tilde{u} = u \cos \alpha + v \sin \alpha$$
$$\tilde{v} = - u \sin \alpha + v \cos \alpha \tag{A.5}$$

$$\phi_\xi = \phi_x \cos \alpha + \phi_y \sin \alpha$$
$$\phi_\xi = - \phi_x \sin \alpha + \phi_y \cos \alpha . \tag{A.6}$$

Total potential energy:

$$\Pi_p = U_{bending} + U_{shear} - W, \tag{A.7}$$

where the strain energy resulting from bending is

$$U_{bending} = \frac{1}{2} \int_L \int_A E(w')^2 dA \, dz =$$
$$= \frac{1}{2} \int_L E(I_x \phi_x'^2 + I_y \phi_y'^2 - 2 I_{xy} \phi_x' \phi_y') \, dz \tag{A.8}$$

that resulting from shear

$$U_{shear} = \frac{1}{2} \int_L GA(\kappa_1 \gamma_{1z}^2 + \kappa_2 \gamma_{2z}^2) \, dz \tag{A.9}$$

where $\kappa_1 = 1/\tilde{\kappa}_1$, $\kappa_2 = 1/\tilde{\kappa}_2$ being shear shape factors in directions 1 and 2, respectively (for definition of κ_1, $\tilde{\kappa}_2$ see /23a,b/),

A is the surface of the cross section while I_x, I_y, I_{xy} are second-order moments.

Work of the system of external forces:

$$W = \int_L (p_x\, u + p_y\, v)dz + \int_L (m_x\, \phi_x + m_y\, \phi_y)dz +$$

$$+ \left[M_x\, \phi_x + F_x\, u\right]\Big|_0^L + \left[M_y\, \phi_y + F_y\, v\right]\Big|_0^L \tag{A.10}$$

Thus, considering the variation of fields u, v, ϕ_x, ϕ_y in Π_p independently of each other, we use the product integration rule to obtain

$$\delta\Pi_p = 0 = -\int_L \left[\delta\phi_x\ \ \delta\phi_y\right]\left(E\begin{bmatrix} I_x & -I_{xy} \\ -I_{xy} & I_y \end{bmatrix}\begin{bmatrix} \phi_x'' \\ \phi_y'' \end{bmatrix} - \begin{bmatrix} F_y \\ -F_x \end{bmatrix} + \begin{bmatrix} m_x \\ m_y \end{bmatrix}\right)dz -$$

$$- \int_L \left[\delta u\ \ \delta v\right]\left(GA\begin{bmatrix} \kappa_x & \kappa_{xy} \\ \kappa_{yx} & \kappa_y \end{bmatrix}\begin{bmatrix} u'' - \phi_y' \\ v'' + \phi_x' \end{bmatrix} + \begin{bmatrix} p_x \\ p_y \end{bmatrix}\right)dz +$$

$$+ \left\{\left[\delta\phi_x\ \ \delta\phi_y\right]\left(E\begin{bmatrix} I_x & -I_{xy} \\ -I_{yx} & I_y \end{bmatrix}\begin{bmatrix} \phi_y' \\ \phi_y' \end{bmatrix} - \begin{bmatrix} M_x \\ M_y \end{bmatrix}\right)\right\}\Bigg|_0^L +$$

$$+ \left\{\left[\delta u\ \ \delta v\right]\left(GA\begin{bmatrix} \kappa_x & \kappa_{xy} \\ \kappa_{xy} & \kappa_y \end{bmatrix}\begin{bmatrix} u' - \phi_y \\ v' + \phi_x \end{bmatrix} - \begin{bmatrix} F_x \\ F_y \end{bmatrix}\right)\right\}\Bigg|_0^L \tag{A.11}$$

where

$$\kappa_x = \kappa_1\, \cos^2\alpha + \kappa_2\, \sin^2\alpha$$
$$\kappa_y = \kappa_1\, \sin^2\alpha + \kappa_2\, \cos^2\alpha \tag{A.12}$$
$$\kappa_{xy} = \kappa_{yx} = (\kappa_1 - \kappa_2)/2\, \sin 2\alpha$$

Introducing tensors

$$\underline{\underline{I}}_s = \begin{bmatrix} I_x & -I_{xy} \\ -I_{yx} & I_y \end{bmatrix}, \qquad \underline{\underline{\kappa}} = \begin{bmatrix} \kappa_x & \kappa_{xy} \\ \kappa_{yx} & \kappa_y \end{bmatrix}$$

and vectors

$$
\underline{\phi} = \begin{bmatrix} \phi_x \\ \phi_y \end{bmatrix}, \quad \underline{m} = \begin{bmatrix} m_x \\ m_y \end{bmatrix}, \quad \underline{p} = \begin{bmatrix} p_x \\ p_y \end{bmatrix}, \quad \underline{u} = \begin{bmatrix} u \\ v \end{bmatrix}, \quad \underline{M} = \begin{bmatrix} M_x \\ M_y \end{bmatrix}, \quad \underline{F} = \begin{bmatrix} F_x \\ F_y \end{bmatrix}
$$

relationships

$$
\underline{F} = GA \; \underline{\underline{\kappa}} \begin{bmatrix} u' - \phi_y \\ v' + \phi_x \end{bmatrix} \tag{A.13}
$$

and

$$
\underline{M} = E\underline{\underline{I}}_s \cdot \underline{\phi}'; \quad \underline{\phi}' = 1/E \; \underline{\underline{I}}_s^{-1} \cdot \underline{M} \tag{A.14}
$$

or, as a result of the vanishing of the integrals, equilibrium equations

$$
E\underline{\underline{I}}_s \; \underline{\phi}'' + \begin{bmatrix} -F_y \\ F_x \end{bmatrix} = - \underline{m}; \quad (\underline{M}' + \underline{e}_z \times \underline{F} + \underline{m} = \underline{0}) \tag{A.15}
$$

and

$$
GA \; \underline{\underline{\kappa}} \cdot \begin{bmatrix} u'' - \phi_y' \\ v'' + \phi_x' \end{bmatrix} = - \underline{p}; \quad (\underline{F}' + \underline{p} = \underline{0}) \tag{A.16}
$$

are obtained from the variation equation according to (A.11) for the internal forces and moments, respectively while from (A.16),

$$
GA \; \underline{\underline{\kappa}} \cdot \underline{u}'' = - p - GA \; \underline{\underline{\kappa}} \begin{bmatrix} -\phi_y' \\ \phi_x' \end{bmatrix} = - p - GA \; \underline{\underline{\kappa}} \cdot (\underline{e}_z \times \underline{\phi}')
$$

that is

$$
\underline{u}'' = - \frac{1}{GA} \; \underline{\underline{\kappa}}^{-1} \cdot \underline{p} - \frac{1}{E} (\underline{e}_z \times \underline{\underline{I}}_s^{-1}) \cdot \underline{M}
$$

$$
\underline{u}'' = \frac{1}{GA} \; \underline{\underline{\kappa}}^{-1} \cdot \underline{F}' - \frac{1}{E} (\underline{e}_z \times \underline{\underline{I}}_s^{-1}) \cdot \underline{M}, \tag{A.17}
$$

where the first term of the right side carries the effects of shear strain.

REFERENCES

1. Theory of Strength (in Hungarian). Panel of the Department of Mechanics, NME (Technical University of Miskolc), Tankönyvkiadó, Budapest 1977

2. Béda, Gy. - Kozák, I. - Verhás, J.: Continuum Mechanics (in Hungarian). Műszaki Könyvkiadó, Budapest 1987

3. Béda, Gy. - Kozák, I.: Mechanics of elastic bodies (in Hungarian). Műszaki Könyvkiadó, Budapest 1987

4. Surana, K. S.: Isoparametric elements for cross-sectional properties and stress analysis of beams. Int. J. Mech. Eng., 14 (1979), 475—497

5. Mason, W. E. - Hermann, L. R.: Elastic shear analysis of general prismatic beams. J. Eng. mech. Division, EM4 (August 1968), 965—983

6. Cowper, G. R.: The shear coefficient in Timoshenko's beam theory. J. of Applied Mechanics, Vol. 33, No. 2 (June 1966)

7. Páczelt, I. - Szabó, T.: FEM-3D substructural finite element program system in education and research (in Hungarian). MicroCAD'91 Conference on Applied Computer Engineering, Miskolc (Hungary), February 26—March 2, 1991, Vol. 1, VIII/66—72

8. Páczelt, I. - Szabó, T.: Estimation of torsional rigidity by means of the finite element method. Acta Technica 104/1—3 (1991/92)

BOOK REVIEW

Dulácska, E. (ed.): <u>Soil settlement effects on buildings</u>. Akadémiai Kiadó, Budapest, 1992

The book contains 447 pages, 211 figures, 72 tables, 24 examples, 3 PC programs and 304 references altogether. It is recommended first of all for civil engineers and architects.

The book written by a team of five expert engineers aims to facilitate the striking of a balance between safety and economy. It presents the most up-to-date results and possibilities, and hence we can utilize it successfully.

We must design the building so that
— it should not fail,
— not too many cracks should develop,
— it should cost no more than necessary.

This book deals essentially with computer calculation methods and programs concerning the foundation, the building and the ground as a whole. By means of these methods the stresses and deformations of the structure and the soil can be calculated with great accuracy.

The book is divided into seven Sections.

In <u>Section 1</u> the importance of interaction between subsoil and construction, together with relevant theories, is reviewed, accompanied with a long list of pertinent literature.

<u>Section 2</u> reminds the reader about soil mechanics and introduces information about the determination of ground surface movements occurring in nature without the effect of a superimposed structure.

<u>Section 3</u> deals with the rigidity of buildings, their adaptive capacity to deformations and peruses questions about the safety of buildings.

In <u>Section 4</u> computerized calculation methods are presented under the title of mathematical procedures. In computations for composite structures the stiffness of the soil must be modelled. The possible systems for modelling is suggested in this Section. During the last decade the finite element method has been used extensively to solve various foundation problems.

In <u>Section 5</u> approximative calculation methods are recommended for practice. These approximative methods are also used for the determination of basic data for the more sophisticated computer analyses. This Section therefore deals with different approximative methods which can be efficiently used for the analysis of either the whole structure or individual structural elements. Accuracy is of secondary importance when we establish an approximate procedure.

Case histories are described in <u>Section 6</u> and various guiding tables and three computer programs are presented in <u>Section 7</u>.

The reader may utilize each Section in itself, since for someone who wants to perform a quick approximative calculation, there is no need to study basic mathematical approaches, or to delve into computer techniques.

J. Farkas

NOTICE TO CONTRIBUTORS

Papers in English* are accepted on condition that they have not been previously published or accepted for publication.

Manuscripts in two copies (the original type-written copy plus a clear duplicate one) complete with figures, tables, and references should be sent to

Acta Technica
Nádor u. 7. I. 118
Budapest, Hungary
H-1051

Although every effort will be made to guard against loss, it is advised that authors retain copies of all material which they submit. The editorial board reserves the right to make editorial changes.

Manuscripts should be typed double-spaced on one side of good quality paper with proper margins and bear the title of the paper and the name(s) of the author(s). The full postal address(es) of the author(s) should be given in a footnote on the first page. An abstract of 50 to 100 words should precede the text of the paper. The approximate locations of the tables and figures should be indicated in the margin. An additional copy of the abstract is needed. Russian words and names should be transliterated into English.

References. Only papers closely related to the author's work should be referred to. The citations should include the name of the author and/or the reference number in brackets. A list of numbered references should follow the end of the manuscript.

References to periodicals should mention: (1) name(s) and initial(s) of the author(s); (2) title of the paper; (3) name of the periodical; (4) volume; (5) year of publication in parentheses; (6) numbers of the first and last pages. Thus: 5. Winokur, A.—Gluck, J.: Ultimate strength analysis of coupled shear walls. American Concrete Institute Journal 65 (1968) 1029-1035

References to books should include: (1) author(s)' name; (2) title; (3) publisher; (4) place and year of publication. Thus: Timoshenko, S.—Gere, J.: Theory of Elastic Stability. McGraw-Hill Company. New York, London 1961

Illustrations should be selected carefully and only up to the necessary quantity. Black-and-white photographs should be in the form of glossy prints. The author's name and the title of the paper together with the serial number of the figure should be written on the back of each print. Legends should be brief and attached on a separate sheet. Tables, each bearing a title, should be self-explanatory and numbered consecutively.

Authors will receive proofs which must be sent back by return mail.

Authors will receive 50 reprints free of charge.

* Hungarian authors can also submit their papers in Hungarian.

ACTA TECHNICA

(22.)

EDITOR-IN-CHIEF: P. MICHELBERGER

CIVIL ENGINEERING — C/7

ACTA TECHNICA

A JOURNAL OF THE HUNGARIAN ACADEMY OF SCIENCES

CONTENTS

MODIFIED DUGDALE MODEL FOR TWO COLLINEAR CRACKS
WITH A UNIFIED PLASTIC ZONE

R. R. BHARGAVA[*]—S. C. AGRAWAL[**]

Crack opening displacement and plastic zone size are determined or two collinear, equal, symmetrical cracks contained in an infinite homogeneous and elastic-plastic matrix. The matrix is subjected to remotely applied Mode I type loading. The cracks faces thus open forming plastic zones ahead of crack tips. The cohesive linearly varying stress distribution is then applied to arrest the plastic zones developed. Closed form solution, based on Dugdale model solution, is obtained using principal of super-position and complex variable technique. Results obtained are used to study relation between load required for crack closure, yield stress, plastic zone size, crack opening displacement and crack length.

1. Introduction

The elastic analysis of stress distribution in vicinity of a crack using complex variable was given by Muskhelishvili /1/. Using Muskhelishvili technique Dugdale /2/ proposed a 'strip yield model' giving elastic-plastic analysis for determining plastic zone size ahead of crack tips. The effect of partial closure on stress intensity factor of a Griffith crack opened by a parabolic distribution was investigated by Burniston and Gurley /3/. A photo-elastic studies for determination of plastic zone size ahead of a crack tip contained in a thin sheet under uniaxial loading has been carried out by Mishra and Parida /4/.

Harrop /5/ extended the Dugdale model for the case when plastic zones are subjected to cohesive parabolic stress distribution.

---

[*]R. R. Bhargava, Department of Mathematics, University of Roorkee, Roorkee-247 667, India

[**]S. C. Agrawal, Department of Mathematics, University of Roorkee, Roorkee-247 667, India

Stress field in an infinite plate, containing two collinear cracks, loaded at an arbitrary location was studied by Vialaton et al. /6/. Theocaris /7/ applied Dugdale model to determine plastic zone size developed in the case of two collinear and unequal cracks under opening mode conditions

The problem investigated in present paper is of an infinite, homogeneous, isotropic, elastic-perfectly plastic matrix containing two equal, collinear and symmetrically situated cracks. The matrix is subjected to Mode I type tension at infinity causing opening of crack faces forming plastic zones ahead of crack tips. Plastic zones develop at the interior crack tips get unified. A linearly varying cohesive stress distribution is applied over plastic zones to effect the cracks closure. Complex variable theory of elasticity has been used to obtain closed form expressions for plastic zone size and crack opening displacement.

2. Basic formula

For two-dimensional theory of elasticity using complex variable method /1/ Cartesian components of stresses P_{ij} (i,j = x,y) and displacement components u_i (i = x,y) may be expressed in terms of two complex potential functions $\phi(z)$ and $\Omega(z)$ as

$$P_{yy} - iP_{xy} = \phi(z) + \Omega(\bar{z}) - (z-\bar{z})\phi'(z), \tag{1}$$

$$2\mu(u_{x,x} + iu_{y,x}) = \kappa\phi(z) - \Omega(\bar{z}) - (z-\bar{z})\phi'(z). \tag{2}$$

A bar indicates the complex conjugate operation. The dash signifies differentiation with respect to the argument while comma after function stands for partial differentiation with respect to subscript following it. Shear modulus is denoted by μ. For plane strain $\kappa = 3-4\nu$ and for generalised plane stress $\kappa = (3-\nu)/(1+\nu)$, ν being Possion's ratio.

Dual problems of linear relationship are obtained using equation (1) when the rims of crack (s) are acted upon by stresses P_{yy}^+, P_{xy}^+ as

$$\phi^+(t) + \Omega^-(t) = P_{yy}^+ - iP_{xy}^+, \tag{3}$$
on crack(s)
$$\phi^-(t) + \Omega^+(t) = P_{yy}^- - iP_{xy}^-, \tag{4}$$

under the assumption $\lim_{y \to 0} y\phi'(t+iy) = 0$.

Supercripts + and - indicate the limiting values from positive y-plane and negative y-plane, respectively. Any point on crack, other then end points, is denoted by t.

The stresses intensity factor, K_I, at crack tip $z = z_1$ may be calculated from

$$K_I = 2\sqrt{2\pi} \lim_{z \to z_1} \{(z-z_1)^{1/2} \phi(z)\}. \tag{5}$$

3. The problem

An infinite, homogeneous, isotropic and elastic-perfectly plastic matrix is subjected to remotely applied uniaxial tension σ_∞ in y-direction. The matrix contains two collinear equal cracks L_1 and L_2 occupying intervals /-b, -a/ and /a, b/, respectively (Fig. 1). The cracks L_1 and L_2 open on account of prescribed tension developing plastic zones ahead of cracks tips. It is assumed that plastic zones developed at the interior tips of cracks are unified. Interior plastic zone Γ_1 lies in /-a, a/ and exterior plastic zones Γ_2: /-c, -b/ and Γ_3: /c, b/, develop at exterior tips of the cracks L_1 and L_2. These plastic zones are, in turn, subjected to linearly varying cohesive stress distribution, $t\sigma_{ye}$, where t is any point on the plastic zones and σ_{ye} is yield point stress.
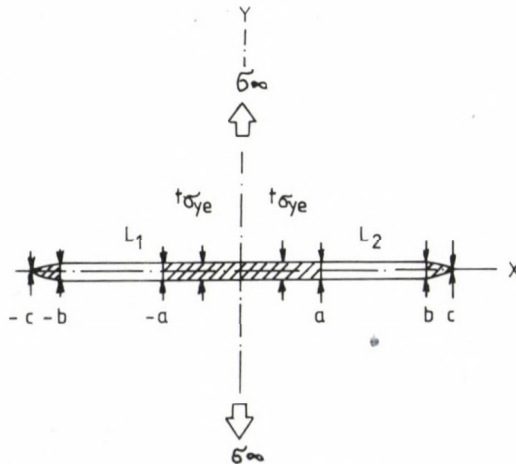
Fig. 1. Configuration

The problem is solved using superimposition of two component problems termed as (a) elastic problem and (b) plastic problem.

(a) Elastic problem

An infinite, homogeneous, isotropic and elastic-perfectly plastic matrix contains a stress free straight crack L: /-c, c/. The matrix is subjected to remotely applied uniform uniaxial tension σ_∞ in y-direction. The complex potential $\phi_e(z)$ for this may be written as in /1/

$$\phi_e(z) = 0.5 \; \sigma_\infty z (z^2 - c^2)^{-1/2}. \tag{6}$$

Opening mode stress intensity factor K_{Ie} is calculated using equation (5) substituting value of $\phi_e(z)$ from equation (6) and may be written as

$$K_{Ie} = 0.5 \; \sigma_\infty \; \sqrt{c/2}. \tag{7}$$

(b) Plastic problem

A stress free infinite, homogeneous, isotropic and elastic-perfectly plastic matrix contains two symmetrically situated cracks L_1: /-b, -a/ and L_2: /a, b/. Interior plastic zone Γ_1 occupies /-a, a/ and exterior plastic zones Γ_2 and Γ_3 occupy /-c, -b/ and /b, c/ ligaments ahead of crack tips -b and b, respectively. Boundary conditions of problem are

(i) No stress are acting at infinite boundary.
(ii) Cohesive stress distribution, $t\sigma_{ye}$, acting on rims of each of the plastic zones Γ_1, Γ_2 and Γ_3, respectively. Any point on plastic zones is denoted by t.

And

(iii) Rims of the cracks L_1 and L_2 are stress free.

Dual Hilbert problems obtained using boundary conditions (ii) and (iii) applied on extended crack (= the actual crack ∪ relevant plastic zone) may be written as follows:

$$\phi_p^+(t) + \Omega_p^-(t) = t\sigma_{ye}$$

$$\text{on } \Gamma_1 \cup \Gamma_2 \cup \Gamma_3. \tag{8}$$

$$\phi_p^-(t) + \Omega_p^+(t) = t\sigma_{ye}$$

The subscript p refers that potentials refer to plastic problem. Using Muskhelishvili /1/ complex variable technique the complex potential $\phi_p(z)$ of interest may be given by

$$
\phi(z) = \frac{\sigma_{ye}}{\pi i}\left[\frac{1}{x(z)}\left\{\frac{c^2}{2}\left(\begin{array}{l}\pi/2 +\sin^{-1}a/c -\sin^{-1}b/c-b/c\,\cos\,\sin^{-1}b/c\\ + a/c\,\cos\,\sin^{-1}a/c\end{array}\right)\atop -z^2(\pi/2-\sin^{-1}b/c + \sin^{-1}a/c)\right\}\atop -z\left\{\tan^{-1}\frac{z}{a}\sqrt{\frac{c^2-a^2}{z^2-c^2}} - \tan^{-1}\frac{z}{b}\sqrt{\frac{c^2-b^2}{z^2-c^2}}\right\}\right] \tag{9}
$$

Stress intensity factor K_{Ip} at the tip $z = c$ may be written using equations (9) and (5) as

$$
K_{Ip} = \frac{\sigma_{ye}}{2\pi}c\sqrt{c/2}\;(\pi/2 + \sin^{-1}a/c - \sin^{-1}b/c + b/c\,\cos\,\sin^{-1}b/c - a/c\,\cos\,\sin^{-1}a/c). \tag{10}
$$

4. Plastic zone and crack opening displacement

Plastic zone size at the tip $z = c$ of crack L_2 determined from condition

$$
K_{Ie} + K_{Ip} = 0. \tag{11}
$$

Substituting values from equations (7) and (10) a non-linear relation for determining plastic zone is obtained in terms of a, b, c, $\sigma_\infty/\sigma_{ye}$.

Crack opening displacement at the crack tip $z = c$ is obtained from

$$
u_c = \frac{4}{E}\,\text{Im}\left[\int\phi(z)\,dz\right], \tag{12}
$$

where function $\phi(z) = \phi_e(z) + \phi_p(z)$ is obtained after the singular parts of $\phi_e(z)$ and $\phi_p(z)$ have balanced each other. Young's modulus is denoted by E and Im // is imaginary part of the quantity in bracker. For present case it may be given by

$$
u_c = \frac{2\sigma_{ye}}{\pi E}\,c(\pi/2 + \sin^{-1}a/c - \sin^{-1}b/c)\,(b/c\,\sqrt{c^2-b^2} + c\,\sin^{-1}b/c). \tag{13}
$$

5. Example of applications

An illustrative numerical example is considered to study effect of crack length, inter crack distance, plastic zone size on the load ratio (load applied at infinity/yield stress) required for crack closure.

Figure 2 depicts variation of required load ratio as inter crack distance is increased. Crack length is taken unity. It is observed as cracks are moved apart, less load is required for plastic zone arrest. Studies also show that larger is plastic zone size more load is required for closure.

Required load ratio is plotted against increasing crack lengths in Fig. 3. As expected, for larger crack lengths less load ratio is required for closing exterior plastic zones. Increase in plastic zone size does require more load for plastic zone arrest.

Crack opening displacement (COD) at exterior crack tip as interior distance between cracks increases is shown in Fig. 4. For the load ratio calculated above, variation of COD shows that bigger the size of plastic zone, crack opens more.
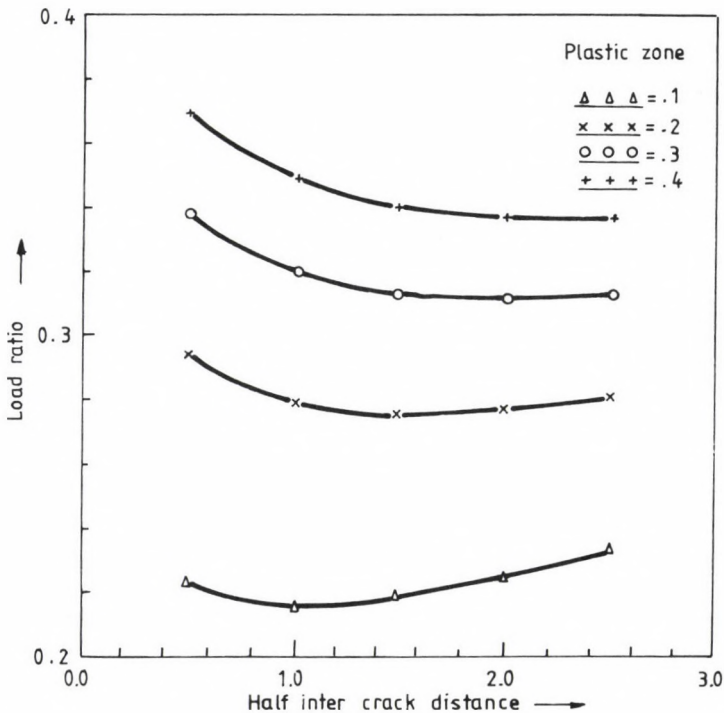
Fig. 2. Variation of load ratio versus inter crack distance
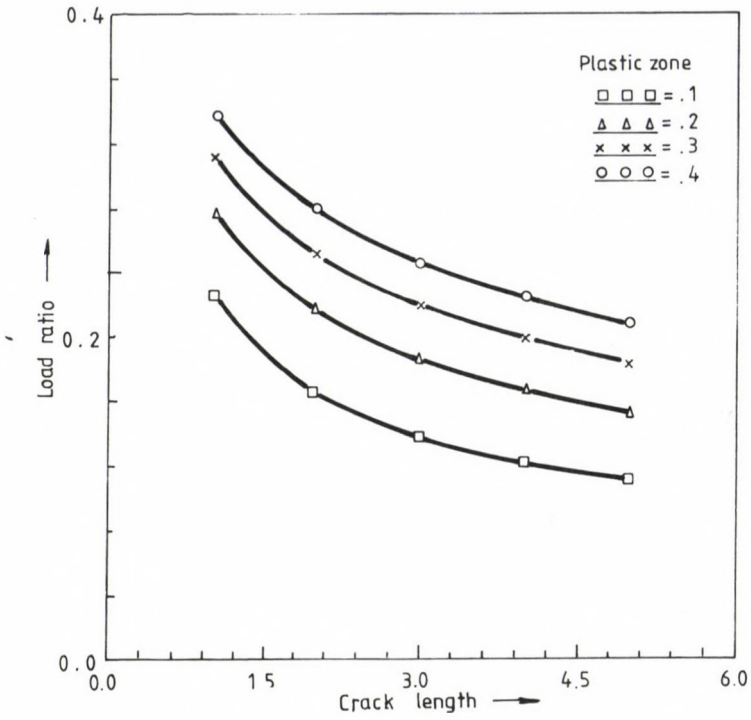
Fig. 3. Normalised load ratio versus crack length

BHARGAVA, R. R.—AGRAWAL, S. C.
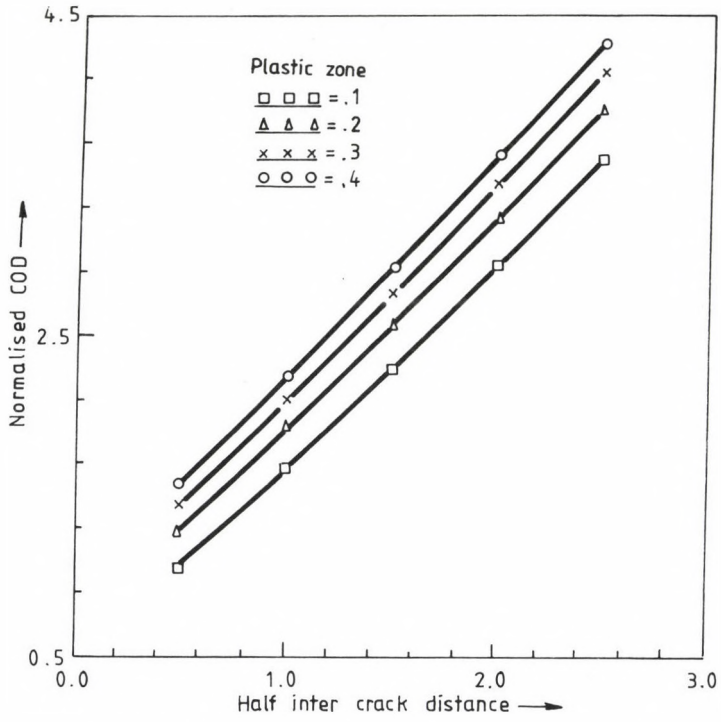
Fig. 4. Normalised crack opening displacement variation
against inter crack distance
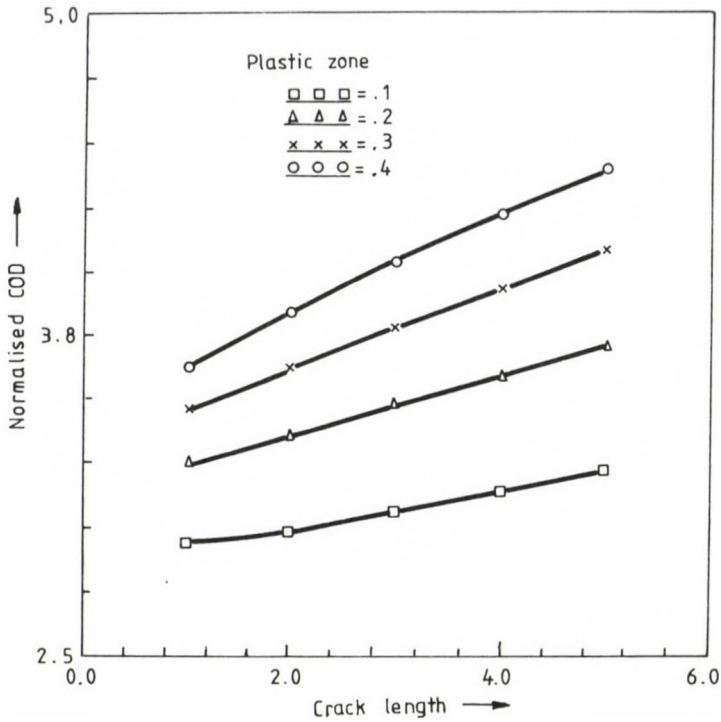
Fig. 5. Normalised COD versus crack length

Behaviour of COD as crack length increase is depicted in Fig. 5. Crack opens more as the crack length increases, as expected.

ACKNOWLEDGEMENT

REFERENCES

1. Muskhelishvili, N. I.: Some Basic Problems of the Mathematical Theory of Elasticity. Nordhoff: Groningen, Holland 1953

2. Dugdale, D. S.: J. Mech. Phys. Solids, 8 (1960), 100—104

3. Burniston, E. E.—Gurley, W. Q.: Int Journal of Fracture, 9 (1973), 9—19

4. Mishra, S. C.—Parida, B. K.: Engineering Fracture Mechanics, 22 (1985), 351—357

5. Harrop, L. P.: Engineering Fracture Mechanics, 10 (1978), 807—816

6. Vialaton, G.—Lhermet, G.—Vessiere, G.—Boivin, M.—Bahuaud, J.: Engineering Fracture Mechanics, 8 (1976), 525—538

7. Theocaris, P. S.: Engineering Fracture Mechanics, 18 (1983), 545—559

FINITE MECHANISMS HAVE NO HIGHER-ORDER RIGIDITY[*]

GÁSPÁR, ZS.[**]—TARNAI, T.[***]

In a paper, R. Connelly and H. Servatius showed an example of a non-rigid bar-and-joint assembly which was third-order rigid by their definition. Seeing this obvious contradiction they concluded that the whole notion of higher-order rigidity is questionable. In this paper, using a definition of higher-order infinitesimal mechanism we will show a method by which this contradiction could be avoided.

1. Introduction

Connelly and Servatius /1/ have examined the finite mechanism shown in Fig. 1, and they have found it to be third-order rigid by their definition. We think it is a contradiction that a structure is finite mechanism and at the same time any-order rigid. So, one of the definitions ought to be changed. Tarnai /6/ has given a definition for nth-order infinitesimal mechanisms, and we know that an nth-order infinitesimal mechanism is $n+1$st-order rigid /2/. Unfortunately, Tarnai's definition is not a constructive one. But if a structure is shown to be minimum nth-order infinitesimal mechanism then it is sure that the structure cannot be nth-order rigid.

In Section 2 a method will be shown which is suitable to determine a one-parameter system of infinitesimal displacements of the joints for this structure where the elongations of the bars have no nth- or lower-order terms. We apply the method for $n = 6$, so the structure cannot be third-order rigid (nor even sixth-order rigid) according to Tarnai's definition.

[**]Gáspár, Zsolt, H-1025 Budapest, Kapy u. 40/b, Hungary
[***]Tarnai, Tibor, H-1037 Budapest, Kolostor u. 17, Hungary
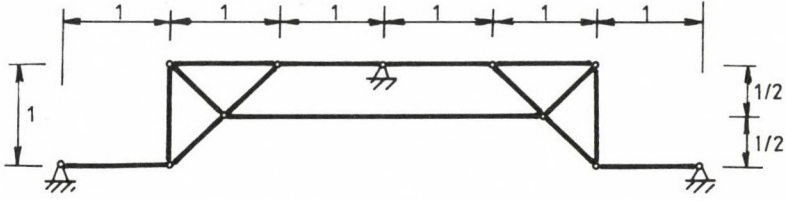
Fig. 1. The framework of Connelly and Servatius

2. Minimum 6th-order mechanism

First we recall the definition of $\underline{n}$th-order mechanism form /6/. Consider a bar-and-joint assembly which contains $\underline{b}$ bars and consider a system γ of infinitesimal displacements of the joints. Let us denote an infinitesimal displacement component of a characteristic joint — as a scalar parameter of motions — by δ and the elongation of the bar $\underline{k}$ due to δ by $\underline{e}_{k\gamma}$. Let $\underline{e}^{(i)}_{k\gamma+}(0)$ denote the $\underline{i}$th one-sided derivative of $\underline{e}_{k\gamma}(\delta)$ at point $\delta = 0$.

DEFINITION. An assembly is an $\underline{n}$th-order infinitesimal mechanism if

$$\underline{n} = \max_{\gamma} \min_{k} \left\{ \underline{h} \,\middle|\, \underline{e}^{(i)}_{k\gamma+}(0) = 0 \quad \text{for} \quad \underline{i} = 1,2,\ldots,\underline{h}; \quad \text{but } \underline{e}^{(h+1)}_{k\gamma+}(0) \neq 0 \right\}$$

$\underline{k} \in \{1,2,\ldots,\underline{b}\}$, $\gamma \in \Gamma$ where Γ is a set of all the possible systems of infinitesimal motions.

Let us consider a 4-parameter change of the nodes where 4 bars have no elongation and the incline bars (the double triangles in Fig. 1 are replaced with incline bars rigid for bending but capable for elongation) remain straight (Fig. 2):

$$\mathbf{p}_1 = \begin{bmatrix} \sqrt{1-a^2} \\ 1+a \end{bmatrix}; \qquad \mathbf{p}_2 = \begin{bmatrix} 3 - \sqrt{1-b^2} \\ b \end{bmatrix}; \qquad (1a)$$

$$\mathbf{p}_3 = \begin{bmatrix} 6 - \sqrt{1-c^2} \\ 1+c \end{bmatrix}; \qquad \mathbf{p}_4 = \begin{bmatrix} 3 + \sqrt{1-d^2} \\ d \end{bmatrix}. \qquad (1b)$$

To show that the structure is minimum $\underline{n}$th-order mechanism it is allowed to substitute the terms in form $\sqrt{1-x^2}$ by their $\underline{n}$-jet (truncation of the
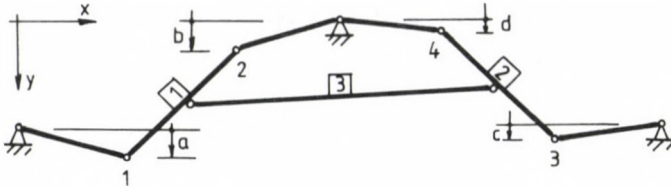
Fig. 2. Simplified model of the framework; displacements of the joints

MacLaurin series at degree $\underline{n}$) because the elongation of four bars even in this way will not have $\underline{n}$th- or lower-order terms.

We want to determine vertical displacement functions $\underline{b(a)}$, $\underline{c(a)}$, $\underline{d(a)}$ such that the first $\underline{n}$ derivatives of the elongation functions

$$e_1(a) = |\mathbf{p}_2 - \mathbf{p}_1| - \sqrt{2},$$

$$e_2(a) = |\mathbf{p}_4 - \mathbf{p}_3| - \sqrt{2}, \tag{2}$$

$$e_3(a) = \frac{1}{2}|\mathbf{p}_3 + \mathbf{p}_4 - \mathbf{p}_1 - \mathbf{p}_2| - 3$$

at the point $\underline{a} = 0$ must be zero. Function $\underline{b(a)}$ is supposed to have the form

$$b(a) = \sum_{i=1}^{n} c_i a^i, \tag{3}$$

and the coefficients can be determined one by one from the conditions

$$e_1^{(i)}(0) = 0 \qquad (i = 1, 2, \ldots, n)$$

where the superscript denotes derivation with respect to $\underline{a}$. If $\underline{n} = 6$ then

$$b = a + a^2 + a^3 + \frac{11}{4}a^4 + \frac{25}{4}a^5 + \frac{131}{8}a^6. \tag{4}$$

Because of symmetry of the structure, the relationship

$$d = c + c^2 + c^3 + \frac{11}{4}c^4 + \frac{25}{4}c^5 + \frac{131}{8}c^6 \tag{5}$$

also holds. Function $\underline{c(a)}$ is supposed to have the form

$$c(a) = a + \sum_{i=1}^{2n-5} C_i a^{1+i/2}. \tag{6}$$

Equations (4--6) are substituted into the function

$$(\mathbf{p}_3 + \mathbf{p}_4 - \mathbf{p}_1 - \mathbf{p}_2)^T(\mathbf{p}_3 + \mathbf{p}_4 - \mathbf{p}_1 - \mathbf{p}_2),$$

and the coefficients $\underline{c}_i$ can be determined one by one from the conditions that all the coefficients of terms $a^{j/2}$ $(\underline{j} \leq 2\underline{n})$ must be zero. If $\underline{n} = 6$ then

$$c = a \pm \sqrt{6}\, a^{3/2} + \frac{9}{2}\, a^2 \pm \frac{95\sqrt{6}}{16}\, a^{5/2} + \frac{93}{2}\, a^3 \pm \frac{35647\sqrt{6}}{512}\, a^{7/2} +$$

$$+ \frac{5079}{8}\, a^4 \pm \frac{24861661\sqrt{6}}{24576}\, a^{9/2}. \tag{7}$$

Depending on which sign is chosen for the terms with fractional exponent bar 3 will incline to the right or to the left.

In this way we have found a system of displacements of the joints where the first six derivatives of the elongation function of each of the bars, in the original position, are equal to zero. It means that the assembly in Fig. 1 is <u>at least sixth-order infinitesimal mechanism</u>, that is, it is at least seventh-order rigid, in contrast with Connelly and Servatius's findings. Using this technique one can continue the series expansion so that the first seven or more derivatives of the elongation functions vanish, that is, can show that the assembly is at least seventh- or higher-order infinitesimal mechanism.

3. Finite mechanism

We can go further and neglecting the visual way we can show also theoretically that the assembly is a <u>finite mechanism</u>. In this section we will use notation different from that in Section 2 (e.g., numbering the bars in Fig. 3 will be different from that in Fig. 2).

Let us consider bar $\underline{k}$ of an assembly joining joints $\underline{i}$ and $\underline{j}$ (Fig. 3a), and denote its elongation by $\underline{e}_k$ such that

$$e_k = /(x_i - x_j)^2 - (y_i - y_j)^2/^{1/2} - l_k$$

where x_i, y_i, x_j, y_j are the Cartesian co-ordinates of joints $\underline{i}$ and $\underline{j}$, and l_k is the length of bar $\underline{k}$; and let λ_k denote force in bar $\underline{k}$.

(a)

(b)
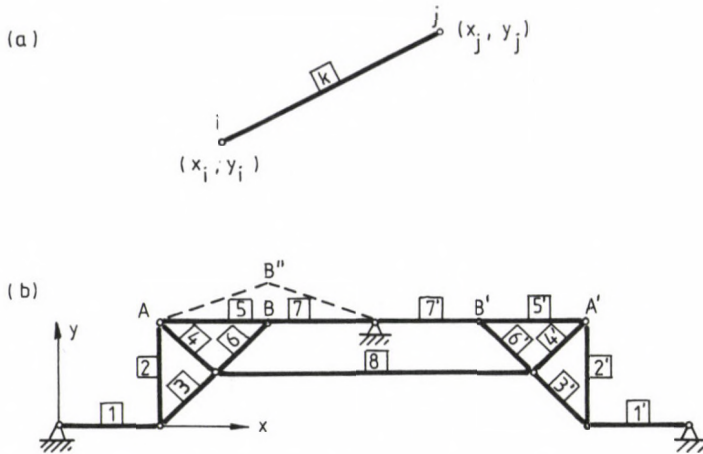
Fig. 3. Notation (a) for a bar, (b) for the whole framework

Due to the classical theory of kinematics /4/ a bar-and-joint assembly, which can have at most one state of self-stress, is a finite mechanism if function Φ such that

$$\Phi = \sum_{k=1}^{b} \lambda_k e_k$$

has no extremum at the investigated position of the assembly. (Following Levi-Civita /5/, Kuznetsov uses the theory of virtual displacements for such a problem /3/.) In fact, e_k and λ_k are constraint functions and Lagrange multiplayers, respectively, with the member constraint: $e_k = 0$ ($\underline{k} = 1, 2, \ldots, \underline{b}$); and Φ is a potential energy function.

The framework of Connelly and Servatius can be in a state of self-stress in the basic position with forces in bars:

$$\lambda_1 = \lambda_1, = 1,$$
$$\lambda_2 = \lambda_2, = -1,$$
$$\lambda_3 = \lambda_3, = \sqrt{2},$$
$$\lambda_4 = \lambda_4, = \sqrt{2},$$
$$\lambda_5 = \lambda_5, = -1,$$
$$\lambda_6 = \lambda_6, = 0,$$
$$\lambda_7 = \lambda_7, = -1,$$
$$\lambda_8 = 2.$$
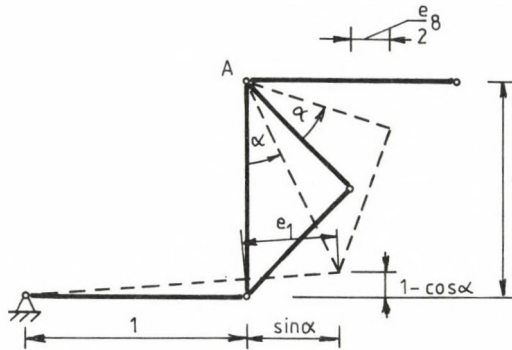
Fig. 4. Motion of members of the framework

Here the subscripts refer to the labels denoting the bars in Fig. 3b.

In the basic position $e_k = 0$ ($k = 1,2,\ldots,b$), consequently $\Phi = 0$. Let us displace joint B parallel with axis y to point B'' (Fig. 3b), but preserve all the other joints at their original place. In this case the length of bars 5, 6 and 7 will increase, the length of the other bars will not change. (An increase in the length of bar 6, however, does not play any role since this bar is inactive.) Let us denote, the common elongation of bars 5 and 7 by e. Since $e > 0$ and $\lambda_5 = \lambda_7 = -1$ we have

$$\Phi = \sum_{k=1}^{b} \lambda_k e_k = \lambda_5 e + \lambda_7 e = -2e < 0,$$

that is, for any e the value of function Φ is negative.

Let us rotate the triangles composed of bars 2, 3, 4 and 2', 3', 4' about points A and A', respectively, by angle α in opposite direction. (In Fig. 4 we have shown only the rotation of triangle 2, 3, 4.) In this case bars 5, 7 and 5', 7' remain at their original place, the lengths of bars 2, 3, 4 and 2', 3', 4' do not change, bar 8 displaces, elongates but remains horizontal. Elongations of bars are as follows:

$$e_1 = e_{1'} = (3 + 2\sin\alpha - 2\cos\alpha)^{1/2} - 1,$$

$$e_8 = 1 - \cos\alpha - \sin\alpha.$$

So we have

$$\Phi = \lambda_1 e_1 + \lambda_{1'} e_{1'} + \lambda_8 e_8 = 2\left[(3 + 2\sin\alpha - 2\cos\alpha)^{1/2} - \cos\alpha - \sin\alpha\right].$$

For small value of α we obtain

$$\Phi \approx \alpha^2 > 0,$$

that is, for small α the value of the function Φ is positive. Consequently, function Φ cannot have an extremum at the basic position of the assembly, therefore the assembly in Fig. 1 is a finite mechanism, that is, not rigid.

4. Conclusions

In spite of the fact that the assembly in the example has a cusp in the configuration space, it seems that the definition of $\underline{n}$th-order infinitesimal mechanism in /6/ works, and we conjecture that the truncation technique with fractional exponents presented in this paper can be applied for any value of $\underline{n}$. If this conjecture is true then it follows that the assembly in Fig. 1 is at least an infinitesimal mechanism of infinite order. In this way the contradiction caused by Connelly and Servatius's definition of higher-order rigidity could be dissolved.

ACKNOWLEDGEMENT

REFERENCES

1. Connelly, R., Servatius, H.: Higher order rigidity — what is the proper definition? Discrete & Computational Geometry 11 (1994), 193—200

2. Connelly, R., Whiteley, W.: Remarks on underconstrained structural systems. Preprint, Department of Mathematics, Cornell University, 1992

3. Kuznetsov, E. N.: Underconstrained structural systems. Int. J. Solids and Structures 24 (1988), 153—163

4. Kötter, E.: Über die Möglichkeit, n Punkte in der Ebene oder im Raume durch weniger als 2n-3 oder 3n-6 Stäbe von ganz unveränderlicher Länge unverschieblich miteinander zu verbinden. Festschrift Heinrich Müller-Breslau, Kröner, Leipzig, 1912, 61—80

5. Levi-Civita, T., Amaldi, U.: Lezioni di Meccanica Razionale, Vol. 1, Bologna, Zanichelli, 1949

6. Tarnai, T.: Higher-order infinitesimal mechanisms. Acta Technica Acad. Sci. Hung. 102 (1989), 363—378

ON THE STABILITY OF VISCOELASTIC SYSTEMS
WITH VISCOSITY COEFFICIENTS VARYING IN TIME

IJJAS, GY.*

Some kind of structures show collapse in the presence of creep. This is called in the literature creep buckling. From the beginning of the sixties it is known that the creep buckling is essentially an elastic one. In the beginning of the eighties the author showed that the phenomenon of collapse in the course of creep corresponds to the singularity of the Hessian of the elastic potential function of the structure where the differentiation was made only with respect to the external parameters. The material investigated was linear viscoelastic with constant coefficients. This study extends this proof to the case of linear viscoelastic material with varying viscosity coefficients, analyse the influence of temperature.

1. Introduction

The stability of viscoelastic structures was probably firstly analysed by Freudenthal /1946/ who examined the stability of an Euler column made of viscoeolastic material. His result was improved by Kempner and Pohle /1953/. Hoff /1954/ examined an Euler column. The constitutive equation of the material of the column corresponded to the constitutive equation of a non-linear dashpot. He obtained that the deformation co-ordinates (deflection) of the column tended to infinity during a finite time. He called that pheno-menon creep buckling. Later Hult /1962/ analysed, among other structures, a simple von Mises truss and he showed that the rate of the deformation of the structure became infinite during finite time, but the deformation co-ordinates remained finite. This von Mises truss was made of Maxwell fluid. That means, he did not neglect the elastic behaviour of the material, as Hoff did, and concluded: "the sudden finite jump (of the structure) is ... the results of the simultaneous occurrance of elastic and creep deformation".

---

*Ijjas, György, H-1147 Budapest, Öv u. 165, Hungary

His example later was refined by Huang /1966/ who explicitly declared: "The buckling process is instantaneous and the response during buckling is elastic." However, he did not explain this declaration. Several authors examined the buckling behaviour of different structures in the sixties and seventies, taking into account or neglecting the elasticity of the materials. Some of them gave different criteria for the buckling of the structures in the course of creep, e.g. Samuelson /1969/ and Leipholtz /1975/, but perhaps the most important studies were published by Hayman /1978, 1980/. He was the first who was looking for the connection between the elastic equilibrium paths and the buckling of simple structures made of viscoelastic materials. He essentially supposed in his study that the buckling of structures showing creep behaviour is elastic buckling. The creep of the material produces only the deformation and stress state of the structure where buckling occurs.

Before continuing our discussion on the problem we should clarify the expression "stability". We can speak about the stability of motion or equilibrium. It is evident that a structure moves during creep. However if the inert mass of the structure is neglected, as usual, than the kinetic energy and the inertia of the structure is zero, as in the case of equilibrium. On the other hand, the system cannot be considered to be in equilibrium, because in the course of creep the entropy of the system is changing. So its entropy cannot be maximum and, consequently, its potential energy cannot be minimum, which is the condition of stable equilibrium. (The definition of the potential energy can be found e.g. in the book of Brush and Almroth /1975/.) However, let us consider that the deformation parameters belong to two groups, external and internal. Their definition will be given later. The author has shown /Ijjas, 1982/ that if in the course of creep the rate of the external parameters become infinite, the Hessian of the potential function will be singular. The Hessian of the potential function contains derivatives with respect to the external parameters only. So we can speak about the stability of the structure in the sense that its potential is minimum in the space of the external parameters. The author presented its derivation in the case of viscoelastic materials with constant coefficients. In this study these results will be extended to the case of viscosity coefficients varying in time. The derivation will be based on the studies of Biot /1954/ and Schapery /1964/.

The fundamental equation of linear viscoelastic materials was set up by Biot who used the theorems of irreversible thermodynamics. Some details

of his derivation can be read in Schapery's study. Schapery pointed out that
Biot's results are valid if the viscosity coefficients are not constants.

For the sake of uniform treatment the derivation of the constitutive
law of linear viscoelastic materials from the thermodinamics will be given
at the beginning.

2. The determination of entropy production

Let us consider a closed thermodynamic system whose volume is unity in
a reference state and which has a prescribed constant temperature. We de-
compose the system into two subsystems: System I where the irreversible
processes take place and System II constituted by a large heat reservoir at
a constant temperature T (see Fig. 1). The whole system is insulated. System
I is immersed into System II. The whole system is defined by n state vari-
ables and either by temperature or by internal energy. Th n state variables
q_i (degrees of freedom, generalized co-ordinates) are of a quite general
nature. In our case they represent mechanical strains or deformation co-
ordinates. Correlatively we assume that the system is under the action of
generalised external forces denoted by Q_i (conjugate to the variable q_i)
such that $Q_i dq_i$ represents the energy furnished to the system. These forces
in our case are externally applied stresses or forces. No external forces
are associated with the temperature variables. In this paper q_i means both
internal (hidden) and external co-ordinates. The hidden co-ordinates are de-
fined by the condition that their conjugate (externally applied) forces are
always zero (see e.g. the Eqs (28) of the structure in Fig. 3).
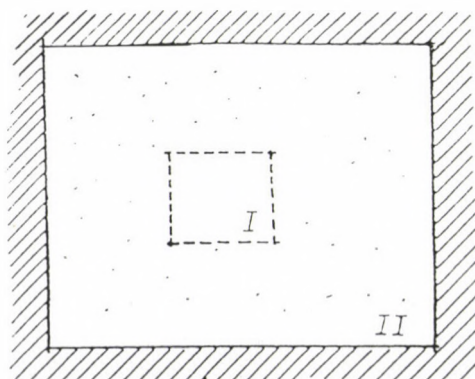
Fig. 1

The basic relationships of the thermodinamics are:

$$dU = dH + dW, \tag{1a}$$

$$dS \geq \frac{dH}{dT}, \tag{1b}$$

where T is the absolute temperature, S is the entropy and U is the internal energy of the system. W is the work done on the system, H is the beat supplied to the system. The kinetic energy is neglected. The repeated indexes mean summation.

Equations (1) show that the entropy is a function of the internal energy and of the co-ordinates of mechanical motion. So the linear increment of the change of entropy is

$$dS = (\partial S/\partial U)_{\mathbf{q}} dU + (\partial S/\partial q_i)_{U,q_k} dq_i, \tag{2}$$

where q_k denotes all co-ordinates $q_1, \ldots, q_n$ exepting q_i. The indices U and $\mathbf{q}$ or q_k mean that these co-ordinates are kept constant in the course of differentiation. (Here the bold $\mathbf{q}$ means the vector of the q_k co-ordinates.) Equation (2) is the linear member of a Taylor series of the entropy, where U and q_k are considered being independent co-ordinates, as defined above.

If the processes are very slow, the state is very near to equilibrium, so it is sufficient to take into account the linear part of entropy change. The structure behaves as if it were in equilibrium during the coursed creep, because the creep is a very slow motion and the inertia forces are negligible. The assumption of linear entropy changes is acceptable for engineering practice.

Let us examine the change of heat of Systems I and II. At first we should define the coefficients of Eq. (2). The coefficient of the first member of Eq. (2) is the partial derivative of the entropy with respect to the internal energy. In this case, all the other co-ordinates are kept constant because of the definition of the partial derivative. From the First Law of Thermodynamics the change of heat, dH, is

$$dH = dU - Q_i dq_i. \tag{3}$$

If $dq_i = 0$, which is the case of the earlier mentioned partial derivative, there is only heat transfer. Since we are examining processes very near to equilibrium, the temperature difference in every increment has to be infinitesimal. So the incremental process is defined to be reversible, and

the Second Law of Thermodynamics has the form $TdS = dH$. Thus from Eq. (3) we have

$$dH = TdS = dU. \tag{4}$$

In the case of $dq_i = 0$ the form of Eq. (2) becomes

$$dS = (\partial S/\partial U)_q dU, \tag{5}$$

Multiplying both sides of Eq. (5) by T, the result is

$$TdS = T(\partial S/\partial U)_q dU. \tag{6}$$

Comparing Eq. (6) and Eq. (4), it is evident that

$$1 = (\partial S/\partial U)_q T. \tag{7}$$

Multiplying Eq. (2) by T and taking into account Eq. (7), Eq. (2) assumes the form

$$TdS = dU + T(\partial S/\partial q_i)_{U,q_k} dq_i. \tag{8}$$

The form of Eq. (8) is the same as Eq. (3), so it is convenient to define the state function $Q_i^{(R)}$ as

$$Q_i^{(R)} \equiv -T(\partial S/\partial q_i)_{U,q_k}, \tag{9}$$

and call $Q_i^{(R)}$ a reversible force.

   While the entropy change of the reservoir, which is reversible, is $dS_{Reservoir} = -dH/T$, where the negative sign stands for the entropy decrease (the heat loss) of the reservoir, the incremental entropy change dS' of the total system is

$$dS' = dS + dS_{Reservoir} = dS - dH/T, \tag{10}$$

which is the entropy change due to irreversibility. This entropy change is readily evaluated for the system under consideration by subtracting Eq. (3) from Eq. (7):

$$dS' = (1/T)(Q_i - Q_i^{(R)})dq_i. \tag{11}$$

Dividing Eq. (11) by the time increment yields the expression for the rate at which the entropy of the whole system is produced

$$\dot{S}' = (1/T) \; X_i \dot{q}_i, \tag{12}$$

where

$$X_i \equiv Q_i - Q_i^{(R)}, \tag{13}$$

and the dot denotes differentiation with respect to time. $\dot{S}'$ is termed the entropy production per unit volume and X_i is the irreversible component of force applied to the co-ordinate q_i.

3. The constitutive law of linear viscoelastic materials

The important principle of Thermodynamics of Irreversible Processes, namely the Onsager's principle is now introduced, which can be stated as follows: If the entropy production is written in the form

$$\dot{S}' = X_i' \dot{q}_i, \tag{14}$$

then the X_i' are forces proportional to the "fluxes" $\dot{q}_i$ ($\dot{q}_i$ mean the creep rate or the rate of strain in mechanics), that is,

$$X_i' = b_{ij}' \dot{q}_j, \tag{15}$$

and the matrix of coefficients b_{ij} is symmetric. Equation (15) is, in fact, the constitutive law of the dashpot, e.g. the Newton liquid. However, b_{ij}' is not necessarily a constant in order to apply Onsager's principle, it is only required that this matrix be a continuous function of state variables for the range of applicability of Eq. (15). Equation (15) can be written in the notations (12) and (13) by setting

$$X_i' = (1/T)X_i; \qquad b_{ij}' = (1/T)b_{ij}, \tag{16}$$

so we obtain the set of equations

$$Q_i^{(R)} + b_{ij}\dot{q}_j = Q_i. \tag{17}$$

A more useful form of these relations is obtained by using definition (9) to express $Q_i^{(R)}$ as a function of q_i and T. To do so, we introduce the Helmholtz free energy F which is defined as

$$F \equiv U - TS. \tag{18}$$

The Helmholtz free energy can be defined as the "useful work" that can be done by the system. (It is different from the Gibbs free energy. The Gibbs free energy can be defined as the the "total work" that can be done by the system. See Ramsay /1971/.) We have to note the natural variables of the Helmholtz free energy are among others the temperature and the deformation co-ordinates (see Callen /1960/).

Substitution of F into Eq. (8) yields

$$dF = - S \, dT + Q_i^{(R)} dq_i, \tag{19}$$

which implies

$$-S = (\partial F / \partial T)_{\mathbf{q}}, \tag{20a}$$

$$Q^{(R)} = (\partial F / \partial q_i)_{T, q_k} \tag{20b}$$

because dF is a total differential. Using the identity (20b) permits to write Eq. (17) as

$$(\partial F / \partial q_i)_{T, q_k} + b_{ij} \dot{q}_j = Q_i, \tag{21}$$

which is a set of n equations of motion for q_i under the action of prescribed forces Q_i and temperature. This system of equations can be called as the constitutiv equations of the linear viscoelastic materials.

Equation (21) is general in the sense that we did not make any restriction on the free energy. If the system is in the neighbourhood of a reference state, the free energy can be expanded in a Taylor series, and powers higher than second order can be neglected. So we obtain

$$F = \left(\frac{\partial F}{\partial T} \right)_r \Theta + \left(\frac{\partial F}{\partial q_j} \right)_r q_j + \frac{1}{2} \left(\frac{\partial^2 F}{\partial q_i \, \partial q_j} \right)_r q_j q_i + \left(\frac{\partial^2 F}{\partial q_j \, \partial T} \right)_r \Theta q_j + \frac{1}{2} \left(\frac{\partial^2 F}{\partial T^2} \right)_r \Theta^2. \tag{22}$$

The expansion here was made according to the natural co-ordinates of the free energy. (The "natural co-ordinates" expression is used by Callen /1960/.)

Here r means the reference state and $\Theta = T - T_r$. If the temperature of the system is constant, i.e. $T = T_r$, and the reference state represents thermodynamic equilibrium, then we obtain

$$F = \frac{1}{2} \left(\frac{\partial^2 F}{\partial q_i \, \partial q_j} \right) q_i q_j. \tag{23}$$

IJJAS, GY.
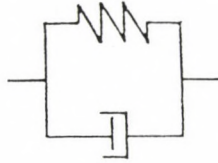
Fig. 2

If we introduce the definition

$$(\partial^2 F/\partial q_i \partial q_j) \equiv a_{ij} \equiv a_{ji},\tag{24}$$

then the expression of the free energy becomes

$$F = \frac{1}{2} a_{ij} q_j q_i.\tag{25}$$

So Eq. (21) can be written as

$$a_{ij} q_j + b_{ij} \dot{q}_j = Q_i.\tag{26}$$

Biot /1954/ called this equation "the fundamental equation of relaxation phenomena", while Schapery /1964/ called it "thermodynamic equation of motion". Let us employ Eq. (26) in the case of a very simple system, which consists of a spring and a dashpot connected in parallel (see Fig. 2). This is the so-called Kelvin model. In this case $i=1$ and $j=1$. a_{11} means the spring constant, while b_{11} is the viscosity of the dashpot /Flügge, 1975/. If a_{11} is equal to zero, then the model becomes a dashpot, while if b_{11} is equal to zero, the model becomes a spring. Let us examine a more complicated model (Fig. 3). The constitutive equations of this system are
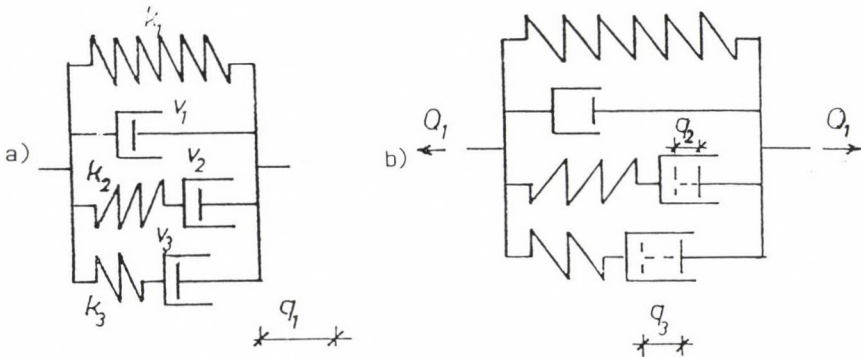
Fig. 3

$$k_1 q_1 + v_1 \dot{q}_1 + k_2(q_1 - q_2) + k_3(q_1 - q_3) = Q_1,$$
$$-k_2(q_1 - q_2) + v_2 \dot{q}_2 = 0, \tag{27}$$
$$-k_2(q_1 - q_3) + v_3 \dot{q}_3 = 0.$$

These equations express the equivalence of the external force and the resistance of the springs and the resistance of the springs and the corresponding dashpots. If Eqs (27) are rearranged, we obtain

$$(k_1 + k_2 + k_3)q_1 - k_2 q_2 - k_3 q_3 + v_1 \dot{q}_1 = Q_1,$$
$$-k_2 q_1 + k_2 q_2 \qquad\qquad v_2 \dot{q}_1 = 0, \tag{28}$$
$$-k_3 q_1 \qquad - k_3 q_3 + v_3 \dot{q}_3 = 0.$$

Taking into account the symbols of (26):

$$
\begin{array}{llll}
a_{11} = k_1 + k_2 + k_3 & a_{12} = -k_2 & a_{13} = -k_3 & b_{11} = v_1 \\
a_{12} = -k_2 & a_{22} = k_2 & a_{23} = 0 & b_{22} = v_2 \\
a_{13} = -k_3 & a_{23} = 0 & a_{33} = k_3 & b_{33} = v_3
\end{array}
$$

The parameter q_1 is an external parameter, while q_2 and q_3 are internal parameters (hidden co-ordinates). The system in Fig. 3 has not an elastic response, due to the dashpot v_1.

4. A necessary condition for the stability of linear viscoelastic materials

Now we make the restriction that we shall examine only structures made of materials having elastic response. That means that the external parameters (more precisely the rate of external parameters, i.e. the strain rates) cannot have viscous coefficient different from zero. In this case the system of Eqs (21) can be written as

$$a_{ij} q_j = Q_i \qquad\qquad i = 1 \ldots k \tag{29a}$$
$$a_{ij} q_j + b_{ij} \dot{q}_j = 0 \qquad i = k+1, \ldots, n \tag{29b}$$

where k is the number of external parameters. Now the viscosity parameters are the function of time.

The external forces usually are not conjugate to the external par-
ameters. So we have to employ a transformation if we calculate the work of
the external forces. If we restrict ourselves to conservative external
forces, i.e. if the forces can be derived from the external work by dif-
ferentiating with respect to conjugate co-ordinates, and the work of ex-
ternal forces is $W = \int P_i df(q_i)$, the (29a) can be written as

$$\frac{\partial F}{\partial q_i} - \frac{\partial W}{\partial q_i} = 0, \tag{30}$$

taking into account that $a_{ij}q_j = \partial F/\partial q_i$.

If we use the notation $V = F - W$ then Eq. (30) becomes

$$\frac{\partial V}{\partial q_i} = 0. \qquad i = 1 \ldots k. \tag{31}$$

Let us examine the stability of a structure made of viscoelastic materials
with viscosity coefficient varying in time. In this case we have to deter-
mine the time when the rate of external parameters tends to infinity (cri-
tical time). That is when the structure collapses. To obtain the rate of ex-
ternal parameters is let us differentiate Eq. (31) with respect to time.
That means

$$\frac{d}{dt}\left[\frac{\partial V}{\partial q_i}\right] = 0. \tag{32}$$

Where it was taken into account that

$$P_i df(q_i) = \int P_1 \frac{df(q_i)}{dq_i} dq_i \tag{33a}$$

and

$$\frac{d}{dt}\left[\frac{\partial W}{\partial q_i}\right] = \frac{d}{dt}\left[P_1 \frac{df(q_i)}{dq_i}\right] = \dot{P}_1 \frac{df(q_i)}{dq_i} + P_1 \frac{d^2 f(q_i)}{dq_i dq_j} = \dot{P}_1 \frac{df(q_i)}{dq_i} + \frac{\partial^2 W}{\partial q_i \partial q_j} q_j. \tag{33b}$$

Let us separate the rate of the internal and external parameters in Eq.
(32). So we have

$$\frac{\partial^2 V}{\partial q_i \partial q_1} \dot{q}_1 + \frac{\partial^2 V}{\partial q_i \partial q_j} \dot{q}_j + \dot{P}_1 \frac{df(q_i)}{dq_i} = 0, \qquad \begin{array}{l}(i = 1,..,k)\\(1 = 1,..,k)\\(j = k+1,..,n)\end{array} \tag{34}$$

where $\dot{q}_1$ means the rate of external parameters.

Equation (34) is a system of linear equations for $\dot{q}_1$. The coefficient matrix of the system is the Hessian matrix of the potential energy. So if we wish to express $\dot{q}_1$ as a solution of the system (34), then the determinant of the system is

$$\left| \frac{\partial^2 V}{\partial q_i \partial q_1} \right|.$$ (35)

One can obtain infinite value for $\dot{q}_1$ if this determinant is zero.

If this determinant becomes zero, that is the coefficient matrix of the system for $\dot{q}_1$, Eqs (34), becomes singular, that means that the Hessian of the system is singular or the minimum of the potential energy of the structure disappears in the space of external parameters. So one can conclude that the structure made of viscoelastic material loses its stability if the Hessian of the potential of the structure is singular. This criterion is very similar to the so called energy criterion of the equilibrium of elastic structures.

Let us take an example. We shall examine the structure in Fig. 4. The bar AB of the structure is made of Dischinger material. The Dischinger model is a spring and a dashpot connected in line. The dashpot has a viscosity coefficient varying with time. (This is the so-called ageing.) The constitutive equation of bar AB is

$$\frac{dq}{dt} = \frac{1}{k} \frac{dQ}{dt} + \frac{Q}{k} \frac{d\phi}{dt},$$ (36)

where q is the elongation, t is the time, Q is the component of the external force in the direction of AB, k is the spring constant and

$$\phi = \phi_{max}(1 - e^{-\lambda t}),$$ (37)

where ϕ_{max} and λ are material constants.

The equation of equilibrium of the structure is

$$-QL \cos\beta + PL \sin\beta = 0,$$ (38)

where P is the external force, β is the angle between the vertical and the BC line, and from geometrical consideration

$$q = q_D + q_{0g} = L \sin\beta,$$ (39)

where q_D is the elongation of the Dischinger model,

q_{0g} is the distance of the points A and B just before loading (geometric imperfection).
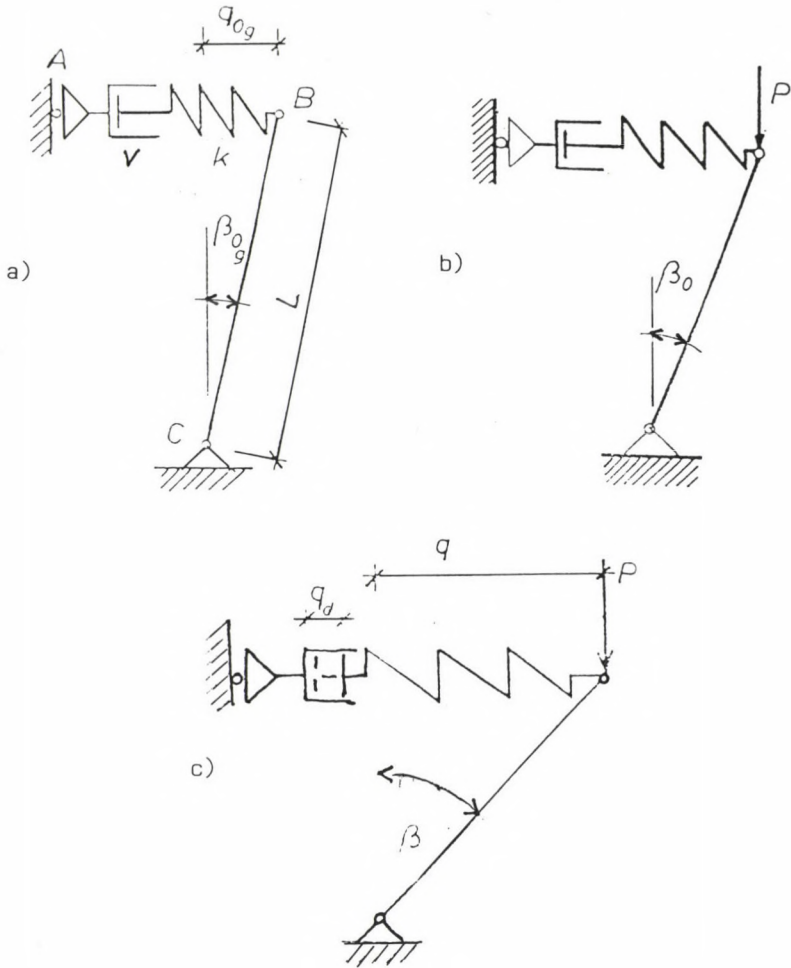
Fig. 4

Using (37), (38) and (39), we obtain from (36)

$$\frac{d\beta}{dt} = \frac{\lambda \phi_{max} \, \sin\beta\cos\beta \, e^{-\lambda t}}{\frac{kL}{P} \cos^3 \beta - 1} . \tag{40}$$

Let us calculate the potential energy of the system:

$$V = \frac{1}{2} k(q - q_d - q_{0g})^2 - PL\left[\sqrt{1 - \left(\frac{q_{0g}}{L}\right)^2} - \sqrt{1 - \left(\frac{q}{L}\right)^2} \right]. \tag{41}$$

Here q_d is the elongation of the dashpot (internal parameter).

Differentiating (41) with respect to q the result is

$$\frac{\partial V}{\partial q} = k(q - q_d - q_{0g}) - P\frac{q/L}{\sqrt{1 - \left(\frac{q}{L}\right)^2}} .$$

(42)

This expression will be used later.

Differentiating (41) two times with respect to q and taking into account Eq. (39), we obtain

$$\frac{\partial^2 V}{\partial q^2} = k - P\frac{\frac{1}{L}\left[1 - \left(\frac{q}{1}\right)^2\right]^{\frac{1}{2}} - \frac{q}{L}\frac{1}{2}\left[1 - \left(\frac{q}{L}\right)^2\right]^{-\frac{1}{2}}(-2)\frac{q}{L}\frac{1}{L}}{1 - \left(\frac{q}{L}\right)^2} = k - \frac{P}{L\left[1 - \left(\frac{\Delta}{L}\right)^2\right]^{\frac{3}{2}}} =$$

$$= \frac{kL\cos^3\beta - P}{L\cos^3\beta} = \frac{\frac{kL}{P}\cos^3\beta - 1}{\frac{L}{P}\cos^3\beta} .$$

(43)

Comparing the numerator of (43) and the denominator of (40), it can be seen that $d\beta/dt$ tends to infinity when the potential energy loses its minimum. This result is naturally, the consequence of the earlier proof.

It is worth to examine the behaviour the structure in Fig. 4 in more detail. Let us determine the rotation-time function in the case of the structure in Fig. 4. The variables in the Eq. (40) can be separated and after integration we obtain

$$t = -\frac{1}{\lambda}\ln\left\{1 - \frac{1}{\phi_{max}}\left[\frac{kL}{P}\cos\beta + \ln\frac{\left(\tan\frac{\beta}{2}\right)^{\frac{kL}{P}}}{\tan\beta}\right]_{\beta_0}^{\beta}\right\} .$$

(44)

In Eq. (44), β_0 means the initial value of β. Two $\beta(t)$ functions are plotted in Fig. 5 for two different ϕ_{max} values. If $\phi_{max} = 13$, then the $\beta(t)$ function tends to a horizontal asymptote, while if $\phi_{max} = 14$ then the $\beta(t)$ function has a vertical tangent, which gives the critical time. It is seen that the curve belonging to $\phi_{max} = 14$ "bends back". That means that the $\beta(t)$ curve has no physical meaning above β_{crit}, which is the point of loss of stability.
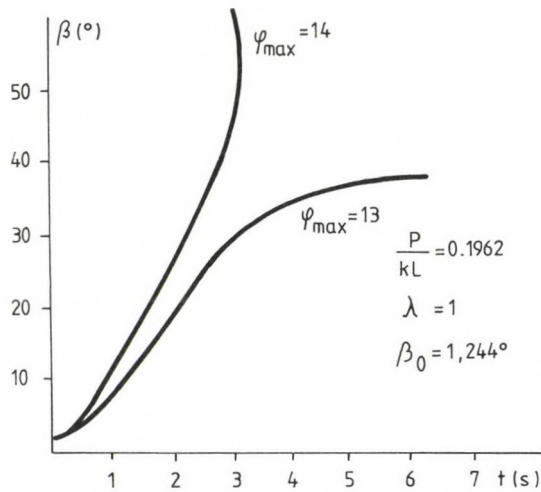
<u>Fig. 5</u>

To be come more familiar with the phenomenon, let us consider Eq. (42). This equation can be directly established by taking into account the equilibrium equation of the structure and the physical equation of the spring. The right-hand side of this equation is equal to zero which is the conclusion of Eq. (21) or (26) of the derivation sketched. Expressing the load P from this equation, a function of two variables is obtained. This function can be seen in Fig. 6 in the case of two different load levels. This figure shows that the phenomenon can be interpreted in the following way. If in the course of the process the creep stops before the load bearing capacity decreases below the load, the structure will not loose its stability (see Fig. 6b). On the other hand, if the creep continues beyond this point the structure will lose its stability (see Fig. 6a).

5. The effect of temperature

In this part we shall examine the case when $T-T_r$ is not equal to zero. Let us change Eqs (30). If we take into consideration that $F \equiv U-TS$ and differentiate it with respect to T, we shall get

$$(\partial F/\partial T)_q = (\partial U/\partial T)_q - S - T(\partial S/\partial T)_q. \qquad (45)$$

a.)

b.)
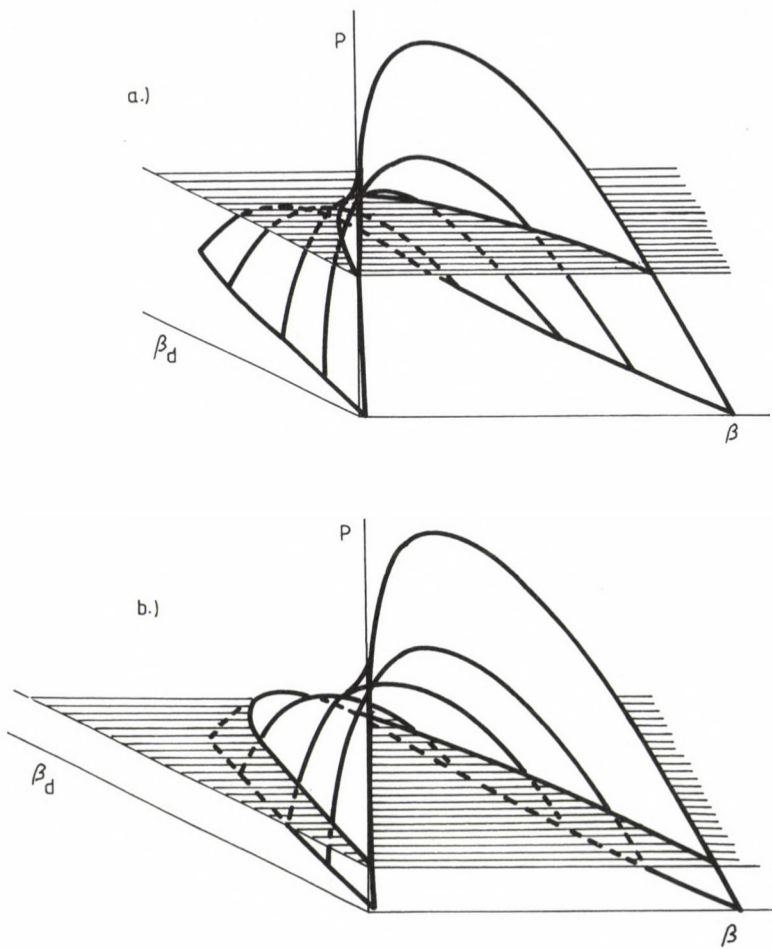
Fig. 6

Introducing (20a) into (45) the result is

$$(\partial U/\partial T)_{\mathbf{q}} = T(\partial S/\partial T)_{\mathbf{q}} = -T(\partial^2 F/\partial T^2)_{\mathbf{q}}.$$ (46)

Now it will be proven that $(\partial U/\partial T)_{\mathbf{q}} = C_{\mathbf{q}}$, where $C_{\mathbf{q}}$ is the heat capacity at constant volume. (The generalized co-ordinates are constant.)

Let us start with Eq. (3). In the case of constant volume

$$dH = dU.$$ (47)

Because of the definition $C_q = \partial H/\partial T$, consequently

$$C_q = \partial H/\partial T = \partial U/\partial T. \tag{48}$$

Taking into account (46) we shall get

$$C_q = -T_r (\partial^2 F/\partial T^2)_r \tag{49}$$

where the subscript r means the reference state at which the heat capacity is given. If we take into account the definition

$$(\partial^2 F/\partial q_i \partial T)_r = -\beta_i \tag{50}$$

and Eq. (24), then Eq. (22) will have the form

$$F = -S_r \theta + \frac{1}{2} a_{ij} q_i q_j - \beta_i \theta q_i - (C_q/2T_r)\theta^2. \tag{51}$$

If we repeat the derivation that has been shown in the fourth part, and take into consideration Eq. (51) for F, then Eqs (33) will have the form

$$\frac{\partial^2 V}{\partial q_i \partial q_1} \dot{q}_1 + \frac{\partial^2 V}{\partial q_i \partial q_j} \dot{q}_j + \dot{P}_1 \frac{df(q_i)}{dq_i} - \beta_i \dot{\theta} = 0. \quad \begin{array}{l} (i = 1...k) \\ (1 = 1...k) \\ (j = k+1...n) \end{array} \tag{52}$$

If we want to solve (52) for $\dot{q}_1$ then the determinant of the system, as was in the case of Eqs (34), will be again $|\partial^2 V/(\partial q_i \partial q_1)|$. $\dot{q}_1$ will tend to infinity if the determinant of the system is equal to zero, or the Hessian of the potential energy of the system is singular.

6. Summary

The stability of viscoelastic structures was analysed by several authors. Because of the neglection of the inert mass this phenomenon cannot be treated as the stability of motion. On the other hand, because of the increasing entropy in the course of creep, this is not identical to the problem of the stability of equilibrium. In the sixties it was recognized that the buckling phenomenon is actually an elastic one, but the connection of this phenomenon with the property of the points of the elastic potential

could not be found. Ijjas /1982/ showed the connection between the infinite
rate of deformation and the critical point of the potential energy of the
analysed system in the case of linear viscoelastic materials with constant
material coefficients. In this paper this result is generalized for material
coefficients varying with time. The influence of the temperature are exam-
ined too.

REFERENCES

Biot, M. A. (1954): Theory of stress strain relations in anisotropic viscoelasticity and re-
    laxation phenomena. J. of Applied Physics, Vol. 25, No. 11, 1385—1391

Brush, don O.—Almroth, bo O. (1975): Buckling of Bars, Plates and Shells. McGraw—Hill

Callen, H. B. (1960): Thermodynamics. John Wiley

Flügge, W. (1975): Viscoelasticity. Springer Verlag

Freudenthal, A. M. (1946): Some time effects in structural analysis. Report 6th International
    Congress for Applied Mechanics, (unpublished) see also

Freudenthal, A. M. (1950): The Inelastic Behaviour of Engineering Materials and Structures.
    John Wiley and Sons, New York

Hayman, B. (1978): Aspects of creep buckling. Proc. R. Soc. Lond. A. 364, 393—414, 415—

Hayman, B. (1980): Creep buckling-A general view of the phenomena. In: Creep in Structures,
    eds: A. R. S. Ponter, D. R. Hayhurst. IUTAM Symposium, Leicester, 289—307

Hult, J. (1962): Oil canning problem in creep. In: Creep in Structures, ed.: N. J. Hoff.
    Academic Press, 161—173

Huang, N. C. (1966): Nonlinear creep buckling of some simple structures. IRPA 66—80,
    April, 1966

Ijjas, Gy. (1982): Buckling of viscoelastic structures. Acta Technica Acad. Sci. Hung.,
    Vol. 95, No. 1—4, 55—61

Kempner, J.—Pohle, F. V. (1953): On the nonexistence of a finite critical time for linear
    viscoelastic columns. J. of the Aeronautical Sciences, 572—573

Leipholtz, H. H. E. (1975): An attempt to refine certain stability concepts. Proc. of the Fifth
    Canadian Congress of Appl. Mech. Fredericton, May 26—30, 1975, G61—G74

Ramsay, J. R. (1971): A Guide to Thermodynamics. Chapman and Hall Ltd.

Samuelson, L. A. (1969): Creep buckling of a circular cylindrical shell. AIAA Journal, Vol. 7,
    No. 1, 42—49

Schapery, R. A. (1964): Application of thermodynamics to thermomechanical fracture, and
    birefringent phenomena in viscoelastic media. J. of Applied Mechanics, Vol. 35, No. 5,
    1451—1465

EXPERIMENT TO INVESTIGATE THE COMMON LOSS
OF STABILITY OF EDGE BEAMS IN COMBINATION WITH HYPERBOLIC
PARABOLOID SHELL SUPPORTED ALONG THE GENERATRICES

JANKÓ, L.[*]—SZITTNER, A.[**]

After preliminary theoretical studies, experiments have been run to investigate the buckling of edge beams of the hyperbolic paraboloid shell supported along the generatrices, with a view to make clear how does the edge beam loose its stability, taking the stiffening effect of the shell into consideration.

By changing the thickness of the edge beams gradually, the effect of flexural rigidity on the loss of stability of the shell interacting with the edge beam could be investigated.

It was found that in the geometrical domain investigated (i.e. in case of a shell relatively rigid as compared with the edge beam), neither shell buckling nor edge beam buckling (bifurcation) had taken place. Instead, a loss of stability by equilibrium limitation (divergence of equilibrium; snap-buckling) has occurred.

An empirical relationship has been set up to calculate the critical load.

1. Introduction

In shell construction, the hyperbolic paraboloid (hypar) shell supported along the generatices is one of the structures most frequently used.

Studies of the simple buckling phenomenon of a hyperbolic paraboloid shell of linearly elastic material supported along the generatrices (hypar limited by straight generatrices), geometrically perfect, flat, isotropic (or orthotropic), rectangular or oblique, under uniformly distributed load in the ground plan, are considered to be a known field /1—4, 9—10, 12—13/.

However, the buckling of edge beams is a different question. The buckling of two-hinged edge beam has been studied theoretically by Dayaratnam and Gerstle /1/ and our accurate calculations based on their approximate results as well as a method we have developed for the buckling of

[*]Jankó, László, H-1091 Budapest, Üllői út 117, Hungary

[**]Szittner, Antal, H-1026 Budapest, Gárdonyi u. 32, Hungary

the cantilever edge beam are presented in /7/. According to this method, the stiffening effect, acting as an "elastic foundation", of the shell interacting with the buckling edge beam to be relieved, was determined on the basis of /5/.

Note that our solution in /5/ applies to a conservative system of forces while the shear force acting upon the edge beam is non-conservative because it follows the shape of the buckling edge beam (i.e. it is directionally not stable). At the same time, the directional stability of the shear force is relatively insignificant because of the flatness.

Leet /10/ was the first to run experiments to thoroughly investigate the buckling of the edge beams of the hyperbolic paraboloid shell supported along the generatrices. An evaluation of his results was also published by Gioncu /4/. In order to make clear the phenomena not investigated by Leet and as a continuation of our theoretical solution given in /7/, we have run experiments. By changing the thickness of the edge beam gradually, we have got suitable information about the effect of flexural rigidity EI (relating to the horizontal axis, cf. Fig. 20) of the edge beam on the loss of stability as well as on the extent of interaction between the shell and the edge beam.

It was investigated whether buckling (bifurcation) of the edge beam had taken place indeed at all. In the geometrical domain investigated (i.e. in case of a shell relatively rigid as compared with the edge beam), the loss of stability was found to result rather from equilibrium limitation than from bifurcation (divergence of equilibrium; snap-buckling).

Presented in this work are the experimental results obtained by Szittner, Kálló, Kaltenbach, Köröndi and Kristóf, described in detail in /14/, together with the evaluation thereof as well as the conclusions drawn by us.

The reader's attention is directed to Section 4 describing the circumstances under which the experiments could have come about.

2. Description of the experiments

2.1. Experimental program

2.1.1. Support conditions

The models are presented in Fig. 1, the dimensions being given in mm in Figs 1 and 8. The edge beams of models 1-5 are <u>cantilever</u> edge beams supported at the low corners continuously along a length of about 45 mm in both directions by means of 2 M6 bolts and washers at each point, by clamping through the ribs (Fig. 2). In models 1 and 5, steel spacers were placed to transfer and/or distribute the clamping force of the bolts.

One of the two supports was a fixed support while the other support was diagonally slightly adjustable so that the adjustment of the geometry of the shell model would best simulate the geometry according to the plan.

The edge beams of model 6 were supported by means of <u>pendulum props</u> at the high corners (Fig. 3) while they were clamped in the way described above at the low corners.

2.1.2. Geometrical data

Theoretical thickness of the plexiglass shell plate: $h = 1.5$ mm. In the ground plan, the hyperbolic paraboloid shell supported along the generatrices is a square with a side length of $2a = 2b = 560$ mm (Fig. 1), the theoretical rise of the hypar shell being $f = 70$ mm.

In the ground plan, the outline dimension is $2A = 2B = 580$ mm in case of each model.

The thickness of the rectangular edge beams is $b_0 = 10$ mm in case of each model, the height varying as follows: $m_1 = 15$ mm, $m_2 = 12$ mm, $m_3 = 8$ mm, $m_4 = 4.5$ mm, $m_5 = h = 1.5$ mm, $m_6 = m_2 = 12$ mm. In model 5, the edge is not stiffened at all.

In this work, **w** is used for the vertical displacements of the surface points (Figs 8 and 15--19). The geometrical <u>imperfections</u> w_0 of the above structure considered to be geometrically perfect are specified in /14/ (for the most important values see Figs 15, 16).
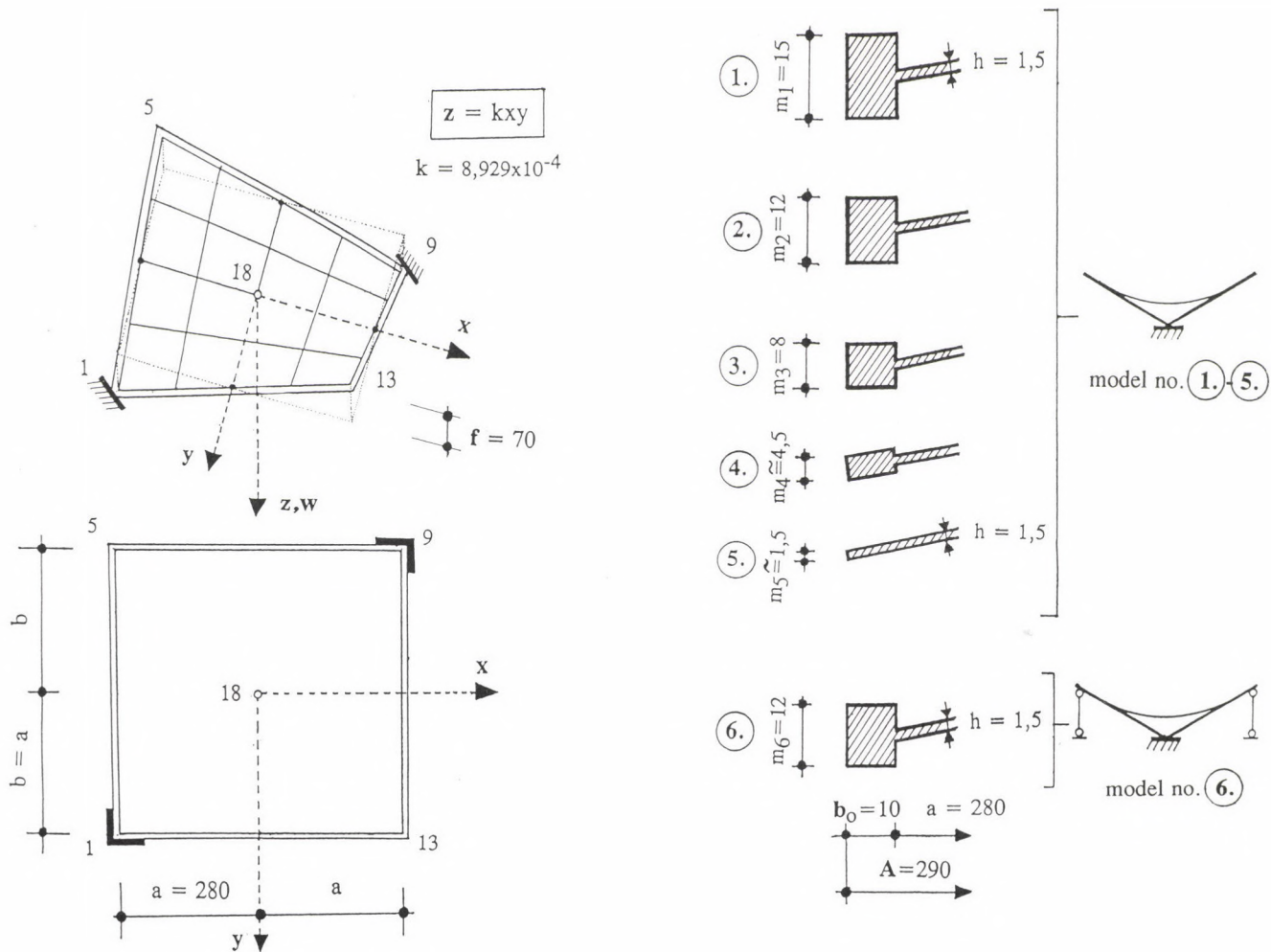
Fig. 1. General arrangement. The models studied
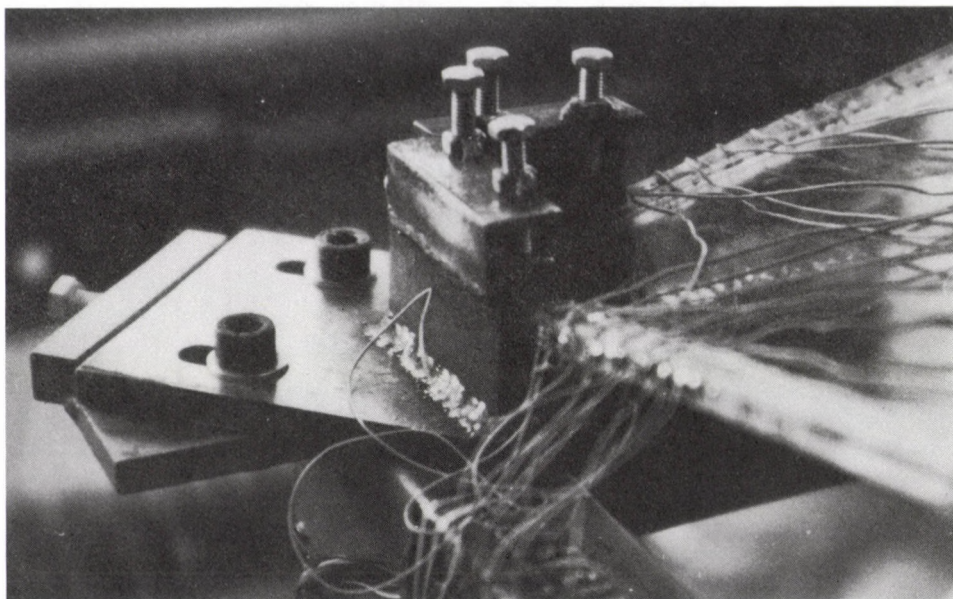
Fig. 2. Clamping fixture (Models 1—6)

2.1.3. Choice of the material of the models

In planning for the program of the model experiments, first thing to do was to choose the appropriate material for the required geometrical parameters (thickness-span relation) to be used in the model experiments, taking the distorted surface geometry of the shell into consideration. The thinnest (1.5 mm) plexiglass (monomethyl metacrylate) plate commercially available in Hungary for the time being was found to be suited for the purpose, among others because the plexiglass could be sticked with its own material relatively successfully and it can be formed at certain temperatures.

The elastic characteristics of the material were determined by means of tensile tests using tensile test bars cut away from the edge of the heat-treated models. Two tensile test bars were used to determine the material characteristics, with 1 longitudinal and 1 transversal resistance strain gage (Kyowa, type KFC-5-C1-11) sticked on either surface of each specimen.

The average values of the results obtained for the modulus of elasticity (E) and transverse contraction factor (μ) on the basis of 16 data for each are tabulated in Table I.

JANKÓ, L.—SZITTNER, A.
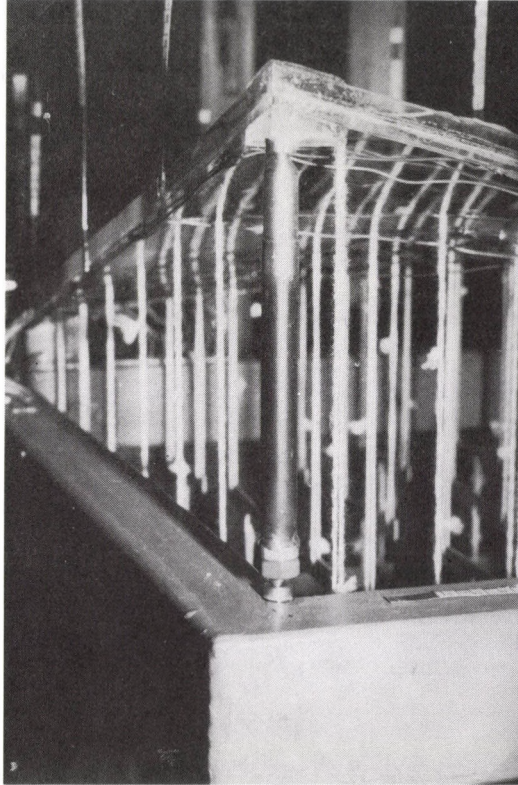
Fig. 3. Pendulum prop (Model 6)

Table I. Material characteristics

σ /Nmm^{-2}/	E /Nmm^{-2}/	μ /-/
Stress domain	Modulus of elasticity	Transverse contraction factor
0—20	3200	0.365

2.1.4. Model making

The plexiglass plate of a thickness of 1.5 mm was cut into six about 650 x 650 mm squares. This pieces of plexiglass plate were used to produce the hyperbolic paraboloid shells of distorted surface. For this purpose that is, to form the surfaces, the heat-treating furnace used for optical stress

measurements by the Department of Mechanics, Faculty of Mechanical Engineering, Technical University of Budapest, was put at our disposal.

The template was made of pieces of a 630 mm long steel strip of a cross section of 0.8 x 19 mm in accordance with the straight surface generatrices. A baseframe was made of full steel sections, with a frame of an inclination of 1:4, made of pieces cut out of a 10 mm thick steel plate, welded on it. Between the two pairs of opposite edges of the frame, there was a difference of 19 mm in height in compliance with the height of the steel strip. The 750 steel strips were arranged edgeways, side by side, on one of the two pairs of opposite edges of the approx. 600 x 600 mm frame. The steel strips, properly pressed together and arranged, were welded together and then to the frame from below. The surface so obtained was smoothed to eliminate the 0.2 mm steps by means of a manual corner grinder: Fig. 4.

The template so produced was used to mould the plexiglass plate of a thickness of 1.5 mm. In doing so, the plexiglass plate was laid onto the template. Six layers of rubber plates of a thickness of 3 mm each were laid onto the plexiglass plate lying on the template, which, due to their own weight, were expected to help the plexiglass plate to take the shape of the template. The plexiglass plate which had experienced thus elastic defor-

Fig. 4. The template used

mation was then placed, together with the template and the rubber plates, in the heat-treating furnace heated to a temperature of 180 $^\circ$C. This relatively high moulding temperature was required because at lower temperatures, a "freezing" of the correct shape could not have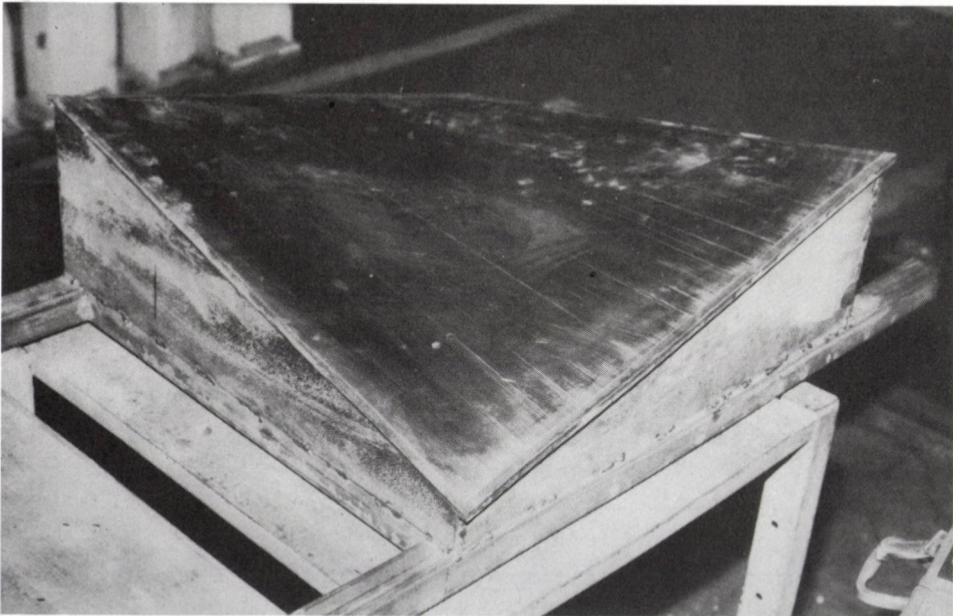 been achieved. The heat-treatment took a time of 1 hour and the furnace, still closed, was allowed to cool for about 24 hours.

The shells so obtained were cut first to the originally planned size of 600 mm. However, it was found that because of deformation of the over-hanging parts, more correct models could be obtained if 10 mm or 15 mm were cut away from the shells on every side. Since imperfections in geometry were still detectable after the edges had been cut away, the finished shells were heat-treated again, one by one, in the way described above.

The ground plan dimensions of the shells of models 1, 2, 3 and 6 are, in the last analysis, 570 x 570 mm because these models have grooved edge beams. The edge beams of these models were made of plexiglass plate of a thickness of 10 mm with a groove of a width of 2 mm and a depth of 5 mm cut into the centre of one of the higher sides of the edge beam, designed to receive the shell. The shell plate fits into the groove of a width of 5 mm which corresponds to half of the edge beam width of $b_o = 10$ mm. The shell so assembled and the edge beams have been sticked together by waste plexiglass dissolved in chloroform.

The ground plan dimensions of the shell of models 4 and 5 are 580 x 580 mm because the edge beam of model 4 has been produced by sticking plexiglass strips of a width of 10 mm and a thickness of 1.5 mm on the top and bottom surfaces while for model 5, no edge beam has been provided at all.

The finished model located on the steel baseframe is shown in Fig. 5.

2.1.5. Load

For the sake of an (approximately) uniform distribution of the load acting upon the models, the load was transferred to the shells at $8 \times 8 = 64$ points located at a uniform spacing in both directions in the ground plan network. Holes of a diameter of 2 mm were bored at the loading points (network nodes) at right angles to the surface, through which as well as through the M2 washers located there the pair of cords connected to the first rocker element was led and then fixed by means of a mandrel.

Two-support distributing rockers were used for load distribution (Fig. 6). Altogether five rows of rockers were used, arranged one under the other and interconnected by cords; with a rocker element connected to the
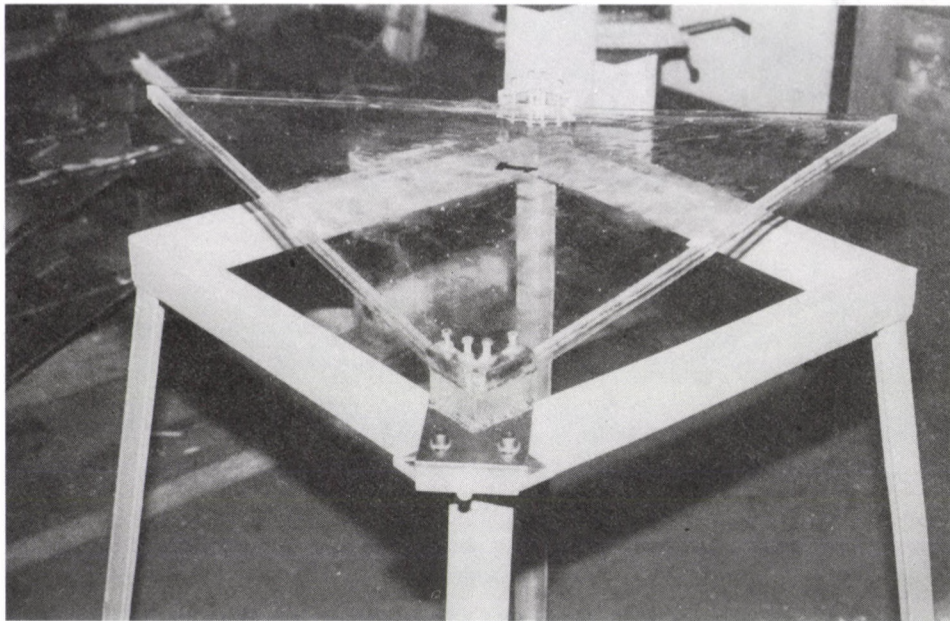
Fig. 5. Model on the baseframe (Models 1—5)
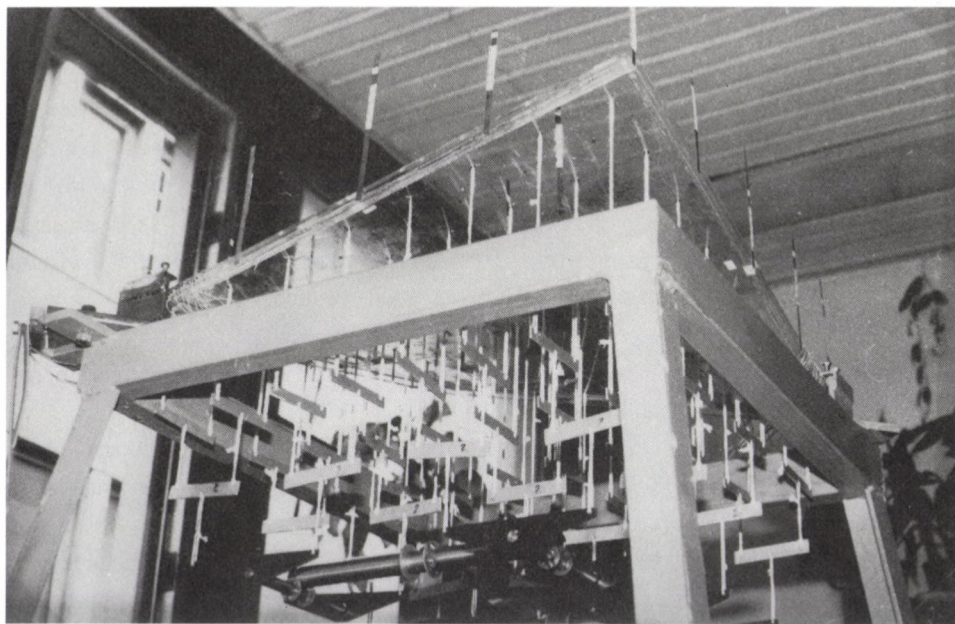
Fig. 6. Rocker system
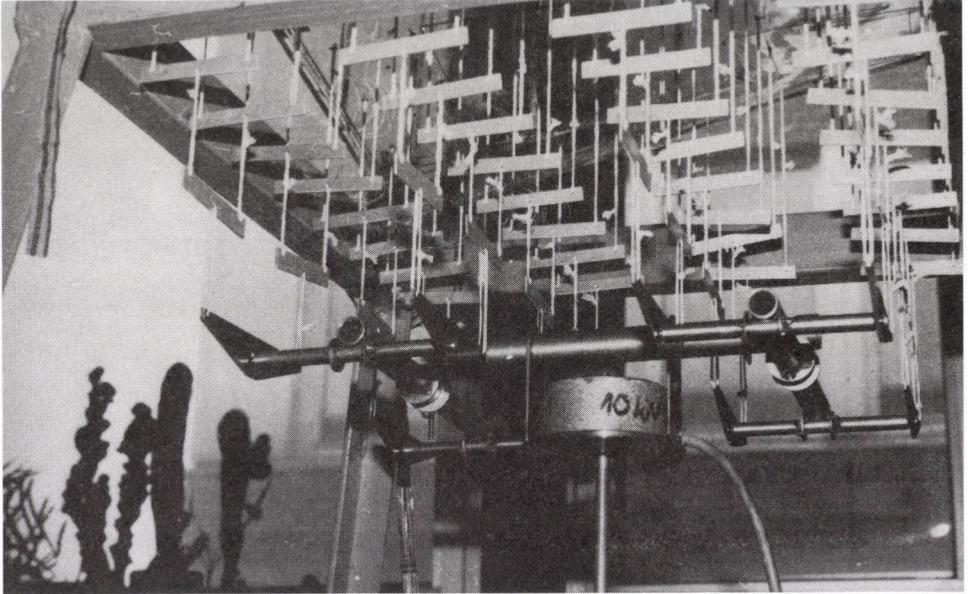
Fig. 7a. Load transfer to the rocker system (Models 1, 2, 3, 6)

loading fixture arranged among the elements of the sixth row. The first row
of rockers included 32 while the second 16 elements, consisting of small
aluminium beams of a cross section of 2 x 12 mm and 2 x 15 mm, respectively,
with a span length of 72.5 mm. The rocker elements with a span length of
145 mm of the third row of rockers were made of steel plate in case of
models 1, 2, 3 and 6 while of aluminium plate in care of models 4 and 5 of
reduced load. The fourth and fifth row of rockers as well as the sixth
rocker element were made of steel in case of models 1, 2, 3 and 6 while,
with a view to reduce the base load, of wood in case of models 4 and 5.

The length of the cords interconnecting the shell and the first row
of rockers was determined so that a rearrangement of the network due to de-
formations would practically not be hindered.

In case of models 1, 2, 3 and 6, the load acting upon the upper steel
plate was transferred to the rocker element in the sixth row through a
pressure load cell (Fig. 7a). A 10 kN load cell was used, permitting the
values of the weight to be recorded electronically with an accuracy of
0.2-0.5% (20-50 N). The loading weights were placed on a rigid steel bar
(Fig. 7b).

In case of models 4 and 5, load was applied to the rocker element in the sixth row simply by suspension, using a loading tray (Fig. 7c). The loading weights weighed in advance were placed in the tray.

In recording the values of load applied to the model, the weights used as well as the dead weight of the rocker system and of the model were taken into consideration.

When load was applied to the model, the first step was to apply a load corresponding to the sum of the dead weight of the model and the weight of the first four rows of the rocker system, called load 0 (zero), in every case. The next step was to add the sum of the weight of the fifth and sixth row of rockers, the loading tray and the load cell to load 0. This load is called load 1. In the subsequent steps, load 1 was considered to be the unloaded condition that is, the basis for comparison. For loading and/or relieving of the model, a hydraulic lifter was placed under the loading tray

Fig. 7b. Load transfer to the rocker system
(Models 1, 2, 3, 6)
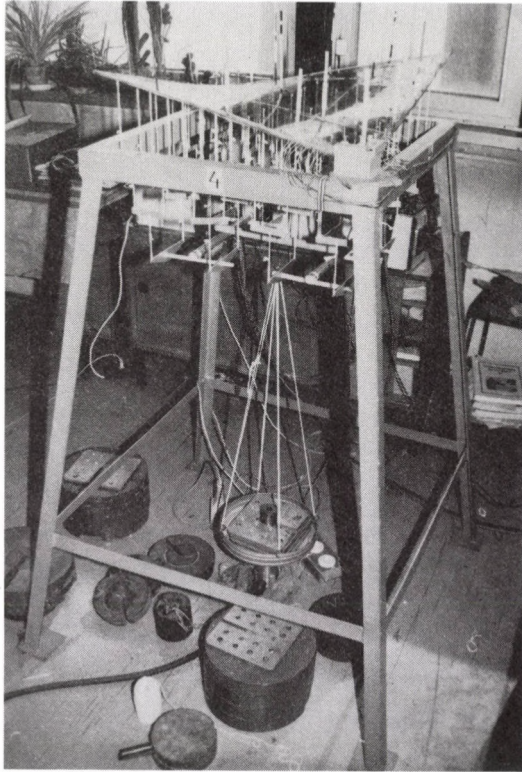
Fig. 7c. Load transfer to the rocker system
(Models 4, 5)

(Fig. 7b), permitting not only the model to be loaded and relieved but also
a complete destruction of the model to be avoided in case of a possible
loss of stability of the model (with the distance between the top of the
lifter and the bottom of the loading tray kept within 1-2 mm upon loading).

Between the different load steps, we have always returned to load 1.
As a result of this relief, also the effect of creep has become negligibly
small.

2.2. Model measurements

Deflection and stress measurements were made under every load and
whenever the model was unloaded.

2.2.1. Deflection measurements

Deflections of the model were measured by levelling by means of 21 levelling gages (Fig. 8) sticked on the upper surface of the model and on the outer edges of the edge beams. Two levelling stations were provided for every model experiment, using MOM Ni A-31 superior-quality levelling instruments for measurement. In accordance with the spacing of the levelling gages (5 mm), the sensitivity of the measurements (minimum unit of measurements) was 0.05 mm. Because of the thickness of the line indicating the points as well as of the inclination of the levelling gages under load, the measuring error was somewhat higher but it still lay below 0.1 mm. To interrelate the two measuring instruments and/or the results of measurements, the saddle point (18) was measured by both instruments. The deflection (vertical displacement) was measured as the difference in height as compared with the initial load (load 0 according to 2.1.5.).

levelling points :   1 – 21
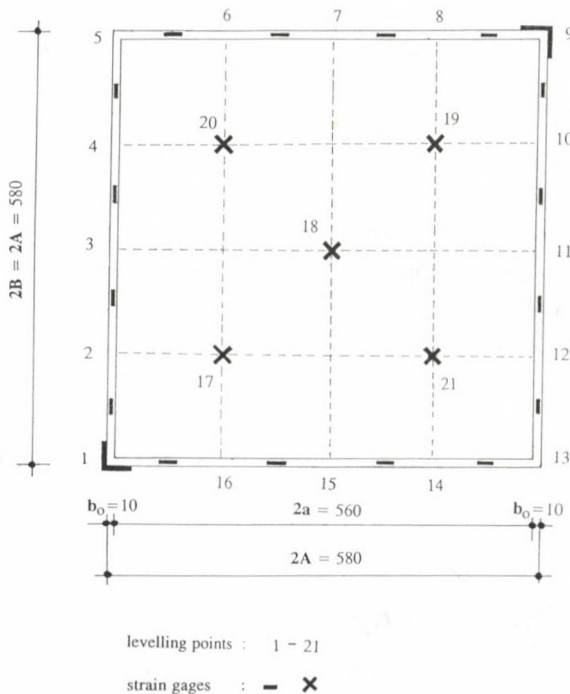
strain gages   : ▬ ✕

Fig. 8. Levelling points for deflection measurements. Arrangement of measuring strain gages (Models 2—6)

2.2.2. Stress measurements

In order to distinguish the normal stresses and bending stresses, a measuring rheostat was located on both the top and bottom surfaces of the shells and edge beams (Fig. 8).

Considering the state of uniaxial stress prevailing there, simple KFC-5-C1-11 measuring rheostats with a measuring base of 5 mm were used for the edge beams and free edges (model 5).

At points arranged coincidently with the axis of symmetry (which could therefore be characterized by known principal stress directions), two rosette type measuring elements (KFC-2-D2-11, measuring base: 2 mm) were arranged at right angles to each other, their direction coinciding with the principal stress direction (with the axis of symmetry). Stresses σ_x, σ_y were calculated on the basis of extensional strains ε_x, ε_y measured, using the well-known relationships of the state of plane stress.

For Model 1, so-called three-dimensional rosettes (KFC-2-D4-11) arranged at angles of 3×120° at points of general position were used. These three-directional rosettes were used for Model 1 only. Namely, significant stresses had not been measured on the shell points but only on the edge beams of Model 1 and therefore, in case of Models 2—6, measuring elements have been located on all the four edge beams with a view to detect a possible asymmetric behaviour of the edge beams more accurately and thus three-directional rosettes have not been used here.

A CMP 16 measurement center with digital display, produced by Hottinger, was used for extension measurements in application with an MG 32 measuring amplifier of a carrier frequency of 225 Hz, with DATCON measuring point transformers interposed. An AT 286 PC was used for data collection and processing.

To document the results of measurements, the extensional strains measured in the lower and upper extreme fibres, the extreme fibre stresses calculatable on the basis thereof as well as the normal and bending stress components determined on the basis of the extreme fibre stresses were tabulated /14/ for each point of measurement.

2.3. Results of the model experiments

2.3.1. Model 1

Some seconds after the last load step had been applied, the model collapsed and it broke into pieces (Fig. 9). The relationship between surface load q and deflection w_{18} of the shell center, determined in the course of the experiment, is diagrammatically illustrated in Figs 15—16.

2.3.2. Model 2

20-30 seconds after the last load step had been applied, the model sunk down and the load got up onto the hydraulic working cylinder. An absolutely elastic loss of stability has taken place, permitting Model 2 to be used later for construction of Model 6. See also Figs 15—16.
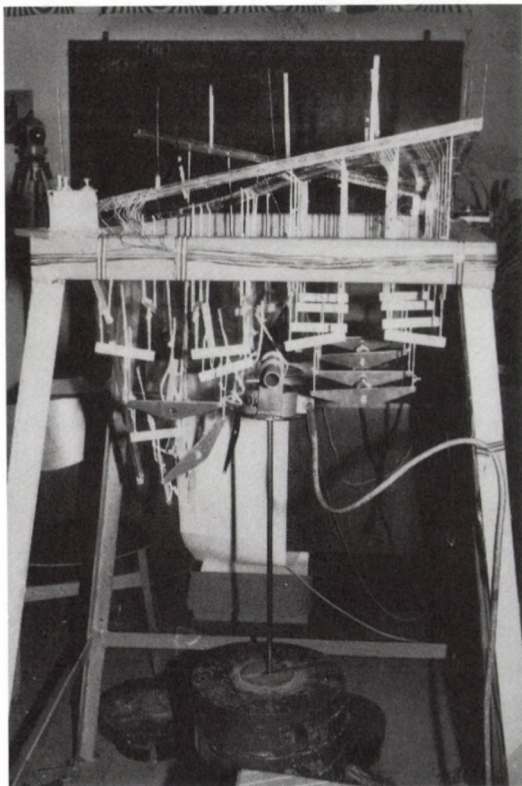
Fig. 9. Loss of stability of Model 1
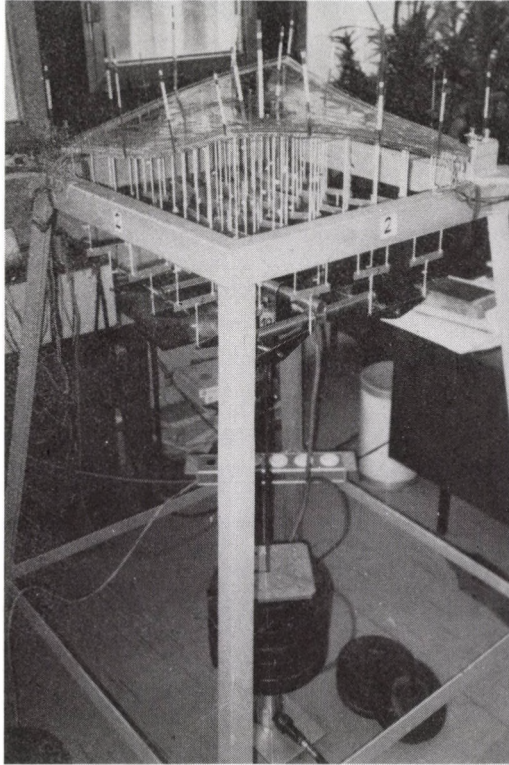
Fig. 10. Loss of stability of Model 2

2.3.3. Model 3

A loss of stability similar to that in case of Model 2 has taken place as shown in Fig. 11. See also Fig. 16.

2.3.4. Model 4

The loss of stability took place shortly after the load had been applied and the model got up onto the hydraulic working cylinder. The state before destruction is shown in Fig. 12. Significant permanent deformations were measured after relief, suggesting that the model had experienced plastic deformation. See also Fig. 16.
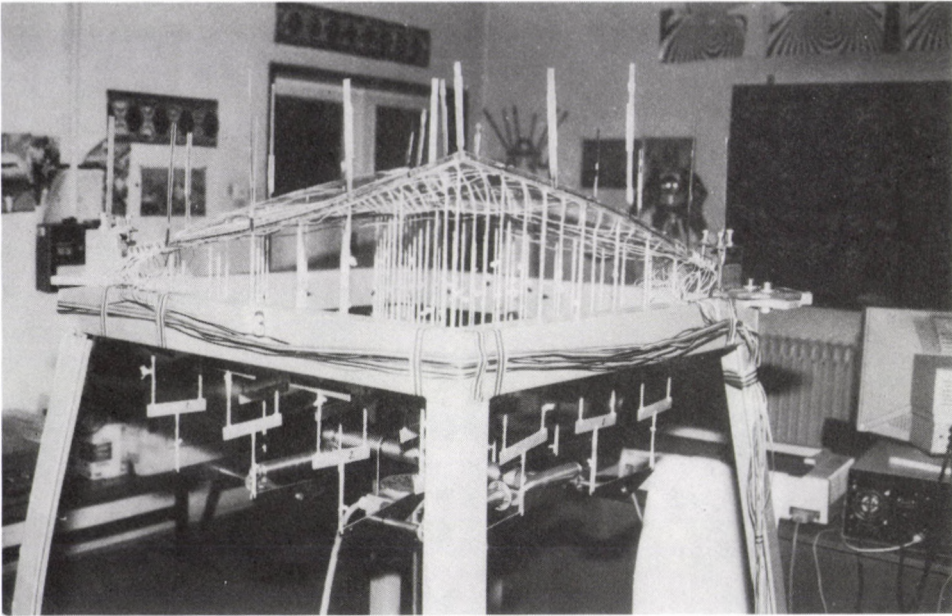
Fig. 11. Loss of stability of Model 3
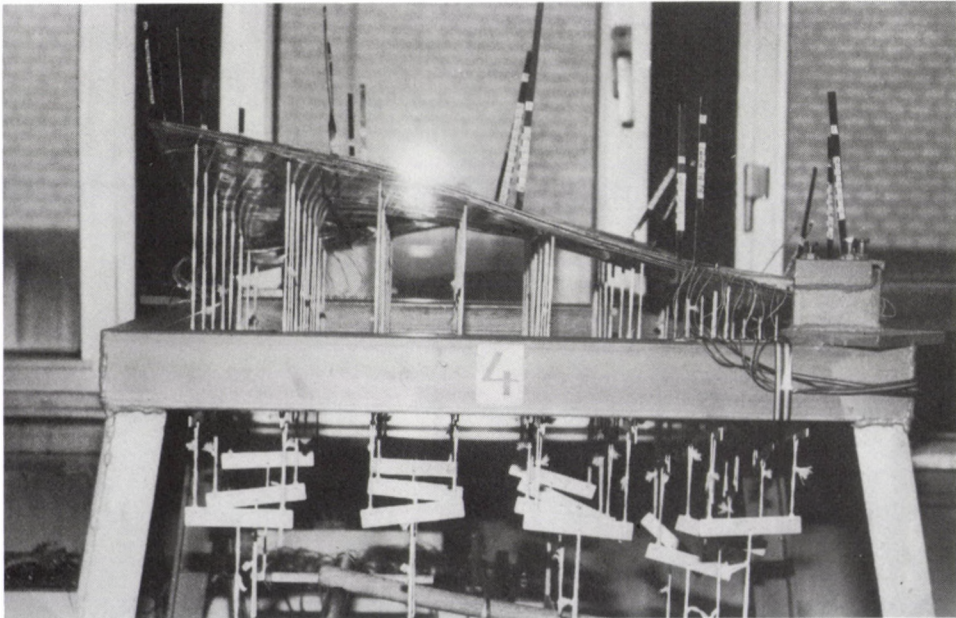
Fig. 12. Loss of stability of Model 4
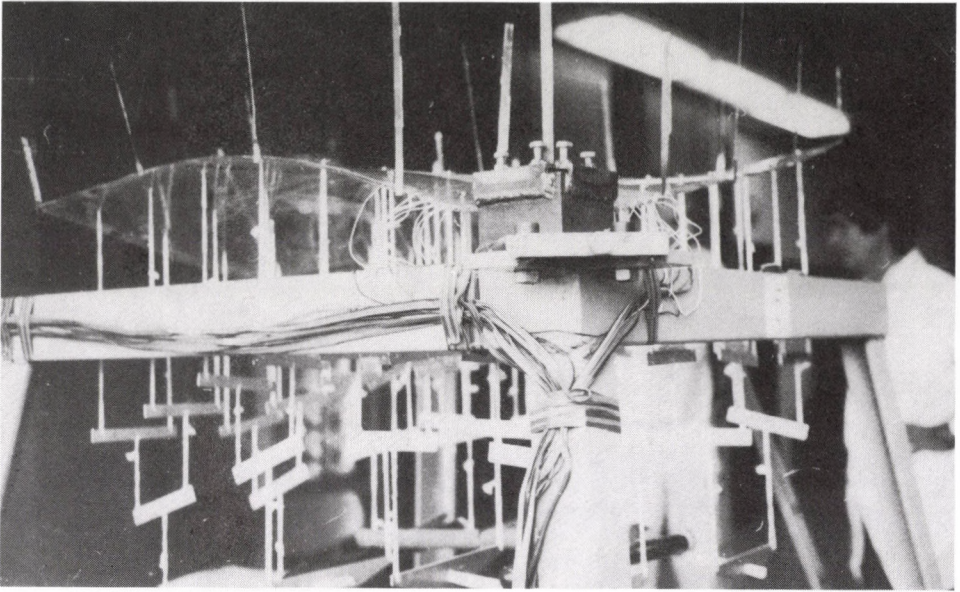
Fig. 13. Loss of stability of Model 5
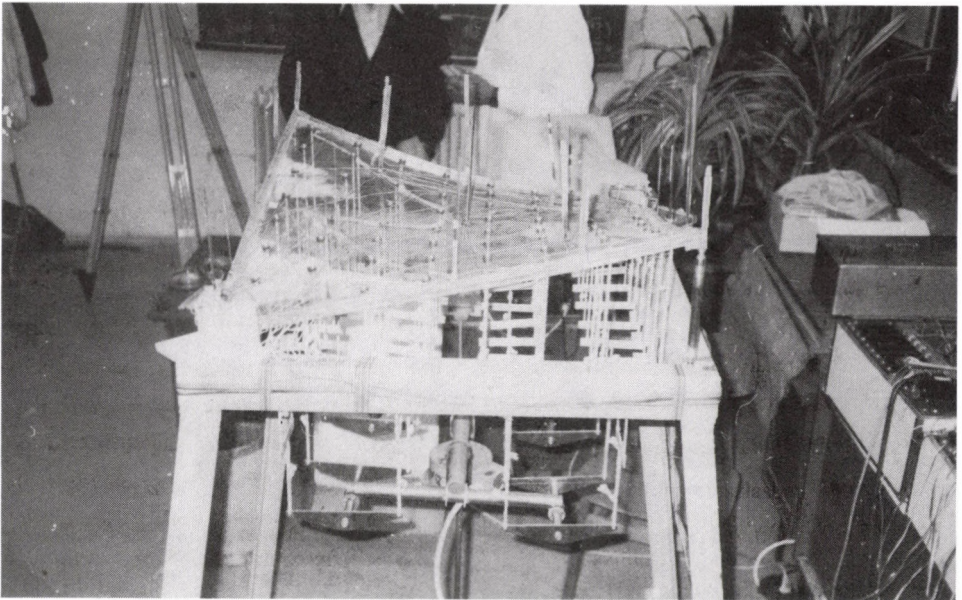
Fig. 14. Loss of stability of Model 6

2.3.5. Model 5

The perfectly unstiffened shell has lost stability after the significant deformation illustrated in Fig. 13 and the model got up onto the hydraulic unit. See also Fig. 16.

2.3.6. Model 6

Figure 14 shows the model, also supported by pendulum props, at the instant before buckling. The model has got up onto the hydraulic press about 5 minutes after the last load step had been applied. A slight permanent deformation has been recorded after relief subsequent to the loss of stability. See also Fig. 15.
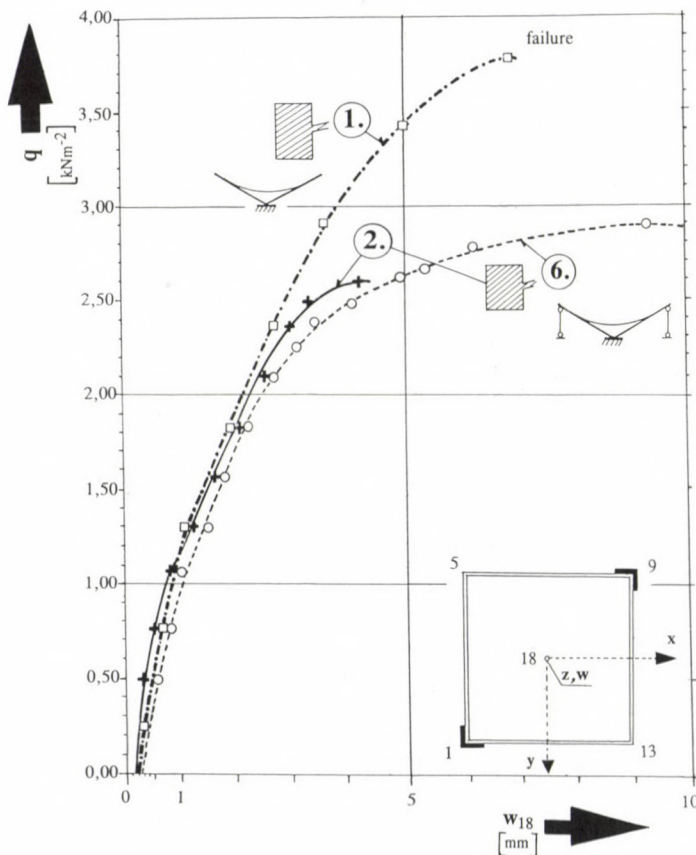
Fig. 15. Experimental equilibrium paths
(Models 1, 2, 6)
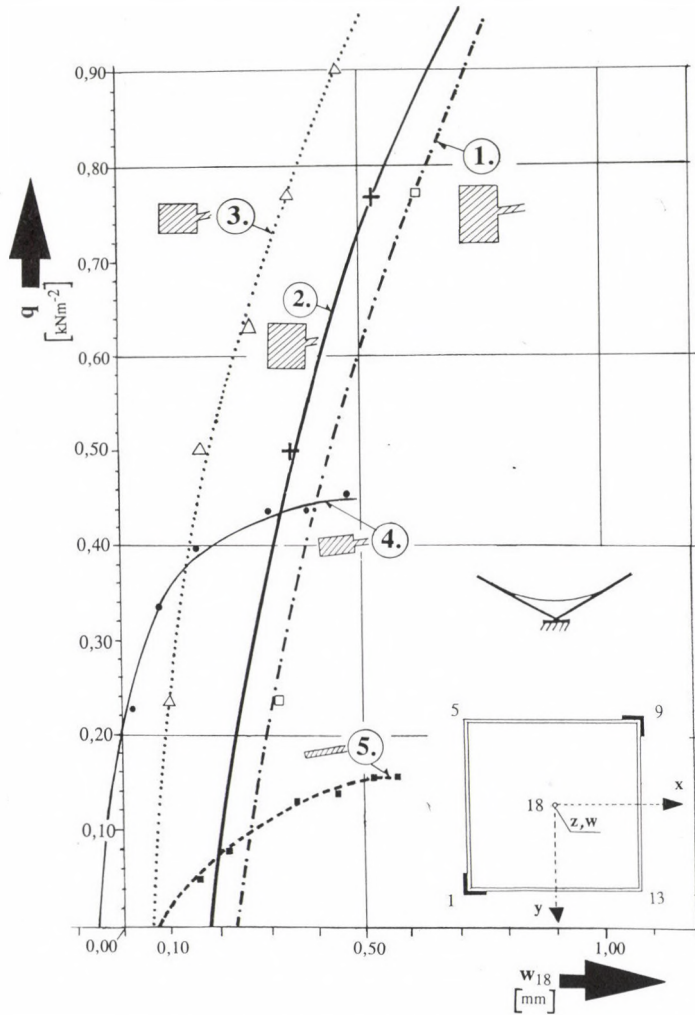
Experimental equilibrium paths
(Models 1—5)

2.3.7. Deflections experienced by the edge beams

Illustrated in Fig. 17 are the deflections of the edge beams experi-
enced immediately before the loss of stability. Note that buckling of the
edge beams has taken place <u>antimetrically</u> (like a frame) as compared with
high corners 5 or 13 (Fig. 1) as also shown in Figs 10—14.

3. Evaluation, conclusions

On the basis of Figs 15--16, the <u>experimental equilibrium paths</u> obtained can be described by characteristic curve **bl** in Fig. 18.

3.1. On shell buckling

The classic <u>linear critical</u>, so-called <u>Reissner--Ralston-load</u> (bifurcation) of the shell can be calculated by means of the following well-known relationship /9, 12, 13/.

$$q_{cr,sh}^{lin} = kE \frac{h^2 f^2}{a^4} = kE \frac{\rho^2}{\omega^4} , \qquad (3.1)$$
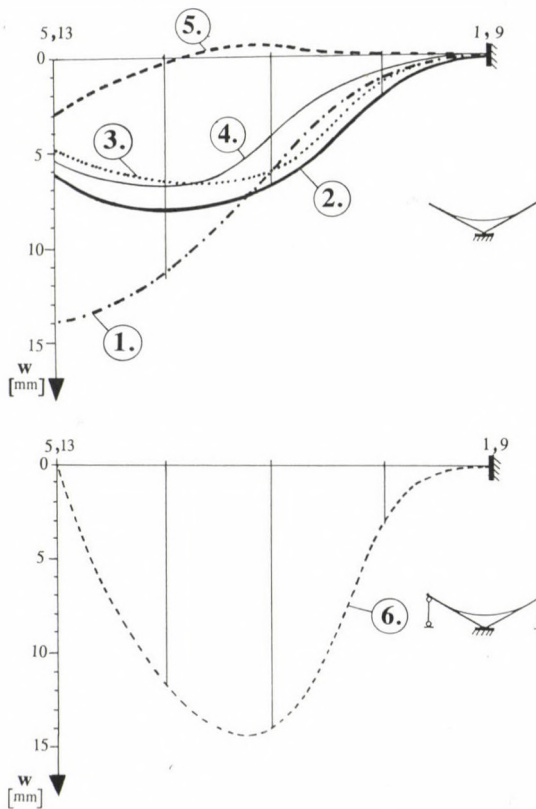
Fig. 17. Edge beam deflection curves
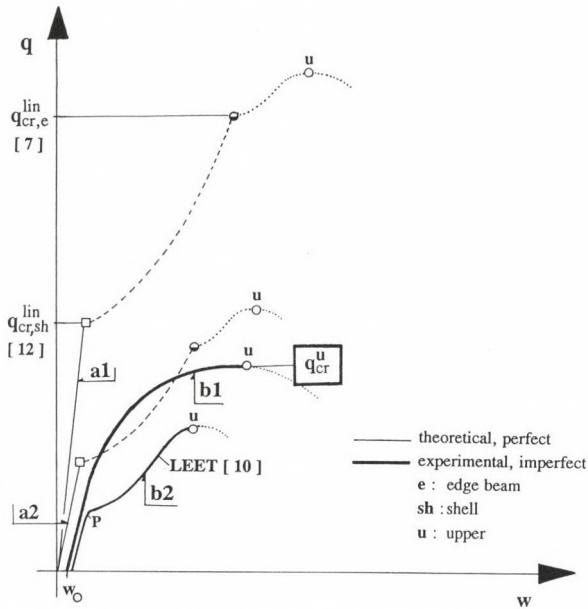
Fig. 18. Type of theoretical and experimental
equilibrium paths
(a1: load-deflection diagram of a geometrically perfect
structure;
a2: same as a1 but for Leet's structures;
b1: experimental load-deflection diagrams;
b2: same as b1 but for Leet's structures)

where

$$k = \frac{2}{\sqrt{3(1 - \mu^2)}} \, ,$$

μ being the transverse contraction factor.

Parameters ρ and ω have been defined in Fig. 21. The subscript sh refers to shell buckling load. With the data of Fig. 1 and Table 1,

$$q_{cr,sh}^{lin} = 7,11 \ kNm^{-2}$$

has been obtained.

Since this theoretical critical load is significant, a shell buckling (bifurcation) has not been expectable and, according to the experiments, it has not taken place either. In Fig. 18, section P of curve b2 corresponds to the buckling of the geometrically imperfect shell. No buckling of this type was shown by curve b1.

Remember that in the experiments of Leet /10/, the shell experienced buckling at about 51-71% of the load calculatable by means of equation (3.1) because of the imperfection (initial waviness) w_0. Also this value is rather high in our case.

As is known, buckling of the shell takes place inextensional ($\varepsilon_x = = \varepsilon_y = 0$; $\gamma_{xy} \neq 0$), in a plate-like way, with a stable symmetric point of bifurcation, that is the postbuckling diagram is rising. The physical explanation of this phenomenon is that in case of properly rigid edge beams, the fibres convex from above (compressed), buckling in small local waves of a large number, are so to say suspended by the fibres concave from above, like by a suspended roof /4, 9/. And this was shown indeed by the Leet models (Fig. 18, curve b2).

Using the data of the Leet shells (a = 406.4 mm, f = 101.6 mm, h = = 0.7747 mm, E = $3,297 \cdot 10^6$ kNm^{-2}, I = $5.549 \cdot 10^{-10}$ m^4), a relatively small critical load,

$$q_{cr,sh}^{lin} = 0,927 \text{ kNm}^{-2}$$

can be calculated for the shell and a shell buckling has taken place indeed in the course of the experiments.

Note that in the investigations of Leet, the load at which shell buckling has taken place decreased continuously as the rigidity of the edge beam decreased. Accordingly, also equation (3.1) remains less and less valid as the edge beam looses its rigidity. Hence, the assumption that the critical load of the shell buckling in small local waves of a large number (in the direction of the arch under pressure) is independent of the boundary conditions (that is, the edges can be considered to be infinitely far from the
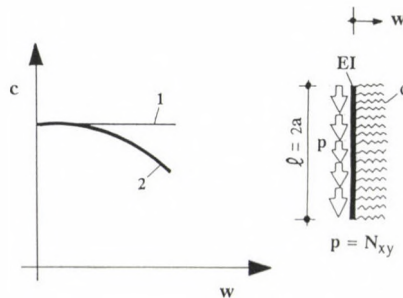
Fig. 19. Illustration to explain
the reduction in load capacity
(1 — theoretical foundation coefficient,
2 — actual foundation coefficient)
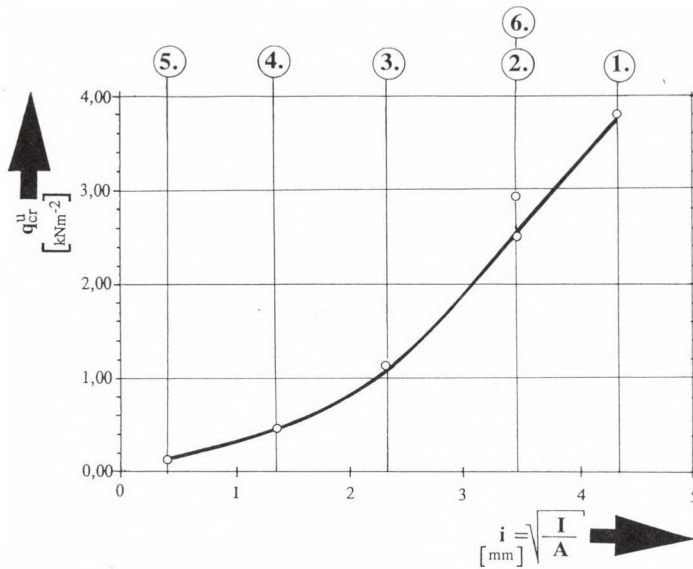
Fig. 20. Change in the upper critical load as a
function of the radius of inertia of the edge beam

buckling wave) remains, below a certain value of edge beam rigidity, no
longer valid. Of course, this is the more true the more we advance towards
the shell of free edge.

3.2. Edge beam buckling

In /7/, the following approximate formula (where subscript e indicates
the edge beam) has been introduced to investigate the buckling of edge beams
(bifurcation phenomenon):

$$q_{cr,e}^{lin} = E \frac{\rho}{\omega^4} (k_1 \alpha + k_2 \rho \sqrt{\alpha}) \tag{3.2}$$

where, in case of two-hinged edge beams, k_1 = 3.094 and k_2 = 1.391
while in case of cantilever edge beams, k_1 = 1.306 and k_2 = 1.035.

For parameters α, ρ and ω see Fig. 21.

In the above relationship, the term proportional to k_1 stands for the
critical load (Euler load) of the bar while the term proportional to k_2 ex-
presses the supporting effect, acting as an elastic foundation, of the shell
interacting with the edge beam (for buckling of the bar on elastic founda-
tion see /5/).

In the present case, the critical load of the edge beam according to (3.2) of <u>models</u> 1--3 and 6 is about 2-6 times as much as the critical load of the shell according to (3.1). Thus an <u>edge beam buckling</u> (<u>bifurcation</u>) has not been expectable. This expectation has been confirmed by our experiments.

Note that an <u>edge beam buckling has not been expected</u>, among others, because the shear force acting upon the edge beam is directionally not stable, instead, it follows the geometry of the buckling edge beam that is, it is <u>non-conservative</u> and thus a <u>static</u> bifurcational critical load (Euler load) is not always acting upon the edge beam either. We think that while a <u>static</u> critical load <u>always exists for the two-hinged bar</u> (without elastic foundation) upon which non-conservative forces are acting, no static critical load but only dynamic critical load exists for the correspond-

$$q_{cr}^{u} \approx 0,09\,E\,\frac{\varrho^{2}\sqrt{\alpha}}{\omega^{4}}$$

$$\alpha = \frac{12I}{h^{3}a}$$

$$\varrho = \frac{f}{h}$$

$$\omega = \frac{a}{h}$$
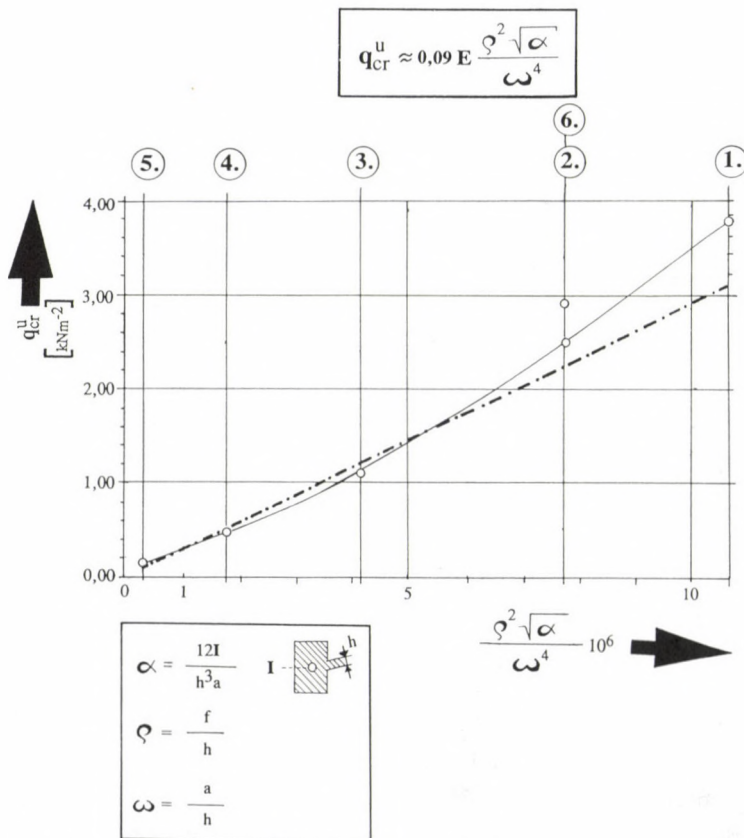
Fig. 21. Approximate formula of the upper critical load

ing <u>cantilever</u> /11/. This means that it is not the frequency but the <u>ampli-</u>
<u>tude</u> that starts to increase beyond every limit. However, this would come
about only if energy were fed which is <u>not possible</u> in case of a shell. On
the other hand, according to the tables given in /11/, the <u>dynamic</u> bifurca-
tion critical load of the unbedded cantilever under load, resulting from non-
conservative forces, is about 5.2-fold as compared with the <u>static</u> critical
load of the cantilever upon which conservative forces are acting. The ten-
dency outlined will most likely prevail also in case of elastic foundation
and thus a bifurcation buckling of the edge beam is <u>not expectable</u>. At the
same time, the effect resulting from the change in direction of the shear
forces is considerably reduced by the <u>flatness</u>.

Of course, either here or in the case according to para 3.1, it is
not the theoretical <u>ideal buckling</u> (<u>bifurcation</u>) a priori excluded because
of the presence of imperfection w_0 but the reduction in rigidity after curve
section P of the Leet diagram in Fig. 18 that fails to come about.

In the geometrical domain investigated, <u>no buckling (bifurcation) of</u>
<u>the edge</u> beams /7/ was observed, certainly because of the relatively signif-
icant rigidity of the shell stiffening the edge beam. Values of the pa-
rameters in formula (3.2): $\alpha = 0.0357 - 35.7$, $\rho = 46.7$, $\omega = 186.6$ (with
$R/h = 746.7$), see Fig. 21.

The <u>theoretical</u> load-deflection diagram of the appropriate, geomet-
rically perfect structure ($w_0 = 0$) is shown in Fig. 18 (curve al). To plot
the diagram, different dash lines were used to indicate that this diagram
has not been determined so far. The solution of the classic <u>shell buckling</u>
(<u>bifurcation</u>) according to /1, 2, 12, 13/, based on the equilibrium path, is
well-known (see expression (3.1) and there exist approximate methods /1, 7/
developed to investigate the <u>buckling (bifurcation) of the edge beam</u> inter-
acting with the shell (see expression (3.2)).

A loss of stability <u>by equilibrium limitation</u> has taken place that is,
the structure has got failed (<u>divergence of equilibrium</u>; <u>snap-buckling</u>)
under the <u>upper critical load</u> corresponding to apex u of the q-w diagram.

The load capacity tends to <u>decrease</u> after apex u. In our view, the
reason for this is that after a certain time, foundation coefficient c of
the edge beam supported elastically by the shell starts decreasing as de-
flection w increases. The reduction in stiffness of the springs is illus-
trated by characteristic 2 in Fig. 19.

Leet /10/ has investigated models (with relatively soft shells as
compared with the edge beam) where the flatter section of load-deflection

diagram P after shell buckling corresponds to the fact that after shell buckling, the edge beam is much less stiffened by the shell. Values of the parameters (see Fig. 21) given in formula (3.2): α = 18.4 - 110.0, ρ = = 131.2 - 151.0, ω = 524.6 - 608.9 (with R/h = 1098 - 2433). After all, the Leet edge beams have got failed either as a result of loss of stability by equilibrium limitation or they have broken before the limit point (horizontal tangent) was reached. Edge beam buckling (bifurcation) has not taken place at all.

3.3. Recommendations

On the basis of Figs 20 and 21, an empirical approximate formula (see Fig. 21) was set up to calculate upper critical loads q_{cr}^{u} (exponent u). The relationship corresponds to formula (3.2) (and also to formula (3.1)) set up in a similar way (using the same shell parameters but now in the form shown below):

$$q_{cr}^{u} \approx k_{u} \, E \, \frac{\rho^{2}\sqrt{\alpha}}{\omega^{4}} , \qquad (3.3)$$

where, for the cantilever edge beam,

$$k_{u} = 0.09.$$

Only experimental data are available for two-hinged edge beams (Model 6). On the basis thereof, k_{u} = 0.105. Hence, the two-hinged edge beam is not much stronger than the cantilever edge beam, the difference being about 17%. Concerning buckling (bifurcation), the buckling two-hinged edge beam was found to be by about 35-50% stronger than the cantilever edge beam in the geometrical domain ivestigated. As is well-known, this ratio will be 1.881/0.784 = 2.40 without elastic foundation.

As seen, zero critical load is associated with the beam without shell (unbedded beam) in formula (3.3). In the last analysis, to eliminate this deficiency, we recommend that Fig. 22 and/or formula (3.4) be used for design purposes. The equation of the two straights in Fig. 22 was produced by equating the measured values of upper critical loads q_{cr}^{u} that can be read from Fig. 21 (or Figs 15 and 16) with the values of linear critical load calculatable on the basis of relationship (3.2) (reduction proportionally to the loads). The measured values of loads q_{cr}^{u} amounted to about 7-14% of the
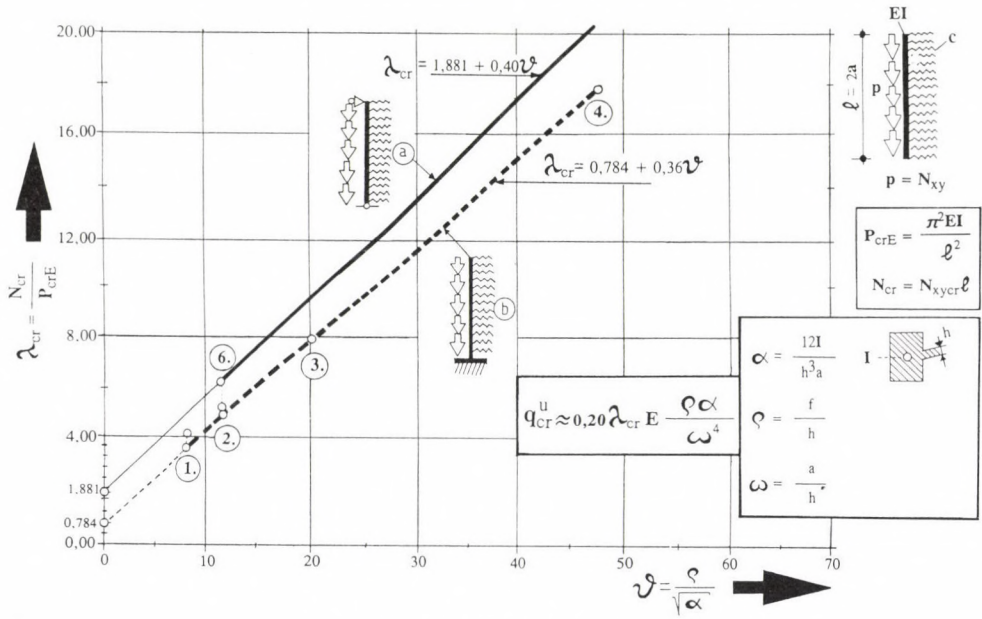
Fig. 22. Approximate design diagrams

values of linear critical loads according to equation (3.2) and also the coefficients of equation (3.2) were reduced accordingly.

After all, the formula of critical load that can be used for <u>design purposes</u> can be written, as follows:

$$q_{cr}^u \approx 0.20 \; \lambda_{cr} \; E \; \frac{\rho \alpha}{\omega^4} \qquad (3.4)$$

where, for two-hinged edge beams,

$$\lambda_{cr} = 1.881 + 0.40 \frac{\rho}{\sqrt{\alpha}} \; ,$$

while for cantilever edge beams,

$$\lambda_{cr} = 0.784 + 0.36 \frac{\rho}{\sqrt{\alpha}} \; .$$

For the sake of a continuous transition to constants <u>1.881</u> and <u>0.784</u> of the unbedded edge beam, the reduction indicated in Fig. 22 (two zero

points along the same vertical line) was used for Models 1 and 2 (and a sim-
ilar reduction was also used in plotting the straight in Fig. 21). That is
why the values of critical load calculatable by means of formula (3.4) are
in general by about 15% lower than those obtained with (3.3). At the same
time, formula (3.4) is advantageous in that it provides a continuous tran-
sition to the case of the unbedded bar.

Of course, the formula of the upper critical load q_{cr}^{u} should be in
principle a function of geometrical imperfection w_o as well. What we can say
here is that in the present case, imperfection (initial waviness) w_o cor-
responding to the load capacity diagrams was smaller than 15% of shell
thickness h (Figs 15--16). The values actually measured can be found in /14/.

When using the process described in /9/, it is recommended that the
properties of reinforced concrete (cracking, creep, plasticity, etc.) be
taken into consideration.

One of our main objects has been to determine the change in critical
load in case of a gradual reduction of flexural rigidity EI of the edge beam
(Fig. 21) until the case of a shell with completely free edges is reached.
In fact, relationship (3.4) complies with this object.

4. ACKNOWLEDGEMENTS

REFERENCES

1. Dayaratnam, P.—Gerstle, K. H.: Buckling of hyperbolic paraboloids. World Conference on Shell Structures, San Francisco, 1962, 289—296

2. Dulácska, E.: Stability of anisotropic hyperbolic paraboloid shells. Acta Techn. Acad. Sci. Hung. 59/1—2 (1967), 123—130

3. Dulácska, E.: Vibration and stability of anisotropic shallow shells. Acta Techn. Acad. Sci. Hung. 65/3—4 (1969), 225—260

4. Gioncu, V.: Thin reinforced concrete shells. Ed. Acad. Rep. Soc. Rumania, J. Willey, Chichester, Toronto 1979

5. Jankó, L.: Buckling of bars on elastic foundation subjected to uniformly distributed axial loads. Acta Techn. Acad. Sci. Hung. 104/1—3 (1991/92), 125—145

6. Jankó, L.: Buckling of a cantilever on elastic foundation loaded on top by concentrated force. Acta Techn. Acad. Sci. Hung. 104/1—3 (1991/92), 147—158

7. Jankó, L.: Buckling of the edge beams of a hyperbolic paraboloid shell supported along the generatrices. Acta Techn. Acad. Sci. Hung. 104/1-3 (1991/92), 159—185

8. Jankó, L.: Buckling of bars on elastic foundation. Építés- Építészettudomány, XXIV/1—2 (1991), (in Hungarian), 33—56

9. Kollár, L.—Dulácska, E.: Buckling of Shells for Engineers. Akadémiai Kiadó, Budapest, 1984

10. Leet, K. M.: Study of stability in the hyperbolic paraboloid. Journ. Eng. Mech. Divis. (Proc. ASCE), 92 (1966), 121—142

11. Petersen, C.: Statik und Stabilität der Baukonstruktionen. Vieweg & Sohn, Braunschweig—Wiesbaden, 1982

12. Ralston, A.: On the problem of buckling of a hyperbolic paraboloidal shell loaded by its own weight. Journ. Math. Phys. 35 (1956), 53—59

13. Reissner, E.. On some aspects of the theory of thin elastic shells. Journ. Boston Soc. Civil Eng. 17 (1955), 100—133

14. Szittner, A.—Kálló, M.—Kaltenbach, L.—Köröndi, L.—Kristóf, L.: Model experiments to study hyperbolic paraboloid shells supported along the generatrices. OTKA Research Report No. 684, Technical University Budapest, Department of Steel Constructions, 1993 (in Hungarian)

RELIABILITY OF ROD-TYPE SUPPORTING
STRUCTURES

MISTÉTH, E.[*]

The objective of this work is to estimate the probability of a possible destruction of rod-type supporting structures. Used for estimation are not the distribution density functions but the calculatable probability characteristics (expectable value, variance, obliquity). The stress resulting from load and the probability characteristics are assumed to be independent of each other and they are easy to calculate.

1. NOTATION

R	load bearing capacity
S	stress resulting from load
Y	load capacity reserve
M	bending or twisting moment
Q	resultant force
g	permanent load
p	effective load
σ_B	normal fracture stress
τ_B	shear fracture stress
T	design life
t	time co-ordinate
W	cross-sectional quantity
A	cross-sectional area
V	cubage of the support
$k = V/V_o$	increase in cubage associated with the standard beam
L	length of beam
q	probability
λ, r σ_1	parameters of the probability distribution function
β	factor expressing probability
$\alpha_1, \alpha_2, \alpha_3$	parameters of the central moments of Weibull distribution
μ_i	ith-order central moment
s	variance
v	relative variance
a	obliquity
ν	safety factor associated with the effective load
$\sigma(t)$	reduction in normal stress
$\nu(t)$	reduction in geometrical dimensions
$w(t)$	reduction in cross-sectional quantity
$\alpha(t)$	reduction resulting from permanent strength

---

[*]Mistéth, Endre, H-1085 Budapest, Csepreghy u. 2, Hungary

2. Introduction

The objective of this work is to estimate the probability of a possible destruction of rod-type supporting structures. Used for estimation are not the distribution density functions but the calculatable probability characteristics (expectable value, variance, obliquity). The stress resulting from load and the probability characteristics are assumed to be independent of each other and they are easy to calculate.

The probability of destruction of one single cross-section can be calculated by expression

$$P\left\{[R(t) - S(t)] \leq 0\right\} < q$$ (1)
$$0 < t \leq T$$

In expression (1), $R(t)$ is the load capacity, $S(t)$ the stress resulting from loads, T the design life and q the probability of destruction. From expression (1), the load capacity and/or the cross-sectional quantity can be calculated at time $t = 0$ /6/.

$$\bar{W}_0^{(R)} = B(T)\, \bar{W}_0^{(S)}$$

where

$$B(T) = \frac{1 + \beta \sqrt{[v_R(T)]^2 + [v_S(T)]^2 - \beta\{[v_R(T)]\,[v_S(T)]\}^2}}{\{1 - \beta^2\,[v_R(T)]^2\}\,[\sigma(T)]\,[\alpha(T)]\,[w(T)]}\,\frac{\bar{S}(T)}{S_0}$$ (2)

$$W_0^{(S)} = \frac{\bar{S}_0}{\bar{\sigma}_{Bo}}$$

In expression (2), $W_0^{(R)}$ is the load capacity at time $t = 0$, $W^{(S)}(T)$ the cross-sectional quantity associated with stress Bo from the stress calculated with regard to the design life, $v_R(T)$ and $v_S(T)$ are the relative variance of the load capacity and the stress resulting from load at the end of the design life, respectively, T is a numerical value depending on the distribution and expressing the possible destruction (e.g. = 3.09 for 1% in case of normal distribution), Bo is the expectable value of the fracture stress of the beam at $t = 0$, (T) is the fracture stress, $w(T)$ the cross-sectional quantity, (T) being the reduction in strength with time.

3. Probability of destruction of lattice girders

The above calculations apply to one single cross-section only. The question is how the probability of destruction of a beam can be determined. Before giving an answer of general validity to the question, let first an example be investigated.

Consider a lattice girder with every chord of it subjected to total load (Fig. 1). For the time being, let the latticing network be left out of consideration. In this case, if q' is the probability of destruction of one single chord of the lattice girder and m is the number of chords, the probability of destruction of the lattice girder will be

$$P = 1 - (1 - q')^m \sim mq' \tag{3}$$

if

$$mq' < 0.15.$$

If the probability of destruction is not equal for every rod and if also the latticing network is taken into consideration, then we can say that under a certain load, destruction of the lattice girder will take place if one of the elements of the latticing network or one of the upper chords or one of the lower chords becomes destroyed. This means that there is a disjunctive relation between the lattice girder elements and thus, if the number of lattice elements in the lattice girder is N, the probability of destruction of the lattice girder will be

$$q_k = 1 - \prod_{i=1}^{N} (1 - q_i) \sim \sum_{i=1}^{N} q_i \tag{4}$$

if

$$q_i \leq 10^{-3}.$$
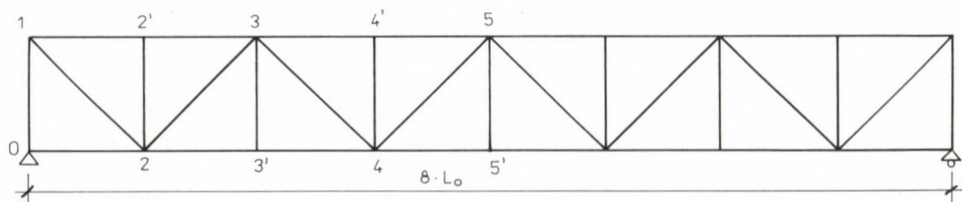
Fig. 1. Lattice girder

Now p_k can be calculated for every one of the different loads (of number ℓ) and the probability of destruction of the lattice girder, denoted by q, will be given by the maximum value from among the values of p_k calculated for every one of the loads of number:

$$q = \max p_{k\ell}. \tag{5}$$

The above calculation is correct. What remains to be answered is how the probability of destruction of the beam can be calculated in case of compact bent beams.

4. Probability of destruction of a beam of plastic material under normal stress condition

Consider a beam of a standard cross-section of A_o and a standard length of L_o as illustrated in Fig. 2, with permanent moment M acting upon both ends. As a result of moment M, an extreme-fibre stress of a magnitude of $\sigma = M/J_x \, y_{max}$ arises along length L_o of the beam. To be determined is the probability of destruction of the beam. In case of beams of plastic material, the distribution of the fracture stress is a Pearson III distribution, the density function being /4/

$$f_1(\sigma_{B'}) = \frac{\lambda_1^{r_1}}{\Gamma(r_1)} (\sigma_{B'} - \sigma_1)^{r_1-1} \exp\left[-\lambda_1 (\sigma_{B'} - \sigma_1)\right]$$

$$\text{if} \quad \sigma_B \geq \sigma_1 \tag{6}$$

$$f_1(\sigma_{B'}) = 0 \qquad\qquad \text{if} \quad \sigma_B \leq \sigma_1.$$
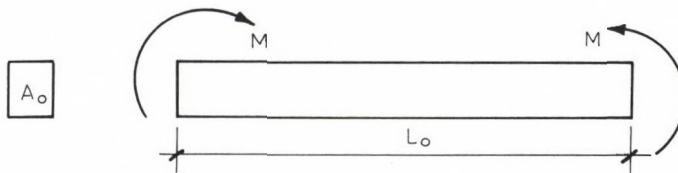
Fig. 2. Standard size beam

Probability characteristics:

Expectable value:
$$\bar{\sigma}_{B'} = \mu_1' = \sigma_1 + r_1/\lambda_1$$

Mean square deviation:
$$s_B^2 = \mu_2' = \frac{r_1}{\lambda_1^2} \tag{7}$$

Obliquity:
$$a_{B'} = 2/\sqrt{r_1} > 0$$

On the basis of expression (7), an arbitrary probability value $[(\sigma_{B'})]_q$ of the fracture stress can be written as

$$[\sigma_B]_q = \bar{\sigma}_{B'} - \beta s_{B'}$$

$$\beta = \beta(a_{B'}, q). \tag{8}$$

A table is available /6/ where the values of β in expression (8) are tabulated as a function of $a_{B'}$ and q.

If the cross-section of the beam under the above load is "A" and its length is L_0, then the density function of the fracture stress will be

$$f_2(\sigma_{B''}) = \frac{\left(\frac{A}{A_0} \lambda_1\right)^{\left(\frac{A}{A_0} r_2\right)}}{\Gamma\left(\frac{A}{A_0} r_2\right)} (\sigma_{B''} - \sigma_2)^{\left(\frac{A}{A_0} r_2\right) - 1} \cdot \exp\left[-\left(\frac{A}{A_0} \lambda_2\right)(\sigma_{B''} - \sigma_2)\right] \tag{9}$$

if

$$\sigma_{B''} \geq \sigma_2,$$

$$f_2(\sigma_{B''}) = 0,$$

if

$$\sigma_{B''} < \sigma_2.$$

Probability characteristics:

Expectable value:
$$\bar{\sigma}_{B''} = \mu_i'' = \sigma_2 + \frac{r_2}{\lambda_2} = \mu_1'$$

Mean square devitation:
$$s_{B''}^2 = \mu_2'' = \frac{r_2}{\lambda_2} \frac{A_0}{A} = \mu_2' \frac{A_0}{A} \tag{10}$$

Obliquity:
$$a_{B''} = \frac{2}{\sqrt{r_1}} \sqrt{\frac{A_0}{A}} = a_{B'} \sqrt{\frac{A_0}{A}} > 0$$

On the basis of expression (1), an arbitrary probability value $(\sigma_B)_q$ of the fracture stress can be written as

$$\left[(\bar{\sigma}_{B''})\right]_q = \bar{\sigma}_{B''} - \beta \sqrt{A_0/A} \; s'_{B''}$$

(11)

$$\beta = \beta \, (a, \, q)$$

According to expression (11), $(\sigma_{B''})_q > (\sigma_{B'})_q$.

The next question is how the probability of destruction of a beam of an arbitrary cross-section A but of a length of $L = n \, L_0$ can be calculated. The subsequent sections of length L_0 are assumed to be independent of each other; the length of sections L_0 has to be determined experimentally /1/. According to the experiments, for round steels, length L_0 that is the length of the independent sections is 70 to 80 times as much as the diameter. In this case

$$_q[L] = n_q[Lo].$$

(12)

According to expression (12), the probability of destruction of a beam n times as long is n times as much.

5. Probability of destruction of a beam of brittle material under normal stress conditions

Consider a beam of standard size, $V_0 = A_0 \, L_0$, according to Fig. 2 but now the beam is assumed to be of brittle material ($a \leq 0$). The distribution of the fracture stress is a Weibull /8/ (II lower extremal) distribution. The distribution function is

$$F_3(\sigma_{B'''}) = 1 - \exp\left\{-\left[\lambda_3 \, (\sigma_{B'''} - \sigma_3)\right]^{r_3}\right\}$$

(13)

$$F_3(\sigma_{B'''}) = 0 \quad \text{if} \quad \begin{matrix} \sigma_{B'''} \geq \sigma_3 \\ \sigma_{B'''} < \sigma_3 \end{matrix}$$

Probability characteristics:

$$\text{Expectable value:} \quad \bar{\sigma}_{B'''} = \sigma_3 + \alpha_1/\lambda_3 = \mu_1'''$$

$$\text{Mean square deviation:} \quad (s_{B'''})^2 = \mu_2''' = \alpha_2/\lambda_3^2 \qquad (14)$$

$$\text{Obliquity:} \quad a_{B'''} = \alpha_3/[\alpha_2]^{3/2} < 0$$

where

$$\alpha_1 = \Pi\left(\frac{1}{\Gamma_3}\right)$$

$$\alpha_2 = \Pi\left(\frac{2}{\Gamma_3}\right) - \Pi^2\left(\frac{1}{\Gamma_3}\right) \qquad (15)$$

$$\alpha_3 = \Pi\left(\frac{3}{\Gamma_3}\right) - 3 \; \Pi\left(\frac{2}{\Gamma_3}\right) \cdot \Pi\left(\frac{1}{\Gamma_3}\right) + 2 \; \Pi^3\left(\frac{1}{\Gamma_3}\right)$$

and $\Pi(Z) = Z!$ is the Gauss function.

The values of expression (15) are found in Tables /6/.

On the basis of expression (14), if

$$q = (100 - 100/n) \; \%,$$

an arbitrary value $(\sigma_{B'''})_q$ of the fracture stress will be

$$(\sigma_{B'''})_q = \sigma_3 + 1/\lambda_3 \; \sqrt[\Gamma_3]{n - \Delta} \qquad (16)$$

where $\lim_{n \to \infty} \Delta = 1/2$.

If the size of the beam is $V = AL$ and $V/V_0 = k$, then the distribution function will be

$$F_4(\sigma_B IV) = 1 - \exp\left\{- k\left[\lambda_3(\sigma_B IV - \sigma_3)\right]^{\Gamma_3}\right\}$$

$$\text{if } \sigma_B IV \geq \sigma_3,$$

$$F_4(\sigma_B IV) = 0 \qquad \text{if } \sigma_B IV < \sigma_3.$$

Probability characteristics:

$$\text{Expectable value:} \quad \bar{\sigma}_B IV = \sigma_3 + \frac{\alpha_1}{\lambda_3 \; \sqrt[\Gamma_3]{k}} < \bar{\sigma}_{B'''}$$

Mean square deviation: $\mu_2 = (s_B IV)^2 = \dfrac{\alpha_2}{\lambda_3^2 \sqrt[r_3]{k^2}} = (s_{B'''})^2 \sqrt[r_3]{\dfrac{1}{k^2}} < (s_{B'''})^2$

$$\tag{17}$$

Obliquity: $a_B IV = \dfrac{\alpha_3}{\alpha_2^{3/2}} = a_{B'''}$

On the basis of expression (17), if q = (100-100/n) %, an arbitrary probability value $(\sigma_B IV)_q$ of the fracture stress can be written as

$$(\sigma_B IV)_q = \sigma_3 + \frac{1}{\lambda_3 \sqrt[r_3]{k(n - \Delta)}} \tag{18}$$

where lim Δ = 1/2.

$$n \rightarrow \infty$$

6. Probability of destruction of a rod of constant cross-section under shear stress conditions

A twisting moment M is acting upon either end of the rod of tubular cross-section and of a length of L_0 illustrated in Fig. 3, the two moments being of opposite sense as compared with each other. As a result of load, shear stress $\tau = M/J_p \, r_{max}$ is prevailing at every point of the periphery of the tube. To be determined is the probability of destruction of the beam or the value of τ_B associated with a certain probability. Assume that rods of plastic or brittle material can be investigated from the point of view of shear stress as well. In this case, their distribution and/or density function will comply with what has been said about normal stress conditions in Sections 4 and 5 accordingly. In case of rods of plastic material with cross-section A and length L_0, the Pearson III density function of the fracture stress will be, provided the rod has a standard cross-section, the following:
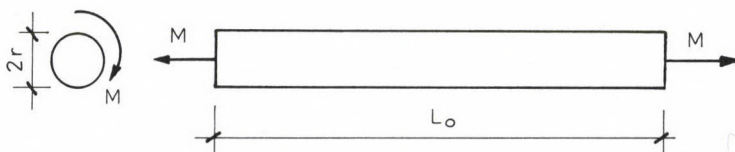
Fig. 3. Standard size tubular beam

$$f_5(\tau_B) = \frac{\left(\frac{A}{A_o}\lambda_5\right)^{\left(\frac{A}{A_o}r_5\right)}}{\Gamma\left(\frac{A}{A_o}r_5\right)}\,(\tau_B - \tau_1)^{\left(\frac{A}{A_o}r_5 - 1\right)}\cdot\exp\left[-\left(\frac{A}{A_o}\lambda_5\right)(\tau_B - \tau_1)\right]$$

$$\text{if } \tau_B \geq \tau_1,$$

$$f_5(\tau_B) = 0 \qquad \text{if } \tau_B < \tau_1.$$

(19)

Probability characteristics:

$$\text{Expectable value:} \qquad \bar{\tau}_{B'} = \mu_1' = r_5/\lambda_5 + \tau_1$$

$$\text{Mean square deviation:} \quad s_{\tau B'}^2 = \mu_2' = \frac{r_5}{\lambda_5^2}\frac{A_o}{A} = \mu_2\frac{A_o}{A}$$

(20)

$$\text{Obliquity:} \qquad a_{B'} = \frac{2}{\sqrt{r_5}}\sqrt{\frac{A_o}{A}} = a_B\sqrt{\frac{A_o}{A}}$$

On the basis of expression (20), an arbitrary probability value $(\tau_B)_q$ of the shear fracture stress can be written as

$$(\tau_B)_q = \bar{\tau}_{B'} - \beta\sqrt{A_o/A}\,s_{\tau B'}$$

(21)

$$\beta = \beta\,(a_B,\,q)$$

If the length of the rod is $L = n\,L_o$, the probability of destruction will be n times as much.

Consider now the case of brittle material $(a \leq 0)$ and assume that all what has been said in Section 5 also applies to shear stress. Then, if the volume of the rod is $V = AL$ and the standard volume $V/V_o = k$ and $V_o = A_o L_o$, the Weibull distribution function of the fracture stress will be

$$F_6(\tau_B) = 1 - \exp\{-k[\lambda_6(\tau_B - \tau_6)]^{r_6}\}$$

$$\text{if } \tau_B \geq \tau_6$$

(22)

$$F_6(\tau_B) = 0 \qquad \text{if } \tau_B < \tau_2$$

Probability characteristics:

Expectable value: $\tau_{B''} = \tau_6 + \dfrac{\alpha_1}{\lambda_6{}^r{}_6\sqrt{k}}$

Mean square deviation: $(s_{\tau B''})^2 = \mu''_2 = \dfrac{\alpha_2}{\lambda_6^2{}^r{}_6\sqrt{k^2}}$ (23)

Obliquity: $a_{B''} = \dfrac{\alpha_3}{\sqrt{\alpha_2^3}},$

if

$$(q = (100 - 100/n) \%,$$

an arbitrary probability value of the shear fracture stress can be written as

$$[\tau_{B''}]_q = \tau_2 + \dfrac{1}{\lambda_6{}^r{}_6\sqrt{k(n - \Delta)}}   \qquad (24)$$

where $\lim \Delta = 1/2$

$\qquad n \to \infty.$

The values of α_i (i = 1, 2, 3) can be calculated similarly to the values of α_i is Section 5. Since no Hungarian experimental data for shear are available, the experimental results obtained for normal stress can be used in numerical calculations but the normal stress values must be multiplied with $1/\sqrt{3} = 0.577$. This factor is based on the Huber—Mises fracture theory.

7. Probability of destruction of statically defined beams of plastic material

The probability of destruction as a result of load varies from cross-section to cross-section in case of the beam of variable cross-section illustrated in Fig. 4. To be determined is the probability of destruction of the beam.

In case of a beam of plastic material and variable cross-section, the beam shall be divided in sections corresponding to 10 to 15 times the height of the beam (a rapid change in cross-section always being a section boundary)
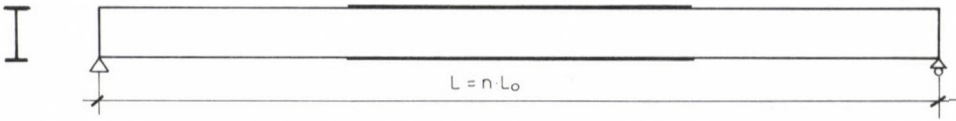
Fig. 4. Beam of variable cross-section

and the probability of destruction shall be determined for each section in-dependently. This means that the probability characteristic of the fracture stress shall be determined for the material and dimensions of the beam ac-cording to expression (10). Of course, the expectable value and the value of mean square deviation are to be understood at the end of the design life. With these values, expression (10) will become for the ith section

$$\bar{\sigma}_B^{(i)}(T) = \sigma_{B0}^{(i)}\ \sigma(T)\ \alpha(T)$$

$$\left[s_B^{(i)}(T)\right]^2 = s^{(\sigma)}(T)\left[s_{B0}^{(i)}\right]^2 \frac{A_0}{A_{(i)}} \tag{25}$$

$$a_B(T) = a_{B0}^{(i)}\sqrt{\frac{A_0}{A_{(i)}}}$$

To be calculated now are the cross-sectional quantity and the proba-bility characteristics at the end of the design life for the ith section:

$$\bar{W}^{(i)}(T) = \bar{W}_0^{(i)}\ w(T)$$

$$\left[s_{(i)}^{(W)}(T)\right]^2 = \left[s_{0_{(i)}}^{(W)}\right]^2 s^{(u)}(T) \tag{26}$$

At the end of the design life, the load capacity and its probability characteristics are

$$\bar{R}^{(i)}(T) = \sigma_B^{(i)}(T) \cdot \bar{W}^{(i)}(T)$$

$$\left[s_{(i)}^{(R)}(T)\right]^2 = \left[\bar{\sigma}_B^{(i)}(T) \cdot s_{(i)}^{(W)}(T)\right]^2 + \left[\bar{W}^{(i)}(T)\ s_{(i)}^{(\sigma)}(T)\right]^2 + \left[s_{(i)}^{(\sigma)}(T) \cdot s_{(i)}^{(W)}(T)\right]^2 \tag{27}$$

$$a_{(i)}^{(R)}(T) = a_{(i)}^{(\sigma)}(T)\left[\bar{W}_{(i)}(T)\ \frac{s_{(i)}^{(\sigma)}(T)}{s_{(i)}^{(R)}(T)}\right]^3 + a_{(i)}^{(W)}(T)\left[\bar{\sigma}_B^{(i)}(T)\ \frac{s_{(i)}^{(W)}(T)}{s_{(i)}^{(R)}(T)}\right]^3$$

Expressions $\sigma(T)$, $\alpha(T)$, $w(T)$, $s^{(\alpha)}(T)$, $s^{(\sigma)}(T)$, and $s^{(w)}(T)$ are found in /7/.

The stress resulting from load along the ith section and its probability characteristics are

$$\bar{S}^{(i)}(T), \quad s_{(i)}^{(S)}(T), \quad a_{(i)}^{(S)}(T).$$

Accordingly, the strength calculation reserve of the ith section and its probability characteristics will be

$$\bar{Y}^{(i)}(T) = \bar{R}^{(i)}(T) - \bar{S}^{(i)}(T)$$

$$\left[s_{(i)}^{Y}(T)\right]^2 = \left[s_{(i)}^{(R)}(T)\right]^2 + \left[s_{(i)}^{(S)}(T)\right]^2 \tag{28}$$

$$a_{(i)}^{Y}(T) = a_{(i)}^{(R)}(T)\left[\frac{s_{(i)}^{(R)}(T)}{s_{(i)}^{Y}(T)}\right]^3 - a_{(i)}^{(S)}(T)\left[\frac{s_{(i)}^{(S)}(T)}{s_{(i)}^{Y}(T)}\right]^3$$

From expression (28), the probability of destruction can be calculated, as follows:

$$\frac{\bar{Y}^{(i)}(T)}{s_{(i)}^{Y}(T)} = \frac{1}{v_Y^{(i)}}$$

$$q'_{(i)} = q\left[v_y^{(i)}, a_{(i)}^{Y}\right] \tag{29}$$

$$q = \sum_{(i)} q'_{(i)}$$

The probability of destruction calculated on the basis of expression (29), denoted by q, must be the optimum probability. If the probability of destruction along the jth section of the beam divided in sections can be calculated on the basis of shear stress $\tau_K(T)$, then it is q associated with this value of shear stress that has to be included among the addable sums of expression (29).

Similarly, if the probability of destruction is attributed to some other strength characteristic (identation), then the value of q_j associated

with that characteristic shall be included among the addable sums of expression (29).

8. Probability of destruction of statically defined beams of brittle material

If the beam of variable cross-section shown in Fig. 4 is made of brittle material, the fracture stress probability characteristics of the beam shall be determined on the basis of formula (17). In this case, the volume of the beam is obtained as the sum of the volumes of the sections of variable cross-section:

$$V = \sum_{(i)} A_i L_i$$

and   (30)

$$k = V/V_o$$

Otherwise expressions (17) and (18) will apply invariably.

9. Statically undetermined beam

The elastic hinges of a statically undetermined beam are arranged on the beam in such a way that the probability of destruction of the beam will be maximum /2, 6/.

Consider an n times undetermined beam of plastic material (Fig. 5) upon which a multiparameter effective load of exptent p is acting in addition to permanent load g. A certain extent $\nu_c p$ of the effective load can be repeated without limit. The beam has standard cross-sections of number $N \geq n$. Standard cross-sections are those where the stress due to load has a relative extreme value or where the cross-section changes rapidly. A load capacity reserve
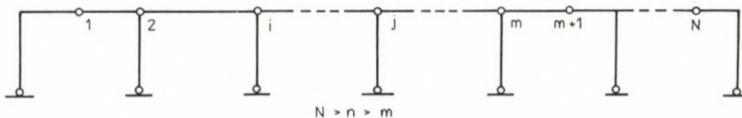
Fig. 5. "n" times undetermined beam

MISTÉTH, E.

$$Y_i = R_i - S_{gi} - S_{pi}$$

can be calculated for each cross-section. In expression (31), R_i denotes the probability characteristics of the load capacity of the cross-section: $\bar{R}_i$ stands for the expectable value, s_{Ri} for variance and a_{Ri} for obliquity. The probability vector variable $\underline{R}$ is

$$\begin{bmatrix} \bar{R}_1 \\ \bar{R}_2 \\ \cdot \\ \cdot \\ \cdot \\ \bar{R}_N \end{bmatrix} = \bar{\underline{R}} \quad \begin{bmatrix} s_{R1} \\ s_{R2} \\ \cdot \\ \cdot \\ \cdot \\ s_{RN} \end{bmatrix} = \underline{s}_R \quad \text{and} \quad \begin{bmatrix} a_{R1} \\ a_{R2} \\ \cdot \\ \cdot \\ \cdot \\ a_{RN} \end{bmatrix} = \underline{a}_R \tag{31}$$

S_{gi} is the internal force due to the own weight, $\bar{S}_{gi}$ the expectable value, e the variance and a is the obliquity. The probability vector variable $\underline{S}_g$ is

$$\begin{bmatrix} \bar{S}_{g1} \\ \bar{S}_{g2} \\ \cdot \\ \cdot \\ \cdot \\ \bar{S}_{gN} \end{bmatrix} = \underline{S}_g \quad \begin{bmatrix} s_{g1} \\ s_{g2} \\ \cdot \\ \cdot \\ \cdot \\ s_{gN} \end{bmatrix} = \underline{s}_g \quad \text{and} \quad \begin{bmatrix} a_{g1} \\ a_{g2} \\ \cdot \\ \cdot \\ \cdot \\ a_{gN} \end{bmatrix} = \underline{a}_g \tag{32}$$

S_{pi} is the internal force due to the effective load applied to the cross-section in a standard way: $\bar{S}_{pi}$ being the expectable value, s_{pi} the variance and a_{pi} the obliquity. The probability vector variable $\underline{S}_p$ is

$$\begin{bmatrix} \bar{S}_{p1} \\ \bar{S}_{p2} \\ \cdot \\ \cdot \\ \cdot \\ \bar{S}_{pN} \end{bmatrix} = \bar{\underline{S}}_p \quad \begin{bmatrix} s_{p1} \\ s_{p2} \\ \cdot \\ \cdot \\ \cdot \\ s_{pN} \end{bmatrix} = \underline{s}_p \quad \text{and} \quad \begin{bmatrix} a_{p1} \\ a_{p2} \\ \cdot \\ \cdot \\ \cdot \\ a_{pN} \end{bmatrix} = \underline{a}_p \tag{33}$$

Stresses S_{gi} and S_{gj} ($i = j = 1, 2, \ldots N$) are not independent since they are internal forces subject to the condition of equilibrium. The same applies to the stresses due to effective loads S_{pi} and S_{pj}.

Probability characteristics of the load capacity reserve:

$$\bar{Y}_i = \bar{R}_i - \bar{S}_{gi} - \bar{S}_{pi}$$

$$s_{Yi}^2 = s_{Ri}^2 + s_{gi}^2 + s_{pi}^2$$

$$a_{Yi} = a_{Ri}\left(\frac{s_{Ri}}{s_{Yi}}\right)^3 - a_{gi}\left(\frac{s_{gi}}{s_{Yi}}\right)^3 - a_{pi}\left(\frac{s_{pi}}{s_{Yi}}\right)^3 \qquad (34)$$

$$(i = 1, 2, \ldots N)$$

$$\frac{1}{v_{Yi}} = \frac{\bar{Y}_i}{s_{Yi}}$$

A safety factor v_i resulting in zero load capacity reserve can be determined for each standard cross-section:

$$\bar{v}_i = (\bar{R}_i - \bar{S}_{gi})/\bar{S}_{pi} \qquad (35)$$

The minimum value of $\bar{v}_i$:

$$\min \bar{v}_i = v_a \quad (i = 1, 2, \ldots N) \qquad (36)$$

where v_a is the value of the load capacity characteristic of the beam. In case of a beam of brittle material, this effective load $v_a\bar{p}$ means the expectable value of the limit load capacity of the beam. The probability of destruction of beams of brittle material can be calculated on the basis of expressions (17), (18) and (30).

Of course, beams of plastic material can be loaded additionally. Associated with standard cross-sections of number N are different load positions of number L ≤ N. In case of each load position, after plastic hinges of number m ≤ n have occurred as a result of the effective load, when also yield of the material takes place in the m+1st cross-section, the beam becomes instable either fully (m=n) or partially (m ≤ n) and its entire load capacity reserve gets exhausted.

At point m in the Lth load position, relative rotation $\kappa_j^{(L)}$ (j = 1, 2, ..., m) occurs and thus the conditional equation will be

$$\nu^{(L)} \, S_{p1}^{(L)} + z_{11} \, \kappa_1^{(L)} + \ldots + z_{1m} \, \kappa_m^{(L)} = R_1 - S_{g1}$$

$$\nu^{(L)} \, S_{p2}^{(L)} + z_{21} \, \kappa_1^{(L)} + \ldots + z_{2m} \, \kappa_m^{(L)} = R_2 - S_{g2}$$

$$\text{--} \quad (37)$$

$$\nu^{(L)} \, S_{pm}^{(L)} + z_{m1} \, \kappa_1^{(L)} + \ldots + z_{mm} \, \kappa_m^{(L)} = R_m - S_{gm}$$

$$\nu^{(L)} \, S_{pm+1}^{(L)} + z_{m+1,1} \, \kappa_1^{(L)} + \ldots + z_{m+1,m} \, \kappa_m^{(L)} = R_{m+1} - S_{gm+1}$$

Of course, with the exception of z_{ij}-k, every expression in equation system (37) is a probability variable and therefore the equation system shall be solved for the expectable values of $\bar{S}_{gi}$, $\bar{S}_{pi}$, $\bar{R}_i$. The value of z_{ij} can be calculated from the geometrical dimensions and from the ratio of the moduli of elasticity. The relative variance of the geometrical dimensions lies below 1%; the variation of the modulus of elasticity along the beam is negligible and thus also its effect is minimum /2/ and therefore, because of their relative variance of about 1%, quantities z_{ij} can be assumed to be determined.

$$\nu^{(L)} = \frac{\begin{vmatrix} \bar{R}_1 - \bar{S}_{g1} & z_{11} & \cdots & z_{1m} \\ \bar{R}_2 - \bar{S}_{g2} & z_{21} & \cdots & z_{2m} \\ \text{------------------} \\ \bar{R}_m - \bar{S}_{gm} & z_{m1} & \cdots & z_{mm} \\ \bar{R}_{m+1} - \bar{S}_{gm+1} & z_{m+1,1} & \cdots & z_{m+1m} \end{vmatrix}}{\begin{vmatrix} \bar{S}_{p1}^{(L)} & z_{11} & \cdots & z_{1m} \\ \bar{S}_{p2}^{(L)} & z_{21} & \cdots & z_{2m} \\ \text{------------------} \\ \bar{S}_{pm}^{(L)} & z_{m1} & \cdots & z_{mm} \\ \bar{S}_{pm+1}^{(L)} & z_{m+1,1} & \cdots & z_{m+1,m} \end{vmatrix}} = \frac{\sum\limits_{(i)} \bar{R}_i \, \underline{\underline{Z}}_{(i)}^{(L)} - \sum\limits_i \bar{S}_{gi} \, \underline{\underline{Z}}_{(i)}^{(L)}}{\sum\limits_{(i)} \bar{S}_{pi}^{(L)} \, \underline{\underline{Z}}_{(i)}^{(L)}} \quad (38)$$

$$(L = I, II, \ldots, X, \ldots)$$
$$(i = j = 1, 2, \ldots m)$$

$$\kappa_j^{(L)} = \frac{\sum\limits_{(i)} \bar{R}_i \, \underline{\underline{Z}}_{(\kappa j)}^{(L)} - \sum\limits_i \bar{S}_{gi} \, \underline{\underline{Z}}_{(\kappa j)}^{(1)}}{\sum\limits_{(i)} \bar{S}_{pi}^{(L)} \underline{\underline{Z}}_{(i)}^{(L)}}$$

Similarly to expression (31), the load capacity reserve of the m+1st cross-section of the Lth load position will be

$$\bar{Y}_{m+1}^{(L)} = \bar{R}_{m+1}^* - \bar{S}_{gm+1} - \bar{S}_{pm+1} \tag{39}$$

where

$$\bar{R}_{m+1}^* = \bar{R}_{m+1} + \sum_{j=1}^{n} z_{m+1j} \, \kappa_j^{(L)}$$

In expression (39), $\kappa_j^{(L)}$ is the relative rotation taking place on the plastic hinges of number m while $z_{m+1,j}$ is the internal force in the m+1st cross-section resulting from relative rotation $\kappa_j = 1$ at the jth point of the undetermined beam.

The surplus load capacity term can be calculated from expression (38) and/or (39). Namely, submatrices $\underline{\underline{Z}}_{(\kappa j)}^{(L)}$ can be considered determined and also the ratio of probability characteristics $\bar{R}_i$ is determined because the load capacity in question is that of a beam of the same material but in different cross-sections and also the ratio of expectable values $\bar{S}_{gi}$, moreover, also that of the values of $\bar{S}_{pi}^{(L)}$ are determined and therefore the relative variance of the second term in expression (41) is approximately identical independently of the cross-sections and thus the probability of destruction is reduced by the surplus load capacity. However, the question will require extra consideration if within the cross-section, the partial internal forces are taken up by beam sections of a different material each.

In general, using the values of z_{ij}, the following matrix can be written:

$$
\begin{bmatrix}
z_{11} & z_{12} & \cdots & z_{1i} & \cdots & z_{1j} & \cdots & z_{1m} & z_{1m+1} & \cdots & z_{1N} \\
z_{21} & z_{22} & \cdots & z_{2i} & \cdots & z_{2j} & \cdots & z_{2m} & z_{2m+1} & \cdots & z_{2N} \\
\hline
z_{i1} & z_{i2} & \cdots & z_{ii} & \cdots & z_{ij} & \cdots & z_{im} & z_{im+1} & \cdots & z_{iN} \\
\hline
z_{j1} & z_{j2} & \cdots & z_{ji} & \cdots & z_{jj} & \cdots & z_{jm} & z_{jm+1} & \cdots & z_{jN} \\
\hline
z_{m1} & z_{m2} & \cdots & z_{mi} & \cdots & z_{mj} & \cdots & z_{mm} & z_{mm+1} & \cdots & z_{mN} \\
z_{m+1,1} & z_{m+1,2} & \cdots & z_{m+1,i} & \cdots & z_{m+1,j} & \cdots & z_{m+1,m} & z_{m+1,m+1} & \cdots & z_{m+1,N} \\
\hline
z_{N1} & z_{N2} & \cdots & z_{Ni} & \cdots & z_{Nj} & \cdots & z_{Nm} & z_{Nm+1} & \cdots & z_{NN}
\end{bmatrix} = \underline{\underline{Z}} \tag{40}
$$

Matrix $\underline{\underline{Z}}$ is a symmetric quadratic matrix. Also submatrices associated with every load position of number L, quadratic and symmetric, can be produced of matrix $\underline{\underline{Z}}^{(L)}$. On the basis thereof, the following matrix equation can be written from relationship (39):

$$\underline{\underline{Z}}^{(L)} \; \underline{\kappa}^{(L)} = \underline{Y}^{(L)} \quad (L = I, II, \ldots X \ldots). \tag{41}$$

The probability characteristics of the denominator of expression (38), a linear sum $S_p^{(L)} = \underline{\underline{Z}}_1^{(L)} S_{p1} + \ldots + \underline{\underline{Z}}_m^{(L)} S_{pm}$, can be simply calculated because they are not independent but there exists the above linear sum relation between them. Therefore, the probability characteristics of the denominator of expression (38) are perfectly identical with those of the effective load:

$$\bar{S}_p^{(L)} = \underline{\underline{Z}}_1^{(L)} \bar{S}_{p1} + \underline{\underline{Z}}_2^{(L)} \bar{S}_{p2} + \ldots + \underline{\underline{Z}}_m^{(L)} \bar{S}_{pm}$$

$$s_p^{(L)} = v_p \bar{S}_p^{(L)} \tag{42}$$

$$a_p^{(L)} = a_p.$$

The probability characteristics of internal forces due to dead weight in the numerator of expression (38) are, similarly to expression (42),

$$\bar{S}_g^{(L)} = \underline{\underline{Z}}_1^{(L)} \bar{S}_{g1} + \underline{\underline{Z}}_2^{(L)} \bar{S}_{g2} + \ldots + \underline{\underline{Z}}_m^{(L)} \bar{S}_{gm}$$

$$s_g^{(L)} = v_g \bar{S}_g^{(L)} \tag{43}$$

$$a_g^{(L)} = a_g.$$

A safety factor $\bar{v}^{(L)}$ (where L is the serial number of the load position) is associated with every load position. The minimum value of $\bar{v}^{(L)}$ is

$$\min \bar{v}^{(L)} = v_b \quad (L = I, II, \ldots X \ldots). \tag{44}$$

This effective load $v_b \bar{p}$ means the fracture load capacity of the beam, taking the plastic properties of the beam into consideration. Should the value of load $v_b \bar{p}$ be continuously repeated, a kinematic destruction of the beam will take place that is, after each loading cycle from among those of

number L, relative rotations κ_b will increase continuously. However, there exists a value of load $\nu_c \bar{p}$ for which

$$\nu_a \leq \nu_c \leq \nu_b \tag{45}$$

and which can be repeated continuously. Thus it will result in a rotation vector $\underline{\kappa}_c$ of a definite value.

On the basis of safety factor ν_a, the order of "cross-sections of minimum load capacity" can be determined. In this less stable cross-sections of number m, a rotation load $\underline{\kappa}_c$ will occur which discontinues increasing independently of how many times the loading has been repeated.

An equation system similar to (37) can be written which differs from (37) in that in may apply to different load positions of number m+1 while (37) applies to one single load position only. The sign of safety factor ν_c so calculated and the sign of each element $\kappa_j^{(c)}$ (j = 1, 2, ..., m+1) of relative displacement (rotation, shift etc.) vector $\underline{\kappa}_c$ associated with it must be identical with the sign of the restraint force arising at the jth place as a result of the load. A safety factor $\nu^{(x)}$ (x = A, B, C ...) is associated with each group of cross-sections of minimum load capacity of number m+1 satisfying the condition given below, from among which the minimum safety factor is

$$\min \nu^{(x)} = \nu_c \quad (X = A, B, C ...) \tag{46}$$

Where A, B, C, ... are the different groups of cross-sections of minimum load capacity with the loads associated with them.

ν_c from expression (46) satisfies expression (45) while for each element of rotation vector $\underline{\kappa}_c$, a matrix equation similar to (41) can be written:

$$\underline{\underline{Z}}^{(x)} \underline{\kappa}^{(x)} = \underline{\bar{Y}}^{(x)} \quad (X = A, B, C ...). \tag{47}$$

If equation (47) is solved for safety factor ν_c, we will arrive at relative rotation vector $\underline{\kappa}_c$ which discontinues increasing as a result of repeated loads because matrix equation (47) does not apply to one single load position like equation (41) but to different load positions associated with cross-sections of minimum load capacity. The cross-sections of minimum stability of number (m+1) cannot be determined immediately. Therefore, more equations associated with the order of cross-sections of minimum stability (A, B, C, ...) must be solved.

A possible value of the three limit load capacity conditions has already been determined by Kossalka /5/ to a good approximation.

If the strength of every standard cross-section that is $\nu_1 = \nu_2 = \ldots = \nu_N = \nu_a$ were calculated so as to result in identical safety, then $\nu_c = \nu_a$ and $\underline{\kappa}_c = 0$. Also beams where $\nu_b = \nu_a$ can be designed. The above condition is satisfied by every lattice girder.

The economically most favourable dimensions of statically undetermined beams suited to carry loads can be determined under rather general conditions by means of elasticity calculations. If the beam is utilized in some privileged cross-sections only and it is made of some material of plastic behaviour, then this plastic reserve will increase the load capacity $(\nu_a > \nu_c)$.

Under operating conditions, the load capacity shall be calculated on the basis of safety factor ν_c. The extraordinary value of load can be calculated by means of factor ν_b.

The correct probability is given by the probability of possible destruction calculatable on the basis of expression (39).

Beams of plastic material will be economically most favourable if the safety is identical in every cross-section. In this case, $\nu_a = \nu_b = \nu_c = \nu$.

The probability of destruction of the beam can be calculated in the way already discussed as the sum of probabilities of destruction of the independent sections.

10. Numerical example

The steel taken as a basis for the numerical example has been made by the Hungarian Millworks. The probability characteristics of the yield limit, calculated on the basis of several thousands of data, of grade 37B-5 plastic steel of Pearson III distribution are given below:

$$\text{Expectable value: } \sigma_{Fo} = 288.3 \text{ N/mm}^2$$

$$\text{Variance: } \quad s_{Fo} = 30.73 \text{ N/mm}^2$$

$$\text{Obliquity: } \quad a_{Fo} = 0.679$$

On the basis of processed data, the relative variance of the dead weight of the steel is $v_g^{(s)} = 0.04$, the obliquity of the load of lognormal distribution, applied to the beam by its own weigth, being 0.40237. The

$$N = H = \frac{0.25\,h^2}{h+2v}\,\sigma_H\,t$$

$$M_H = \sigma_H\left[\frac{b\cdot v}{h+2v}\left(h^2 + 2vh + \frac{4}{3}v^2\right) + \frac{t\cdot h^3}{6(h+2v)}\right]$$

$$E = 206\,000 \text{ N/mm}^2$$

$$N = H = 0.3839\,\sigma_p\,t\,h$$

$$R = \sigma_F\left[0.23\,t\,h^2 + bv(h+v)\right]$$

$J_1 = 16\,513.70667 \cdot 10^6 \text{ mm}^4$

$W_1 = 25\,802\,667 \text{ mm}^3$

$a_{11} = 6.900483184 \cdot 10^{-12}$

$q_{01} = 0.60055924 \cdot 10^{-3} \text{ Nmm}$

$J_2 = 8\,175.438453 \text{ mm}^4$

$W_2 = 13\,143\,792 \text{ mm}^3$

$Z_{11} = 144\,917\,388.2 \cdot 10^3$

$W_{10} = 27\,616\,000 \text{ mm}^3$
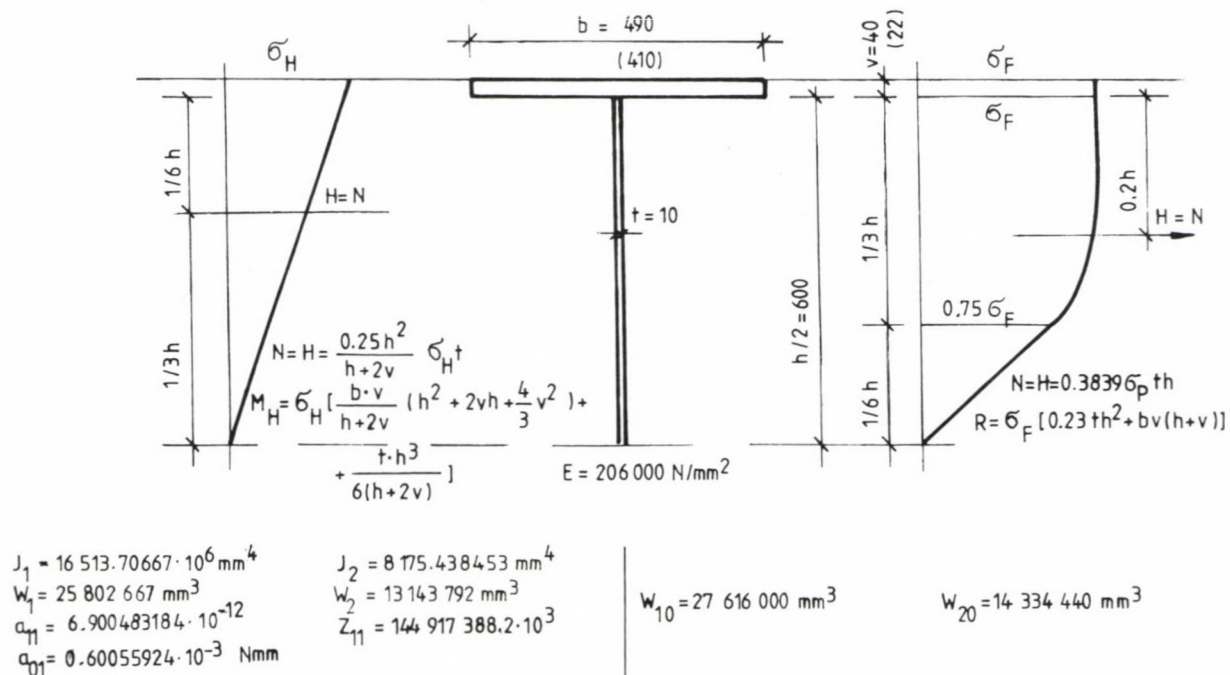
$W_{20} = 14\,334\,440 \text{ mm}^3$

Fig. 6. Cross-sectional data for the numerical example
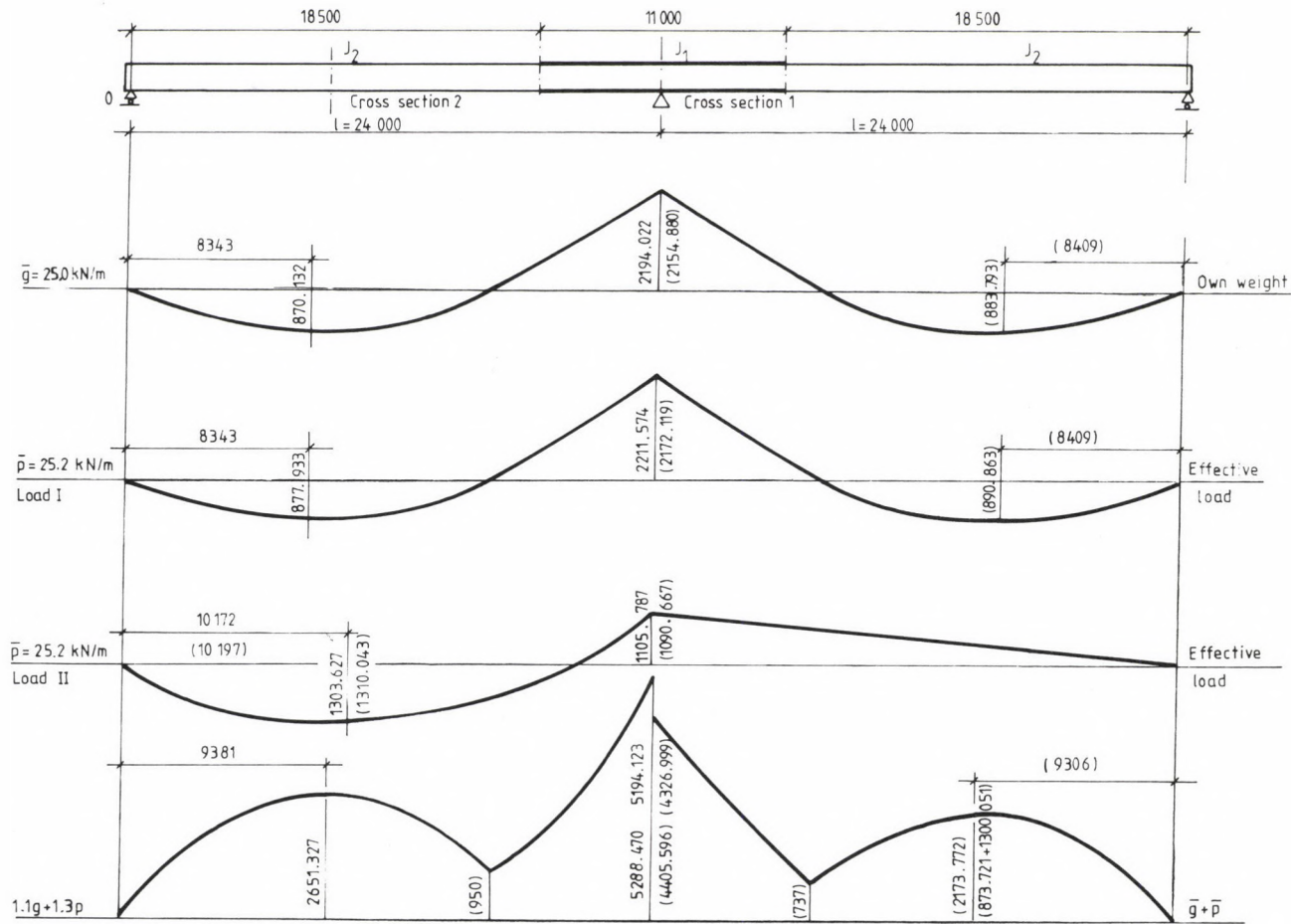(the values in brackets applying to cross-section 2)

Fig. 7. Internal forces of loads

relative variance of the effective load of twice exponential (Gumbel) distribution is, on the basis of measurements, 0.1608, and as is well-known, the obliquity is 1.13955.

The main girder, a steel construction illustrated in Figs 6 and 7, carries the floor of a lecture-room. A permanent load of $g = 25.0$ kN/m is acting upon the main girder, the effective load being 3 kN/m^2 that is $p = 25.2$ kN/m. Standard moment of the floor of a strength calculated according to Hungarian Standard MSZ 15024:

$$\text{At place 1:} \quad M_{M1} = 1.1 \cdot 2194.022 + 1.3 \cdot 2211.574 -$$
$$- (391.418 \cdot 1.1 + 394.549 \cdot 1.3) \cdot 0.1 =$$
$$= 5194.123 \text{ kNm}$$

$$\text{At place 2:} \quad M_{M2} = 1.1 \cdot 873.721 + 1.3 \cdot 1300.051 =$$
$$= 2651.159 \text{ kNm}$$

Standard stress:

$$\text{At place 1:} \quad \sigma_{M1} = 5194.123 \cdot 10^6 / 25\,802\,667 = 201.3 \text{ N/mm}^2$$
$$\text{At place 2:} \quad \sigma_{M2} = 2651.159 \cdot 10^6 / 13\,143\,792 = 201.7 \text{ N/mm}^2$$

Shear test result at place 1:

$$Q_1 = 1.1 \cdot 344.893 + 1.3 \cdot 347.652 = 831.330 \text{ kN}$$

Static moment of the half-section: $S_1 = 13\,952\,000$ mm^3.

$$\tau_{M1} = 831\,330 \cdot 13\,952\,000 / 16\,513\,706\,670 \cdot 10.0 = 70.24 \text{ N/mm}^2$$

For further studies, the plastic properties of the girder were utilized (for starting data see the right side of Fig. 6).

Cross-sectional and strength data and their probability characteristics:

Cross section 1:

Cross-sectional modulus:
$$\bar{W}_{10} = 27\,616\,000 \text{ mm}^3$$

Variance:
$$s_{10}^W = 519\,643 \text{ mm}^3$$

Cross section 2:

$$\bar{W}_{20} = 14\,334\,440 \text{ mm}^3$$

$$s_{20}^W = 237\,385 \text{ mm}^3$$

Cross section 1:   Cross section 2:

Relative variance:
$$v_{10}^{W} = 0.018817$$
$$\qquad\qquad\qquad\qquad\qquad\qquad v_{20}^{W} = 0.016560$$
$$u(50) = 1 - \frac{1}{2}\left(\frac{50}{500}\right) - \frac{1}{2}\left(\frac{50}{500}\right)^2 =$$
$$= 0.94500$$

Reduction in cross-sectional modulus:

$$w_1(50) = 1 - \frac{10(1 - 0.945)}{27\,616\,000}\,1\,031\,520 = \qquad w_2(50) = 1 - \frac{10(1 - 0.945)}{14\,334\,440}\,\cdot$$
$$= 0.97946 \qquad\qquad\qquad\qquad\qquad \cdot\,882\,180 = 0.96615$$

Endurance: $\bar{\alpha}(50) = 1 - 0.15\left(\dfrac{2154.88 + 0.2\cdot 2172.119}{2154.880 + 2172.119}\right)^4 = 0.98077$

Variance: $s_{\alpha}(50) = 0.03$

Design life: $T = 50$ year

Reduction in strength: $\sigma(50) = 1 - \dfrac{1}{2}\left(\dfrac{50}{500}\right)^2 - \dfrac{1}{2}\left(\dfrac{50}{500}\right)^2 = 0.99450$

Increase in strength variance: $s^{(\sigma)}(50) = 1 + 2\left(\dfrac{50}{500}\right) = 1.2$

<center>Load capacity:</center>

$$\bar{R}_1(50) = 288.3\cdot 27\,616\,000\cdot 0.99450\cdot 0.97946\cdot 0.98077 = 7606.136 \text{ kNm}$$
$$\bar{R}_2(50) = 288.3\cdot 14\,334\,440\cdot 0.99450\cdot 0.96615\cdot 0.98077 = 3894.412 \text{ kNm}$$

$$\frac{\bar{R}_2}{\bar{R}_1} = 0.51200925$$

<center>Variance:</center>

$$s_1^{(R)}(50) = 7606.136\sqrt{\left(\frac{0.10659}{0.99450}\right)^2 1.2 + \left(\frac{0.018817}{0.97946}\right)^2 1.2 + 0.03^2} = 935.519 \text{ kNm}$$

$$s_2^{(R)}(50) = 3894.412\sqrt{\left(\frac{0.10659}{0.99450}\right)^2 1.2 + \left(\frac{0.01656}{0.96615}\right)^2 1.2 + 0.03^2} = 477.562 \text{ kNm}$$

Obliquity:

$$a_1^{(R)}(50) = 0.679 \left(\frac{893.031}{935.519}\right)^3 = 0.59062$$

$$a_2^{(R)}(50) = 0.679 \left(\frac{457.240}{477.562}\right)^3 = 0.59595$$

Stress due to load:

Permanent load:

$$\bar{S}_{g1}(50) = -2154.880 \text{ kNm} \qquad \frac{S_{g2}}{S_{g1}} = 0.40542156 \qquad \bar{S}_{g2}(50) = 873.721 \text{ kNm}$$

Variance:

$$s_{g1}(50) = 0.04 \cdot 2154.880 = 86.195 \text{ kNm}$$

$$s_{g2}(50) = 0.04 \cdot 873.721 = 34.949 \text{ kNm}$$

Obliquity:

$$a_{g1}(50) = 0.40237 \qquad\qquad\qquad a_{g2}(50) = 0.40237$$

Effective load:

$$\bar{S}_{p1}(50) = -2172.119 \text{ kNm} \qquad \frac{S_{p2}}{S_{p1}} = -0.59851739 \qquad \bar{S}_{p2}(50) = 1300.051 \text{ kNm}$$

Variance:

$$s_{p1}(50) = 0.1608 \cdot 2172.119 = 349.277 \text{ kNm}$$

$$s_{p2}(50) = 0.1608 \cdot 1300.051 = 209.048 \text{ kNm}$$

Obliquity:

$$a_{p1}(50) = 1.13955 \qquad\qquad\qquad a_{p2}(50) = 1.13955$$

Total load:

$$\bar{S}_1(50) = -2154.880 - 2172.119 = -4326.999 \text{ kNm}$$

$$\bar{S}_2(50) = 873.721 + 1300.051 = 2173.772 \text{ kNm}$$

Variance:

$$s_{S1}(50) = \sqrt{86.195^2 + 349.277^2} = 359.755 \text{ kNm}$$

$$s_{S2}(50) = \sqrt{34.949^2 + 209.048^2} = 211.949 \text{ kNm}$$

Obliquity:

$$a_{S1}(50) = 0.40237 \left(\frac{86.195}{359.755}\right)^3 + 1.13955 \left(\frac{349.277}{359.755}\right)^3 = 1.04387$$

$$a_{S2}(50) = 0.40237 \left(\frac{34.949}{211.949}\right)^3 + 1.13955 \left(\frac{209.048}{211.949}\right)^3 = 1.095200$$

Strength calculation reserve:

$$\bar{Y}_1(50) = 7606.136 - 4326.999 = 3279.137 \text{ kNm}$$

$$\bar{Y}_2(50) = 3894.412 - 2173.772 = 1720.640 \text{ kNm}$$

Variance:

$$s_{Y1}(50) = \sqrt{935.519^2 + 359.755^2} = 1002.307 \text{ kNm}$$

$$s_{Y2}(50) = \sqrt{477.562^2 + 211.949^2} = 522.482 \text{ kNm}$$

Obliquity:

$$a_{Y1}(50) = 0.59062 \left(\frac{935.519}{1002.307}\right)^3 - 1.04387 \left(\frac{359.755}{1002.307}\right)^3 = 0.43198$$

$$a_{Y2}(50) = 0.59595 \left(\frac{477.562}{522.482}\right)^3 - 1.095200 \left(\frac{211.949}{522.482}\right)^3 = 0.38197$$

$$\beta_1(50) = \frac{3279.137}{1002.307} = 3.2716$$

$$\beta_2(50) = \frac{1720.640}{522.482} = 3.2932$$

$$q_1 \sim 1.81 \cdot 10^{-6} \qquad\qquad q_2 \sim 5.71 \cdot 10^{-6}$$

Fracture shear stress: $\bar{\tau}_F = \frac{1}{\sqrt{3}} \, 288.3 = 166.45 \text{ N/mm}^2$

Variance: $s_{\tau F} = \frac{1}{\sqrt{3}} \, 30.79 = 17.777 \text{ N/m}^2$

Obliquity: $a_{\tau F} = 0.679$

    Shear load capacity of the cross-section above the central support:

Load capacity: $\bar{R}_{1Q}(50) = 166.45 \cdot 16\,513\,706\,670 \cdot 10 \cdot$

$$\cdot \frac{0.99450 \cdot 0.98077 \cdot 0.97946}{13\,952\,000} = 1882.134 \text{ kN}$$

Variance: $s_{1QR}(50) = 1882.134 \sqrt{\left(\frac{0.10659}{0.99450}\right)^2 1.2 + \left(\frac{0.018817}{0.97946}\right)^2 1.2 + 0.03^2} =$

$$= 231.494 \text{ kN}$$

Obliquity: $a_{1QR}(50) = 0.59062$

        Maximum resultant and its probability characteristics:

Permanent load: $\bar{Q}_{1g}(50) = 344.893 \text{ kN}$

Variance: $s_{1g}(50) = 0.04 \cdot 344.893 = 13.796 \text{ kN}$

Obliquity: $a_{1g}(50) = 0.40237$

Effective load: $\bar{Q}_{1p}(50) = 347.652 \text{ kN}$

Variance: $s_{1p}(50) = 0.1608 \cdot 347.652 = 55.902 \text{ kN}$

Obliquity: $a_{1p}(50) = 1.13955$

Total load: $\bar{Q}_{1}(50) = 344.893 + 347.652 = 692.545 \text{ kN}$

Variance: $s_{1Q}(50) = \sqrt{13.796^2 + 55.902^2} = 57.579 \text{ kN}$

Obliquity: $a_{1Q}(50) = 0.40237 \left(\frac{13.796}{57.579}\right)^3 + 1.13955 \cdot \left(\frac{55.902}{57.579}\right)^3 = 1.04839$

        Shear strength calculation reserve:

$\bar{Y}_Q(50) = 1882.134 - 692.545 = 1189.589 \text{ kN}$

$s_{YQ}(50) = \sqrt{231.494^2 + 57.579^2} = 238.547 \text{ kN}$

$a_{YQ}(50) = 0.59062 \left(\frac{231.494}{238.547}\right)^3 - 1.04839 \left(\frac{57.579}{238.547}\right)^3 = 0.52502$

$\beta_{YQ}(50) = \frac{1189.589}{238.547} = 4.9868$

$q_Q(50) < 10^{-6}$

The shear load capacity is not a governing characteristic. Probability of destruction of the girder:

$$q = (4 \cdot 5.71 + 1.81) \, 10^{-6} = 24.65 \cdot 10^{-6} \quad \underline{2.47 \cdot 10^{-5}}$$

Safety factors:

$$\nu_{a1} = \frac{7606.136 - 2154.880}{2172.119} = 2.5096$$

$$\nu_{a2} = \frac{3894.412 - 873.721}{1300.051} = 2.3235$$

$$\nu_{b1} = 2.9787; \quad \kappa_1 = 7.0307 \cdot 10^{-3}$$

$$\nu_{b2} = 3.1940; \quad \kappa_2 = -18.3795 \cdot 10^{-3}$$

Calculation of the value of ν_c:

From equations

$$\bar{S}_{p1} \quad \nu_c + z_{11} \quad \kappa_1 = -\bar{R}_1 - \bar{S}_{g1}$$
$$\bar{S}_{p2} \quad \nu_c + z_{21} \quad \kappa_1 = \bar{R}_2 - \bar{S}_{g2}$$

$$\nu_c = \frac{\bar{R}_1 \left(z_{21} + \dfrac{\bar{R}_2}{\bar{R}_1} z_{11} \right) + \bar{S}_{g1} \left(z_{21} - \dfrac{\bar{S}_{g2}}{\bar{S}_{g1}} z_{11} \right)}{- \bar{S}_{p1} \left(z_{21} - \dfrac{\bar{S}_{p2}}{\bar{S}_{p1}} z_{11} \right)} = 2.3967$$

$$\kappa_1 = \frac{\bar{R}_1 \left(\dfrac{\bar{S}_{p2}}{\bar{S}_{p1}} + \dfrac{\bar{R}_2}{\bar{R}_1} \right) - \bar{S}_{g1} \left(\dfrac{\bar{S}_{p2}}{\bar{S}_{p1}} + \dfrac{\bar{S}_{g2}}{\bar{S}_{g1}} \right)}{z_{21} - \dfrac{\bar{S}_{p2}}{\bar{S}_{p1}} z_{11}} = 1.6930 \cdot 10^{-3}$$

On the basis thereof, the increase in load capacity is

$$\bar{R}_2^x = 3894.412 + 1.6930 \cdot 10^{-3} \cdot \frac{9.306}{24.0} \cdot 144\,917.39 = 3989.544 \text{ kNm}$$

κ_1 increasing the variance of the fracture load capacity:

$$(s_{\kappa 1})^2 = \left(\frac{\dfrac{\bar{S}_{p2}}{\bar{S}_{p1}} + \dfrac{\bar{R}_2}{\bar{R}_1}}{z_{21} - \dfrac{\bar{S}_{p2}}{\bar{S}_{p1}} z_{11}} \; s_{R2} \right)^2 + \left(\frac{\dfrac{\bar{S}_{p2}}{\bar{S}_{p1}} + \dfrac{\bar{S}_{g2}}{\bar{S}_{g1}}}{z_{21} - \dfrac{\bar{S}_{p2}}{\bar{S}_{p1}} z_{11}} \; s_{g1} \right)^2$$

$$(s_{\kappa 1})^2 = \left[\frac{(-0.59851739 + 0.51200925)\ 477.562}{(0.38775 + 0.59851739)\ 144917.39} \right]^2 +$$

$$+ \left[\frac{(-0.59851739 - 0.40546156) \cdot 34.989}{(0.38775 + 0.59851739)\ 144917.39} \right]^2 = 14.381757 \cdot 10^{-8}$$

Variance of surplus load capacity:

$s_{\kappa 1} = 3.79233 \cdot 10^{-4}$

$s_R' = 3.79233 \cdot 10^{-4} \dfrac{9.306}{24.00} \; 144\,917.39 = 21.310 \text{ kNm}$

$s_R = \sqrt{477.562^2 + 21.310^2} = 478.037 \text{ kNm}$

$\bar{Y}_{(50)} = 3989.544 - 2173.772 = 1815.772 \text{ kNm}$

$s_{Y(50)} = \sqrt{478.037^2 + 211.949^2} = 522.917 \text{ kNm}$

$a_{Y(50)} = 0.59595\ (478.037/522.917)^3 - 1.0952\ (211.949/522.917)^3 = 0.38237$

$\beta_2 = 1815.772/522.917 = 3.4724$

$q_2 \sim 0.998 \cdot 10^{-6}$

On the basis thereof, the probability of destruction of the girder decreases to $(4 \cdot 0.998 + 1.81) \cdot 10^{-6} = q' = 5.80 \cdot 10^{-6}$, that is, to a quarter of the original value.

11. Summary

Presented in this work is a method to determine the reliability of a rod-type supporting structure.

a) The reliability of lattice girders is given by the sum of probabilities calculated for the rods under identical load.

b) The probability of destruction of compact-walled supporting structures is given by the sum of probabilities of destruction of cross-sections independent of each other, lying at a distance of 10-15 times the height of the beam from each other.

c) A possible destruction of statically undetermined beams will take place at that of the possible plastic hinges for which the probability of destruction is highest.

REFERENCES

1. Bölcskei, E.—Mistéth, E.: Elastic properties of reinforcing wires. Mélyépítési Szemle (4), 1972 (in Hungarian)

2. Éliás, E.: Random variability of the elasticity modulus. Acta Technica Acad. Sci. Hung., Vol. 70 (1—2), 251—263 (1971)

3. Gniegienko, B. V.—Beliaiev, J. K.—Soloviev, A. O.: Mathematical Methods of the Reliability Theory. Műszaki Könyvkiadó Budapest, 1970 (in Hungarian)

4. Korda, J.: Classification of the tensile and compressive strength of elastoplastic materials on the basis of the probability theory. Mélyépítési Szemle (4), 1972 (in Hungarian)

5. Kossalka, J.: Statics and Kinematics of Beams. Budapest 1941

6. Mistéth, E.: Principles of calculations for the economies of size of multipurpose projects using the probability theory. Doctor-thesis, Budapest 1977 (in Hungarian)

7. Mistéth, E.: Change in load cpacity with time. Közlekedésépítési és Mélyépítéstudományi Szemle (3), 1987 (in Hungarian)

8. Weibull, W.: A statistical theory of the strength of materials. Proc. Roy. Swedish. Inst. Eng. Ros. Stockholm, No. 2, 1939

GEOMETRICALLY SIMPLE EXPONENTIAL WEIR

KESHAVA MURTHY, K.[*]—RANGARAJ, C.[**]

This paper presents a practical exponential weir of simple geometric profile formed by quadrants of a circle of radius 'R'. The flow through this weir of crest width '2t', top width 2(R+t) and altitude R, is proportional to the exponential power of head 'h' for flows above a threshold depth, in the range of $0.55 \, R \leq h \leq R$ within a maximum deviation of $\pm$ 2% from the exact theoretical discharge.

The exponential relationship between the discharge and head is determined based on a numerical optimization procedure developed for the purpose. Nearly 45% of the height of the weir can be used effectively as the measuring range. Experiments with the two weirs show excellent agreement with theory by giving a constant average coefficient of discharge C_d equal to 0.62. The use of the weir in measurement of large discharges in canals during floods is highlighted. Another unique feature of this weir is that it is a double purpose weir as it can alternatively be used as a linear proportional weir when inverted.

NOTATION

a, b	constant of the replaced exponential relationship
e	deviation of Q_E from Q_T
g	acceleration due to gravity
h	head above the weir crest
m	slope constant
n	exponent in the term H^n
q	discharge
q_E	proposed relationship in exact exponential form
t	half crest width of the poebing weir
x	vertical co-ordinate
y	horizontal co-ordinate
A, B	nondimensional counterpart of a, b
C	intercept constant
C_d	coefficient of discharge
E	prefixed maximum percentage of error

[*]Keshava Murthy, K., Indian Inst. of Sci., Bangalore — 560 012, India
[**]Rangaraj, C., Indian Inst. of Sci., Bangalore — 560 012, India

H	h/R
H_d	H measured from a datum such that $B = 1$ in the replaced exponential relationship
K	$2C_d \sqrt{2g}$ a dimensional constant
P_R	proportionality range
Q_E	nondimensional replaced exponential discharge
Q_{MAX}, Q_{MIN}	nondimensional discharges at the upper and lower limit of the proportionality range respectively
Q_T	$q/KR^{5/2}$
R	radius of the quadrant
S_1, S_2	curves defining the permissible region for Q_E to lie in Q vs. H plot
T	t/R
X	x/R
Y	y/R
y_1, y_2	counterparts of S_1, S_2 in $\ln(Q)$ vs. H plot respectively
α	base flow depth or lower limit of proportionality range
β	upper limit of the proportionality range

Introduction

Weirs have been classified /4/ into two categories as non-base weirs and base weirs, depending on the value of the exponent 'n' in the discharge-head relationship of the weir, "$Q \propto H^n$". When $n \geq 3/2$ the weirs can be designed without a base. They are called as 'non-base weirs'. The conventional rectangular weir, V-notch and parabolic weirs are examples of this kind. When $n < 3/2$ the weirs invariably require a base and are called 'base weirs'. The linear (Sutro 1908, /9/, Keshava Murthy 1968 and 1978, /10/), quadratic /3/ and logarithmic weirs /2/ belong to the base weir category.

Exact linear weirs have applications in irrigation, hydraulic, chemical and environmental engineering. The complementary profile of these weirs is complex (as is generally the case with all base wier profiles) requiring sophisticated equipment and skilled manpower for their fabrications which are scarce in field conditions.

Troskolanski /11/ in his well-known book on hydrometry mentions about two geometrically simple plate weirs that give near linear head-discharge characteristics. He mentions that the flow through the intervening space obtained by keeping a semicircular cylinder in a rectangular channel produces a near linear characteristic. Troskolanski /11/ also mentions that a closed trapezoidal weir with a vertex angle approximately equal to 50°, gives almost a linear head-discharge relationship. Surprisingly these weirs

were never investigated for about three decades. These weirs, called the bell mouth weir and the inverted V-notch (IVN), were theoretically investigated and experimentally verified by Keshava Murthy and Giridhar (/6/ and /8/). The IVN and the bell mouth weir have been further improved with regards to their range in the chimney weir and the extended bell mouth weir, respectively (/7/ and /8/).

Exponential weir (referred to as the logarithmic weir by Banks, Burch and Shaw /1/) gives a discharge proportional to the exponential power of head, $q \propto e^h$. It could find an application in flood discharge measurement since it is a quick discharging weir. This weir falls under the base weir category since the term e^h in the discharge-head relationship, $q = be^{ah}$, contains a term h. The weir profile obtained using Abel's Integral equations is complex.

The present inquiry into the Poebing weir is motivated by a casual reference made by Troskolanski in his aforementioned book on Hydrometry in which be states that the 'Poebing weir' formed by inserting a semicircular disc of diameter (2R) in a rectangular channel also of width (2R) with the straight portion resting on the channel bed, would result in an approximate exponential weir. This has not been analytically studied. Neither its explicit exponential discharge-head relationship has been determined nor the range of validity of the same has been established. Troskolanski also suggests that a small gap has to be provided between the quadrants of the weir to avoid the surface tension effects. This gap which necessarily has to be provided should also be optimized. The exponential wier (henceforth referred to as 'E-weir') gives the smallest value of relative error so that among the weirs of circular shapes it is perfect from the metrological point of view /11/. In the paper /11/ we relook into this Poebing weir and analyse the characteristics as an E-weir in the framework of the general theory of proportional weirs underlining the existence of a unique reference plane for every weir /3, 4/.

Formulation of the problem

Exponential weirs are those weirs which give an exponential discharge-head relationship in the form

$$q \propto e^{ah} \qquad\qquad ...(1a)$$
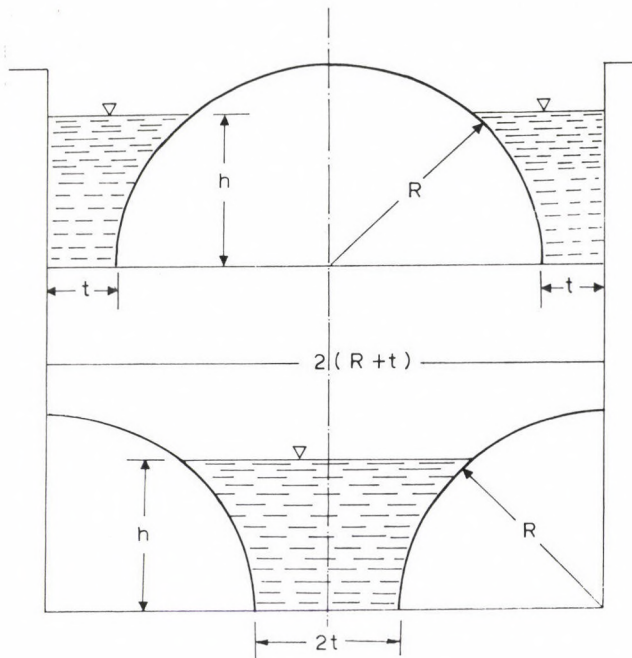
$$q = be^{ah} \qquad\qquad ...(1b)$$

<u>Fig. 1.</u> Poebing weir

The discharge through any symmetrical sharp-crested weir, whose profile is defined by $y = f(x)$ (where x and y are the vertical and horizontal co-ordinate axes, respectively), neglecting the velocity of approach is

$$q = 2C_d \sqrt{2g} \int_0^h \sqrt{(h - x)} f(x) dx,$$

where, q = discharge, h = head above the crest, g = acceleration due to gravity, C_d = coefficient of discharge and $f(x)$ = equation of the profile.

The equation of the profile of the Poebing weir is shown in Fig. 1

$$f(x) = t + R - \sqrt{(R^2 - x^2)},$$

where, t = half crest width, R = radius of the quadrants.

The discharge through it is given by

$$q = 2C_d \sqrt{2g} \int_0^h \sqrt{(h - x)}/t + R - \sqrt{(R^2 - x^2)}/dx \quad 0 \leq h \leq R \qquad \ldots (2)$$

The coefficient of discharge is assumed to be constant, for sharp crested weirs and streamlined flows. The coefficient of discharge is generally a function of several parameters including the head causing flow, dimensions of the weir in relation to the channel and the crest height. The value of C_d has to be ascertained from experiments as in conventional weirs and the variation in C_d will normally be within $\pm$ 1% of the average C_d for any weir and hence can be considered as practically invariable with respect to head.

Equation (2) can be expressed for convenience in the nondimensional from as

$$Q_T = \frac{2}{3}(1 + T)H^{3/2} - \int_0^H \sqrt{(H - X)} \sqrt{(1 - X^2)}dX \quad 0 \leq H \leq 1 \qquad ...(3)$$

where, $Q_T = q/KR^{5/2}$; $H = h/R$; $X = x/R$; $T = t/R$ and $K = 2C_d \sqrt{2g}$.

The integration of Eq. (3) is done by Simpson's one-third rule. The discharge Q vs. head H graph for various values of T is shown in Fig. 2. The same are plotted in Fig. 3 to a semi-log graph ($\log_e Q$ vs. H) where it is seen that the plot is nearly linear for a wide range of head. This implies the existence of a near exponential relationship in the Q versus H graph over a certain range of head.
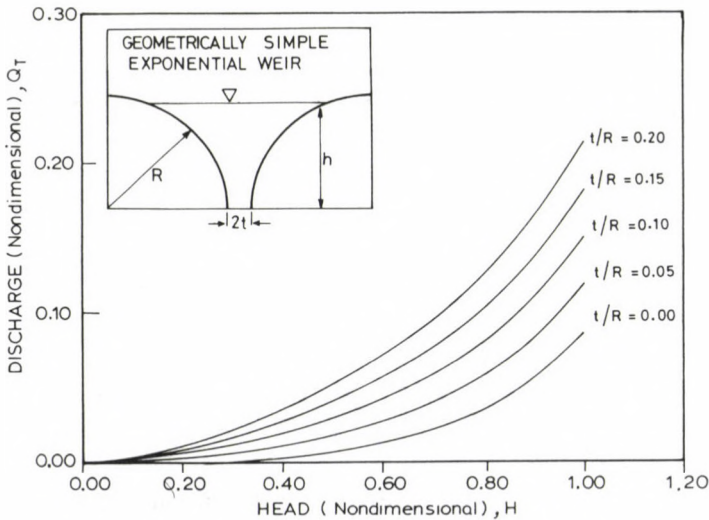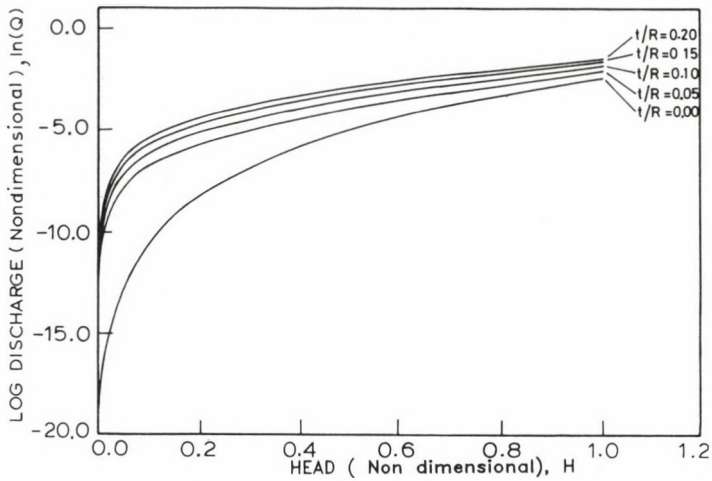

Fig. 2. Theoretical discharge (Q_T) vs. head (H)

Fig. 3. Variation of theoretical discharge w.r.t.
head on a semi-log graph (to the base e)

Analysis

We exploit the near exponential nature of curves in Fig. 2 by propos-
ing a formal exponential relationship

$$Q_E = Be^{AH} \qquad\qquad ...(4)$$

where A and B are constants; such that Q_E gives almost the same discharge
characteristic within a certain range and within a prefixed percentage of
error E. Suppose e, is the deviation of Q_E from Q_T then

$$e = \frac{|Q_T - Q_E|}{Q_T} \times 100 \leq E \qquad\qquad (5a)$$

In most discharge measurements in practice, involving weirs and
notches, a maximum weir indication error (E) of $\pm$ 2% is normally allowed
/11/. This results in a reasonably high degree of accuracy under field con-
ditions. This value of E is adopted in the analysis.

It is seen that the curve Q_E has to lie within the prescribed bounds
of Eq. (5a). This leads to the plotting of the permissible region. Fixing
this region beforehand makes the problem amenable to theoretical treatment.
From Eq. (5a),

$$Q_E = Q_T(1 \pm e/100) \qquad (5b)$$

The appropriate sign, positive if $Q_T < Q_E$ and negative if $Q_T > Q_e$, is considered in Eq. (5b). In the limits Eq. (5b) defines the pair of curves S_1 and S_2 when e attains the value of E. Curves S_1 and S_2 form the lower and upper bound of the permissible region for Q_E.

$$S_1 = Q_T(1 - E/100) \qquad ...(6a)$$

$$S_2 = Q_T(1 + E/100) \qquad ...(6b)$$

The sketch in Fig. 4 shows the region formed by the two curves S_1 and S_2 and the curve Q_E with a part of it embedded in it. The projection on the H-axis (shown as the length between α and β in Fig. 4) of that part of the curve Q_E which lies entirely between the curves S_1 and S_2, defines the proportionality range (P_R). Hence the "Proportionality range", P_R, is

$$P_R = \beta - \alpha \qquad ...(7)$$

The region bounded by Eqs (6a) and (6b) and Eq. (4) is transferred to the semi-log graph. The resulting pair of curves are given by

$$y_2 = \ln S_2 \qquad ...(8a)$$
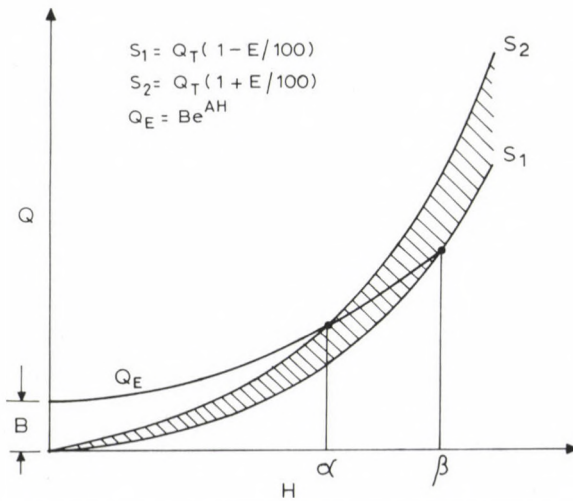
$$y_1 = \ln S_1 \qquad ...(8b)$$

Fig. 4. Typical diagram showing the exact exponential
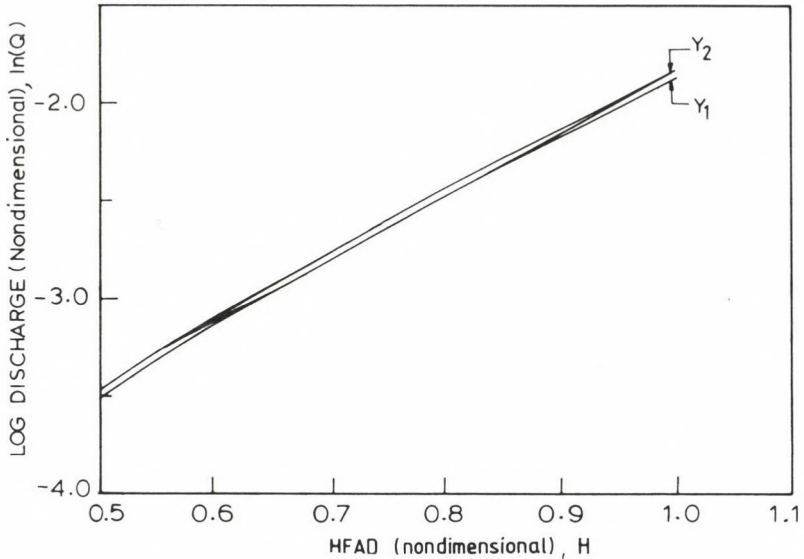discharge curve within the permissible region

<u>Fig. 5a.</u> The exact exponential discharge curve within a
permissible region on a semi-log graph

These curves, with the relevant portion in which the curves are nearly
linear, are shown expanded in Fig. 5a. Since the precise exponential curve
given by Eq. (4) appears as an exact straight line in the semi-log graph
(ln Q vs. H), given by

$$\ln Q_E = \ln B + AH \qquad \ldots(9)$$

already a rough estimate of the maximum proportionality range possible with
its starting and ending points can be obtained as shown in Fig. 5a by moving
a straight edge within the region manually. This would prove useful as a
check and in deciding about the feasibility of the problem in the early
stages.

Optimization procedure

The original problem of stimulating the near exponential character-
istic of the Poebing weir using $Q_E = Be^{ah}$ within the bounds of error and
with the proportionality range maximum, is simplified in the semi-log plane
into finding, by process of optimization, a straight line,

$$y = mH + C \qquad \ldots(10)$$

whose horizontal projection is maximum, subject to the constraint that the entire straight line be in the region bounded by y_2 and y_1. Comparing Eqs (9) and (10), we obtain

$$\ln Q_E = y \qquad \qquad \dots(11a)$$

$$A = m \qquad \qquad \dots(11b)$$

$$B = e^C \qquad \qquad \dots(11c)$$

Expressing the same in dimensional form Eqs (11a) and (11b), we get

$$b = 2C_d \sqrt{2ge} \, {}^C R^{5/2} \qquad \qquad \dots(12a)$$

$$a = m/R \qquad \qquad \dots(12b)$$

A systematic numerical optimization procedure was developed to find the line with the greatest horizontal projection in the region formed by the curves y_2 and y_1 (Fig. 5b) which are monotonically increasing.

A point P_1 is chosen on the extreme right of the y_1 curve and joined to a point P_2 on the extreme left of the y_2 curve. The entire line P_1P_2 may not be in the region. Point P_2 is moved successively on the y_2 curve until the entire line is in the region. The horizontal projection of this line
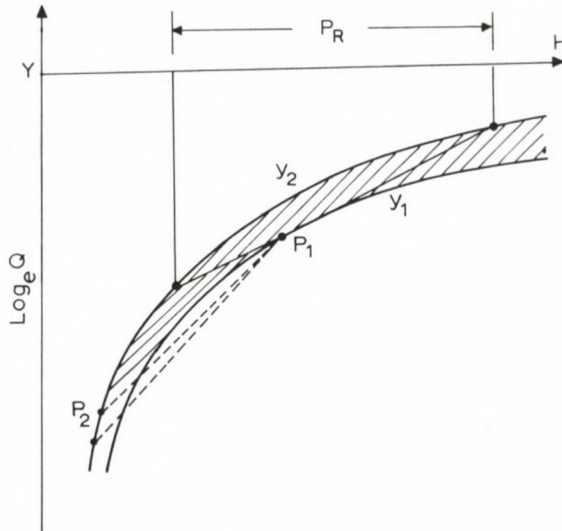

Fig. 5b. Optimization procedure to find the line with the maximum horizontal projection

with any possible extension within the region formed by y_2 and y_1 is then determined.

The procedure is repeated for all possible points P_1 on the y_1 curve such that each time, that straight line inclusive for any extension, which is entirely in the region, is obtained. The line which has the maximum horizontal projection is selected. A computer software was developed for the method on the VAX-88 mainframe computer.

Optimization of the weir parameters

The optimization procedure developed in the previous section is followed to obtain the proportionality range (P_R) for numerous values of t/R, the geometric parameter of the weir. In the light of the fact that Troskolanski /11/ recommends a gap of 3-5 mm between the quadrants, in the actual construction of the Poebing weir to satisfy the practical requirement of avoidance of surface tension effects, it is logical that this geometric parameter of the weir be optimized. The proportionality range (P_R) plotted against the half width t/R is shown in Fig. 6a.

The same is expanded in the range $0 \leq t/R \leq 0.2$ in Fig. 6b. Figure 6b reveals that the proportionality range (P_R) is almost constant in $0.1 \leq \leq t/R \leq 0.2$. A convenient value of t/R = 0.1 is chosen for our experiments.

Analysis of results

From the above optimization procedure we obtain the values A and B (for t/R = 0.1) and the following exponential relationship is proposed.

$$Q_E = 6.396 \times 10^{-3} e^{3.2280H} \quad 0.552 \leq H \leq 1.00 \qquad \ldots(13a)$$

or,

$$Q_E = e^{3.22(H-1.5651)} \qquad \ldots(13b)$$

or,

$$Q_E = e^{3.22(H_d)} \qquad \ldots(13c)$$

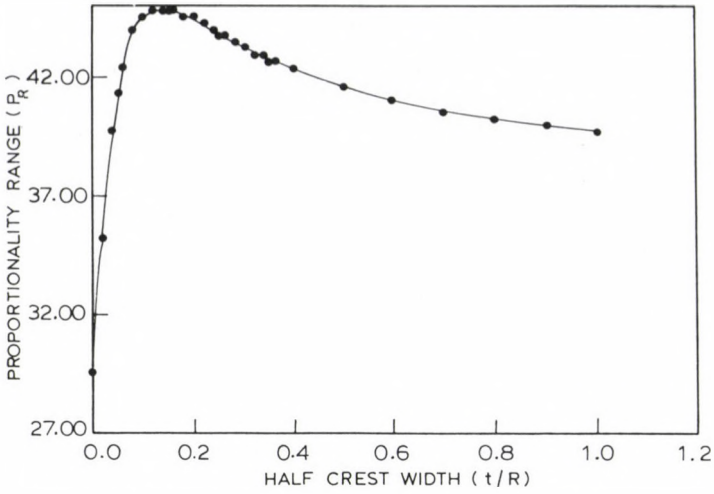where, H_d is the nondimensional head measured from a datum situated at 1.5651R above the crest.

Fig. 6a. Variation of the proportionality range P_r
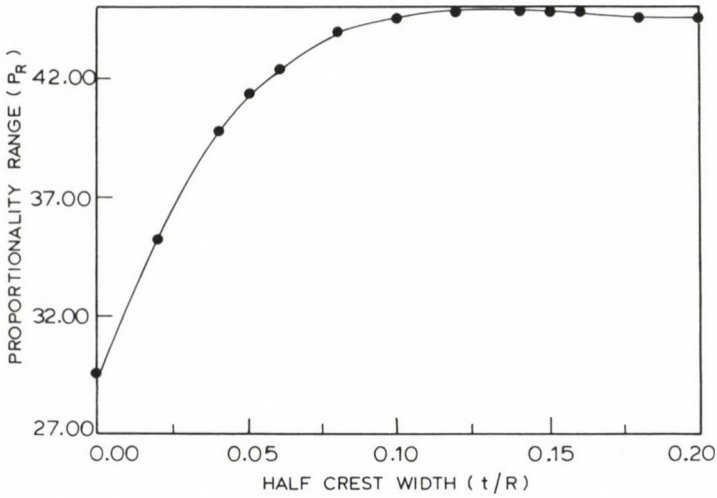with half crest width ratio t/R

Fig. 6b. Variation of the proportionality range with the
half crest width ratio expanded in the region $0 \leq t/R \leq 0.2$

Dimensionally it can be expressed as

$$q_E = q_E K R^{5/2} \qquad\qquad ...(13d)$$

Table 1

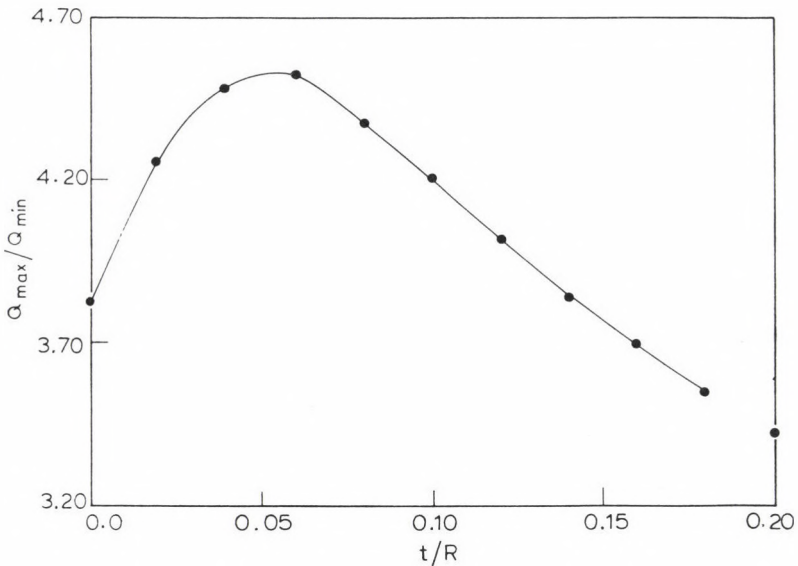| t/R	A	B	Discharge equation
0.12	3.09914	7.8×10^{-3}	$Q = 7.8 \times 10^{-3} e^{3.09914H}$ or, $Q = e^{(3.09914H - 4.85363)}$
0.14	2.997197	9.39742×10^{-3}	$Q = 9.3979 \times 10^{-3} e^{2.9972H}$ or, $Q = e^{(2.9972H - 4.66727)}$
0.16	2.91476154	10.9515×10^{-3}	$Q = 10.9515 \times 10^{-3} e^{2.91476H}$ or, $Q = e^{(2.91476H - 4.51428)}$
0.18	2.84562612	12.537×10^{-3}	$Q = 12.537 \times 10^{-3} e^{2.84562H}$ or, $Q = e^{(2.84562H - 4.37907)}$

Fig. 7. Variation of the ratio of the discharge at the top
and bottom of the measuring range with half crest width ratio

The details of the exponential relationship for various other values of t/R are given in Table 1. The limits of the proportionality range remains constant for $0.1 \leq t/R \leq 0.18$. Figure 7 shows the plot of the ratio of the discharge at the end points (Q_{MAX}, Q_{MIN}) of the measurement range versus the ratio t/R.

It is significant to note that this weir when inverted is the bell mouth weir /8/, a linear proportional weir. At t/R = 0.18 a design close to

the optimum design of the bell-mouth weir is obtained and this value of t/R is within the optimum range of t/R of the Poebing weir. At the value of t/R = 0.1 used in our experiment, 53% of the total height of the bell-mouth weir can be used for the linear measurement. The linear discharge-head relationship is given by

$$Q = 0.2815(H - 0.0437), \quad \text{for} \quad 0.16 \leq H \leq 0.69 \qquad \qquad ...(14)$$

where, $Q = q/KR^{5/2}$; $H = h/R$; $X = x/R$; $T = t/R$; $K = 2C_d\sqrt{2g}$.

Experiments

Experiments were conducted on two geometrically simple E-weirs of R = 0.25 m and R = 0.30 m with t/R = 0.1. The weirs were cut from 6.5 mm thick mild steel plates according to standards. The weirs had a sharp edge of 1.5 mm with a 45° chamfer. Figure 8 shows a schematic arrangement of the laboratory set up used. The weirs are fixed at the end of a rectangular channel 19.5 m long, 1.2 m wide and 1.1 m deep, with crests set 20 cm above the channel bed. The channel had adequate stilling arrangements. The head over the weir was measured using a point gauge, which was fixed 4 m upstream of the weir section, with accuracy of measurements to the third decimal place, 0.001 in (0.1254 mm).
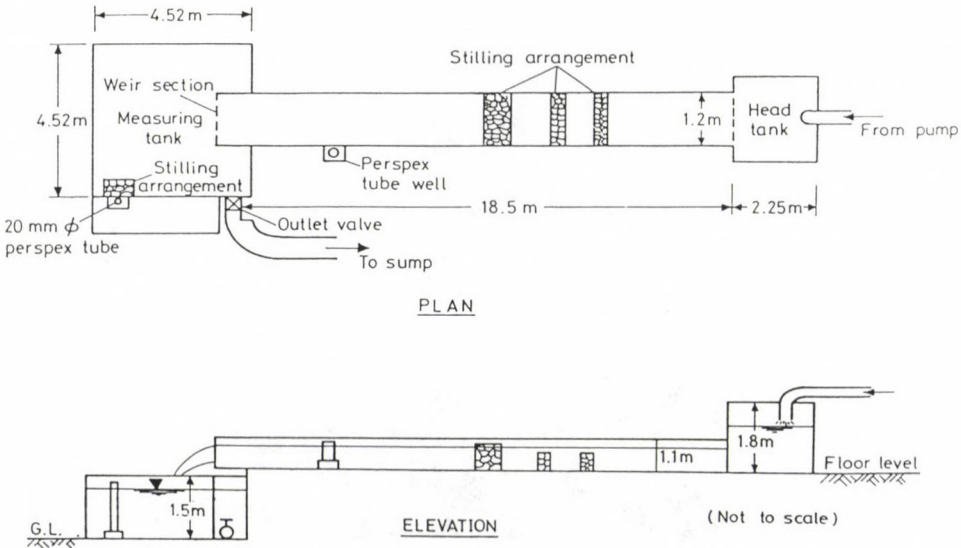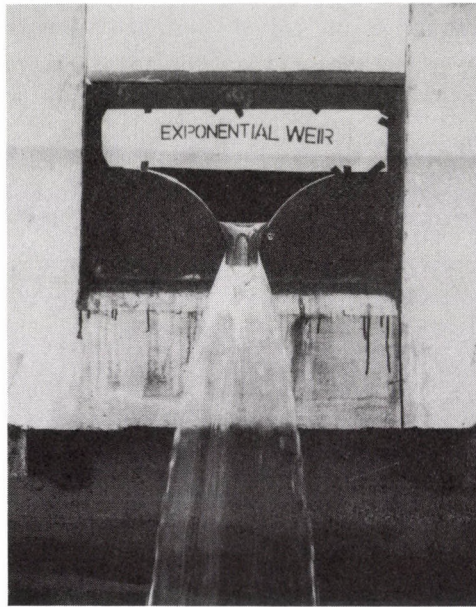

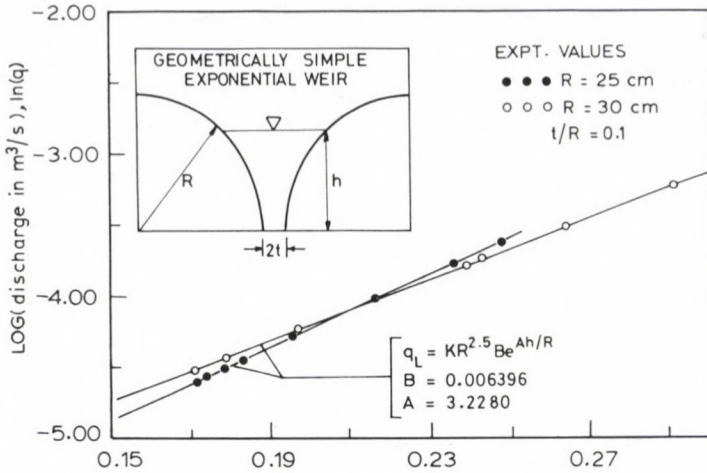Fig. 8. Experimental set-up

Fig. 9a

Fig. 9b

Fig. 10. Semi-log plot of actual discharge versus head

The discharges were measured volumetrically in a measuring tank 4.52 x 4.52 m x 1.5 m through readings in a perspex tube of 20 mm internal diameter, connected to the bottom of the tank at one end. The discharges were determined by finding the time taken for the water level to rise from one indicator, fixed in the perspex tube, to another, which was exactly at a height of 50 cm above the first indicator. The indicators were connected to the leads of an electronic timer through a start and stop mechanism. Figures 9a, 9b shows the photograph of the weir discharging.

Figure 10 shows the variation of measured discharge versus head on a semi-log graph (ln q vs. h). It is seen that the experiments are in very good agreement the theory by giving a constant average C_d. Figure 11 shows the variation of C_d with head for two weirs with R = 0.24 m and R = 0.3 m and t/R = 0.1. The C_d is obtained as the ratio of the experimental discharge to the discharge obtained from the proposed exponential relationship. It is seen that the C_d, does not vary by more than $\pm 1\%$ from the average C_d for any head which adequately supports the assumption of a constant coefficient of discharge in analysis.
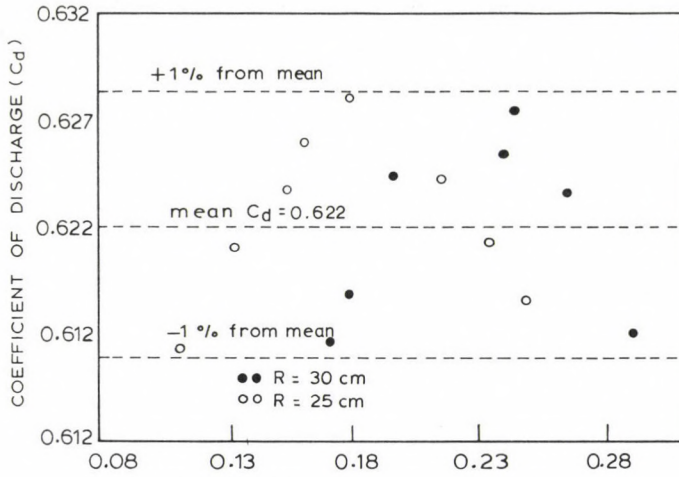
Fig. 11. Variation of C_d with depth of flow

Concluding remarks

1. It is shown that the weir formed by two quadrants of a circle of radius R with a gap of 2t between them can be used to give a exponential discharge-head relationship within a maximum percentage deviation of ± 2 from the theoretical discharge in a range of head determined by the value of t/R.

2. This weir is a unique weir where the reference plane could be adjusted.

3. When t/R lies between 0.1 and 0.18 maximum range of measurable head is obtained. For the above range of t/R nearly 45% of the effective depth of the weir can be used in the range of head $0.55R \leq h \leq R$.

4. Experiments on two weirs give a constant average coefficient of discharge, C_d equal to 0.62. The variation of C_d is within ± 1% of the mean value.

5. The geometrically simple E-weir can also be used as a linear weir (bell mouth weir) when inverted. For t/R = 0.1 it has the linear relationship in the range $0.16R \leq h \leq 0.69R$.

6. On account of its geometric simplicity and its quick discharging characteristic it should prove useful in practice as a quick discharge measuring device during floods.

ACKNOWLEDGEMENT

REFERENCES

1. Banks, W. H. H.—Burch, C. R.—Shaw, T. L.: The design of proportional and logarithmic thin plate weirs. J. Hydr. Res., Vol. 6, No. 2 (1968), 75—105

2. Govinda Rao, N. S.—Keshava Murthy, K.: On the design of logarithmic weirs. J. Hydr. Res., Vol. 4, No. 1 (1966), 51—59

3. Keshava Murthy, K.: On the design of quadratic weirs. J. of the Franklin Inst., Vol. 287, No. 2 (1969), 159—174

4. Keshava Murthy, K.—Gopalakrishna Pillai, K.: Design of constant accuracy linear proportional weirs. J. Hydr. Div., ASCE, Vol. 106 (4), (1978), 527—541

5. Keshava Murthy, K.—Pillai, G. K.: Modified proportional V-notch. J. Hydr. Div., ASCE, Vol. 104, No. HY5, May 1978, 715—791

6. Keshava Murthy, K.—Giridhar, D. P.: Inverted V-notch: A practical proportional weir. J. Irrig. and Drain. Engrg., ASCE, Vol. 115 (6), (1989), 1035—1050

7. Keshava Murthy, K.—Giridhar, D. P.: Improved inverted V-notch or chimney weir. J. Irrig. and Drain. Engrg., ASCE, Vol. 116 (3), (1990), 374—386

8. Keshava Murthy, K.—Giridhar, D. P.: Geometrically simple linear weirs using circular quadrants-bell mouth weirs. J. Hydr. Res., IAHR, Vol. 29, No. 4 (1991),

9. Lakshman Rao, N. S.—Abdul Bhukari, C. H.: Linear proportional weirs with Trapezoidal bottoms. J. Hydr. Res., IAHR, Vol. 9, No. 3 (1971), 413

10. Srinivasulu, P.—Raghavendra, R.: Linear proportional weirs. J. Hydr. Div., ASCE, Vol. 96, No. HY2, Proc. Paper 7062 (1970), 379—389

11. Troskolanski, A. T.: Hydrometry: Theory and Practice of Hydraulic Measurements. Pergamon Press, New York (1960)

12. Venkataraman, P.—Subramanya, K.: A practical proportional weir. Water Power, Vol. 25 (5), (1973), 189—190

USE OF A HYPERBOLIC FUNCTION
TO DESIGN A SELF-BASING LINEAR WEIR

KESHAVA MURTHY, K.[*]—RANGARAJ, C.[**]—RAMESH, H. S.[***]

This paper is concerned with the theory and design of a new improved self-basing linear weir of small base flow depth and constant indication accuracy. The design is achieved by utilising the characteristics of a simple hyperbolic function. It is seen that the 'reference plane' or the 'datum' of the weir lies with the crest, so that the discharge through this weir, for all flows above a threshold depth, is proportional to the head measured above the crest within a prefixed maximum percentage deviation of $\pm 1\%$ of the theoretical discharge. Experiments with two typical weirs confirm the theory by giving a constant co-efficient of discharge of 0.64. Its application in irrigation and environmental engineering is highlighted.

NOTATIONS

a	a constant
b	a constant, here equal to the co-efficient of the term $h^{3/2}$ in $\phi(H)H$
e	relative error $= \left\| \dfrac{Q - Q_L}{Q} \right\|$
e_{max}	maximum permissible 'e' adopted in the design
g	acceleration due to gravity
h	head above the weir crest
m	slope constant
n	exponent
q	discharge
α	a parameter controlling the shape of the generating function and the base depth
x	vertical co-ordinate
κ_0	the value of x at which the function becomes nearly constant/linear
y	horizontal co-ordinate
$\phi(H)$	$\tanh(\alpha\sqrt{(H)})$, a function which becomes rapidly constant beyond an initial non-linear portion

[*]Keshava Murthy, K., Indian Institute of Sci., Bangalore — 560 012, India

[**]Rangaraj, C., Indian Institute of Sci., Bangalore — 560 012, India

[***]Ramesh, H. S., Indian Institute of Sci., Bangalore — 560 012, India

Γ the well-known gamma function
C_d coefficient of discharge
E absolute error
H h/W
H_c h/H_c
Q $q/KW^{5/2}$
Q_c $q/KW_c^{5/2}$
Q_L linear discharge relationship replacing the theoretical discharge Q
X x/W
X_c x/W_c
Y y/W
Y_c y/W_c
W a dimensional length constant
W_c half crest width of the weir depending on α

1. Introduction

Linear proportional weir has attracted interest in recent years /1—4/ owing to its simplicity in head-discharge relationship as well as its practical applications in varied fields like chemical, environmental and irrigation engineering /5/.

Exact linear proportional weirs are invariably compound weirs consisting of a base weir and a complementary weir /6/ fitted over it and achieve a discharge directly proportional to the linear power of the head measured above a datum, generally non-coincident with the crest. As compared with the exact linear proportional weirs, geometrically simple weirs /7—9/ have a profile consisting only of straight lines and segments of circles and are thus easy to fabricate. However geometrically simple linear weirs produce a discharge proportional to the linear power of the head in a limited range controlled by the choice of the maximum permissible error deviation from the theoretical discharge.

Self-basing linear weirs (henceforth referred to as 'SBL weirs') /10, 11/, are a new class of weirs consisting of a single profile with a portion of the weir above the creast acting as the base weir. In comparison, with the geometrically simple linear weirs, the self-basing linear weirs have a marked advantage in having unlimited linearity range. Self-basing linear weirs are also free of the criticism directed against the conventional linear weirs questioning the rationality of choosing a common value of the coefficient of discharge C_d, for the flow, in the base weir as well as the complementary weir above.

A problem common to most of the physically feasible exact linear weirs is that the reference plane does not lie with the crest. This makes the indication accuracy (error caused in the discharge computation for a $\pm 1\%$ error in the head) to vary with the head which is undesirable /12/.

The two main disadvantages of the self-basing linear weir designed earlier by Keshava Murthy and Giridhar, are

(i) the reference plane of the weir does not lie with the crest so that the indication accuracy is not a constant but varies with the head,

(ii) the base depth is sufficiently large so that a large amount of water flows before the linearity law of the weir starts.

The above two limitations are overcome in the present design.

2. Choice of the generating function

A self-basing linear weir can be obtained in any one of the following ways:

(i) Using a discharge function $q = f(h)$ (generating function) which is non-linear in the range $0 \le h \le d$ but becomes near linear in $d \le h \le \infty$ (SBL-1 type) (Fig. 1a).

(ii) Using a function, $\dfrac{dq}{dh} = f(h)$ which is non-linear in the range $0 \le h \le d$ but is nearly constant in $d \le h \le \infty$ (SBL-2 type) (Fig. 1b).

Consider the function

$$\phi(x) = \tanh(\alpha \sqrt{x}) \qquad \qquad \ldots(1)$$
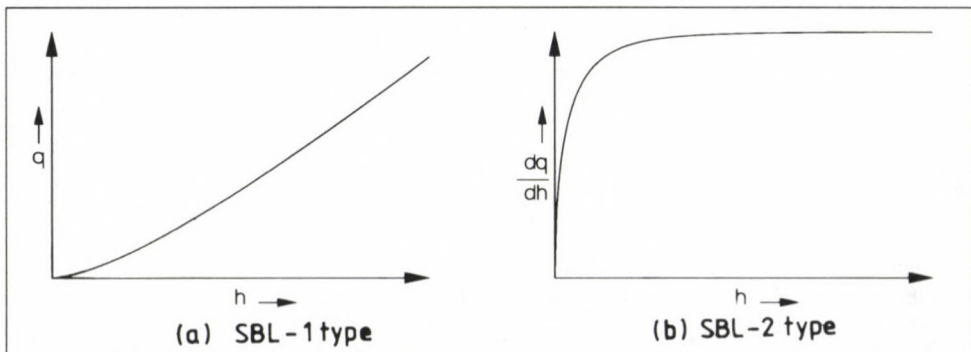

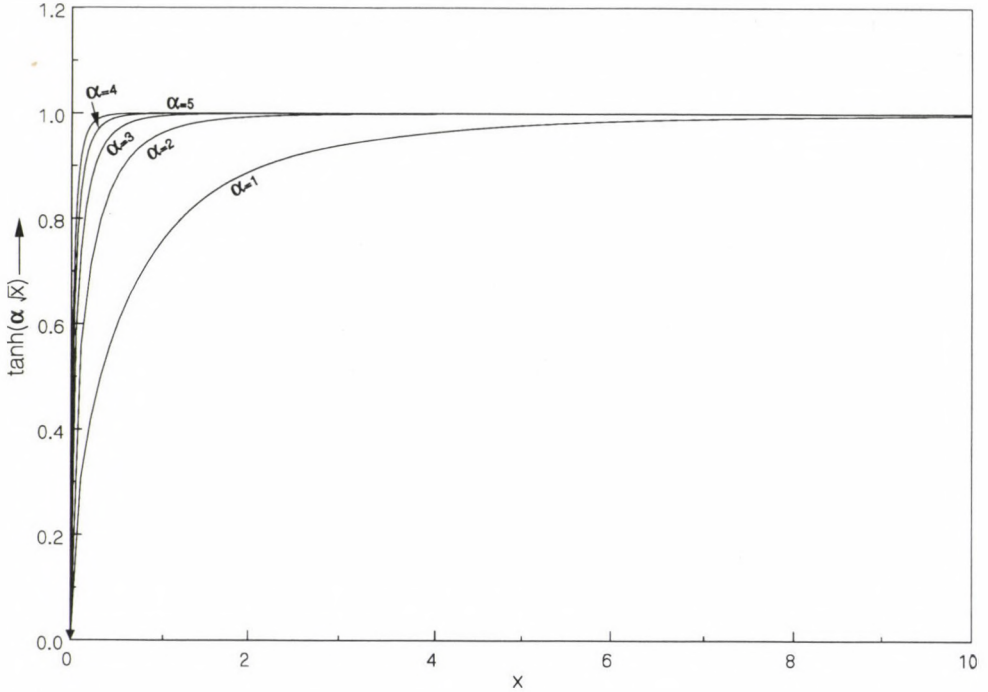(a) SBL-1 type   (b) SBL-2 type

Fig. 1. Forms of primary generating function

Fig. 2. Plots of $\tanh(\alpha\sqrt{x})$ ⟶

where α is a constant. It is seen from Fig. 2 that ϕ is non-linear in $0 \leq x \leq x_0$ and is nearly constant for $x \geq x_0$. The value of x_0 decreases as α increases. However it is advantageous to use the function of the form, $x\phi(x)$ which is non-linear in the range $0 \leq x \leq x_0$ and nearly linear in $x \geq x_0$ as SBL-1 type as will be clear in the foregoing sections. Hence we take

$$Q = \tanh(\alpha\sqrt{H})H) = \phi(H)H \qquad \qquad \ldots(2)$$

as the generating function in non-dimensional form (ref. Eq. (6)) to derive the weir profile. It is seen that $Q(0) = 0$, $Q(\infty) = \infty$, $Q(H)$ is monotonically increasing and $\frac{dQ}{dH} = 0$ at $H = 0$, which are the conditions to be satisfied by any discharge-head function.

A weir with a zero crest width at the origin will increase in width and reach a maximum and once again decrease which will lead to sharp kinks which are difficult to fabricate and are undesirable in a weir. Whereas a weir with a finite crest width at the origin will give rise to a profile which is continuously decreasing. Hence we look forward for an additional

requirement of a profile with finite crest width at the origin. It is clear from the works of Cowgill /13/ and Banks /14/ that a weir will have a finite crest width if and only if Q(H) has $H^{3/2}$ as the lowest term. Expanding Q in terms of power series we have,

$$Q = (\alpha H^{3/2} - (1/3)\alpha^3 H^{5/2} + \ldots) \qquad \ldots(3)$$

it is seen that the least power of head is 3/2, assuring that the weir will have non-zero, finite crest width /13, 14/. Hence $Q = \phi(H)H$ is choses as the primary H-Q function to achieve a constant accuracy self-basing linear weir.

The crest width for the weir can be derived as below. For a weir producing a discharge $q = bh^m$ the weir profile is given by /13, 14/:

$$y = f(x) = \frac{b}{C_d \sqrt{2g\pi}} \frac{\Gamma(m + 1)}{\Gamma(m - 1/2)} x^{m-3/2}$$

Substituting $b = 2C_d \sqrt{2g}\alpha W$ and $m = \frac{3}{2}$ in the above equation,

$$y(0) = \frac{2\alpha W}{\sqrt{\pi}} \frac{\Gamma(3/2 + 1)}{\Gamma(3/2 - 1/2)} = \frac{3W\alpha}{2}$$

or,

$$Y(0) = \frac{3\alpha}{2} . \qquad \ldots(4)$$

3. Mathematical analysis

The discharge through a sharp crested weir defined by $y = f(x)$ is given by

$$q(h) = 2C_d \sqrt{2g} \int_0^h \sqrt{(h - x)} f(x) dx \qquad \ldots(5)$$

where, q = discharge or rate of flow,
       h = depth of flow measured above the weir crest,
       g = acceleration due to gravity,
       C_d = coefficient of discharge.

The coefficient of discharge is assumed to be constant, for sharp creasted weirs and streamlined flows. Coefficient of discharge is generally a function of several parameters including surface tension, viscosity, head
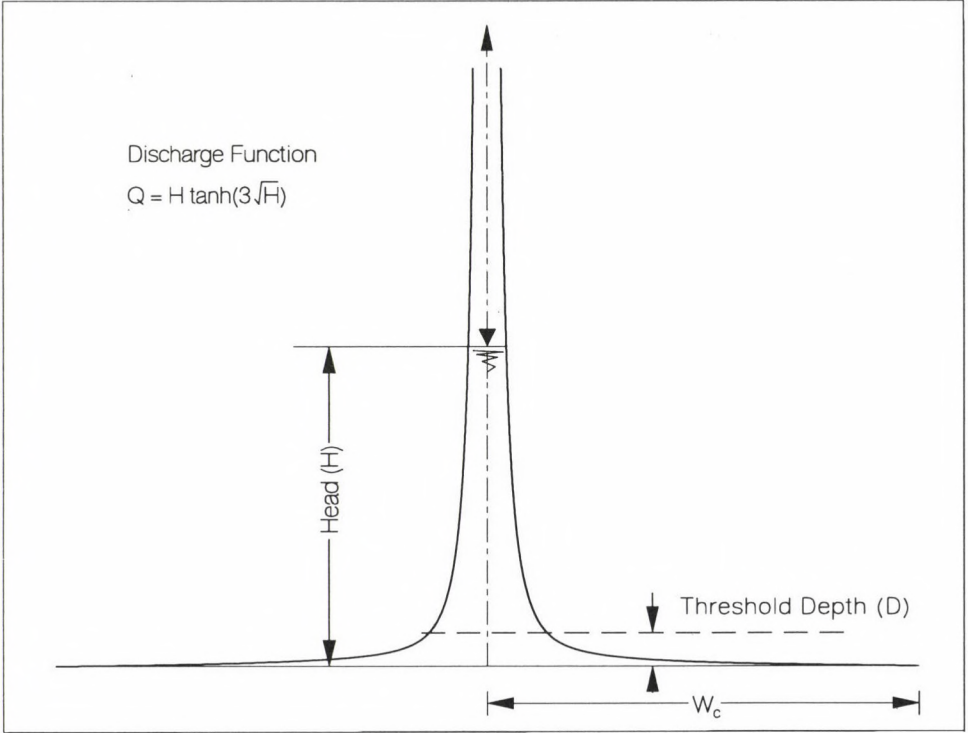
Fig. 3. Profile of the weir

causing flow, dimensions of the weir in relation to the channel and the
crest height. The value of C_d has to be ascertained from experiments as in
all sharp crested weirs. The variation in C_d will normally be within $\pm 1\%$
of the average C_d for any weir.

Non-dimensionalising Eq. (5)

$$Q(H) = \int_0^H \sqrt{(H - X)} F(X) dX \qquad \qquad \dots (6)$$

where, $H = h/W$,

$\quad x = x/W$,

$\quad Q = q/(2C_d \sqrt{2g} W^{5/2})$,

$\quad W =$ a dimensional length constant.
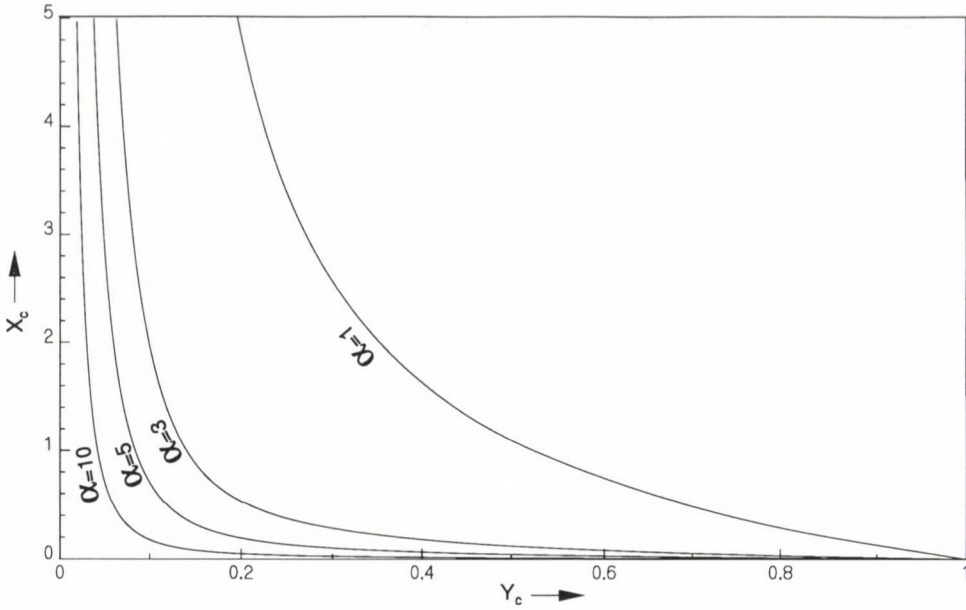
<u>Fig. 3a.</u> Shows the weir profiles (y/W_c) for various values of α

Differentiating Eq. (5) with respect to h using Leibnitz's rule

$$\int_0^H \frac{F(X)}{\sqrt{(H - X)}} \, dX = 2Q'(H) \qquad \qquad \ldots(7)$$

The left-hand side of Eq. (7) is in the form of Abel's integral equation and the solution of Eq. (7) is /14, 15/

$$F(X) = \frac{2}{\pi} \int_0^X \frac{Q''(H)}{\sqrt{(X - H)}} \, dH \qquad \qquad \ldots(8)$$

The integration in the above equation was performed on the UNIX system using the 'Mathematica' package to get the weir profile. The profile of the weir for $\alpha = 3$ is shown in Fig. 3. For the purpose of comparison the half profile of the weirs for different values of α are shown in Fig. 3a.

4. Linear discharge characteristic of the weir

Let

$$Q_L = mH + C \qquad \qquad ...(9)$$

represent the asymptote, of the theoretical head-discharge curve.

$$m = \lim_{H \to \infty} \frac{dQ(H)}{dH} = 1 \qquad \qquad ...(10)$$

$$C = \lim_{H \to \infty} (Q(H) - mH) = 0 \qquad \qquad ...(11)$$

The equation of the asymptote, which if the linear relationship replacing the actual discharge-head curve (for $H \geq H_0$) is

$$Q_L = H \qquad \qquad ...(12)$$

By takint $q = kh \tan n(\alpha \sqrt{h})$, where k is a constant, inclination of the q-h curve could be varied, to get a weir of the desired sensitivity.

5. Analysis of error

If E(H) is the absolute deviation of Q from Q_L

$$E(H) = |Q - Q_L| \qquad \qquad ...(13)$$

it is seen that $E(0) = 0$, $E(\infty) = 0$.

The relative error as defined by

$$e = \left| \frac{Q - Q_L}{Q} \right| \qquad \qquad ...(14)$$

is continuously decreasing with H in the range $0 \leq H \leq \infty$ and rapidly approaches zero. It is seen from Fig. 4, that the error is equal to $\pm 1\%$ at $H = 0.781$ (for $\alpha = 3$), beyond which for all practical purposes, the designed weir is almost as accurate as any exact linear weir. In most discharge measurements in practice, involving weirs and notches, a maximum relative error of $\pm 2\%$ is normally allowed /15/. This results in a reasonably high degree of accuracy under field conditions. Taking the maximum permissible
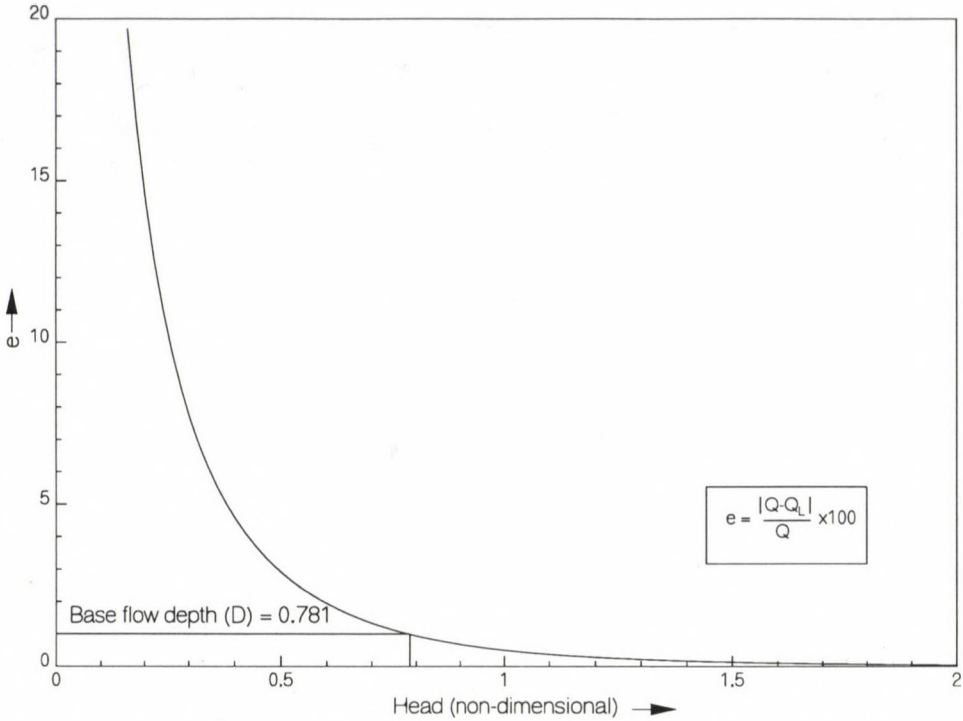
Fig. 4. Distribution of percentage relative error

error as $\pm 1\%$ for our design, the depth of flow at which this error occurs can be considered as the threshold depth, which is analogous to the base weir in conventional weirs.

From Eq. (2), Eq. (12) and Eq. (14) the base depth for a given value of e_{max} is

$$D = \frac{c_1}{\alpha^2} \qquad \qquad \ldots(15)$$

where, $c_1 = (ArcTAnh(\frac{1}{1 + e_{max}/100}))^2$,

   D = nondimensional base flow depth, d/W.

From Eq. (15) the value of α giving the same base depth of 0.4 obtained from the earlier designed SBL weir /10, 11/ is 2.271, corresponding for a $\pm 1\%$ relative error in discharge.

Table 1

x/W$_c$	Co-ordinates of y/W$_c$ for values of α =			
	6	5	7	10
0.00	1.0000	1.0000	1.0000	1.0000
0.05	0.7170	0.4664	0.3088	0.1958
0.10	0.5515	0.3047	0.1982	0.1334
0.15	0.4467	0.2341	0.1570	0.1088
0.20	0.3761	0.1958	0.1348	0.0944
0.25	0.3263	0.1719	0.1204	0.0846
0.30	0.2898	0.1553	0.1099	0.0773
0.35	0.2620	0.1430	0.1019	0.0716
0.40	0.2403	0.1334	0.0954	0.0670
0.45	0.2230	0.1257	0.0900	0.0632
0.50	0.2088	0.1192	0.0854	0.0599
0.55	0.1970	0.1136	0.0815	0.0571
0.60	0.1870	0.1088	0.0781	0.0547
0.65	0.1785	0.1046	0.0750	0.0526
0.70	0.1711	0.1009	0.0723	0.0507
0.75	0.1646	0.0975	0.0699	0.0489
0.80	0.1588	0.0944	0.0677	0.0474
0.85	0.1536	0.0916	0.0657	0.0460
0.90	0.1490	0.0891	0.0638	0.0447
0.95	0.1448	0.0867	0.0621	0.0435
1.00	0.1409	0.0846	0.0605	0.0424
3.00	0.0814	0.0489	0.0350	0.0245
5.00	0.0632	0.0379	0.0271	0.0189
7.00	0.0534	0.0320	0.0229	0.0160
9.00	0.0471	0.0282	0.0202	0.0141
11.0	0.0426	0.0255	0.0182	0.0127
13.00	0.0392	0.0235	0.0168	0.0117
15.00	0.0365	0.0219	0.0156	0.0109
17.00	0.0343	0.0205	0.0147	0.0102
19.00	0.0324	0.0194	0.0139	0.0097
21.00	0.0308	0.0185	0.0132	0.0092

5. Universalisation of the weir parameters

The primary discharge-head function is non-dimensionalised with re-spect to a dimensional length parameter W. However it is desirable to non-dimensionalise the profile equation of the designed weir with respect to its own dimension namely, the half crest width W_c. It is apparent from this non-dimensionalisation that $\frac{y(0)}{W_c} = 1$ and from Eq. (4) $\frac{W_c}{W} = \frac{3\alpha}{2}$.

The corresponding threshold depth is

$$D_c = \frac{d}{W_c} = \frac{2D}{3\alpha} \qquad \qquad ...(16)$$

From Eqs (4), (12) and (19),

$$Q_c = aH_c \qquad \qquad ...(17)$$

where $a = \left(\frac{3}{2}\alpha\right)^{-3/2}$. For the designed weir with $\alpha = 3$, $y(0) = W_c = 4.5$, $D_c = 0.1736$ and $Q_c = 0.10476\ H_c$. Table 1 gives the co-ordinates of the weir for $\alpha = 3, 5, 7$ and 10.
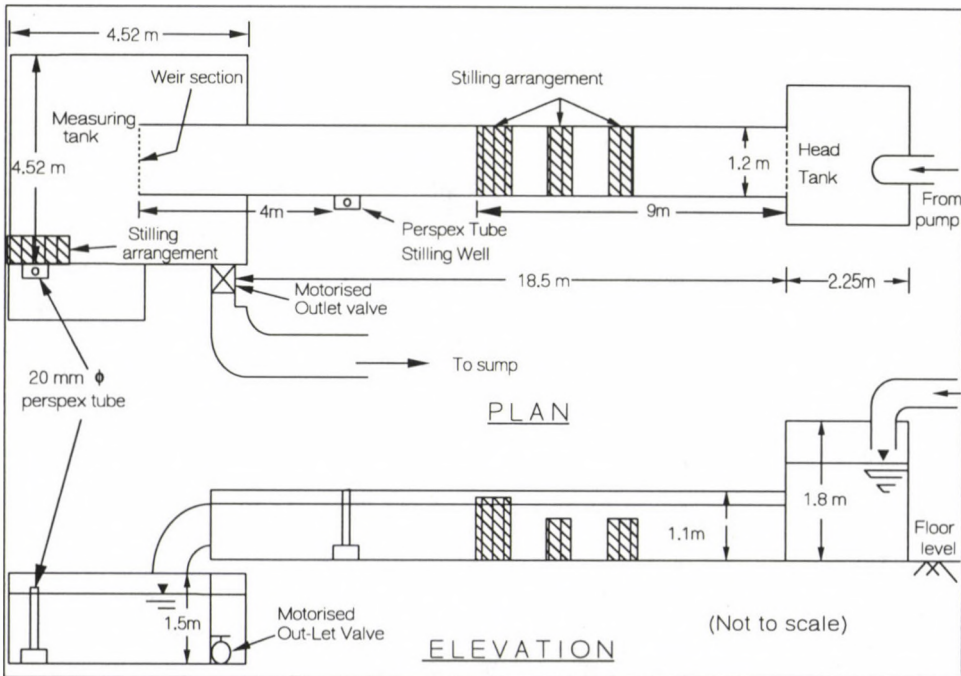
Fig. 5. Experimental setup
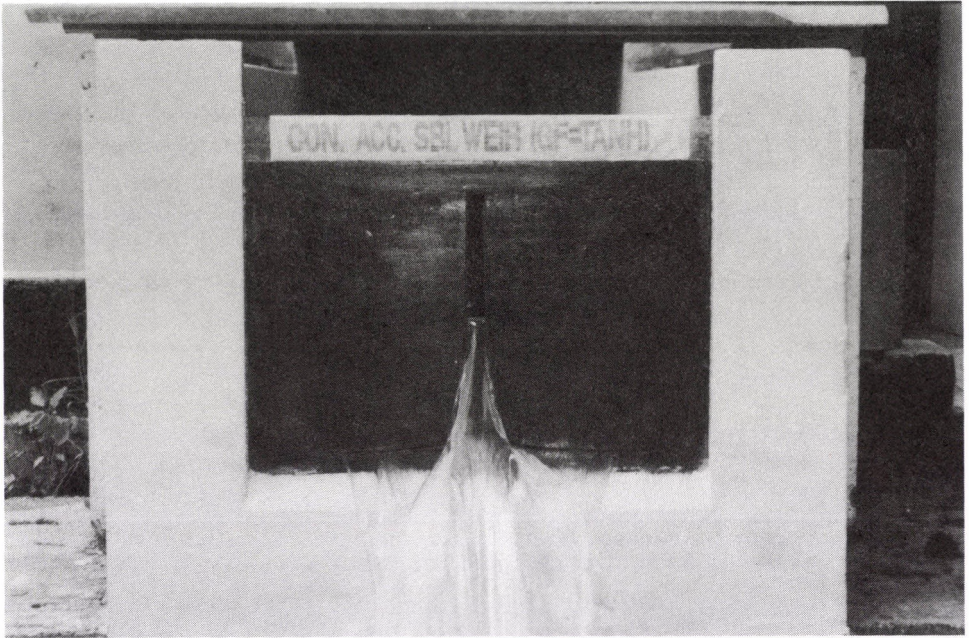
Fig. 6a. Front view
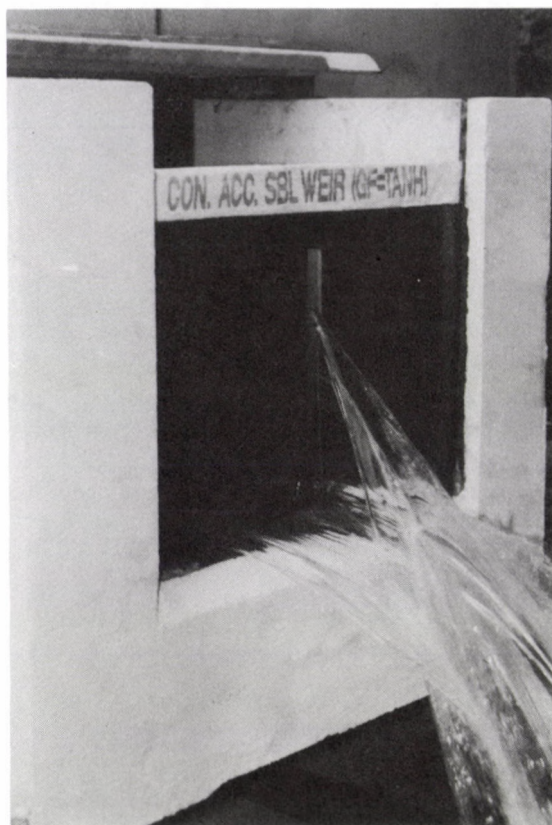
Fig. 6b. Side view showing the nappe
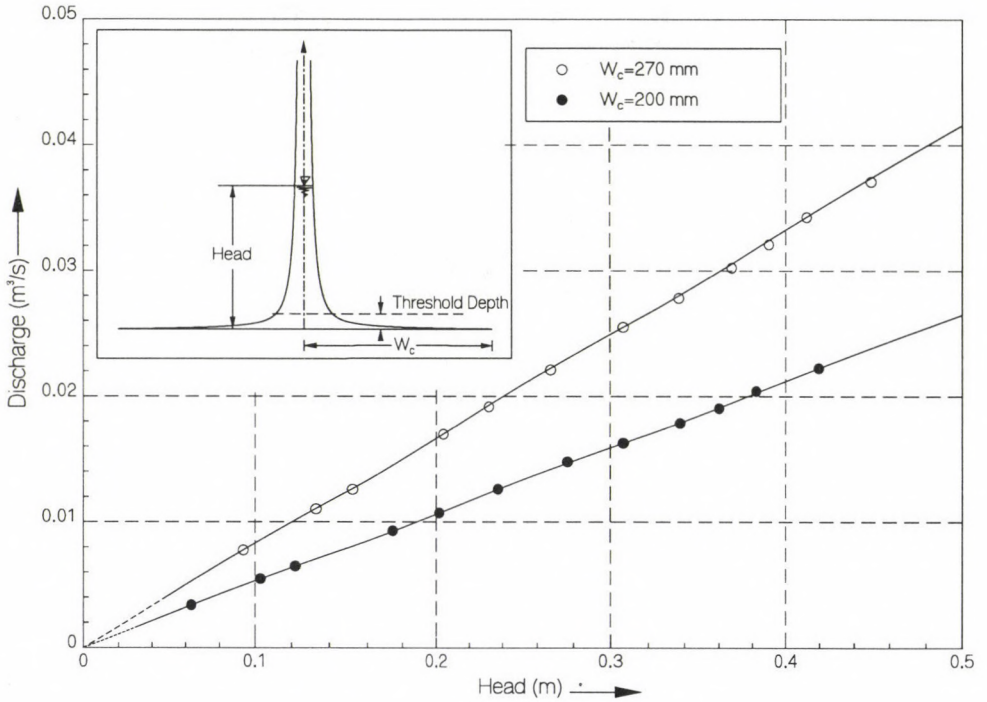
Fig.-7. Experimental head-discharge plot

6. Experiments

The experimental setup is shown in Fig. 5. The profile of the weir is cut on a nibbing machine using 914.4 mm x 609.6 mm x 6.5 mm thick M.S. Sheets. The depth of flow over the crest was measured with an electronic point gauge having a least count of 0.01 mm located 4 m upstream of the weir section in a stilling well. The surface waves were dampened by using graded boulders on the upstream of the channel section. The time required to collect a fixed volume of water in a measuring tank (4.52 m x 4.52 m x 1.5 m) was recorded with the help of an electronic timer triggered by impulse signals attached to the level indicators. Figure 6 (Photo) shows the view of the discharging weir. Figure 7 shows the plot of actual discharge versus head measured above the crest of the weir. The graph is a straight line passing through the origin, confirming the theoretical analysis. The plot of coefficient of discharge versus head is shown in Fig. 8 and the average coefficient of discharge for the weir is 0.63. The coefficient of discharge for any head is
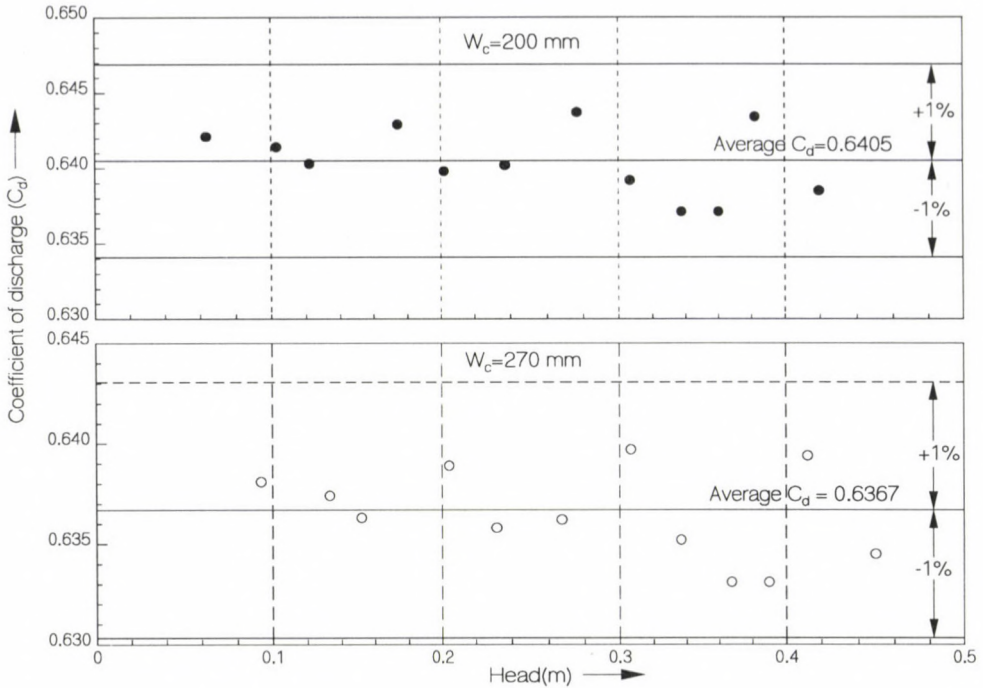
Fig. 8. Plot of C_d vs. head

well within $\pm$ 1% of the average C_d which justifies the assumption of con-
stant coefficient of discharge in the analysis.

7. Conclusions

1. A hyperbolic function is used as a generating function to design a con-
   stant accuracy linear weir.
2. The weir has a non-zero finite crest width.
3. The base flow depth or the threshold depth (depth at which $\pm$ 1% error oc-
   curs) varies with the parameter α.
4. For $\alpha \geq 2.271$, the base flow depth of the designed weir is smaller than
   the base depth of the earlier designed SBL weir using quadratic weir
   profile.
5. The reference plane of the weir significantly, lies with the crest ren-
   dering it as a constant accuracy weir.
6. Experiments with two typical weirs are in good agreement with the theory
   by giving a constant co-efficient of discharge of 0.64.

ACKNOWLEDGEMENT

REFERENCES

1. Stout, O. V. P.: The proportional flow weir devised in 1896. Engineering News Record, 72 (3) (1914), 148—149

2. Pratt: Another proportional weir. Engineering News Record 72 (9) (1914), 462—463

3. Srinivasulu, P.—Raghavendra, R.: Linear proportional weirs. J. Hyrd. Div., ASCE, 96 (2) (1970), 379—389

4. Lakshman Rao, N. S.—Abdul Bhukari, C. H.: Linear proportional weirs with trapezoidal bottoms. J. Hydr. Res., IAHR, 9 (3) (1971), 413—427

5. Singer, J.—Lewis, D. C. G.: Proportional weirs for automatic sampling or dosing. Water and Engineering, 70 (841) (1966), 105—111

6. Keshava Murthy, K.—Seshagiri: A generalised mathematical theory of proportional weirs. J. of the Franklin Institute, 285 (5) (1968), 347—363

7. Keshava Murthy, K.—Giridhar, D. P.: Inverted V-notch: A practical proportional weir. J. Irrig. and Drain. Engrg., ASCE, 115 (6) (1989), 1035—1050

8. Keshava Murthy, K.—Giridhar, D. P.: Improved inverted V-notch or chimney weir. J. Irrig. and Drain. Engrg., ASCE, 116 (3) (1990), 374—386

9. Keshava Murthy, K.—Giridhar, D. P.: Geometrically simple linear weirs using circular quadrants-bell mouth weirs. J. Hydr. Res., IAHR, 29 (4) (1991), 497—509

10. Keshava Murthy, K.—Giridhar, D. P.: On the design of self basing weirs (under review)

11. Giridhar, D. P.: Mathematical theory and experimental verification on geometrically simple and self basing linear weirs. Ph. D. Thesis, 1990, Indian Institute of Science Bangalore, India

12. Keshava Murthy, K.—Gopalakrishna Pillai, K.: Design of constant accuracy linear proportional weirs. J. Hydr. Div., ASCE, 106 (4) (1978), 527—541

13. Cowgill, A. P.: The Mathematics of Weir Forms, 2 (2) (1944), 142—147

14. Banks, R. B.: A Note on Generalized Weir Equation. Dept. of Civil Engg., North Western University, Paper HP 0654, Illinois, 1954

15. Troskolanski, A. T.: Hydrometry: Theory and Practice of Hydraulic Measurements. Pergamon Press, New York, 1960

A SIMPLIFIED DERIVATION OF THE EQUATIONS
OF SHALLOW-SHELL THEORY IN CURVILINEAR CO-ORDINATES

MBAKOGU, F. C.[x]—PAVLOVIĆ, M. N.[xx]

The differential equations describing the behaviour of a shallow shell within the broad framework of curvilinear co-ordinates corresponding to the mutually orthogonal lines of curvature of the shell middle surface are derived on the basis of the two-surface shell theory. This approach to the derivation of the shell equations is, in essence, a generalization of an earlier formulation, due to Calladine /1/, in terms of plane Cartesian co-ordinates. Specific examples of the present formulation are then given with reference to more complex frames of reference such as spherical, cylindrical, polar and quasi-polar co-ordinate systems. As will be seen, the proposed derivation scheme — which may also be extended so as to encompass completely general, oblique frames of reference — is, in the spirit of the two-surface idealization of shells, more direct, simpler and, above all, more instructive than conventional treatments.

Introduction

The complex interaction between bending and stretching actions, which generally combine to sustain loads applied to shell structures, can be effectively studied by means of a two-surface theory of shells proposed by Calladine /1/. In this theory the interaction between bending and stretching actions is brought out in physical terms by the conceptual splitting of the actual surface of a shell into two distinct, but coincident, surfaces, designated B and S, each of which is endowed with a different part of the stiffness of an element of the shell. The S- (or stretching) surface possesses in-plane stiffness only, and thus carries membrane (i.e. in-plane) forces but is physically incapable of transmitting bending (and twisting)

---

[x]F. C. Mbakogu, Allied Tropical Consultants Ltd., 5 Akinola Cole Crescent, Ikeja, Lagos, Nigeria

[xx]M. N. Pavlović, Department of Civil Engineering, Imperial College of Science, Technology and Medicine, London SW7 2BU, U.K.

moments and transverse shear forces. On the other hand, the B- (or bending) surface is provided with flexural stiffness only, and hence sustains bending (and twisting) moments and transverse shear forces but offers no resistance whatsoever to in-plane forces. The device of splitting the action of a shell into two distinct parts affords the possibility of thinking separately about the two aspects of behaviour, and the interaction between them. Thus, for example, the load-sharing between the two surfaces provides ready insight into the regime of behaviour into which a given problem falls /2--4/.

In /5--8/, the didactic potential of the two-surface model was illustrated by means of a numerical model. Here, the teaching potential of the method is demonstrated by reference to analytical derivations. Specifically, the differential equations describing the behaviour of a shallow shell within the broad framework of curvilinear co-ordinates corresponding to the lines of curvature of the shell middle surface are derived on the basis of the two-surface theory. This approach to the derivation of the shell equations is essentially a generalization of an earlier formulations, due to Calladine /1/, in terms of plane Cartesian co-ordinates. Special cases of the present treatment -- corresponding to cylindrical, spherical, polar and quasi-polar co-ordinate systems -- are then used to illustrate the inherent advantages of the approach. Apart from its elegance, when compared to existing derivations /9--14/, the present approach also has clear didactic advantages, notably, the elucidation of the meanings of the various quantities in the field equations in simple, physical terms. These advantages stem from the use, in the present scheme, of the two-surface notion of separable bending and stretching effects, and of the Gaussian curvature change as the prime kinematic variable.

General derivation

Figure 1 shows the various stress resultants and couples acting on a differential element of a shell, as well as the surface tractions to which the element is subjected. The orthogonal curvilinear co-ordinates α_1 and α_2 coincide with the lines of principal curvatures of the middle surface of the shell. The applied loading consists of a normal pressure p and a pair of tangential surface tractions q_1 and q_2 aligned with the directions of principal curvature. The diagram defines the positive senses of the in-plane direct and shearing stress resultants N_1, N_2, $N_{12}(=N_{21})$, out-of-plane (or

Fig. 1. Infinitestimal shell element under in-plane and bending
actions (only actions on sides AB and BC are shown)

transverse) shear stress resultants Q_1, Q_2 and bending and twisting stress
resultants (or couples) M_1, M_2, M_{12} (= M_{21}).

Let the principal curvatures of the middle surface of the shell be de-
noted by K_1 (= $1/R_1$), K_2 (= $1/R_2$) while the associated Lamé parameters be de-
noted by A_1 = A_1 (α_1, α_2), A_2 = A_2 (α_1, α_2). It will be recalled, from the
theory of surfaces, that these geometric parameters are related thus:

$$\frac{\partial}{\partial \alpha_1}\left(\frac{1}{A_1}\frac{\partial A_2}{\partial \alpha_1}\right) + \frac{\partial}{\partial \alpha_2}\left(\frac{1}{A_2}\frac{\partial A_1}{\partial \alpha_2}\right) = - K_1 K_2 A_1 A_2 \tag{1}$$

$$\frac{\partial}{\partial \alpha_1}(K_2 A_2) = K_1 \frac{\partial A_2}{\partial \alpha_1} \tag{2}$$

$$\frac{\partial}{\partial \alpha_2}(K_1 A_1) = K_2 \frac{\partial A_1}{\partial \alpha_2} \tag{3}$$

The above relations are the well-known Gauss—Codazzi equations (the first
is Gauss's equation, while the other two are due to Codazzi), the signifi-
cance of which rests on the fact that the quantities A_1, A_2, K_1 and K_2 can-
not be expressed arbitrarily as function of the co-ordinates (α_1, α_2) of a
point on the surface /15, 16/.

Now consider the equilibrium of the differential shell element. In-
stead of formulating the equilibrium equations for the actual shell element
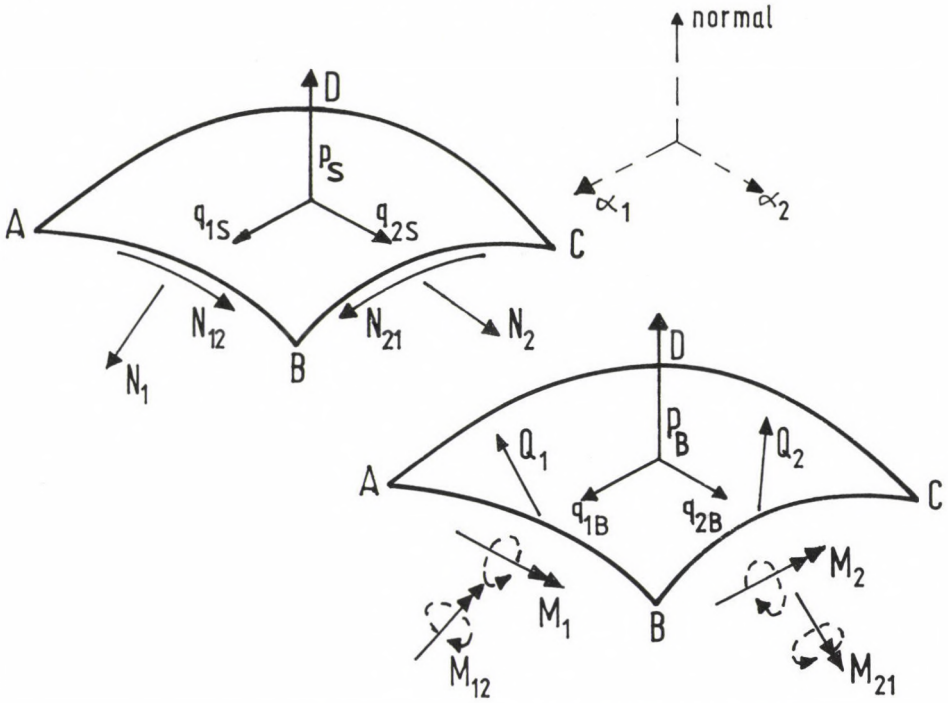
Fig. 2. Mathematical model for the infinitesimal shell element
of Fig. 1 obtained by splitting the shell into two separate surfaces
a) S-surface ("stretching"); b) B-surface ("bending")

directly, as in conventional treatments, we shall, in keeping with the two-surface idealization, set up the corresponding equations for each of the distinct conceptual surfaces used in modelling the shell. As shown in Fig. 2(a) and Fig. 2(b), the S-surface element carries only the membrane stress resultants while the B-surface element sustains the flexural actions exclusively. The diagrams also show that the B-surface element is subjected to a normal pressure p_B and two tangential surface tractions q_{1B}, q_{2B} while its S-surface counterpart is, in turn, subjected to a normal pressure p_S and a pair of tangential loadings q_{1S} and q_{2S}. It is obvious that, since the actual applied loading is generally carried partly by the S-surface and partly by the B-surface, the following interaction conditions of overall equilibrium linking the carrying capacities of the two surfaces hold true:

$$p_S + p_B = p \tag{4}$$

$$q_{1S} + q_{1B} = q_1 \tag{5}$$

$$q_{2S} + q_{2B} = q_2 \tag{6}$$

It may readily be shown that the equilibrium equations for the two surfaces are as follows:

$$K_1 N_1 + K_2 N_2 = p_S \tag{7}$$

$$\frac{1}{A_1 A_2} \left[\frac{\partial(A_2 N_1)}{\partial \alpha_1} - N_2 \frac{\partial A_2}{\partial \alpha_1} + \frac{\partial(A_1 N_{12})}{\partial \alpha_2} + N_{12} \frac{\partial A_1}{\partial \alpha_2} \right] = -q_{1S} \tag{8}$$

$$\frac{1}{A_1 A_2} \left[\frac{\partial(A_1 N_2)}{\partial \alpha_2} - N_1 \frac{\partial A_1}{\partial \alpha_2} + \frac{\partial(A_2 N_{12})}{\partial \alpha_1} + N_{12} \frac{\partial A_2}{\partial \alpha_1} \right] = -q_{2S} \tag{9}$$

$$\frac{1}{A_1 A_2} \left[\frac{\partial(A_2 Q_1)}{\partial \alpha_1} + \frac{\partial(A_1 Q_2)}{\partial \alpha_2} \right] = -p_B \tag{10}$$

$$\frac{Q_1}{R_1} = -q_{1B} \tag{11}$$

$$\frac{Q_2}{R_2} = -q_{2B} \tag{12}$$

$$\frac{1}{A_1 A_2} \left[\frac{\partial(A_2 M_1)}{\partial \alpha_1} + \frac{\partial(A_1 M_{12})}{\partial \alpha_2} + M_{12} \frac{\partial A_1}{\partial \alpha_2} - M_2 \frac{\partial A_2}{\partial \alpha_1} \right] = Q_1 \tag{13}$$

$$\frac{1}{A_1 A_2} \left[\frac{\partial(A_1 M_2)}{\partial \alpha_2} + \frac{\partial(A_2 M_{12})}{\partial \alpha_1} + M_{12} \frac{\partial A_2}{\partial \alpha_1} - M_1 \frac{\partial A_1}{\partial \alpha_2} \right] = Q_2 \tag{14}$$

Equations (7)--(9) relate to the S-surface while expressions (10)--(14) are associated with the B-surface. For the former, equation (7) expresses the condition of force equilibrium in the normal direction while equations (8) and (9) are the corresponding equations for the tangential directions. For the B-surface, equation (10) represents the condition of force equilibrium in the normal direction while equations (11) and (12) are the corresponding equations for the tangential directions; in addition, equations (13) and (14) represent the conditions of moment equilibrium about the α_1 and α_2 axes.

Clearly, the S-surface equilibrium equations (7)--(9) are of the same form as the corresponding equations of a membrane shell (see, for example, Gol'denveizer /17/). In the present case, however, the load components acting

on the S-surface element represent only some portion of the actual (i.e. total) applied load components.

By combining equations (10), (13) and (14), one may express the B-surface pressure loading p_B in terms of the bending and twisting moments as follows:

$$
\begin{aligned}
-A_1 A_2 p_B &= \frac{\partial}{\partial \alpha_1} \left\{ \frac{1}{A_1} \left[\frac{\partial(A_2 M_1)}{\partial \alpha_1} + \frac{\partial(A_1 M_{12})}{\partial \alpha_2} + M_{12} \frac{\partial A_1}{\partial \alpha_2} - M_2 \frac{\partial A_2}{\partial \alpha_1} \right] \right\} \\
&+ \frac{\partial}{\partial \alpha_2} \left\{ \frac{1}{A_2} \left[\frac{\partial(A_1 M_2)}{\partial \alpha_2} + \frac{\partial(A_2 M_{12})}{\partial \alpha_1} + M_{12} \frac{\partial A_2}{\partial \alpha_1} - M_1 \frac{\partial A_1}{\partial \alpha_2} \right] \right\}
\end{aligned}
\tag{15}
$$

In view of the mechanical characteristics of the B-surface, one would expect that the above expression (15) represents the equation of equilibrium of an element of a flat plate which is locally tangential to the curved surface of the shell. However, unlike a flat-plate element, which is incapable of carrying any tangential loading, the curved B-surface element demands some tangential loading in order to secure its equilibrium in the tangential direction. This is confirmed by equations (11) and (12), which reveal that the required B-surface loadings q_{1B}, q_{2B} depend on the disposition of the transverse shear forces Q_1, Q_2 within the B-surface. By reason of the smallness of the B-surface tangential loadings in the present context of shallow shells, it is obvious that they can provide but very feeble coupling between the bending and stretching effects, which coupling disappears in the limiting case of a flat plate. Thus, it seems reasonable to ignore the terms q_{1B} and q_{2B} in equations (5), (6), (11) and (12), thereby transferring the entire applied tangential loadings to the S-surface. Evidently, the neglect of the tangential force interaction between the S- and B-surfaces is consistent with the Donnell—Mushtari—Vlasov simplifications of the shell equations; and, also, with Gol'denveizer's approximation for shells with 'large indices of variation' /17/. Moreover, such a move implies that the interaction conditions of overall equilibrium are expressed solely in terms of normal loading components /3, 18/.

The constitutive and compatibility relations for the two imaginary surfaces may also be formulated separately. In the following, these relations, together with the equilibrium equations, are collected together in separate columns for the two surfaces. (For present purposes, tangential surface tractions are neglected — this point will be taken up again later.)

S-surface

B-surface

$$\frac{N_1}{R_1} + \frac{N_2}{R_2} = p_S \qquad (16S)$$

$$\frac{\kappa_2}{R_1} + \frac{\kappa_1}{R_2} = g_B \qquad (16B)$$

$$\frac{\partial(A_2 N_1)}{\partial\alpha_1} - N_2 \frac{\partial A_2}{\partial\alpha_1} + \frac{\partial(A_1 N_{12})}{\partial\alpha_2} +$$

$$\frac{\partial(A_2 \kappa_2)}{\partial\alpha_1} - \kappa_1 \frac{\partial A_2}{\partial\alpha_1} - \frac{\partial(A_1 \kappa_{12})}{\partial\alpha_2} -$$

$$+ N_{12} \frac{\partial A_1}{\partial\alpha_2} = 0 \qquad (17S)$$

$$- \kappa_{12} \frac{\partial A_1}{\partial\alpha_2} = 0 \qquad (17B)$$

$$\frac{\partial(A_1 N_2)}{\partial\alpha_2} - N_1 \frac{\partial A_1}{\partial\alpha_2} + \frac{\partial(A_2 N_{12})}{\partial\alpha_1} +$$

$$\frac{\partial(A_1 \kappa_1)}{\partial\alpha_2} - \kappa_2 \frac{\partial A_1}{\partial\alpha_2} - \frac{\partial(A_2 \kappa_{12})}{\partial\alpha_1} -$$

$$+ N_{12} \frac{\partial A_2}{\partial\alpha_1} = 0 \qquad (18S)$$

$$- \kappa_{12} \frac{\partial A_2}{\partial\alpha_1} = 0 \qquad (18B)$$

- -

$$N_1 = \frac{1}{A_2} \frac{\partial}{\partial\alpha_2} \left(\frac{1}{A_2} \frac{\partial\Phi}{\partial\alpha_2} \right) +$$

$$\kappa_2 = - \frac{1}{A_2} \frac{\partial}{\partial\alpha_2} \left(\frac{1}{A_2} \frac{\partial w}{\partial\alpha_2} \right) -$$

$$+ \frac{1}{A_1^2 A_2} \frac{\partial A_2}{\partial\alpha_1} \frac{\partial\Phi}{\partial\alpha_1} \qquad (19S)$$

$$- \frac{1}{A_1^2 A_2} \frac{\partial A_2}{\partial\alpha_1} \frac{\partial w}{\partial\alpha_1} \qquad (19B)$$

$$N_2 = \frac{1}{A_1} \frac{\partial}{\partial\alpha_1} \left(\frac{1}{A_1} \frac{\partial\Phi}{\partial\alpha_1} \right) +$$

$$\kappa_1 = - \frac{1}{A_1} \frac{\partial}{\partial\alpha_1} \left(\frac{1}{A_1} \frac{\partial w}{\partial\alpha_1} \right) -$$

$$+ \frac{1}{A_1 A_2^2} \frac{\partial A_1}{\partial\alpha_2} \frac{\partial\Phi}{\partial\alpha_2} \qquad (20S)$$

$$- \frac{1}{A_1 A_2^2} \frac{\partial A_1}{\partial\alpha_2} \frac{\partial w}{\partial\alpha_2} \qquad (20B)$$

$$N_{12} = - \frac{1}{A_1 A_2} \left(\frac{\partial^2 \Phi}{\partial\alpha_1 \partial\alpha_2} - \right.$$

$$\kappa_{12} = - \frac{1}{A_1 A_2} \left(\frac{\partial^2 w}{\partial\alpha_1 \partial\alpha_2} - \right.$$

$$\left. - \frac{1}{A_2} \frac{\partial A_2}{\partial\alpha_1} \frac{\partial\Phi}{\partial\alpha_2} - \frac{1}{A_1} \frac{\partial A_1}{\partial\alpha_2} \frac{\partial\Phi}{\partial\alpha_1} \right) \qquad (21S)$$

$$\left. - \frac{1}{A_2} \frac{\partial A_2}{\partial\alpha_1} \frac{\partial w}{\partial\alpha_2} - \frac{1}{A_1} \frac{\partial A_1}{\partial\alpha_2} \frac{\partial w}{\partial\alpha_1} \right) \qquad (21B)$$

$$\varepsilon_1 = \frac{1}{Et} (N_1 - \nu N_2) \qquad (22S)$$

$$M_2 = D (\kappa_2 + \nu \kappa_1) \qquad (22B)$$

$$\varepsilon_2 = \frac{1}{Et} (N_2 - \nu N_1) \qquad (23S)$$

$$M_1 = D (\kappa_1 + \nu \kappa_2) \qquad (23B)$$

$$\gamma_{12} = \frac{2(1 + \nu)}{Et} N_{12} \qquad (24S)$$

$$2M_{12} = 2D (1 - \nu)\kappa_{12} \qquad (24B)$$

$$-g_S = \frac{1}{A_1 A_2} \left\{ \frac{\partial}{\partial \alpha_1} \left[\frac{1}{A_1} \frac{\partial(A_2 \varepsilon_2)}{\partial \alpha_1} - \frac{\varepsilon_1}{A_1} \frac{\partial A_2}{\partial \alpha_1} - \frac{\gamma_{12}}{A_1} \frac{\partial A_1}{\partial \alpha_2} \right] + \frac{\partial}{\partial \alpha_2} \left[\frac{1}{A_2} \frac{\partial(A_1 \varepsilon_1)}{\partial \alpha_2} - \frac{\varepsilon_2}{A_2} \frac{\partial A_1}{\partial \alpha_2} - \frac{\gamma_{12}}{A_2} \frac{\partial A_2}{\partial \alpha_1} \right] - \frac{\partial^2 \gamma_{12}}{\partial \alpha_1 \partial \alpha_2} \right\} \quad (25S)$$

$$-p_B = \frac{1}{A_1 A_2} \left\{ \frac{\partial}{\partial \alpha_1} \left[\frac{1}{A_1} \frac{\partial(A_2 M_1)}{\partial \alpha_1} - \frac{M_2}{A_1} \frac{\partial A_2}{\partial \alpha_1} + \frac{2M_{12}}{A_1} \frac{\partial A_1}{\partial \alpha_2} \right] + \frac{\partial}{\partial \alpha_2} \left[\frac{1}{A_2} \frac{\partial(A_1 M_2)}{\partial \alpha_2} - \frac{M_1}{A_2} \frac{\partial A_1}{\partial \alpha_2} + \frac{2M_{12}}{A_2} \frac{\partial A_2}{\partial \alpha_1} \right] + 2 \frac{\partial^2 M_{12}}{\partial \alpha_1 \partial \alpha_2} \right\} \quad (25B)$$

The behaviour of the S-surface is described by the set of equations (16S)—(25S). Expressions (16S)—(18S) represent the equations of equilibrium of the S-surface for the present case of vanishing tangential surface tractions; as is well known, equations of this type may be conveniently dealt with by introducing an Airy-type stress function Φ /19/, and this is defined by relations (19S)—(21S). Equations (22S)—(24S) are the constitutive relations for the S-surface while equation (25S) represents the compatibility equation relating the S-surface Gaussian curvature change g_S to the in-plane strain components /3, 20/.

The set of equations (16B)—(25B) describes the behaviour of the B-surface. Expressions (16B)—(18B) are the compatibility equations relating the B-surface Gaussian curvature change g_B to the ordinary curvature-change components κ_1, κ_2 and κ_{12}. Expressions (19B)—(19B) are the simplified geometric relations which define the curvature-change components solely in terms of the normal displacement component w. Equations (22B)—(24B) are the constitutive relations for the B-surface while expression (25B), which may be obtained from equation (15) by means of simple transformations, represents the B-surface equilibrium equation relating the loading p_B to the bending and twisting moments M_1, M_2 and M_{12}.

The formal similarity between the corresponding expressions for the two surfaces, as indicated by the common numbering, is evident. It is, of course, a consequence of the extended static-geometric analogy of Calladine /1/ and clearly indicates that the set of equations describing the behaviour of the S-surface can be transformed into the corresponding set of equations for the B-surface, and vice versa, by merely interchanging analogous variables and material constants ($N_1 \leftrightarrow \kappa_2$, $N_2 \leftrightarrow \kappa_1$, $N_{12} \leftrightarrow -\kappa_{12}$, $\varepsilon_1 \leftrightarrow M_2$,

$\varepsilon_2 \leftrightarrow M_1$, $\quad \gamma_{12} \leftrightarrow -2M_{12}$, $\quad \Phi \leftrightarrow -w$, $\quad \nu_{(S)} \leftrightarrow -\nu_{(B)}$, $\quad \frac{1}{Et} \leftrightarrow D$, $\quad P_S \leftrightarrow g_B$, $g_S \leftrightarrow P_B$).

A full description of each of the two conceptual surfaces has been presented. In order to ensure that the surfaces do not behave independently of one another, it is necessary to impose interaction conditions of overall equilibrium and compatibility. As noted earlier, overall equilibrium is assured by equating the total applied (normal) load p to the sum of the separate (normal) loadings carried by the S- and B-surfaces, as expressed by equation (4). Overall compatibility, on the other hand, is assured by equating the B-surface Gaussian curvature change to its S-surface counterpart, that is, by the condition

$$g_S = g_B \tag{26}$$

Since the above interaction conditions are, in fact, statements of the sought governing equations, it is evident that the latter may be obtained by determining the variables P_S, P_B, g_S and g_B separately and then combining them by means of equations (4) and (26).

Consider, first, the equations of the S-surface. By substituting expressions (19S) and (20S) into the equilibrium equation (16S) and taking account of the Codazzi equations (2) and (3), the S-surface loading P_S can be expressed in terms of the stress function Φ as follows:

$$P_S = \nabla_k^2 \Phi \tag{27}$$

where the symbol ∇_k^2 denotes the second-order mixed differential operator defined by

$$\nabla_k^2 = \frac{1}{A_1 A_2} \left[\frac{\partial}{\partial \alpha_1} \left(\frac{A_2}{A_1} K_2 \frac{\partial}{\partial \alpha_1} \right) + \frac{\partial}{\partial \alpha_2} \left(\frac{A_1}{A_2} K_1 \frac{\partial}{\partial \alpha_2} \right) \right] \tag{28}$$

Now, in special cases (such as, for example, Cartesian, polar and quasi-polar co-ordinates) the two tangential equilibrium equations become identically satisfied once they are expressed in terms of the stress function Φ. In the present, general case, this does not happen, but these equations take the following forms. By substituting the stress-function definitions (19S)--(21S) into the tangential equilibrium equation (17S), one obtains, after some manipulations (amongst which, account is taken of Gauss's equation (1)), the relation

$$\frac{\partial(A_2 N_1)}{\partial \alpha_1} - N_2 \frac{\partial A_2}{\partial \alpha_1} + \frac{\partial(A_1 N_{12})}{\partial \alpha_2} + N_{12} \frac{\partial A_1}{\partial \alpha_2} = - \frac{A_2}{R_1 R_2} \frac{\partial \Phi}{\partial \alpha_1} \qquad (29)$$

Similarly, the second tangential equilibrium equation (18S) may be expressed in the following form:

$$\frac{\partial(A_1 N_2)}{\partial \alpha_2} - N_1 \frac{\partial A_1}{\partial \alpha_2} + \frac{\partial(A_2 N_{12})}{\partial \alpha_1} + N_{12} \frac{\partial A_2}{\partial \alpha_1} = - \frac{A_1}{R_1 R_2} \frac{\partial \Phi}{\partial \alpha_2} \qquad (30)$$

Evidently, the right-hand side terms in equations (29) and (30) vanish for shells with zero Gaussian curvature (as they do in the case of flat plates). However, for a shell of non-vanishing Gaussian curvature the terms may, as an approximation, be assumed to be equal to zero if the middle surface is shallow, by reason of the smallness of the curvatures of the shell; such an approximation can also be used if the state of stress in the shell exhibits rapid variation by virtue of the negligible magnitude of the first derivatives of Φ in comparison with its higher derivatives.

The S-surface Gaussian curvature change can also be expressed in terms of the stress function Φ. This can be achieved by substituting the constitutive relations (22S)—(24S) into expression (25S) and taking account of the tangential equilibrium equations (17S) and (18S) as well as the stress-function definitions. In this way, one obtains:

$$- g_S = \frac{1}{Et} \nabla_g^2 \nabla_g^2 \Phi \qquad (31)$$

where the symbol ∇_g^2 denotes the generalized Laplace operator defined by

$$\nabla_g^2 = \frac{1}{A_1 A_2} \left[\frac{\partial}{\partial \alpha_1} \left(\frac{A_2}{A_1} \frac{\partial}{\partial \alpha_1} \right) + \frac{\partial}{\partial \alpha_2} \left(\frac{A_1}{A_2} \frac{\partial}{\partial \alpha_2} \right) \right] \qquad (32)$$

Now consider the set of equations describing the behaviour of the B-surface. By substituting expressions (19B) and (20B) into the compatibility equation (16B) and taking account of the Codazzi equations (2) and (3), the B-surface Gaussian curvature change g_B may be expressed in terms of the transverse displacement function w in the following form:

$$g_B = - \nabla_k^2 w \qquad (33)$$

As for the tangential equilibrium of the S-surface, the remaining two compatibility equations of the B-surface are not identically satisfied when w is inserted into them for the present, general case, but they take the following forms. By substituting the curvature-change definitions (19B)-- (21B) into the compatibility equation (17B) one obtains, after some manipulations (amongst which, account is taken of Gauss's equation (1)), the following relation:

$$\frac{\partial(A_2\kappa_2)}{\partial\alpha_1} - \kappa_1\frac{\partial A_1}{\partial\alpha_1} - \frac{\partial(A_1\kappa_{12})}{\partial\alpha_2} - \kappa_{12}\frac{\partial A_1}{\partial\alpha_2} = \frac{A_2}{R_1 R_2}\frac{\partial w}{\partial\alpha_1} \tag{34}$$

Similarly, the second compatibility equation (18B) may be expressed as follows:

$$\frac{\partial(A_1\kappa_1)}{\partial\alpha_2} - \kappa_2\frac{\partial A_1}{\partial\alpha_2} - \frac{\partial(A_2\kappa_{12})}{\partial\alpha_1} - \kappa_{12}\frac{\partial A_2}{\partial\alpha_1} = \frac{A_1}{R_1 R_2}\frac{\partial w}{\partial\alpha_2} \tag{35}$$

For shells of zero Gaussian curvature, the right-hand side terms in the above equations vanish; they may also be assumed to vanish in non-zero Gaussian curvature shells which are shallow and/or exhibit rapidly-varying states of stress, for reasons stated earlier.

We now turn our attention to the B-surface loading p_B, which can be expressed in terms of the displacement function w. This may be achieved by substituting the constitutive relations (22B)—(24B) into expression (25B) and taking account of the compatibility relations (17B) and (18B) as well as the curvature-change definitions. In this manner, one obtains the following expression

$$p_B = D\nabla_g^2\nabla_g^2 w \tag{36}$$

Finally, by combining the overall equilibrium and compatibility conditions ((4) and (26), respectively) with expressions (27), (31), (33) and (36) one obtains the sought governing equations:

$$D\nabla_g^1\nabla_g^2 w + \nabla_k^2\Phi = p \tag{37}$$

$$\frac{1}{Et}\nabla_g^2\nabla_g^2\Phi - \nabla_k^2 w = 0 \tag{38}$$

It is interesting to note that the effort required for the derivation of the above equations may be considerably reduced if one invokes the static-geometric analogy. This important feature of the present method is clearly absent in conventional derivations: it stems from the fact that the static-geometric analogy enables the various expressions for the parameters associated with one surface to be written down by inspection once the expressions for the corresponding parameters of the other surface have been obtained. In particular, one could readily have established expressions (33) and (36), for the B-surface parameters g_B and p_B, from the expressions (27) and (31), for the S-surface quantities p_S and g_S, and vice versa, by invoking the appropriate interchanges consistent with the extended static-geometric analogy.

Specific examples

It was noted earlier that the present formulation is a generalization of Calladine's derivation in terms of Cartesian co-ordinates. Indeed, this may readily be verified — and serves as a useful introductory exercise — by making the following substitutions (which relate the Cartesian (x,y) co-ordinate system to the more general orthogonal curvilinear system presently employed) in the foregoing expressions: $\alpha_1 = x$, $\alpha_2 = y$, $A_1 = 1$, $A_2 = 1$. Similarly, the present formulation may be specialized to other co-ordinate systems. Four cases are considered in what follows.

Example I: Cylindrical co-ordinate system

This co-ordinate system may be used for the description of shells the reference surfaces of which are surfaces of revolution. It will be recalled that a surface of revolution is formed by rotating a plane curve, as a rigid body, about an axis (the axis of revolution) in the plane of the curve. The plane containing the axis of revolution is called the meridional plane, and the intersection of this plane with the surface is called a meridian. Furthermore, the intersection of the surface with a plane which is perpendicular to the axis of revolution is a circle known as a latitude circle or parallel; and it may be shown that the meridians and parallels are the lines of principal curvature of the surface of revolution /21/.
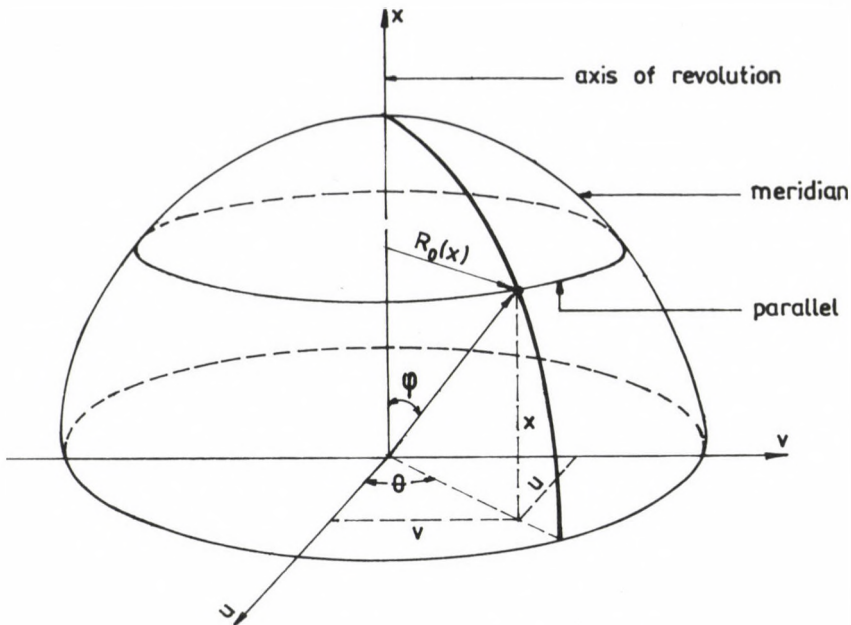
Fig. 3. Co-ordinate systems: Examples I and II

In the present co-ordinate system the position of a point on the surface is defined by the angle θ and the distance x; the co-ordinate θ represents the angle between the meridional plane passing through the point and a fixed meridional plane, while the other co-ordinate, x, defines the distance, measured along the axis of revolution, of the associated latitude circle from a suitable datum (see Fig. 3). The parameters α_1, α_2, A_1 and A_2 can be shown to be given by /21/

$$\alpha_1 = x, \quad \alpha_2 = \theta, \quad A_1 = \left[1 + (R_0')^2\right]^{1/2}, \quad A_2 = R_0 \tag{39}$$

where R_0 is the radius of the latitude circle at position x and a prime denotes differentiation with respect to x. In addition, the principal radii of curvature of the middle surface are given by

$$R_1 = - \frac{\left[1 + (R_0')^2\right]^{3/2}}{R_0''}; \quad R_2 = R_0 \left[1 + (R_0')^2\right]^{1/2} \tag{40}$$

where R_1 represents the radius of curvature of the meridian curve $R_o(x)$ while R_2 is the distance along the normal to the curve $R_o(x)$ drawn from a point on the curve to the axis of revolution of the surface /21/.

On the basis of the above relations (39) and (40), which can readily be shown to identically satisfy the Gauss—Codazzi equations (1)—(3), one can easily transform the S- and B-surface equations into the present co-ordinate system, and these are listed below. (The subscripts have been sub-stituted thus: $1 \rightarrow x$; $2 \rightarrow \theta$; $12 \rightarrow x\theta$.)

S-surface

$$\frac{N_x}{R_1} + \frac{N_\theta}{R_2} = p_S \qquad (41S)$$

$$\frac{\partial(N_x \cdot R_o)}{\partial x} - N_\theta \cdot R_o' +$$

$$+ \frac{R_2}{R_o} \frac{\partial N_{x\theta}}{\partial \theta} = 0 \qquad (42S)$$

$$\frac{\partial(N_{x\theta} \cdot R_o)}{\partial x} + N_{x\theta} \cdot R_o' +$$

$$+ \frac{R_2}{R_o} \frac{\partial N_\theta}{\partial \theta} = 0 \qquad (43S)$$

$$N_x = \frac{1}{R_o^2} \frac{\partial^2 \phi}{\partial \theta^2} + \frac{R_o}{R_2^2} \cdot R_o' \cdot \frac{\partial \phi}{\partial x} \qquad (44S)$$

$$N_\theta = \frac{R_o}{R_2} \left(\frac{R_o}{R_2} \frac{\partial^2 \phi}{\partial x^2} + \frac{R_o'}{R_1} \frac{\partial \phi}{\partial x} \right) \qquad (45S)$$

$$N_{x\theta} = - \frac{1}{R_2} \left(\frac{\partial^2 \phi}{\partial x \partial \theta} - \frac{R_o'}{R_o} \frac{\partial \phi}{\partial \theta} \right) \qquad (46S)$$

$$\varepsilon_x = \frac{1}{Et} (N_x - \nu N_\theta) \qquad (47S)$$

$$\varepsilon_\theta = \frac{1}{Et} (N_\theta - \nu N_x) \qquad (48S)$$

B-surface

$$\frac{\kappa_\theta}{R_1} + \frac{\kappa_x}{R_2} = g_B \qquad (41B)$$

$$\frac{\partial(\kappa_\theta \cdot R_o)}{\partial x} - \kappa_x \cdot R_o' -$$

$$- \frac{R_2}{R_o} \frac{\partial \kappa_{x\theta}}{\partial \theta} = 0 \qquad (42B)$$

$$- \frac{\partial(\kappa_{x\theta} \cdot R_o)}{\partial x} - \kappa_{x\theta} \cdot R_o' +$$

$$+ \frac{R_2}{R_o} \frac{\partial \kappa_x}{\partial \theta} = 0 \qquad (43B)$$

$$\kappa_\theta = - \frac{1}{R_o^2} \frac{\partial^2 w}{\partial \theta^2} - \frac{R_o}{R_2^2} \cdot R_o' \cdot \frac{\partial w}{\partial x} \qquad (44B)$$

$$\kappa_x = - \frac{R_o}{R_2} \left(\frac{R_o}{R_2} \frac{\partial^2 w}{\partial x^2} + \frac{R_o'}{R_1} \frac{\partial w}{\partial x} \right) \qquad (45B)$$

$$\kappa_{x\theta} = - \frac{1}{R_2} \left(\frac{\partial^2 w}{\partial x \partial \theta} - \frac{R_o'}{R_o} \frac{\partial w}{\partial \theta} \right) \qquad (46B)$$

$$M_\theta = D(\kappa_\theta + \nu \kappa_x) \qquad (47B)$$

$$M_x = D(\kappa_x + \nu \kappa_\theta) \qquad (48B)$$

$$\gamma_{x\theta} = \frac{2(1 + \nu)}{Et} N_{x\theta} \qquad (49S) \qquad 2M_{x\theta} = 2D(1 - \nu)\kappa_{x\theta} \qquad (49B)$$

$$-g_S = \frac{1}{R_2}\left\{\frac{\partial}{\partial x}\left[\frac{R_0}{R_2}\frac{\partial(\varepsilon_\theta \cdot R_0)}{\partial x}\right] - \right.$$

$$\qquad\qquad -\varepsilon_x \cdot \frac{R_0 R_0'}{R_2}\right] + \frac{1}{R_0}\frac{\partial}{\partial\theta}\left[\frac{R_2}{R_0}\frac{\partial\varepsilon_x}{\partial\theta}\right] - $$

$$\qquad\qquad \left. -\gamma_{x\theta} \cdot R_0'\right] - \frac{\partial^2\gamma_{x\theta}}{\partial x\partial\theta}\right\} \qquad (50S)$$

$$-p_B = \frac{1}{R_2}\left\{\frac{\partial}{\partial x}\left[\frac{R_0}{R_2}\frac{\partial(M_x \cdot R_0)}{\partial x}\right] - \right.$$

$$\qquad\qquad -M_\theta \cdot \frac{R_0 R_0'}{R_2}\right] + \frac{1}{R_0}\frac{\partial}{\partial\theta}\left[\frac{R_2}{R_0}\frac{\partial M_\theta}{\partial\theta}\right] + $$

$$\qquad\qquad \left. +2M_{x\theta} \cdot R_0'\right] + 2\frac{\partial^2 M_{x\theta}}{\partial x\partial\theta}\right\} \qquad (50B)$$

Further, it can readily be shown that, for the present co-ordinate system, expressions (28) and (32), defining the differential operators ∇_k^2 and ∇_g^2 (which appear in expression (27), (31), (33) and (36), defining the S- and B-surface normal loadings and Gaussian curvature changes, as well as in the coupled differential equations (37) and (38)), reduce to the following forms:

$$\nabla_k^2 = \frac{R_0^2}{R_2^3}\frac{\partial^2}{\partial x^2} + 2\frac{R_0 R_0'}{R_1 R_2^2}\frac{\partial}{\partial x} + \frac{1}{R_0^2 R_1}\frac{\partial^2}{\partial\theta^2} \qquad (51)$$

$$\nabla_g^2 = \left(\frac{R_0}{R_2}\right)^2\frac{\partial^2}{\partial x^2} + \frac{R_0 R_0'}{R_2}\left(\frac{1}{R_1} + \frac{1}{R_2}\right)\frac{\partial}{\partial x} + \frac{1}{R_0^2}\frac{\partial^2}{\partial\theta^2} \qquad (52)$$

To our knowledge, no similar expressions exist in the literature for this co-ordinate system in its general form.

In the special case when the generating curve (i.e. meridian) is straight and parallel to the axis of revolution, the radius R_0 of the latitude circle becomes constant (i.e. independent of the co-ordinate x), so that all derivatives of R_0 with respect to x vanish. Thus, the following relations hold true:

$$A_1 = 1, \qquad R_1 = \infty, \qquad R_2 = R_0 \qquad (53)$$

and the middle surface corresponds to a circular cylinder of radius R_0 ($= R_2$). In this case the formulation is considerably simplified. In particular, the differential operators ∇_k^2 and ∇_g^2 reduce to the following forms:

$$\nabla_k^2 = \frac{1}{R_o} \frac{\partial^2}{\partial x^2} \tag{54}$$

$$\nabla_g^2 = \frac{\partial^2}{\partial x^2} + \frac{1}{R_o^2} \frac{\partial^2}{\partial \theta^2} \tag{55}$$

The relative simplicity of the governing equations for circular cylindrical shells is evident; for conventional derivations of these equations, see, for example, Billington /22/ and Soedel /14/.

Example II: Spherical co-ordinate system

This co-ordinate system may also be used for the description of shells of revolution, in analogy with the cylindrical co-ordinate system discussed above. In this case the position of a point on a surface of revolution is defined by the angular co-ordinates θ and ϕ; as shown in Fig. 3, the co-ordinate ϕ is the angle between the axis of revolution of the surface and a normal to the surface at the point in question (note that, as in the preceding co-ordinate system, θ represents the angle between the meridional plane passing through the point and a fixed meridional datum plane). The parameters α_1, α_2, A_1 and A_2 are defined thus /14, 21/:

$$\alpha_1 = \phi, \quad \alpha_2 = \theta, \quad A_1 = R_1, \quad A_2 = R_o \tag{56}$$

where R_o is the radius of the latitude circle at position ϕ. The principal radii of curvature of the middle surface depend only on the co-ordinate ϕ, and the following relations hold true /14, 21/:

$$R_o = R_2 \sin \phi; \quad \frac{dR_o}{d\phi} = R_1 \cos \phi \tag{57}$$

On the basis of the above relations (56) and (57), which can readily be shown to identically satisfy the Gauss—Codazzi equations (1)--(3), one can easily transform the S- and B-surface equations into the present co-ordinate system, and these are listed below. (The subcripts have been substituted thus: $1 \rightarrow \phi$; $2 \rightarrow \theta$; $12 \rightarrow \phi\theta$.)

<u>S-surface</u>   <u>B-surface</u>

$$\frac{N_\phi}{R_1} + \frac{N_\theta}{R_2} = p_S \qquad (58S) \qquad \frac{\kappa_\theta}{R_1} + \frac{\kappa_\phi}{R_2} = g_B \qquad (58B)$$

$$\frac{\partial(N_\phi \cdot R_o)}{\partial\phi} - N_\theta \cdot R_1 \cos \phi + \qquad\qquad \frac{\partial(\kappa_\phi \cdot R_o)}{\partial\phi} - \kappa_\phi \cdot R_1 \cos \phi -$$

$$+ R_1 \frac{\partial N_{\phi\theta}}{\partial\theta} = 0 \qquad (59S) \qquad - R_1 \frac{\partial \kappa_{\phi\theta}}{\partial\theta} = 0 \qquad (59B)$$

$$\frac{\partial(N_{\phi\theta} \cdot R_o)}{\partial\phi} + N_{\phi\theta} \cdot R_1 \cos \phi + \qquad\qquad - \frac{\partial(\kappa_{\phi\theta} \cdot R_o)}{\partial\phi} - \kappa_{\phi\theta} \cdot R_1 \cos \phi +$$

$$+ R_1 \frac{\partial N_\theta}{\partial\theta} = 0 \qquad (60S) \qquad + R_1 \frac{\partial \kappa_\phi}{\partial\theta} = 0 \qquad (60B)$$

- -

$$N_\phi = \frac{1}{R_o^2} \frac{\partial^2\Phi}{\partial\theta^2} + \frac{1}{R_o R_1} \cos \phi \frac{\partial\Phi}{\partial\phi} \quad (61S) \qquad \kappa_\theta = -\frac{1}{R_o^2}\frac{\partial^2 w}{\partial\theta^2} - \frac{1}{R_o R_1} \cos \phi \frac{\partial w}{\partial\phi} \quad (61B)$$

$$N_\theta = \frac{1}{R_1} \frac{\partial}{\partial\phi}\left(\frac{1}{R_1}\frac{\partial\Phi}{\partial\phi}\right) \qquad (62S) \qquad \kappa_\phi = -\frac{1}{R_1}\frac{\partial}{\partial\phi}\left(\frac{1}{R_1}\frac{\partial w}{\partial\phi}\right) \qquad (62B)$$

$$N_{\phi\theta} = -\frac{1}{R_o R_1}\frac{\partial^2\Phi}{\partial\phi\partial\theta} + \qquad\qquad \kappa_{\phi\theta} = -\frac{1}{R_o R_1}\frac{\partial^2 w}{\partial\phi\partial\theta} +$$

$$+ \frac{1}{R_o^1} \cos \phi \frac{\partial\Phi}{\partial\theta} \qquad (63S) \qquad + \frac{1}{R_o^2} \cos \phi \frac{\partial w}{\partial\theta} \qquad (63B)$$

$$\varepsilon_\phi = \frac{1}{Et}(N_\phi - \nu N_\theta) \qquad (64S) \qquad M_\theta = D(\kappa_\theta + \nu\kappa_\phi) \qquad (64B)$$

$$\varepsilon_\theta = \frac{1}{Et}(N_\theta - \nu N_\phi) \qquad (65S) \qquad M_\phi = D(\kappa_\phi + \nu\kappa_\theta) \qquad (65B)$$

$$\gamma_{\phi\theta} = \frac{2(1 + \nu)}{Et} N_{\phi\theta} \qquad (66S) \qquad 2M_{\phi\theta} = 2D(1 - \nu)\kappa_{\phi\theta} \qquad (66B)$$

$$- g_S = \frac{1}{R_o R_1} \left\{ \frac{\partial}{\partial \phi} \left[\frac{1}{R_1} \frac{\partial (\varepsilon_\theta \cdot R_o)}{\partial \phi} - \right. \right.$$

$$\left. - \varepsilon_\phi \cos \phi \right] + \frac{R_1}{R_o} \frac{\partial}{\partial \theta} \left[\frac{\partial \varepsilon_\phi}{\partial \theta} - \right.$$

$$\left. - \gamma_{\phi\theta} \cos \phi \right] - \frac{\partial^2 \gamma_{\phi\theta}}{\partial \phi \partial \theta} \right\} \qquad (67S)$$

$$- p_B = \frac{1}{R_o R_1} \left\{ \frac{\partial}{\partial \phi} \left[\frac{1}{R_1} \frac{\partial (M_\phi \cdot R_o)}{\partial \phi} - \right. \right.$$

$$\left. - M_\theta \cos \phi \right] + \frac{R_1}{R_o} \frac{\partial}{\partial \theta} \left[\frac{\partial M_\theta}{\partial \theta} + \right.$$

$$\left. + 2 M_{\phi\theta} \cos \phi \right] + 2 \frac{\partial^2 M_{\phi\theta}}{\partial \phi \partial \theta} \right\} \qquad (67B)$$

In addition, one can easily show that the differential operators ∇_k^2 and ∇_g^2 now become

$$\nabla_k^2 = \frac{1}{R_1} \left[\frac{1}{R_2} \frac{\partial}{\partial \phi} \left(\frac{1}{R_1} \frac{\partial}{\partial \phi} \right) + \frac{1}{R_o R_1} \cos \phi \frac{\partial}{\partial \phi} + \frac{1}{R_o^2} \frac{\partial^2}{\partial \theta^2} \right] \qquad (68)$$

$$\nabla_g^2 = \frac{1}{R_1} \frac{\partial}{\partial \phi} \left(\frac{1}{R_1} \frac{\partial}{\partial \phi} \right) + \frac{1}{R_o R_1} \cos \phi \frac{\partial}{\partial \phi} + \frac{1}{R_o^2} \frac{\partial^2}{\partial \theta^2} \qquad (69)$$

Again, to our knowledge, no similar expression exist in the literature for this co-ordinate system in its general form.

In the case of spherical shells (for which $R_1 = R_2 = R$) the formulation is somewhat simplified. In particular, it is a straightforward matter to show that the operator ∇_g^2 reduces to the well-known Laplace operator referred to the spherical co-ordinate system, that is,

$$\nabla_g^2 = \frac{1}{R^2} \left\{ \frac{\partial^2}{\partial \phi^2} + \cos \phi \frac{\partial}{\partial \phi} + \frac{1}{\sin^2 \phi} \frac{\partial^2}{\partial \theta^2} \right\} \qquad (70)$$

while its counterpart ∇_k^2 becomes

$$\nabla_k^2 = \frac{1}{R} \nabla_g^2 \qquad (71)$$

Example III: Polar co-ordinate system

In the polar co-ordinate system the parameters α_1, α_2, A_1 and A_2 given by:

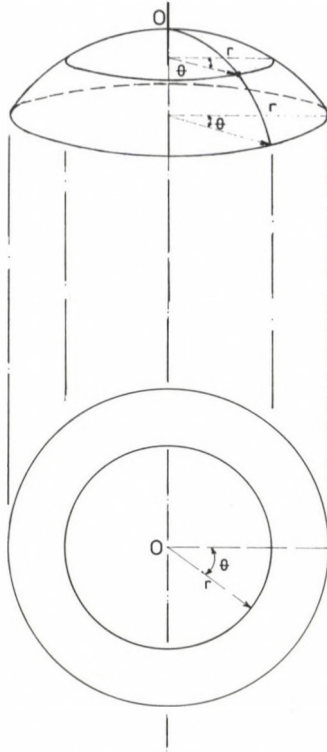$$\alpha_1 = r, \quad \alpha_2 = \theta, \quad A_1 = 1, \quad A_2 = r \qquad (72)$$

Fig. 4. Co-ordinate systems:
Examples III and IV

where r and θ denote the polar distance and polar angle, respectively (see Fig. 4). The S- and B-surface equations referred to the polar co-ordinate system are listed below. (The subscripts have been substituted thus: $1 \rightarrow r$; $2 \rightarrow \theta$; $12 \rightarrow r\theta$.)

	S-surface		B-surface

$$\frac{N_r}{R_1} + \frac{N_\theta}{R_2} = p_S \qquad\qquad (73S)$$

$$\frac{\kappa_\theta}{R_1} + \frac{\kappa_r}{R_2} = g_B \qquad\qquad (73B)$$

$$\frac{\partial(rN_r)}{\partial r} - N_\theta + \frac{\partial N_{r\theta}}{\partial \theta} = 0 \qquad (74S)$$

$$\frac{\partial(r\kappa_\theta)}{\partial r} - \kappa_r - \frac{\partial \kappa_{r\theta}}{\partial \theta} = 0 \qquad (74B)$$

$$\frac{\partial(rN_{r\theta})}{\partial r} + \frac{\partial N_\theta}{\partial \theta} + N_{r\theta} = 0 \qquad (75S)$$

$$-\frac{\partial(r\kappa_{r\theta})}{\partial r} + \frac{\partial \kappa_r}{\partial \theta} - \kappa_{r\theta} = 0 \qquad (75B)$$

$$N_r = \frac{1}{r^2}\frac{\partial^2 \phi}{\partial \theta^2} + \frac{1}{r}\frac{\partial \phi}{\partial r} \qquad (76S) \qquad \kappa_\theta = -\frac{1}{r^2}\frac{\partial^2 w}{\partial \theta^2} - \frac{1}{r}\frac{\partial w}{\partial r} \qquad (76B)$$

$$N_\theta = \frac{\partial^2 \phi}{\partial r^2} \qquad (77S) \qquad \kappa_r = -\frac{\partial^2 w}{\partial r^2} \qquad (77B)$$

$$N_{r\theta} = \frac{1}{r^2}\frac{\partial \phi}{\partial \theta} - \frac{1}{r}\frac{\partial^2 \phi}{\partial r\partial \theta} \qquad (78S) \qquad \kappa_{r\theta} = \frac{1}{r^2}\frac{\partial w}{\partial \theta} - \frac{1}{r}\frac{\partial^2 w}{\partial r\partial \theta} \qquad (78B)$$

$$\varepsilon_r = \frac{1}{Et}(N_r - \nu N_\theta) \qquad (79S) \qquad M_\theta = D(\kappa_\theta + \nu\kappa_r) \qquad (79B)$$

$$\varepsilon_\theta = \frac{1}{Et}(N_\theta - \nu N_r) \qquad (80S) \qquad M_r = D(\kappa_r + \nu\kappa_\theta) \qquad (80B)$$

$$\gamma_{r\theta} = \frac{2(1+\nu)}{Et}N_{r\theta} \qquad (81S) \qquad 2M_{r\theta} = 2D(1-\nu)\kappa_{r\theta} \qquad (81B)$$

$$-g_S = \frac{\partial^2 \varepsilon_\theta}{\partial r^2} + \frac{2}{r}\frac{\partial \varepsilon_\theta}{\partial r} - \frac{1}{r}\frac{\partial \varepsilon_r}{\partial r} + \qquad\qquad -p_B = \frac{\partial^2 M_r}{\partial r^2} + \frac{2}{r}\frac{\partial M_r}{\partial r} - \frac{1}{r}\frac{\partial M_\theta}{\partial r} +$$

$$+ \frac{1}{r^2}\frac{\partial^2 \varepsilon_r}{\partial \theta^2} - \frac{1}{r^2}\frac{\partial \gamma_{r\theta}}{\partial \theta} - \frac{1}{r}\frac{\partial^2 \gamma_{r\theta}}{\partial r\partial \theta} \quad (82S) \qquad + \frac{1}{r^2}\frac{\partial^2 M_\theta}{\partial \theta^2} + \frac{2}{r^2}\frac{\partial M_{r\theta}}{\partial \theta} + \frac{2}{r}\frac{\partial^2 M_{r\theta}}{\partial r\partial \theta} \quad (82B)$$

The differential operators ∇_k^2 and ∇_g^2 corresponding to the present frame of reference can be expressed thus:

$$\nabla_k^2 = \frac{1}{R_1}\left(\frac{1}{r^2}\frac{\partial^2}{\partial \theta^2} + \frac{1}{r}\frac{\partial}{\partial r}\right) + \frac{1}{R_2}\frac{\partial^2}{\partial r^2} \qquad (83)$$

$$\nabla_g^2 = \frac{\partial^2}{\partial r^2} + \frac{1}{r}\frac{\partial}{\partial r} + \frac{1}{r^2}\frac{\partial^2}{\partial \theta^2} \qquad (84)$$

It can easily be verified that, on setting the S-surface Gaussian curvature change g_S to zero in the appropriate expression relating the latter to the stress function ϕ, the well-known biharmonic equation for plane stress in terms of polar co-ordinates /23/ is obtained. Also, it can readily be seen that the expression relating the B-surface loading p_B to the transverse displacement function w represents the governing equation (referred to polar co-ordinates) for a flat plate which is locally tangential to the curved

surface of the shell /24/. Finally, it is worth noting that, when $R_1 = R_2 =$ = R, the reduced set of equations describing the behaviour of shallow spherical shells within the framework of plane polar co-ordinates is obtained, the present simple derivation should be compared to the more involved traditional derivation (e.g. Reissner /12/).

Example IV: Quasi-polar co-ordinate system

In this co-ordinate system the position of a point on a reference plane is determined by the polar angle θ and a non-dimensional parameter α which is connected to the polar radius r through the following relation

$$r = r_o \alpha \tag{85}$$

in which r_o is a constant having the dimensions of length. This co-ordinate system is also described by Fig. 4, with the (radial) non-dimensional co-ordinate α corresponding to a given point on the surface defined in terms of the associated polar distance r through the above equation (85) (as noted in /10/, the constant r_o may be regarded as a "conversion" factor for transforming the absolute co-ordinate r into its non-dimensional counterpart α). Thus, the parameters α_1, α_2, A_1 and A_2 take the following values /10, 25/:

$$\alpha_1 = \alpha, \quad \alpha_1 = \theta, \quad A_1 = r_o, \quad A_2 = r_o \alpha \tag{86}$$

The S- and B-surface equations in the present co-ordinate system may be derived from the more general relations in terms of orthogonal curvilinear coordinates, and these are listed below. (The subscripts have been substituted thus: 1 → α; 2 → θ; 12 → αθ.)

S-surface

$$\frac{N_\alpha}{R_1} + \frac{N_\theta}{R_2} = p_S \tag{87S}$$

$$\frac{\partial(\alpha \cdot N_\alpha)}{\partial \alpha} - N_\theta + \frac{\partial N_{\alpha\theta}}{\partial \theta} = 0 \tag{88S}$$

$$\frac{\partial(\alpha \cdot N_{\alpha\theta})}{\partial \alpha} + \frac{\partial N_\theta}{\partial \theta} + N_{\alpha\theta} = 0 \tag{89S}$$

B-surface

$$\frac{\kappa_\theta}{R_1} + \frac{\kappa_\alpha}{R_2} = g_B \tag{87B}$$

$$\frac{\partial(\alpha \cdot \kappa_\theta)}{\partial \alpha} - \kappa_\alpha - \frac{\partial \kappa_{\alpha\theta}}{\partial \theta} = 0 \tag{88B}$$

$$-\frac{\partial(\alpha \cdot \kappa_{\alpha\theta})}{\partial \alpha} + \frac{\partial \kappa_\alpha}{\partial \theta} - \kappa_{\alpha\theta} = 0 \tag{89B}$$

S-surface   B-surface

$$N_\alpha = \frac{1}{r_o^2}\left(\frac{1}{\alpha}\frac{\partial\Phi}{\partial\alpha} + \frac{1}{\alpha^2}\frac{\partial^2\Phi}{\partial\theta^2}\right) \tag{90S}$$

$$\kappa_\theta = -\frac{1}{r_o^2}\left(\frac{1}{\alpha}\frac{\partial w}{\partial\alpha} + \frac{1}{\alpha^2}\frac{\partial^2 w}{\partial\theta^2}\right) \tag{90B}$$

$$N_\theta = \frac{1}{r_o^2}\frac{\partial^2\Phi}{\partial\alpha^2} \tag{91S}$$

$$\kappa_\alpha = \frac{1}{r_o^2}\frac{\partial^2 w}{\partial\alpha^2} \tag{91B}$$

$$N_{\alpha\theta} = -\frac{1}{r_o^2}\left(\frac{1}{\alpha}\frac{\partial^2\Phi}{\partial\alpha\partial\theta} - \frac{1}{\alpha^2}\frac{\partial\Phi}{\partial\theta}\right) \tag{92S}$$

$$\kappa_{\alpha\theta} = -\frac{1}{r_o^2}\left(\frac{1}{\alpha}\frac{\partial^2 w}{\partial\alpha\partial\theta} - \frac{1}{\alpha^2}\frac{\partial w}{\partial\theta}\right) \tag{92B}$$

$$\varepsilon_\alpha = \frac{1}{Et}(N_\alpha - \nu N_\theta) \tag{93S}$$

$$M_\theta = D(\kappa_\theta + \nu\kappa_\alpha) \tag{93B}$$

$$\varepsilon_\theta = \frac{1}{Et}(N_\theta - \nu N_\alpha) \tag{94S}$$

$$M_\alpha = D(\kappa_\alpha + \nu\kappa_\theta) \tag{94B}$$

$$\gamma_{\alpha\theta} = \frac{2(1+\nu)}{Et}N_{\alpha\theta} \tag{95S}$$

$$2M_{\alpha\theta} = 2D(1-\nu)\kappa_{\alpha\theta} \tag{95B}$$

$$-g_S = \frac{1}{r_o^2}\frac{\partial^2\varepsilon_\theta}{\partial\alpha^2} + \frac{2}{r_o^2\alpha}\frac{\partial\varepsilon_\theta}{\partial\alpha} -$$

$$-P_B = \frac{1}{r_o^2}\frac{\partial^2 M_\alpha}{\partial\alpha^2} + \frac{2}{r_o^2\alpha}\frac{\partial M_\alpha}{\partial\alpha} -$$

$$-\frac{1}{r_o^2\alpha}\frac{\partial\varepsilon_\alpha}{\partial\alpha} + \frac{1}{r_o^2\alpha^2}\frac{\partial^2\varepsilon_\alpha}{\partial\theta^2} -$$

$$-\frac{1}{r_o^2\alpha}\frac{\partial M_\theta}{\partial\alpha} + \frac{1}{r_o^2\alpha^2}\frac{\partial^2 M_\theta}{\partial\theta^2} +$$

$$-\frac{1}{r_0^2\alpha^2}\frac{\partial\gamma_{\alpha\theta}}{\partial\theta} - \frac{1}{r_0^2\alpha}\frac{\partial^2\gamma_{\alpha\theta}}{\partial\alpha\partial\theta} \tag{96S}$$

$$+\frac{2}{r_0^2\alpha^2}\frac{\partial M_{\alpha\theta}}{\partial\theta} + \frac{2}{r_0^2\alpha}\frac{\partial^2 M_{\alpha\theta}}{\partial\alpha\partial\theta} \tag{96B}$$

The differential operators ∇_k^2 and ∇_g^2 now become

$$\nabla_k^2 = \frac{1}{R_1}\left(\frac{1}{\alpha}\frac{\partial}{\partial\alpha} + \frac{1}{\alpha^2}\frac{\partial^2}{\partial\theta^2}\right) + \frac{1}{R_2}\frac{\partial^2}{\partial\alpha^2} \tag{97}$$

$$\nabla_g^2 = \frac{\partial^2}{\partial\alpha^2} + \frac{1}{\alpha}\frac{\partial}{\partial\alpha} + \frac{1}{\alpha^2}\frac{\partial^2}{\partial\theta^2} \tag{98}$$

Specialised versions of the above — but not previously derived by the present simple and direct formulation — have been used to advantage in the analytical treatment of shallow spherical shells and parabolic domes with circular plan /10, 25, 26/. (An alternative approach to the analytical investigations of the response of such shells, based on the two-surface model, has recently been proposed /27/; the latter possesses several advantages over the conventional presentations, notably, the clarification of the structural response of a loaded shell by reference to the portion of the total applied load sustained by each of the two imaginary (i.e. S- and B-) surfaces used in modelling the actual shell.)

Conclusions

The analytical two-surface theory approach to the formulation of the shallow-shell equations has been generalized so as to encompass curvilinear co-ordinates corresponding to the (mutually orthogonal) lines of curvature of the middle surface of a shell. Apart from its elegance, when compared to existing derivations, the present method also has clear didactic advantages, notably, the elucidation of the meanings of the various terms in the field equations in a simple and "physical" manner. From this general form of the shallow-shell equations, it is a simple and useful exercise to specialize them to the various specific co-ordinate systems of interest. These include Cartesian, cylindrical, spherical, polar and quasi-polar frames of reference, all of which have presently been listed. It is worth pointing out that the expressions corresponding to at least two of these co-ordinate systems do not appear to exist in the available literature.

The governing equations outlined here, with reference to the lines-of-curvature co-ordinates, apply to transversely-loaded shells endowed with isotropic material properties. However, extensions of the formulation to cater for more general conditions are not difficult to envisage. For a start, tangential surface tractions can easily be incorporated into the scheme: in this connection, it should be noted that, in keeping with the two-surface idealization of a shell, the tangential loads must be applied exclusively to the S-surface, since, by definition, the B-surface cannot resist loads lying in its plane — a move which is tantamount to a neglect of the feeble tangential-force interaction between the S- and B-surfaces, in accordance with conventional shallow-shell theory /18, 28/. Secondly, the

method can readily be applied to anisotropic shells, with the proviso that there be no coupling, at the constitutive-relations level, between bending and stretching actions relating to the reference surface. A detailed discussion of the bending stretching coupling phenomenon exhibited by cetain anisotropic shells, and its implications for the two-surface model for a shell, can be found in /28/. In fact, the didactic advantages of the two-surface theory in the analytical derivation of shallow-shell equations for arbitrary loading and material anisotropy are presented elsewhere /29, 30/. Finally, it should be clear that an extension of the present scheme of derivation to encompass general, oblique frames of reference poses no conceptual difficulties; however, such extensions lie beyond the curricula of most existing engineering courses (including postgraduate ones).

REFERENCES

1. Calladine, C. R.: The static-geometric analogy in the equations of thin shell structures. Math. Proc. Camb. Phil. Soc., 82 (1977), 335—351

2. Calladine, C. R.: The theory of shell structures: Aims and methods. Int. J. Mech. Sci., 24 (4) (1982), 219—230

3. Calladine, C. R.: Theory of Shell Structures. Cambridge University Press, Cambridge, 1983

4. Pavlović, M. N.: A statically determinate truss model for thin shells: Two-surface analysis (bending theory). Int. J. Numer. Meth. Engng., 20 (10) (1984), 1863—1884

5. Pavlović, M. N.: A simple model for thin shell theory — Part 1: General concepts. Int. J. Mech. Engng. Educ., 13 (2) (1985), 97—111

6. Pavlović, M. N.: A simple model for thin shell theory — Part 2: Discretized surface, bending theory, and membrane hypothesis. Int. J. Mech. Engng. Educ., 13 (3) (1985), 199—222

7. Pavlović, M. N.: A simple model for thin shell theory — Part 3: Static-geometric analogy and the theorem of virtual work. Int. J. Mech. Engng. Educ., 13 (4) (1985), 281—287

8. Pavlović, M. N.: A simple model for thin shell theory — Part 4: Boundary conditions, singularities and uncoupling of the shell equations. Int. J. Mech. Engng. Educ. 14 (1) (1986), 1—11

9. Vlasov, V. Z.: Osnovnye differentsialnye uravnenia obshche teorii uprugikh obolochek. Prikl. Mat. Mekh, 8 (1944), 109—140. English translation. Basic Differential Equations in General Theory of Elastic Shells. NACA TM 1241, 1951

10. Vlasov, V. Z.: Obshchaya teoriya obolochek i yeye prilozheniya v tekhnike. Gosudarstvennoye Izdatelstvo Tekhniko — Teoreticheskoy Literatury, Moscow—Leningrad, 1949. English translation: General Theory of Shells and its Applications in Engineering. NASA TT-F99, 1964

11. Novozhilov, V. V.: Teoriya tonkikh obolochek. Gosudarstvennoye Izdatelstvo Sudostroitelnoy Literatury, Leningrad, 1951. English version of the 2nd Russian edn. (transl. P. G. Lowe, ed. J. R. M. Radok): Thin Shell Theory. P. Noordhoff Ltd., Groningen, 1964

12. Reissner, E.: Stresses and small displacement of shallow spherical shells. J. Math. Phys., 25 (1946), 80—85, 279—300 (see also corrections to this paper in 27 (1948), 240)

13. Seide, P.: Small Elastic Deformation of Thin Shells. Noordhoff International Publishing, Leyden, 1975

14. Soedel, W.: Vibrations of Shells and Plates. Marcel Dekker, Inc., New York, 1981

15. Forsyth, A. R.: Lectures on the Differential Geometry of Curves and Surfaces. Cambridge University Press, Cambridge, 1912

16. Weatherburn, C. E.: Differential Geometry of Three Dimensions. Cambridge at the University Press, Vol. I (1927) and Vol. II (1930)

17. Gol'denveizer, A. L.: Teoriia uprugykh tonkikh obolochek. Gostekhteoretizdat, Moscow, 1953. English translation ed. by G. Herrmann: Theory of Elastic Thin Shells. Pergamon Press, Oxford, 1961

18. Mbakogu, F. C.—Pavlović, M. N.: Shallow shells under arbitrary loading: Analysis by the two-surface truss model. Commun. Appl. Numer. Meth., 3 (3) (1987), 235—242

19. Novozhilov, V. V.: Theory of Elasticity. Pergamon Press, Oxford, 1961. (A translation, by J. K. Lusher, of the original Russian volume: Teoriya uprugosti. Sudpromgiz, Leningrad, 1958)

20. Calladine, C. R.: Thin-walled elastic shells analysed by a Rayleigh method. Int. J. Sol. Struct., 13 (1977), 515—530

21. Kraus, H.: Thin Elastic Shells. John Wiley and Sons, inc., New York, 1967

22. Billington, D. P.: Thin Shell Concrete Structures. McGraw—Hill Book Co., New York, 1982

23. Timoshenko, S. P.—Goodier, J. N.: Theory of Elasticity. McGraw—Hill, New York, 1951

24. Jaeger, L. G.: Elementary Theory of Elastic Plates. Pergamon Press, Oxford, 1964

25. Beles, A. A.—Soare, M. V.: Elliptic and Hyperbolic Paraboloidal Shells used in Constructions. S. P. Christie & Partners, London—Editura Academiei, Bucuresti, 1976

26. Mišonov, M.: Zur Theorie der flachen Kugelschalen in achsensymmetrischen Aufgaben. Comptes rendus de l'Académie Bulgare des Sciences, 12 (6) (1959), 541—544

27. Mbakogu, F. C.—Pavlović, M. N.: Bending and stretching actions in shallow domes. Thin-Walled Struct. (submitted for publication)

28. Mbakogu, F. C.: Analysis of elastic thin shells by the two-surface truss model. Ph.D. thesis, University of London, 1989

29. Mbakogu, F. C.—Pavlović, M. N.: Two-surface approach to the derivation of anisotropic shallow-shell theory equations — Part 1. Transverse loading. Int. J. Mech. Engng. Educ. (in press)

30. Mbakogu, F. C.—Pavlović, M. N.: Two-surface approach to the derivation of anisotropic shallow-shell theory equations — Part 2: Arbitrary loading. Int. J. Mech. Engng. Educ. (in press)

DIAGONAL BRACING OF SPECIAL CUBE GRIDS

NAGY, GY.*

Consider a cube grid in the space as a rod and joint framework supposing that each cube is a rhomboid during the motion of the joints. The paper describes the economical placing of diagonal braces for making this special cube grid rigid.

1. Introduction

One of the simplest structures in statics are the frameworks.

Definition 1: A framework consists of rigid rods connected by rotatable joints.

Definition 2: A framework is rigid if any continuous motion of the joints that keeps the length of every rod fixed, also keeps fixed the distance between every pair of vertices in the framework.

Let us consider an $n \times m$ square grid in the plane. The corresponding rod and joint framework is a mechanism in the plane. Let the length of the rods be unit. An $n \times m$ square grid framework consists of $n(m+1)$ pieces of horizontal and $(n+1)m$ pieces of vertical rods connected by $(n+1)(m+1)$ pieces of rotatable joints. There is a 3×4 square grid on the left-hand side of Fig. 1 (disregard the six diagonals). We want to make the original square grid rigid using braces in the diagonals of some squares. Thus some squares will become rhombi, others remain squares during any motion of the vertices (Fig. 1). Hence the horizontal rods of the i-th column are parallel with each other during any motion of the joints so they can be denoted by vector X_i. Similarly, the vertical rods of the j-th row are parallel with each

---

*Nagy, Gyula, H-1131 Budapest, Béke u. 118/A, 7. em. 2, Hungary
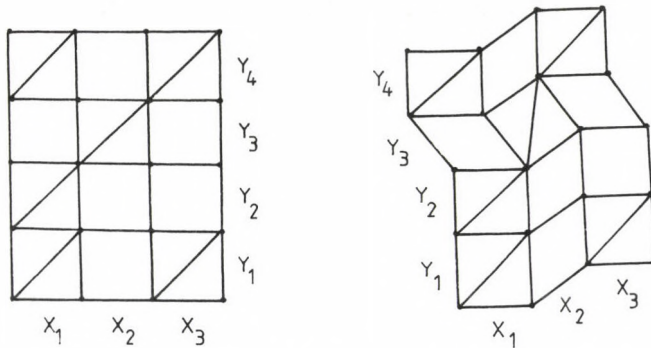
Fig. 1

other during any motion of the vertices so they can be denoted by vector Y_j (Fig. 1). Thus we can describe the move of the n x m square grid framework with n+m vectors, disregarding the translation of the framework only.

According to Definition 2, if every square remains square for any motion of the vertices then the square grid is rigid in the plane. How to brace the square grid if it must be rigid? How many diagonal braces are necessary? This problem have been solved by Bolker and Crapo /3/. In this note we give a new proof of Bolker—Crapo's theorem and extend their theorem to the space, namely to the l x m x n special cube grid. Recski /6/ gave a simpler proof to the theorem of Bolker and Crapo. We use other tools which are also useful in case of the special cube grids below. We are going to use elementary geometry, graph theory and continuity only.

Define the graph c of the framework F as follows: the Vertices of the graph c correspond to the joints of the framework F and there is an edge between two points of c if there is a rod between the corresponding two joints of the framework.

Consider a rod and joint framework in one dimension (line or arc).

Lemma: A framework is rigid in one dimension if and only if its graph c is connected.

Proof: The connectivity of c means we can get from every point to every point along edges of the graph, that means, the joints of the framework can move together to the same direction with the same velocity. If c is not connected then the frameworks corresponding to its components can move independently of each other.

2. Square grid

At the beginning every vector X_i is perpendicular to every vector Y_j, where X_i and Y_j are the horizontal and vertical vectors of the grid, respectively (Fig. 2).

We want to make the grid rigid by inserting diagonal braces. If the square in the intersection of the first column and the second row has a diagonal brace then vector X_1 is perpendicular to vector Y_2 during any motion. Thus the diagonal bracing is described by a bipartite graph (Fig. 3): the X_i's are in the first vertex class, the Y_j's are in the second vertex class, and an edge $X_i Y_j$ exists if and only if there is a diagonal brace in the square determined by the i-th column and the j-th row. We call this bipartite graph the bracing graph.

We denote the vector, its end points and the corresponding point of the bracing graph with the same letter because it will not cause any confusion.

Bolker--Crapo's theorem: An n x m square grid with some diagonal braces is rigid if and only if its bracing graph is connected.

Proof: The end points of the vectors are on a unit circle and some of them are of half π distance from each other (Fig. 5). These vectors are perpendicular in the grid. Let a framework be on the circle. Its joints are the end points of the vectors and its rods exist if there is a diagonal brace in the corresponding square, that means these two vectors must be perpendicular to each other. The grid is rigid in the plane if and only if the former framework is rigid on the circle. This framework lies on a one dimensional circular arc. Using the lemma; this framework is rigid if and only if its graph c is connected. But c is isomorphic to the bracing graph, because their points correspond to the columns and the rows of the square grid framework, and their edges correspond to the diagonal bracing.
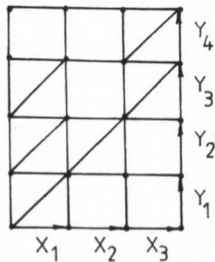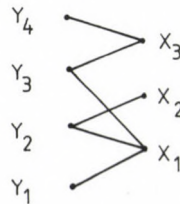
Fig. 2   Fig. 3
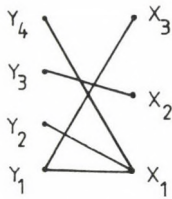
Fig. 4
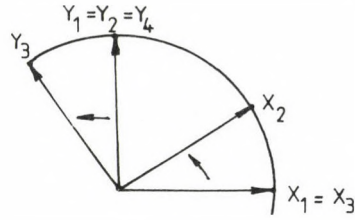
Fig. 5

If the bracing graph of the square grid framework is not connected then the square grid framework is not rigid, see the graph in Fig. 4, which is the bracing graph of the square grid framework on the left-hand side of Fig. 1. We can see a possible motion of the vectors on Fig. 5 since $X_2 Y_3$ is an independent component of the bracing graph. The corresponding motion of the joints and the rods is shown on the right-hand side of Fig. 1.

3. Special cube grid

Consider a $1 \times m \times n$ cube grid in the space as a rod and joint framework supposing each cube is a rhomboid during any motion of the vertices (thus we disregard those motions of the cube where the vertices of any "square" face do not remain coplanar). This is the special assumption. (Throughout, quotation marks will refer to the original situation.) Naturally the special assumption is not satisfied in the space but I think this condition is realizable, and is useful in the general case.

We want to make the special cube grid rigid using some diagonals along the square faces of the unit cubes as diagonal bracing. The consequence of our special assumption is that the "vertical" rods of the first floor are parallel with the vector Z_1, those of the second are parallel with Z_2 and so on. The "parallel tube" indicated by heavy line in Fig. 6 will be denoted by $/X_2, Z_1/$. All the rhombi "perpendicular" to the heavy lines are parallel; applying a diagonal brace for any of them will fix the others as well.

The special cube grid is rigid if and only if all the rhombi remain square during any motion. We have three point classes X_i, Y_j, Z_k similarly to the planar case. Thus we have a tripartite graph T (Fig. 7). We indicate the diagonal braces as edges in the tripartite graph. If T is complete,
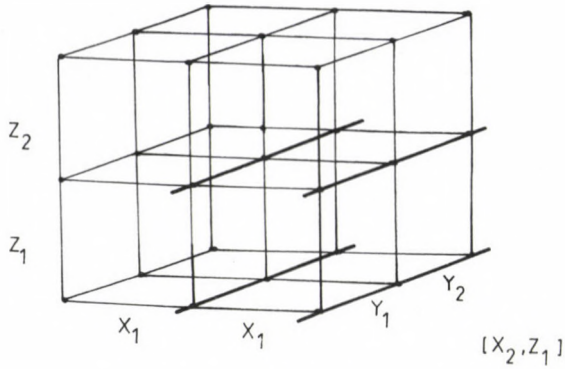
Fig. 6
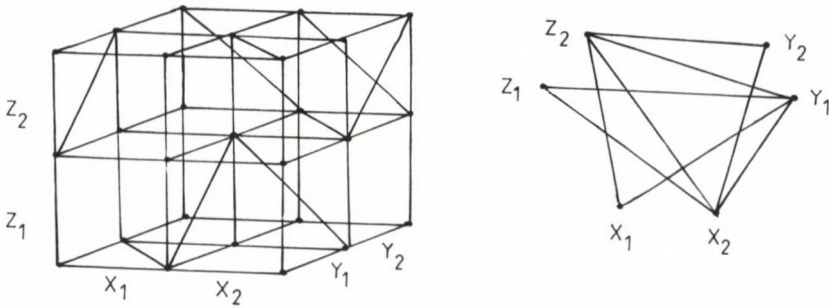
Fig. 7

that is, if there exists an edge between every pair of points if they are in different point classes then the cube grid is rigid, because each rhomboid is a cube in the grid. However, less diagonal bracing may also be sufficient. Consider the three bipartite subgraphs of the bracing tripartite graph T.

Necessity

Theorem 1: If the special cube grid is rigid then the bipartite subgraphs of the bracing tripartite graph are connected.

Proof: If the subgraph $X_i Y_j$ is disconnected then there exists a move whose direction is perpendicular to Z_k, as a consequence of Bolker—Crapo's theorem (Fig. 8).
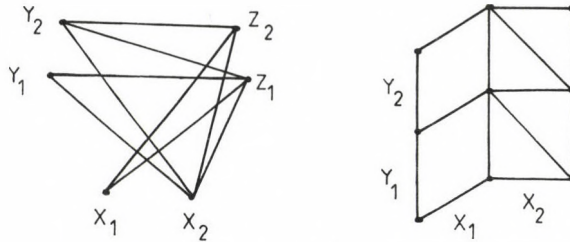
Fig. 8

The necessary condition is sufficient, that is:

Theorem 2: The special cube grid as a bar and joint framework is rigid if and only if the bipartite graphs of the bracing tripartite graph are connected.

Motivation

X_i, Y_j, Z_k are the end points of the respective grid vectors on the unit sphere. The special cube grid is rigid if and only if every X_i is perpendicular to Y_j and Z_k, and Y_j are perpendicular to Z_k during any motion. If there is a diagonal brace in the parallel tube $/X_2$, $Y_2/$ then the vector X_2 is perpendicular to Y_2. We denoted it by a rod on the unit sphere between the points X_2, Y_2. Thus a framework s arises on the sphere (Fig. 9). If this framework s is rigid on the sphere then the special cube grid is rigid in the space. We have a framework on the sphere and its graph c is tripartite and its 3 bipartite subgraph are connected. This type of framework is generic rigid as a consequence of the following theorem /5/.

Lovász—Yemini's theorem: Let G denote a graph c of a planar framework F with v joints and e = 2 v - 3 rods. Then F is generic rigid if and only if the edge set of G_e, obtained from G by doubling any edge e of G, can be recovered by two edge disjoint spanning trees.

We say that a given framework F is generic if all frameworks sufficiently near to F have the same rigidity properties as F does.

Lovász—Yemini's theorem is true intuitively on an open half sphere. Our graph c has l+m+n points and l+m-1 + m+n-1 + n+l-1 = 2(l+m+n)-3 edges since the bipartites are connected, where the dimensions of the grid are l x m x n. It is clear from the definitions of the graph c of the framework s and the bracing graph T that the graph c of s and the tripartite bracing
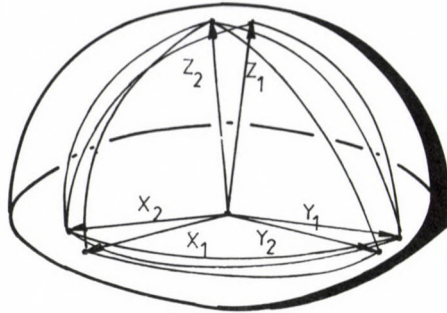
Fig. 9

graph T are isomorphic. Thus we can apply the Lovász—Yemini's theorem for either one of them, say for T. T_e is obtained from the tripartite bracing graph T by doubling an edge e of T. T_e can be covered by two edge disjoing spanning trees. Let $B/X_i,Y_j/$ denote the bipartite graph between X_i, Y_j. Let the doubling edge from $B/X_iY_j/$ be, say, X_1Y_1. $B/X_i,Y_j/$ has two subgraphs so that we can get from some X_i to each Y_j in the first subgraph along edges, and we can get from some Y_j to each X_i in the second subgraph along edges. They are denoted by $S/X,Y/$ and $S/Y,X/$, respectively. Thus we have two spanning trees: $B/X_i,Z_k/ \cup S/X,Y/$ and $B/Y_j,Z_k/ \cup S/Y,X/$.

Sufficiency

If we can prove that the framework s is rigid on the sphere then Theorem 2 is true. In this case we need the co-ordinates of the points X_i, Y_j, Z_k. Let us introduce a new system of co-ordinates, where the origin of the co-ordinate system is still at the unit sphere's centre and let the plane determined by the points X_i, Y_j, Z_k be parallel to the new X', Y' axes. The rank of the rigidity matrix /6/ depends on the new X' and Y' co-ordinates of the points X_i, Y_j, Z_k and on the graph c only, since these points form an equilateral triangle which is parallel to the new X', Y' plane. Thus we can simplify the original problem.

Consider a special cube grid bracing with some diagonal braces along square faces; it is rigid if and only if framework p is rigid on the plane. The joints of p are the same as those of framework s and there is a rod between two joints if there is rod in framework s. Since joints of s are on a plane at the beginning of the motion, it suffices to consider the rigidity of the framework p in the plane.

$$> 2\sqrt{2-\varepsilon^2}$$
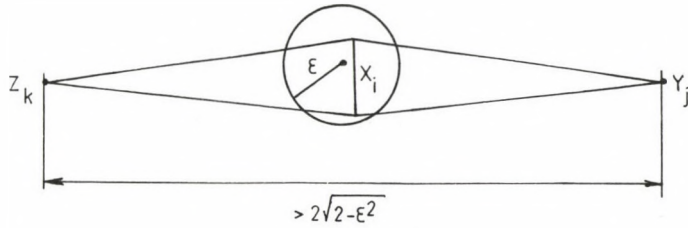
Fig. 10

Choose the joint X_1 among the joints X_i. There are some joints among the joints Y_j and Z_k that are adjacent with joint X_1. These joints are on a circle. The center of the circle is X_1, the radius of the circle is $\sqrt{2}$. Choosing every joint from joints X_1 we get some congruent circles. These circles are denoted by X_i as well.

Assuming that framework p is not rigid, there are at least two X_i circles or two Y_j circles or two Z_k circles with a continuous motion relative to each other. Let us suppose at first that they are X_i circles.

Since the moving is continuous we can choose three circles with radius ε around the vertices of the original equilateral triangle. Every point X_i, Y_j and Z_k are in these three different circles with radius ε.

The circles X_i intersect each other in points Y_j and Z_k or are identical. There are at least two circles that are not identical.

Every circle has two intersection points, one among the points Y_j and the other among the points Z_k since the three bipartite subgraphs of the bracing graph are connected.

If ε is less than 0.1 then the distances of the intersections of the X_i circles are more than $2\sqrt{2-\varepsilon^2} \approx 2.8213$ (Fig. 10) but the distances between points Y_j and points Z_k are less than $\sqrt{2} + 2\varepsilon \approx 1.643$. It is obvious that the X_i's are not different i.e. they do not move. A similar argument can be applied if two Y_j circles or two Z_k circles have a continuous motion relative to each other. This completes the proof of the theorem.

In the proof we show a new framework (framework p) in a plane that is rigid in its plane if and only if the special cube grid is rigid in the space and the graph c of the framework p is isomorphic to the bracing graph of the special cube grid.

This result shows that $l \times m \times n$ special cube grids consisting of ideal frictionless rods connected by joints are rigid if and only if the three

edge direction projections of the grid with face diagonal braces are rigid in the plane.

Thus we need $2(1+m+n)-3$ face diagonal braces for the rigidity of an $1 \times m \times n$ special cube grid. This result could probably be generalized for higher dimensions.

ACKNOWLEDGEMENTS

REFERENCES

1. Asimov, L.—Roth, B.: The rigidity of graphs, Part I. Trans. Amer. Math. Soc. 245 (1978), 279—289; Part II, J. Math. Anal. Appl. 68 (1979), 171—190

2. Bolker, E. D.: Bracing rectangular frameworks II. SIAM J. Appl. Math. 36, No. 3 (1979), 491—508

3. Bolker, E. D.—Crapo, H.: Bracing rectangular frameworks I. SIAM J. Appl. Math. 36, No. 3 (1979), 473—490

4. Connelly, R.: A counterexample to the rigidity conjecture for polyhedra. Publ. Math. I.H.E.S., 47 (1978), 333—338

5. Lovász, L.—Yemini, Y.: On the generic rigidity in the plane. SIAM J. Algebraic and Discrete Methods 3 (1982), 91—98

6. Recski, A.: Matroid Theory and its Applications in Electric Network Theory and in Statics. Akadémiai Kiadó, Budapest and Springer, Berlin (1989)

7. Recski, A.: Bracing cubic grids — A necessary condition. Discrete Mathematics 73 (1988/89), 199—206

8. Whiteley, W.: The union of matroids and the rigidity of frameworks. SIAM J. Disc. Math. 1, No. 2 (1988), 237—255

PACKING OF 5 REGULAR PENTAGONS ON A SPHERE

TARNAI, T.[*]—GÁSPÁR, ZS.[**]

How must n equal non-overlapping regular spherical pentagons be packed on a sphere so that the angular radius of the circum-circles of the pentagons will be as great as possible? In the paper, the conjectured solution of this problem for n = 5 is presented.

1. Introduction

The arrangement of pentamer structural units composed of protein molecules in the capsids of certain spherical viruses has inspired the following mathematical problem /3/: To determine the largest angular circumradius r_n of n equal regular spherical pentagons which can be packed on the surface of a sphere without overlapping.

Conjectured solutions to this problem are known for n = 6, 8 /5/ and, under symmetry constraints, for n = 24, 72 /6/. For n → ∞ a packing in the plane is obtained. The conjectured best arrangement of equal regular pentagons in the plane is published in /2/.

Density D_n of a pentagon packing is defined as the ratio of the total area of the surface of the spherical pentagons to the surface area of the sphere:

$$D_n = \frac{n}{4}\left(\frac{5\alpha}{\pi} - 3\right)$$

where α is an angle of the pentagons measured in radians.

[*]Tarnai, Tibor, H-1037 Budapest, Kolostor u. 17, Hungary
[**]Gáspár, Zsolt, H-1025 Budapest, Kapy u. 40/b, Hungary

The aim of this paper is to present a conjecture for the densest packing of 5 pentagons on a sphere. The best arrangement will be selected from packing constructions resulting in local maxima of the circum-radius of the pentagons and so local maxima of the density of packing.

2. Packing constructions

This pentagon packing problem is similar to the Tammes problem of packing of equal circles on a sphere. However, because a circle is strictly convex but a pentagon is not, there are dissimilarities between the two problems. The most important one is that to a packing of circles there can be associated a graph /1/, but to a packing of pentagons there exist no graph of the same sort. In a circle packing, two circles can touch only in one way; but in a pentagon packing, two pentagons can touch in three different ways: with (a) edge-to-edge, (b) vertex-to-edge, (c) vertex-to-vertex contact.

The pentagon packing problem will be investigated by a method similar to the "heating technique" developed for spherical circle packings /4/, resulting in a local optimum. The principle of this method /5/ is that the pentagons are considered as rigid bodies lying on the surface of the sphere such that their size can be changed simultaneously and in the same proportion. Change in size is attributed to a change in "temperature". Due to a change in temperature the pentagons move on the surface of the sphere, and the boundaries of pentagons in contact can slide on each other. The temperature of the pentagons and so the size of the pentagons is increased uniformly while the system of pentagons remains free of stress. The circum-radius is looked for, for which the pentagons just start to press each other and the system of pentagons gets to a stable state of self-stress. In this state the size of the pentagons cannot be increased any further with continuous increase of the temperature. Appearance of a stable state of self-stress with no contacts in tension indicates a local optimum.

We have applied the method for packing of 5 equal regular pentagons on a sphere. We have worked out a computer program for finding the best configuration, but here we omit the details of the calculation and present only the main points and the results.

Consider first the best packing of six pentagons on a sphere where the radius of the circum-circle of a pentagon with six-decimal accuracy is equal

to 48.719106° /5/. Let us take two pentagons of this packing and join them in such a way that they have a vertex in common, then pack them on the sphere so that the common vertex and the centres of the pentagons lie on the equator. Then let us consider a copy of this pair of pentagons, obtained from the original by a rotation of 90° about the common vertex, and translate the two rotated pentagons in the opposite direction perpendicular to the equator until they contact the original pentagons. (The compound of the four pentagons has two planes of symmetry.) Between the two rotated-translated pentagons, antipodally to the common vertex, there is space for the fifth pentagon. This arrangement is considered as the starting configuration for the heating process. The temperature, that is, the size of the pentagons can be increased until the fifth pentagon contacts the two rotated-translated ones. However, if the two-fold mirror symmetry of the compound of the four pentagons and the common vertex is preserved, the system of forces arising at all the contacts of the pentagons can be in equilibrium only in two cases:

(1) The fifth pentagon and one of the rotated-translated pentagons have a side in common and the vertex of the fifth pentagon, opposite to this common side, is lying on a side of the other rotated-translated pentagon as is shown in Fig. 1. (Considering its position, the fifth pentagon will be called a standing pentagon at the rear.) The radius of the circum-circles of the pentagons in this arrangement with seven-decimal accuracy is $r_5 = 49.5338118^{\circ}$.

(a)   (b)
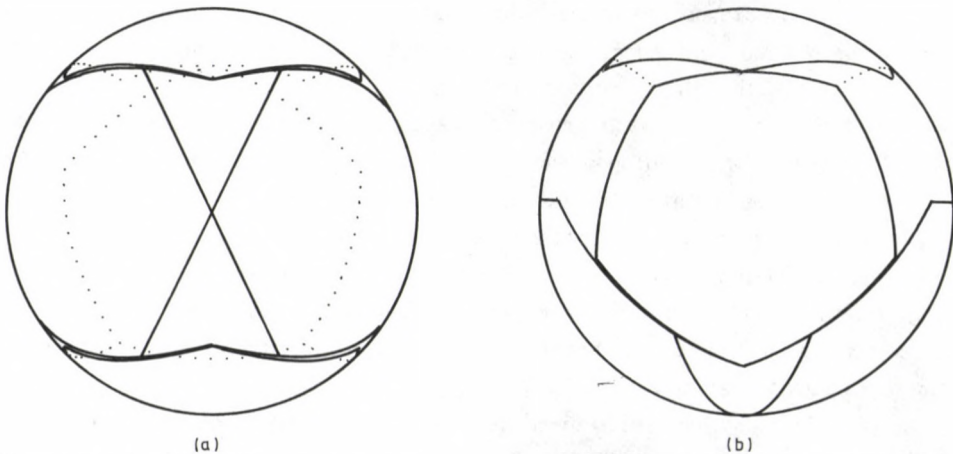
Fig. 1. Packing with 4 pentagons in D_2 symmetry in front and a standing pentagon at the rear, where 2 pentagons have a vertex in common, (a) front-view, (b) view from above

(a)   (b)
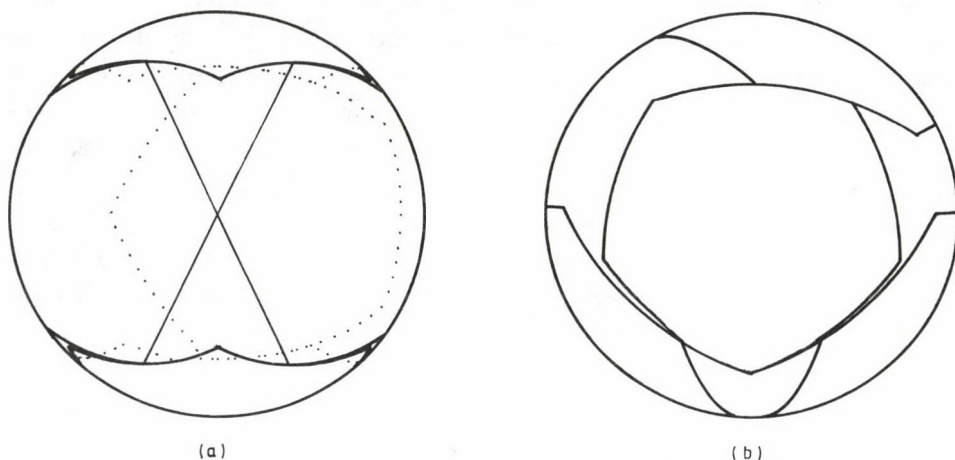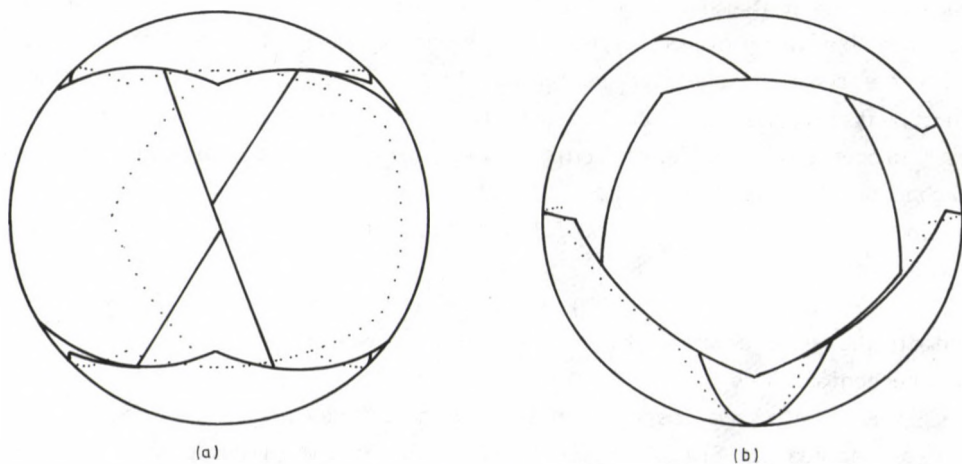
Fig. 2. Packing with 4 pentagons in D_2 symmetry in front and a lying pentagon at the rear, where 2 pentagons have a vertex in common, (a) front-view, (b) view from above

(2) The fifth pentagon and each of the rotated-translated pentagons have a side segment in common as is shown in Fig. 2. (Considering its position, the fifth pentagon will be called a lying pentagon at the rear.) The radius of the circum-circles of the pentagons in this arrangement is $r_5 = 49.5683744^\circ$.

In both cases a state of self-stress can be detected, however, none of the two configurations results in a local maximum of the density, since in both cases, at the common vertex a tensional contact force appears while all the other contacts are in compression. Appearance of a tensional force means that one of two pentagons, between which the tensional force acts, wants to depart from the other. We must not prevent this departure, so the contact of the two pentagons must be removed. Repeating the heating process for the modified assembly of pentagons we can improve the packing. We can do it, for instance, if we rotate the two original pentagons lying on the equator equally and in the same direction (say clockwise), then join them with edge overlapping. Doing so we can increase the size of the pentagons, and depending on the position of the fifth pentagon we obtain two additional equilibrium configurations where the compound of the four front pentagons has a two-fold rotational symmetry:

(3) In the case where there is a standing pentagon at the rear, by an increase in the size of the pentagons we arrive at the configuration in Fig. 3. Here the radius of the circum-circles of the pentagons is obtained
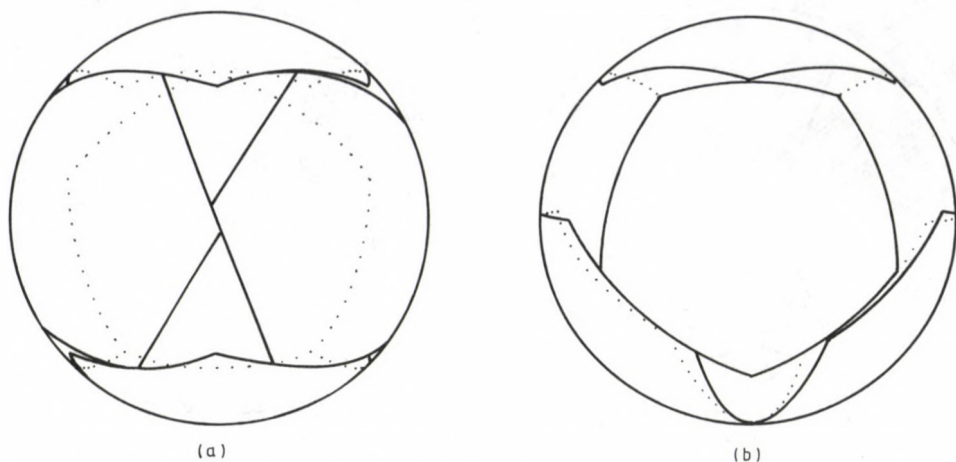
Fig. 3. Packing with 4 pentagons in C_2 symmetry in front and a standing pentagon at the rear, where 2 pentagons have an edge segment in common at the axis of symmetry, (a) front-view, (b) view from above

at an edge-overlap of 7.1542381^O of the two pentagons lying on the equator, and its value is $r_5 = 49.5564816^O$

(4) In the case where there is a lying pentagon at the rear, by an increase in the size of the pentagons we arrive at the configuration in Fig. 4. Here the radius of the circum-circles of the pentagons is obtained

Fig. 4. Packing with 4 pentagons in C_2 symmetry in front and a lying pentagon at the rear, where 2 pentagons have an edge segment in common at the axis of symmetry, (a) front-view, (b) view from above
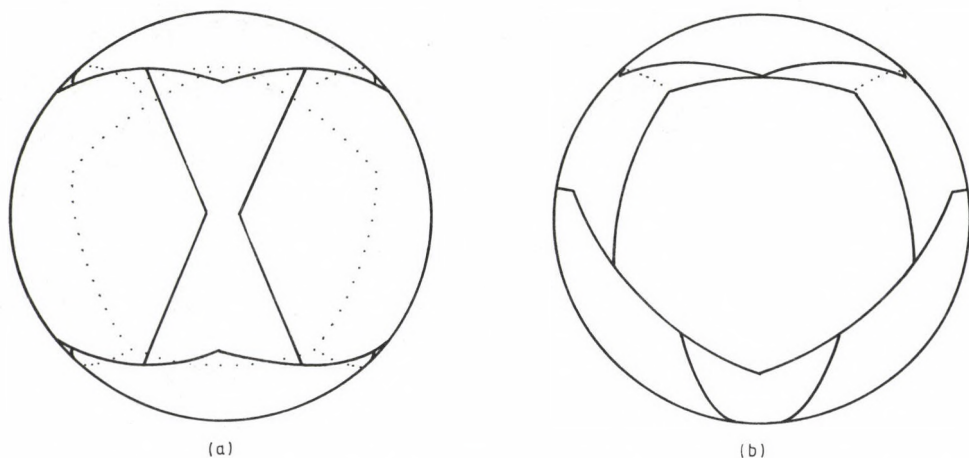
Fig. 5. Locally optimal packing with 4 pentagons in D_2 symmetry in front and a standing
pentagon at the rear, (a) front-view, (b) view from above

at an edge-overlap of 6.9989408^O of the two pentagons lying on the equator,
and its value is $r_5 = 49.5903228^O$.

In both cases a state of self-stress can be detected, however, none of
the two configurations in Figs 3, 4 results in a local maximum of the den-
sity, since in both cases at the edge-to-edge contact of the pentagons lying
on the equator a tensional force appears again. This shows that-the packing
is improvable further after removing this edge-to-edge contact. Indeed, we
can make the pentagons larger if first we arrange the four front pentagons
so that the two pentagons lying on the equator have edge-to-edge contacts
with the rotated-translated pentagons. In this case the compound of these
four pentagons has two planes of symmetry. Preserving this symmetry and con-
tact properties of the four front pentagons we increase the size of the pen-
tagons until the fifth pentagon blocks the motion of the system. Depending
again on the orientation of the fifth pentagon we get to two new equilibrium
configurations:

(5) In the case where there is a standing pentagon at the rear, we
obtain the arrangement in Fig. 5 in which the radius of the circum-circles
of the pentagons is $r_5 = 49.5794094^O$.

(6) In the case where there is a lying pentagon at the rear, we obtain
the arrangement in Fig. 6 in which the radius of the circum-circles of the
pentagons is $r_5 = 49.6138224^O$.

                    (a)   (b)
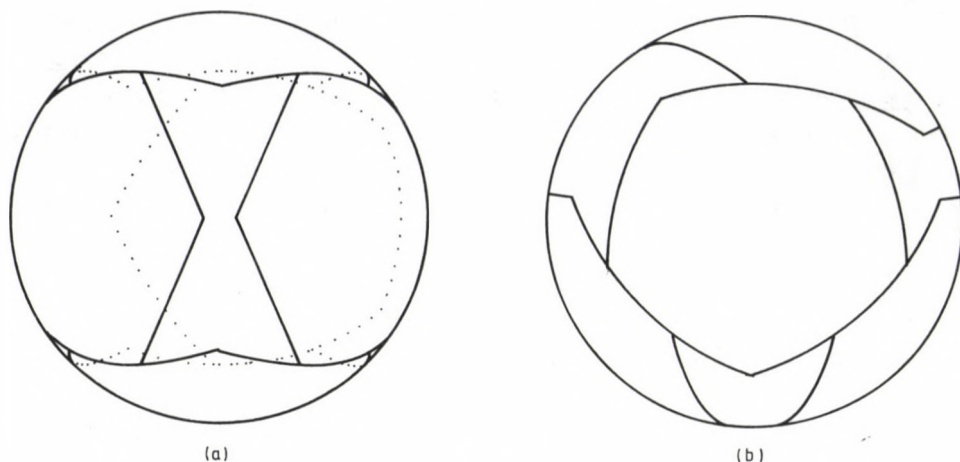
Fig. 6. Locally optimal (the conjectured best) packing with 4 pentagons in D_2 symmetry in front and a lying pentagon at the rear, (a) front-view, (b) view from above

In both cases a stable state of self-stress can be shown, and each contact is in compression. This means that in both cases we have a locally extremal arrangement.

3. Conclusions

We have collected the results of all the investigated equilibrium configurations of pentagons in Table 1 where the packing densities and the crystallographic symmetry groups are also given.

Table 1. Packing of 5 equal regular pentagons on the sphere

Figure	Circumradius r_5 ($^\circ$)	Density D_5	Symmetry	Remark
1	49.5338118	0.7468699	C_s	
2	49.5683744	0.7479557	C_s	
3	49.5564816	0.7475820	C_1	
4	49.5903228	0.7486456	C_1	
5	49.5794094	0.7483025	C_s	local optimum
6	49.6138224	0.7493847	C_s	local optimum

We could not find more than two local optima, so we think that one of them is the solution of the problem, that is, we have the following <u>Conjecture</u>. The densest packing of five equal regular spherical pentagons on a sphere is the packing in Fig. 6 where a pentagon is packed at the north pole, another one at the south pole and the remaining three pentagons on the equator with consecutive distances 108°, 144°, 108° between their centres, and where the circum-radius of the pentagons is $r_5 = 49.6138224...^O$.

The density of the conjectured best packing is $D_5 = 0.7493847$. The plane of the equator is a plane of symmetry of this packing configuration. The centres of the pentagons form a trigonal bipyramid in which the edge lengths of the base triangle are 108°, 144°, 108° and the length of the incline edges is 90°. We note that, for the densest packing of 5 circles on the sphere /1/, the radius of the circles is 45° and the density is 0.7322330, and because the circle packing is not rigid (the solution is not unique) the centres of the circles can form also a trigonal bipyramid, in particular, with the same edge lengths as the conjectured best packing of 5 pentagons.

ACKNOWLEDGEMENTS

REFERENCES

1. Fejes Tóth, L.: Lagerungen in der Ebene auf der Kugel und im Raum. 2nd edition, Springer-Verlag, 1972

2. Kuperberg, G.—Kuperberg, W.: Double-lattice packings of convex bodies in the plane. Discrete Comput. Geom. 5 (1990), 389—397

3. Salunke, D. M.—Caspar, D. L. D.—Garcea, R. L.: Polymorphism in the assembly of polyomavirus capsid protein VP_1. Biophys. J. 56 (1989), 887—900

4. Tarnai, T.—Gáspár, Zs.: Improved packing of equal circles on a sphere and rigidity of its graph. Math. Proc. Camb. Phil. Soc. 93 (1983), 191—218

5. Tarnai, T.—Gáspár, Zs.: Packing of regular pentagons on a sphere. Colloquia Math. Soc. János Bolyai, Intuitive Geometry (ed.: K. Böröczky and G. Fejes Tóth). North-Holland, Amsterdam 63 (1994), 475—480

6. Tarnai, T.—Gáspár, Zs.—Szalai, L.: Pentagon packing models for 'all-pentamer' virus structures. Biophys. J. 69 (1995), 612—618
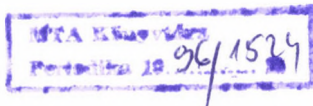
BOOK REVIEW

Prékopa, A.: <u>Stochastic Programming</u>. Akadémiai Kiadó, Budapest, 1995

Stochastic Programming is the science that provides us with tools to design and control stochastic systems by the aid of mathematical programming techniques. It is on the border line of statistics and mathematical programming. The book is a comprehensive introduction to the field and its basic mathematical tools. While its mathematics is of high level, the developed models offer powerful applications, shown by a large number of examples. The presented material ranges from basic linear programming to algoritmic solutions of sophisticated system problems and applications in water resources and power systems, ship manufacturing, inventory control, etc. It is the first graduate level textbook written on the topic.

<u>About the author</u>: András Prékopa, founder of teaching and research of Operations Research in Hungary, professor at the Eötvös Loránd University, Budapest, member of the Hungarian Academy of Sciences, member of the New York Academy of Sciences, foreign member of the National Academy of Engineering of Mexico, member of the International Statistical Institute, fellow of the Econometric Society.

<u>Readership</u>: operations researches, mathematicians, statisticians, engineers (all kinds), economists, computer scientists, business specialists, scientists.

In English, 1995, approx. 600 pages, 17 x 25 cm,
Hardbound, USD 85.00
ISBN 963 05 6872 1

Co-edition with Kluwer Academic Publishers, Dordrecht

Distributed by Akadémiai Kiadó in Albania, Armenia, Bosnia-Herzegovina, Bulgaria, China, C.I.S., Croatia, Cuba, Czech Republic, Estonia, Hungary, Korean People's Republic, Latvia, Lithuania, Macedonia, Mongolia, Poland, Romania, Slovenia, Vietnam, Yugoslavia. For all other countries exclusive distribution right belongs to the co-publisher.

ACTA
TECHNICA

ACADEMIAE SCIENTIARUM HUNGARICAE

EDITOR-IN-CHIEF: P. MICHELBERGER

VOLUME 106
NUMBERS 3–4

ACTA TECHNICA

Volume 106 Nos 1—4

CONTENTS

NOTICE TO CONTRIBUTORS

Papers in English* are accepted on condition that they have not been previously published or accepted for publication.

Only original papers will be published and a copy of the Publishing Agreement will be sent to the authors of papers accepted for publication. Manuscripts will be processed only after receiving the signed copy of the agreement.

Manuscripts in two copies (the original type-written copy plus a clear duplicate one) complete with figures, tables, and references should be sent to

Acta Technica
Nádor u. 7. I. 118
Budapest, Hungary
H-1051

Although every effort will be made to guard against loss, it is advised that authors retain copies of all material which they submit. The editorial board reserves the right to make editorial changes.

Manuscripts should be typed double-spaced on one side of good quality paper with proper margins and bear the title of the paper and the name(s) of the author(s). The full postal address(es) of the author(s) should be given in a footnote on the first page. An abstract of 50 to 100 words should precede the text of the paper. The approximate locations of the tables and figures should be indicated in the margin. An additional copy of the abstract is needed. Russian words and names should be transliterated into English.

References. Only papers closely related to the author's work should be referred to. The citations should include the name of the author and/or the reference number in brackets. A list of numbered references should follow the end of the manuscript.

References to periodicals should mention: (1) name(s) and initial(s) of the author(s); (2) title of the paper; (3) name of the periodical; (4) volume; (5) year of publication in parentheses; (6) numbers of the first and last pages. Thus: 5. Winokur, A.—Gluck, J.: Ultimate strength analysis of coupled shear walls. American Concrete Institute Journal 65 (1968) 1029-1035

References to books should include: (1) author(s)' name; (2) title; (3) publisher; (4) place and year of publication. Thus: Timoshenko, S.—Gere, J.: Theory of Elastic Stability. McGraw-Hill Company. New York, London 1961

Illustrations should be selected carefully and only up to the necessary quantity. Black-and-white photographs should be in the form of glossy prints. The author's name and the title of the paper together with the serial number of the figure should be written on the back of each print. Legends should be brief and attached on a separate sheet. Tables, each bearing a title, should be self-explanatory and numbered consecutively.

Authors will receive proofs which must be sent back by return mail.

Authors will receive 50 reprints free of charge.

* Hungarian authors can also submit their papers in Hungarian.